12-11-2014

Structure-Based Drug Design and Synthesis of Anti-infective and Anticancer Agents

Narendran Gummudipundi Dayanandan
University of Connecticut - Storrs, gdnarendran@gmail.com

Structure-Based Drug Design and Synthesis of Inhibitors as Anti-infective and Anticancer Agents

Narendran G-Dayanandan, Ph. D.

University of Connecticut, 2014

ABSTRACT

Resistance to antibiotics is on the rise at an alarming pace. The problem is exacerbated by the lack of new class of therapeutic agents and targets. Modes of resistance include alteration of drug target, modification of ligand, and reduction of the intracellular concentration of drug. Dihydrofolate reductase (DHFR) is a validated drug target for the treatment of infectious diseases and cancer. The binding of ligands to DHFR inhibits the downstream folate pathway that is vital for purine and thymidylate synthesis. Trimethoprim (TMP), a clinically used antifolate exhibits resistance in both gram-positive and gram-negative bacteria. In this thesis, methods have been refined to expedite the synthesis of propargyl linked antifolates for lead optimization. As a result, novel antifolate inhibitors with better pharmacokinetic profile have been designed and synthesized for methicillin resistant *Staphylococcus aureus* (MRSA). Ligands with minimal inhibitory concentration (MIC) of 0.3 - 0.6 μg/mL exhibiting an *in-vitro* half life of 60 minutes were achieved. Similarly, to overcome resistance to azole antifungal

agents, propargylic linked antifolates exhibiting dual inhibition against *Candida albicans* and *Candida glabrata* were developed. Antifolate activity of less than 0.1 μg/mL has been achieved against the clinically indistinguishable pathogens. In the development of antifolates for gram negative bacteria – *Escherichia coli* and *Klebsiella pneumoniae*, studies were carried out to understand the factors that influence the permeability and efflux of the ligands. With a 1,3 benzodioxole moiety of the antifolate exhibiting low efflux activity, new leads are in progress to synthesize ligands with potent antibacterial activity.

In another project, simplified analogs of the natural product, cyclopamine, have been synthesized. Cyclopamine inhibits the smoothened (Smo) transmembrane of the hedgehog signaling pathway. The synthesis utilizes a furan based Diels Alder reaction to generate a functionalized oxabicyclic adduct. The adduct eventually undergoes a cascade reaction involving a tandem ring-opening, ring closing metathesis reaction to generate the spirocyclic core of cyclopamine.

Structure-Based Drug Design and Synthesis of Inhibitors as Anti-infective and Anticancer Agents

Narendran G-Dayanandan

M.Sc., University of Madras, 2002

M.S., University of Connecticut, 2008

A Dissertation

Submitted in Partial Fulfillment of the

Requirements for the Degree of

Doctor of Philosophy

at the

University of Connecticut

2014

APPROVAL PAGE

Doctor of Philosophy Dissertation

Structure-Based Drug Design and Synthesis of Inhibitors as Anti-infective and Anticancer Agents

Presented by

Narendran G-Dayanandan, M.Sc., M.S.

Major Advisor _____

Dennis L.Wright

Associate Advisor _____

Amy C. Anderson

Associate Advisor _____

M. Kyle Hadden

Associate Advisor _____

Amy R. Howell

ACKNOWLEDGEMENTS

I would like to express my heartfelt gratitude to my advisor Dr. Dennis Wright for giving me the opportunity to pursue my dreams of being a student of science. Dennis' philosophy of "keep it simple" and his infectious excitement and encouragement have enabled me to push beyond my limitations and thereby explore different aspects of drug design and organic synthesis. I acquired a sense of appreciation for organic synthesis while working on the spirocyclic core of cyclopamine, which was based on a very simple retrosynthesis designed by Dennis.

I would also like to thank Dr. Amy Anderson for imparting in me a deep understanding of the biological aspects of drug design. I still recollect with great fondness, Amy's class on drug design that steered me towards discovering my natural aptitude for drug discovery. A special thanks to my committee members- Dr. M. Kyle Hadden, Dr. Amy R. Howell and Dr. Ashis K. Basu for their valuable time and suggestions during my general exam and dissertation defense.

I am greatly indebted to Dr. Zachary E. Oblak, my first mentor in this lab. It was from Zach that I learnt that there is no substitute for perseverance when it comes to organic synthesis and his work ethic has always been an inspiration to me. Another mentor without whom I might not have completed my journey is Dr. Kishore Viswanathan. The endless conversations we had about science and philosophy kept me grounded and helped me understand the true nature of doing research. He also helped me learn more about myself, for which I will be eternally grateful.

Dr. Santosh Keshipeddy has been the soundboard for my ideas. Santosh comes up with unique questions during discussions that steers my thought process in the right direction. Dr. Michael Vanheyst was a fun guy to hang around with and our morning, afternoon and evening walks to the café while talking about synthesis was always the highlight of my day. I can never thank Eric Scocherra enough for making my tranisition to this lab easy and helping me become part of the group. In the last six years, we have had interesting and illuminating conversations about anything and everything. I am also thankful to members of Dr. Anderson's lab – Dr. Janet Paulsen, Dr. Wangda Zhou, Dr. Kristen Lamb, Stephanie Reeve, Michael Lombardo, Behnoush Hajian for their biological studies and also Eric Falcone, Alex Estrada for their help with synthesis.

On a personal note, I would like to thank my cousin Vedhanarayanan and my uncle Santhana Krishnan for their help and support during my graduate studies. I was blessed with great friends – Dr. Magesh Nandagopal, whom I knew from my undergraduate days and Dr. Balaji Raman who has always been my greatest cheerleader. The weekends with Kishore and his wife Dr. Aparna Iyer were truly memborable for my wife and me, while we were all pursuing our doctoral studies.

My brother – Surendran, has shouldered all the family responsibilities in my absence and although younger to me, has always been the more mature and responsible of the both of us. If not for my parents – Leelavathy and Dayanandan, I would not have been able to undertake this long jouney. The sheer magnitude of their sacrifice pales in comparison to what I have accomplished so far and I hope to continue to make them proud. Apart from my parents, if there is one person in the world who believes in me

more than I do in myself, it's my wife – Dr. Archana Krishnan. Archana is my best friend and critic, and she has expanded my horizons, while remaining my inner strength.

DEDICATION

To

Amma & Appa

But see that the imagination of Nature is far, far greater than the imagination of man.

Nobody ever figures out what life is all about, and it doesn't matter. Explore the world.

Nearly everything is really interesting if you go into it deeply enough.

Richard P. Feynman

TABLE OF CONTENTS

LIST OF FIGURES

LIST OF TABLES

LIST OF SCHEMES

CHAPTER 1

INTRODUCTION

Antibiotics – Mechanism of Action and Mode of resistance

The World Health Organization report of 2012 identifies infectious diseases as one of the leading causes of death[1] worldwide. Emergence of antibiotic resistance is of growing concern, which was forewarned by Alexander Fleming in his Nobel Prize[2] speech of 1945. Though the normal evolutionary process of drug resistance cannot be discounted in bacteria, the accelerated rate of resistance is fueled by indiscriminate use of antibiotics. According to a report by The New England Journal of Medicine,[3] nearly 80% of antibiotics in the Unites States are in the argriculture and aquaculture sectors. The increase in resistance to antibacterials is compounded by the lack of new class of antibiotics since the 1990's. (Fig.1)

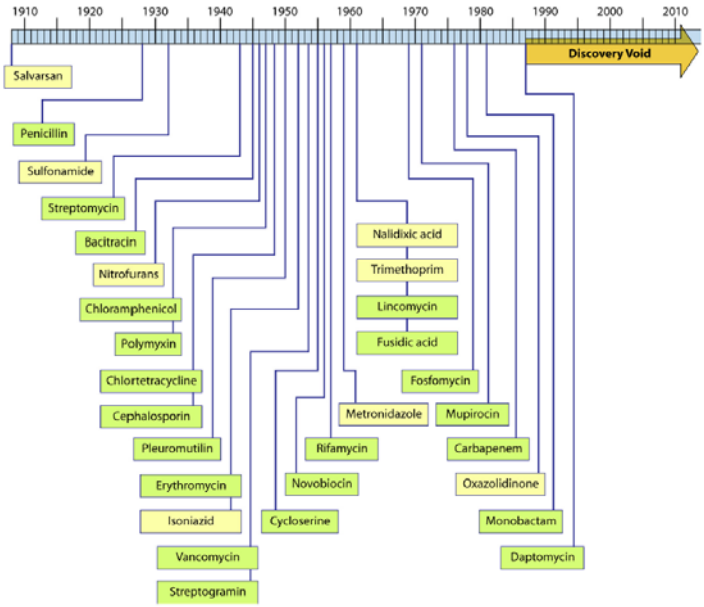

Figure 1 Discovery timeline of antibiotic. Reproduced from Lynn Silver, Clin. Micro.Rev.,2011, 24, 71-109.

A short preview of the anti-bacterials with their mode of action and factors influencing their resistance is discussed below.

1.1 Antibacterial Classification based on Mechanism of Action and Resistance

Antibiotics can be broadly classified into 3 major classes (Fig.2) based on their mode of action. They are inhibition of cell wall synthesis, nucleic acid synthesis and protein synthesis. For the inhibition of protein and nucleic acid targets, the antibacterials have to permeate the outer membrane and enter the cytoplasm of the bacterial cell.

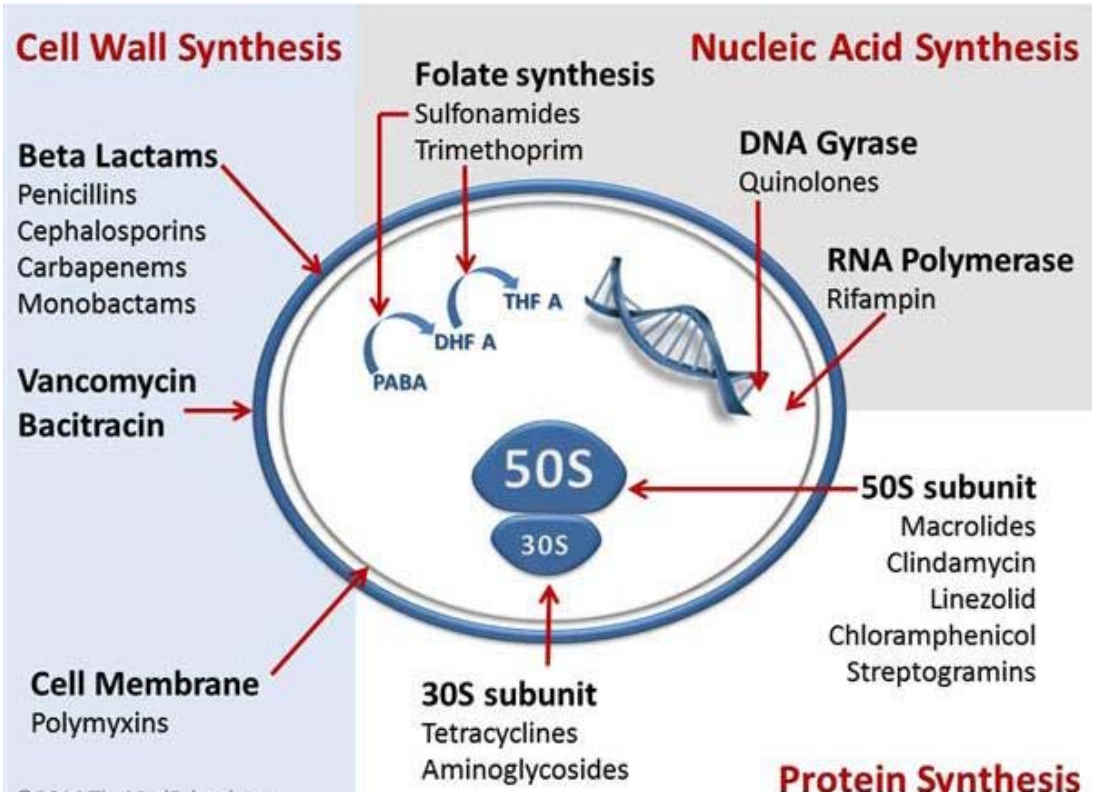

Figure 2 Mechanism of action of antibiotics Reproduced from http://www.orthobullets.com/basic-science/9059/antibiotic-classification-and-mechanism

1.1.1 Inhibition of Cell Wall synthesis

1.1.1A β-lactams

The bacterial cell wall synthesis occurs in the cytoplasm of the bacteria through a series of enzymatic reactions and transported outside as N-acetylmuramyl – pentapeptide containing D-alanine-D-alanine chain. For the crosslinking to occur with another peptidoglycan chain, the D-alanine is cleaved and the resulting acyl group combines with the amino group of a neighboring chain. For the β-lactam antibiotic to effective, it has to be recognized by the penicillin binding proteins (PBPs). The recognition results in the formation of a stable acyl –enzyme species. The resulting enzyme lactam ester complex is resistant to hydrolysis[4]. This feature of irreversibility of the deacylation step in PBPs constitutes the mechanism of action of β-lactams against susceptible strains of pathogens.

For a strain to possess a resistance mechanism (Fig.3) to evade β-lactam[4], either more copies of PBPs exist or the PBPs have evolved to preferentially select for the native endogenous peptides than the xenobiotics. Although both processes cannot be discounted, it's the latter that is responsible for evolution of resistance in gram positive bacteria. Susceptible strains of *Staphylococcus aureus* possess four PBPs (PBP1, PBP2, PBP3, PBP4), but the PBP2 is the target for β-lactam agents, inhibiting its transpeptidase activity. In resistant S.aureus strains an additional PBP2a is present, which crosslinks the peptidoglycan layer for the sustenance of the pathogens. The mechanism of methicillin resitant *S. aureus* involves the acquisition of a mecA gene that codes for the PBP2a protein.

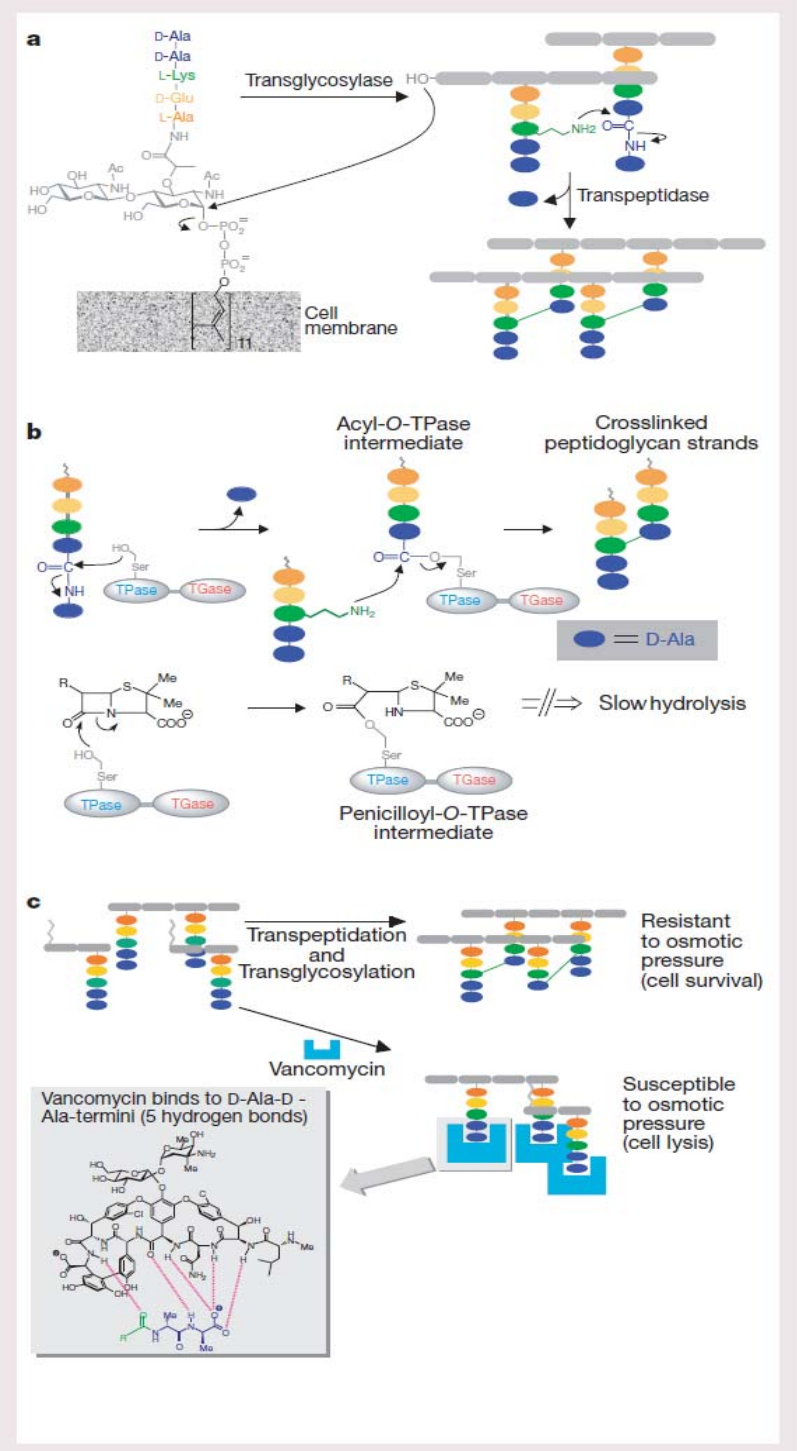

Figure 3. Mechanism of action by β lactam and vancomycin.

Reproduced from Nature. 2000, 17, 406(6797):775-81

A different kind of mechanism (Fig.4) plays out in the case of gram negative bacteria. Here, resistance operates through the acquisition of enzymes called β-lactamases. The existence of these enzymes predates the large scale use of penicillins. The β-lactamases are classified as serine dependent enzymes A,C,D and a metal-based B class. They are found in the periplasmic layer of the gram negative bacteria. These enzymes hydrolyse the β-lactam ring thereby inactivating the drug.

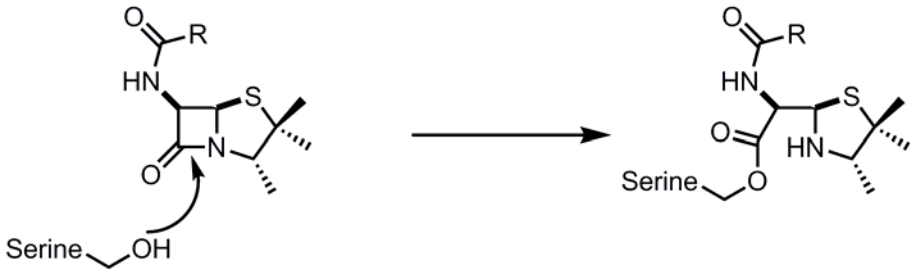

Figure 4. Mechanism of resistance by β lactamases

1.1.1B Vancomycin

The glycopeptide vancomycin inhibits earlier stages of the cell wall synthesis. It prevents the growth of peptidoglycan layer by forming a complex with D-alanine-D-alanine dipeptide through hydrogen bonding. This prevents transglycosylation and transpeptidation reactions that are important for building up the peptidoglycan chain.

The resistance mechanism for vancomycin[5,6] operates through the acquisition of a plasmid containing *van* genes (Fig.5) within a transposon. Courvalin et al proved that the five genes *van* S,R,H,A,X imparted resistance to vancomycin. The vanHAX gene encodes a protein to synthesize D-Ala-D-Lac instead of D-Ala-D-Ala. This results in a

loss of a single hydrogen bond out of the five with vancomycin leading to 1000 fold loss in potency.

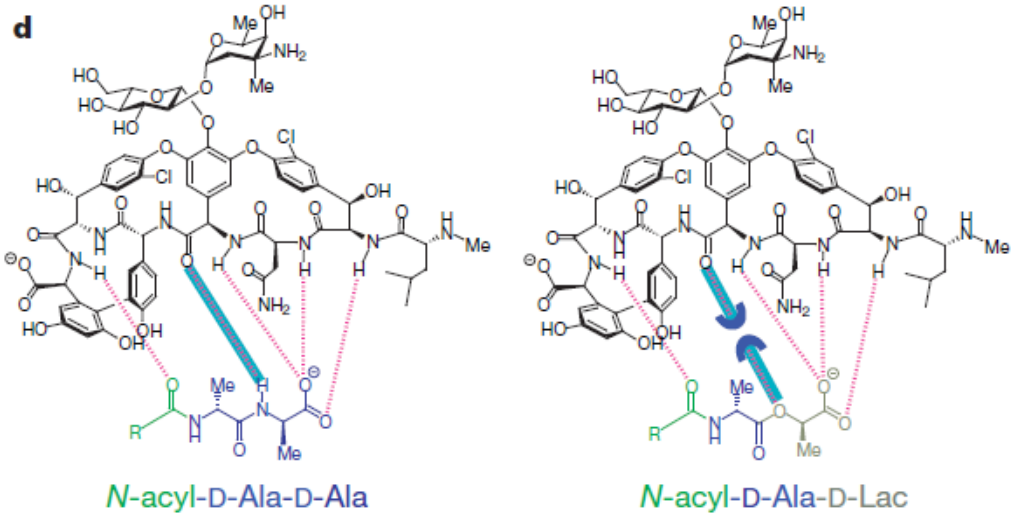

Figure 5. Mode of resistance in vancomycin

Reproduced from Nature. 2000, 17, 406(6797):775-81

1.1.2 Inhibition of Protein Synthesis

1.1.2A Aminoglycosides

Ribosomes catalyze two chemical transformation namely peptide bond formation and ester hydrolysis for polypeptide synthesis. For the initiation of peptide chain, the 30S subunit acts as a receptacle for m-RNA and initiator t-RNA. This ensemble for the initiation of peptide synthesis is complemented with the docking of the 50S subunit of bacterial ribosomes. Aminoglycosides intercept the peptide synthesis process by binding to the 30s of ribosomal subunit. More specifically, binding to the subunit-16S[7, 8] of rRNA interferes with the translation process resulting in defective protein synthesis.

Resistance to aminoglycosides can occur in three ways (a) modification of the target – rRNA or ribosomal protein, (b) alteration in the transport system of aminoglycosides – import and efflux and (c) modification of the ligand by the synthesis of aminoglycoside modifying enzymes. The last mode of resistance seems to be prevalent in most of the clinical isolates of resistant bacteria. Modification of the target by point mutations in the 16S subunit of rRNA is representative of neomycin[9] resistance in *E.coli*, while genes for the methylation of 16S rRNA were encoded on transposons[10,11] and R-plasmids on *Pseudomonas*. The other mode of resistance for aminoglycosides prevalent in gram negative bacteria is the efflux pump.

The most clinically relevant mode of resistance is the enzyme-catalyzed modification of aminoglycoside antibiotics.[12] The enzymes are group into 3 major families (a) aminoglycoside N-acetyltransferases, (b) the aminoglycoside O-nucleotidylyltransferases and (c) the aminoglycoside O-phophotransferases. As implied by the names of these enzymes, they modify the aminoglycoside by acetylation, adenylation or phosphorylation of amino or hydroxyl groups. These modifications render the antiobiotic incapable of binding to the ribosome.

1.1.3 Inhibition of Nucleic Acid Synthesis

1.1.3A Fluoroquinolones

Bacterial gyrase and DNA topoisomerase IV are enzymes[13] that belong to the family of topoisomerases II. The two enzymes relieve the strain of the supercoiled DNA during replication and transcription. They stabilize the conformation by cleaving both strands of the duplex DNA and ligate them together after the uncut ends of DNA slide

through the temporary gap. The scissor action[14] of the topoisomerase occurs by the transesterification reaction of tyrosyl oxygen of the topoisomerase with phosphate of the DNA, resulting in a phosphotyrosine link, while the stitching reaction occurs in a reverse transesterification reaction between the hydroxyl of DNA and phosphate of the topoisomerase. DNA gyrase relaxes the positively or negatively supercoiled DNA and topisomerase IV is involved in the catenation and decatenation of daughter DNA. DNA gyrase is the enzyme target for fluoroquinolones in the case of gram negative bacteria, while topoisomerase IV is inhibited in some gram positive bacteria.

Two major modes of acquisition of drug resistance for fluoroquinolone[15,16] exists. First is the alteration of drug target – DNA gyrase, more specifically in the Gyr A subunit. In *E.coli*, resistant mutations occur between amino acid residues 67 and 106, called the quinolone-resistance determining region (QRDR). These residues reside close to the tyrosine amino acid that transiently anchors itself to the DNA during the relaxation process. The most common mutations occur with Ser83 and Asp87 residues. The mutation Ser83Trp has been shown to reduce the binding affinity of norfloxacin to gyrase-DNA complexes. The second mechanism of resitance is by reducing the intracellular concentration of quinolones. This is carried out by efflux pumps belonging to resistance nodule divison (RND).

1.1.3B Folate pathway

The folate metabolic cycle of prokaryotes differs from eukaryotes in the upstream process of biosynthesis, while the downstream process overlaps for all species (Fig.6). In higher order organisms, folic acid ingested through diet serve as the source of folates, while plants, fungi, bacteria and protozoa have an in-built machinery for the *de novo* synthesis of folates. Gene Brown[17-24] in 1960 -70 identified the essential enzymes for the biosynthesis[25] of folate metabolites involved in bacteria. Folates consist of a pterin moiety coupled to glutamate residues through a p-aminobenzoate linker. The upstream biosynthesis involves the condensation of pABA and 6-hydroxymethyl-7,8-dihydropterin pyrophosphate to form 7,8 dihydropteroate catalyzed by dihydropteroate synthase, DHPS. The glutamate residue is appended to the pterin benzoate motif by the enzyme dihydrofolate synthase, DHFS, to give 7,8-dihydrofolate, DHF. DHF forms the substrate for the dihydrofolate reductase, DHFR enzyme to create 7,8 tetrahydrofolate through an hydride transfer. In humans, DHF is synthesized directly by hydride transfer to folic acid catalyzed by DHFR, while the rest of the folate cycle is akin to the prokaryotes.

The downstream operations of C1 unit transfer for the synthesis of deoxythymidine monophosphate (dTMP), the biosynthesis of purine nucleotides and the amino acids histidine and methionine constitute the most important metabolic processes of the folate pathway.

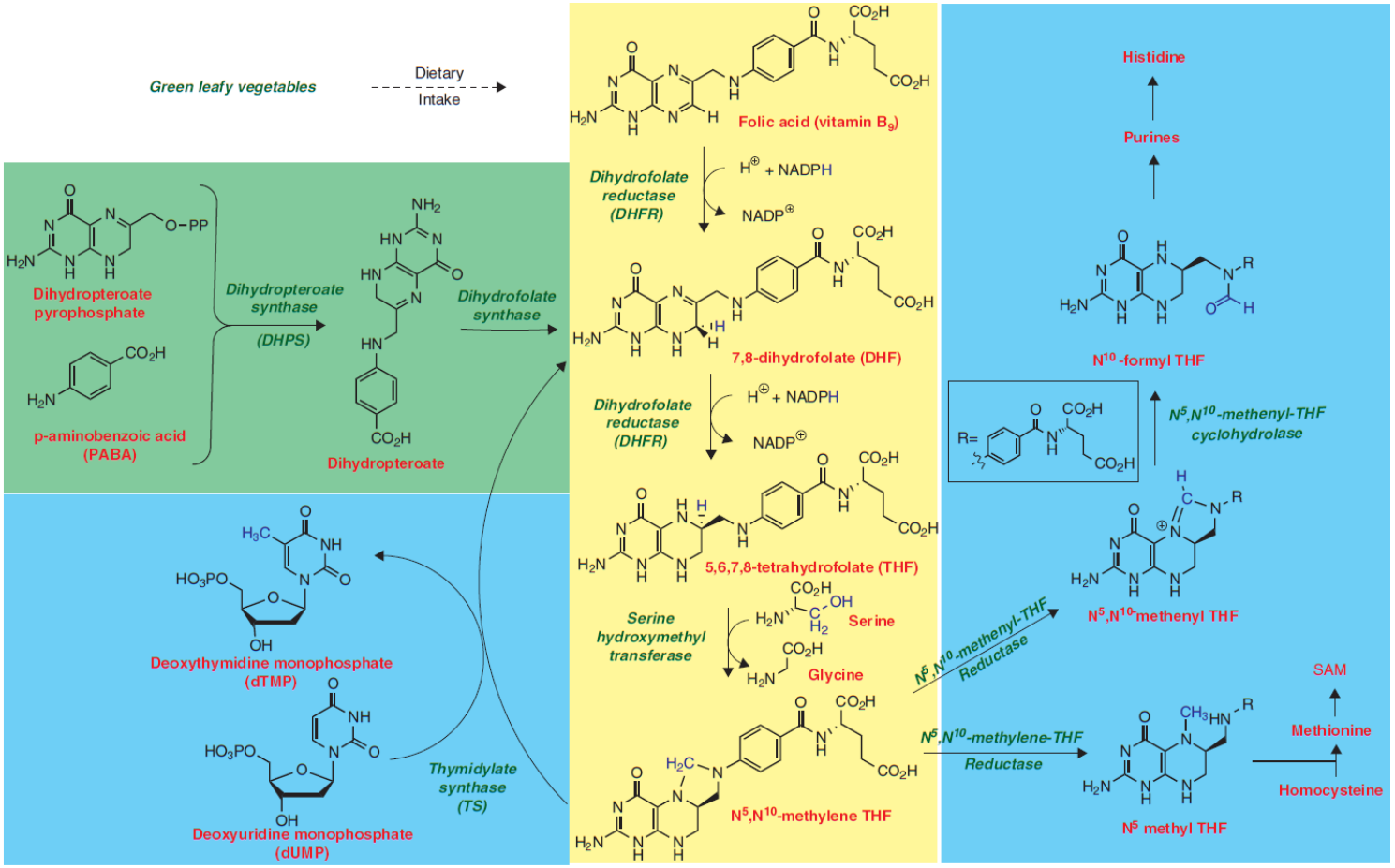

Fig ure 6. Folate pathway. Reproduced from Expert Opin. Ther. Patents (2011) 21(9):1293-1308

1.1.3B.1 Clinical Inhibitors of the Folate Pathway

The very first inhibitor of the DHPS enzyme was prontosil (Fig.7) – for which Gerhard Domagk was awarded the Nobel Prize in Medicine in 1939. He discovered that prontosil was active only in bacterial cells and later research revealed its activity as a prodrug. The use of the folate pathway as an antibacterial target was observed by Woods[26] who carried out experiments with sulfonamides to competitively exclude pABA and thereby stall the synthesis of folates. Further research led to the development of sulfamethoxazole as a bacteriostatic antibiotic.

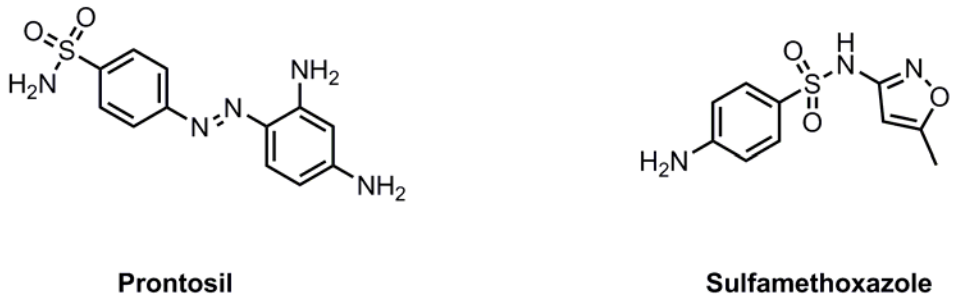

Figure 7. Inhibitors of DHPS

DHFR, because of its role in cellular metabolism has become an ideal target of antibacterials, antiprotozoal and antineoplastic agents. Nobel laureates George H Hitchings and Gerard B. Elion showed the utility of diaminopyrimidine antifolates as potent inhibitors of the folate cofactors. Their discovery of 6-mercaptopurine as an antineoplastic agent set the tone for a flurry of antifolates – pyrimethamine for protozoal infections, trimethoprim as an antibacterial. Later TMP was used in combination with sulfamethoxazole to treat methicillin- resistant *Staphylococcus aureus* (MRSA) and

urinary tract infections (UTI) caused by *Escherichia coli*. Along with cycloguanil and its derivatives, these inhibitors belong to the class of non-classical antifolates characterized by their lipophilic nature. Methotrexate and aminopterin (Fig.8) - classical antifolates bearing resemblance to the natural substrate, folic acid, are potent antineoplastic agents.

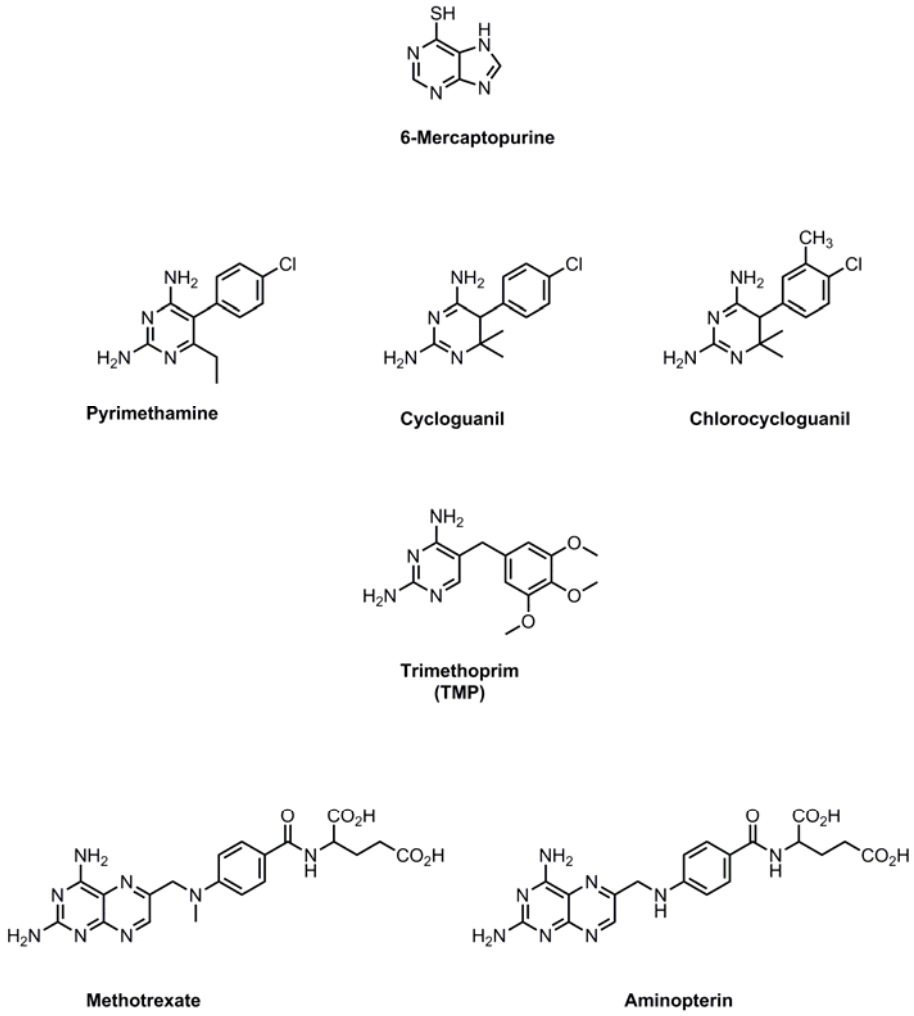

Figure 8. Inhibitors of DHFR

1.1.3B.2 Resistance in Antifolates

Antifolates are not immune to the evolutionary process of resistance by bacteria. The sulfonamide mechanism of resistance is through chromosomal mutation in the *dhps* gene – *folP*. In a sequence analysis of *E.coli* mutants, Phe28Ileu and Phe28Leu were found to confer resistance to sulfonamide[27] while maintaining normal binding to pABA. Plasmid mediated resistance was found in the clinical isolates of enteric bacteria that enable the pathogens to evade sulfonamides and bind to pABA with a Km of 0.6μM.

Use of TMP, chromosomal DHFR undergoes point mutation[28] to impart resistance in *Staphylococcus aureus*. The Phe98Tyr mutation in S1 DHFR right below the TMP inhibitor competes for hydrogen bonding with the carbonyl of Leu5, which in Sa DHFR normally hydrogen bonds with N-4 amine nitrogen of TMP. Another site of mutation occurs in the binding site of NADPH with Gly43Ala. Steric induced conformational change displaces the NADPH from its native state lowering its affinity in the enzyme pocket. This in turn destroys the synergistic affinity of TMP to the active site induced by NADPH in Sa DHFR.

The rise in resistance for antifolates necessitates the design of new pharmacophores to enhance the affinity of ligands in the active site. Research in Dr.Wright and Dr. Anderson's lab pivots around Structure Activity Relationship (SAR) based design, synthesis and evaluation of new pharmacophores as antibiotics against resistant pathogens.

1.1.3B.3 Evolution in the design of Propargyl linked antifoaltes

TMP as an antibiotic catered only to a subset of pathogenic DHFR enzymes. This sowed the seeds for the exploration and optimization of TMP as an antibiotic[29] against *Cryptosporidium hominis* and *Toxoplasma gondii*. TMP inhibits DHFR of *C.hominis* and *T.gondii* with an IC_{50} of 14μM and 8μM respectively. Intrigued by the lack of potency, refinement was carried out with TMP as the scaffold. The diaminopyrimidine A ring of the TMP is retained since it acts as anchor into the active site of DHFR. This interaction of pyrimidine ring is conserved across all species. On investigating the crystal structure (Fig.9) of *Staphylococcus aureus* (Sa) DHFR[12], TMP forms four hydrogen bonding interactions with main chain and side chain residues in the active site. The N1 and N2 amine of TMP interacts with the oxygen atoms of the Asp27 residue. An additional two hydrogen bonds occur between N4 amine and carbonyl oxygen atoms of Leu5 and Phe92. Another water mediated hydrogen bond between the N2 amine and oxygen of Thr111 lends additional affinity for TMP. Apart from the hydrogen bond interactions, a number of van der Waals interactions with Leu5, Val 6, Ala7, Val31 and Phe92 along with the nicotinamide ring of NADPH have been observed. The trimethoxybenzyl group occupies a hydrophobic pocket forming van der Waals interactions with the side chain atoms of Leu20 and Leu28 on one side and Ile50 and Leu54 on the other. The oxygen atoms of the methoxy group do not interact with the enzyme or the cofactor but forms hydrogen bonds with water molecules.

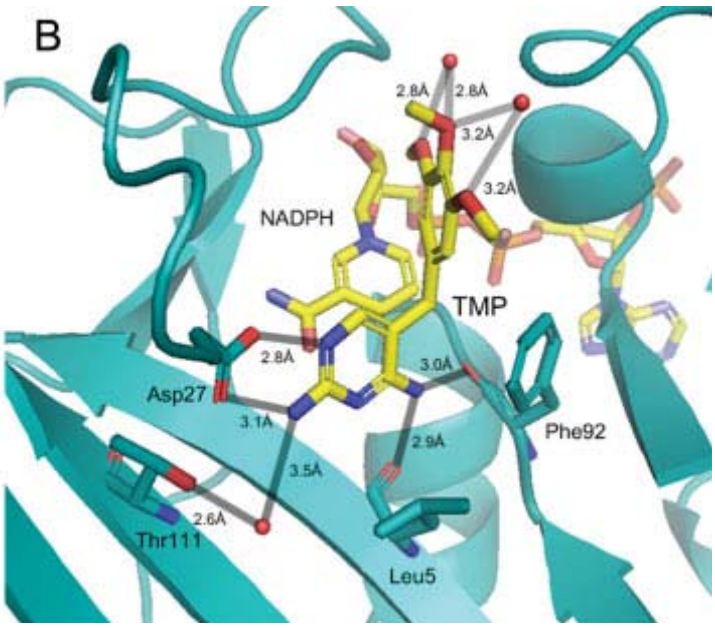

Figure 9. TMP crystallized with Sa DHFR along with the cofactor NADPH. Reproduced from *Proteins* 2009, *76*, 706-717.

However comparing the linker of TMP with MTX in the active site, it was evident that the trimethoxy benzyl group does not extend as deeply into the hydrophobic pocket as observed with the hydrophobic pABA moiety of MTX. A simple strategy to increase the affinity of TMP into the active site by increasing the linker length[13] of TMP was envisioned (Fig.10). The linker length was increased to 2 and 3 carbon atoms between the diaminopyrimidine-A and trimethoxy phenyl-B ring. The two carbon linker was introduced by an acetylene moiety connecting the two fragments. Further chemical modification of acetylene led to cis/trans olefinic substrates and a fully saturated ethylene linker. The enzymatic inhibition studies revealed that the two linker strategy suffered from entropic and conformational effects. Though the saturated linker provided the ease for both aromatic moieties to occupy the active site, the increase in entropy caused by the

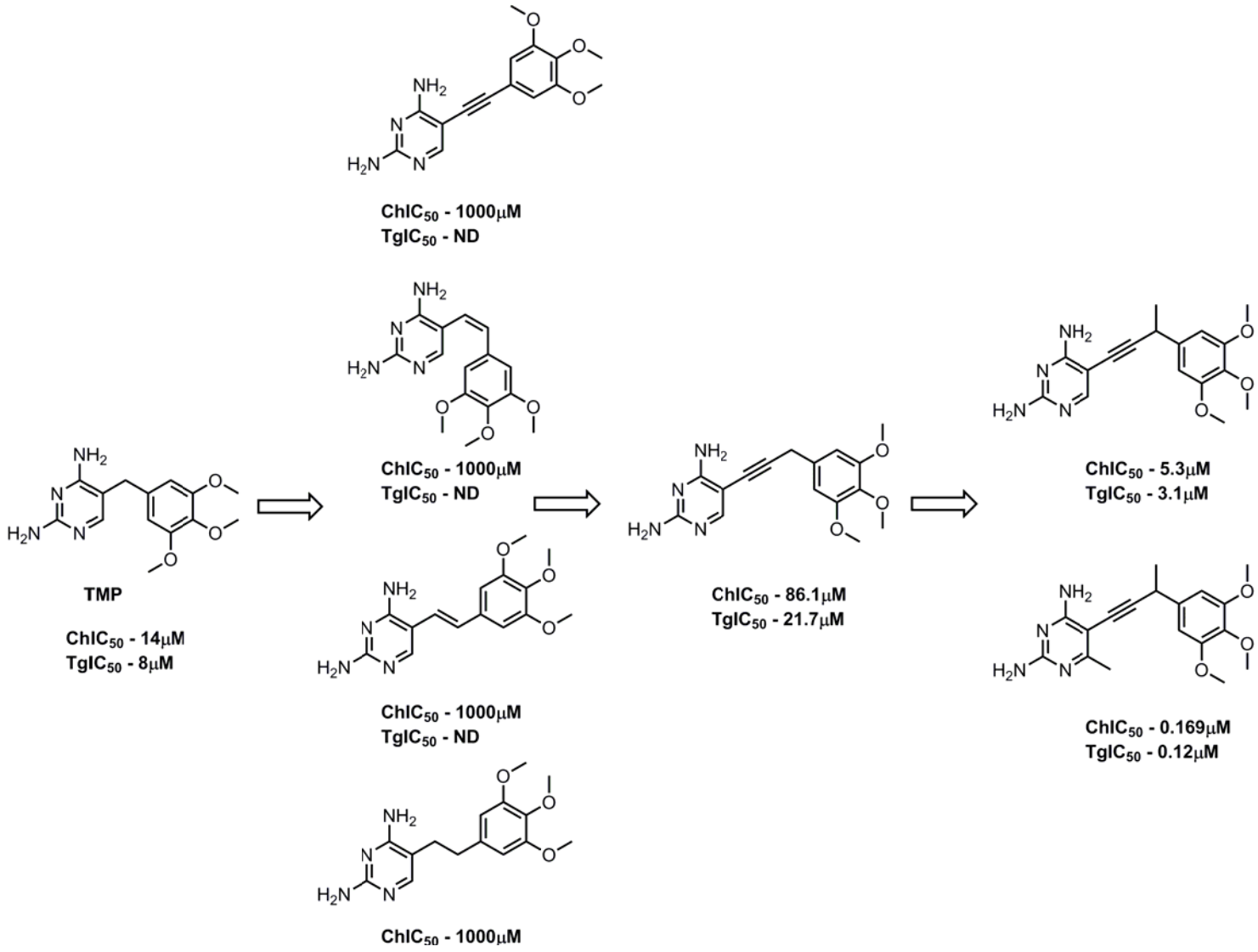

Figure 10. Generations of Propargyl linked Antifolates

organization of the highly flexible linker. The other three compounds, though restricted by the actylenic and olefinic linkage, are also stricted in their conformations to adopt for a productive binding.

A balance between conformation and entropy was achieved when a 3 carbon linker in the form of a propargyl group was introduced between the two aromatic rings. This design enabled the two rings to bind in their respective binding pockets, while maintaining the same number of degrees of freedom as in TMP. The propargylic linker though did not improve the potency relative to TMP. This was attributed to the loss of lipophilic interactions with Leu 25, Leu 33, and Phe 36. This also created a pocket near the C6 position of the pyrimidine ring. Further modifications of the propargylic linker with substitutions at C6 of the pyrimidine A-ring and at the propargylic position engendered a new propargyl linked pharmacophore with potent enzyme inhibition.

While the 1st generation compounds with the propargylic linker afforded potent compounds, their selectivity over human DHFR was only 36-fold. Continued refinement by the addition of a C-ring to the B-ring generated the 2nd generation propargyl linked antifolates (Fig.11) with a potency of 1.8 nM for *Cryptosporidium hominis* and a selectivity of 944-fold over human DHFR. The aromatic C-ring was designed so that a steric interaction can be tuned to destabilize the interaction with human DHFR while maintaining potency against the pathogenic species. The aromatic C-ring projects into the lipophilic opening of the active site generating favorable contacts in the pathogen. When the 2nd generation ligand was tested against *Staphylococcus aureus*, it exhibited an enzyme potency of 61nM compared to TMP's IC_{50} of 23nM.

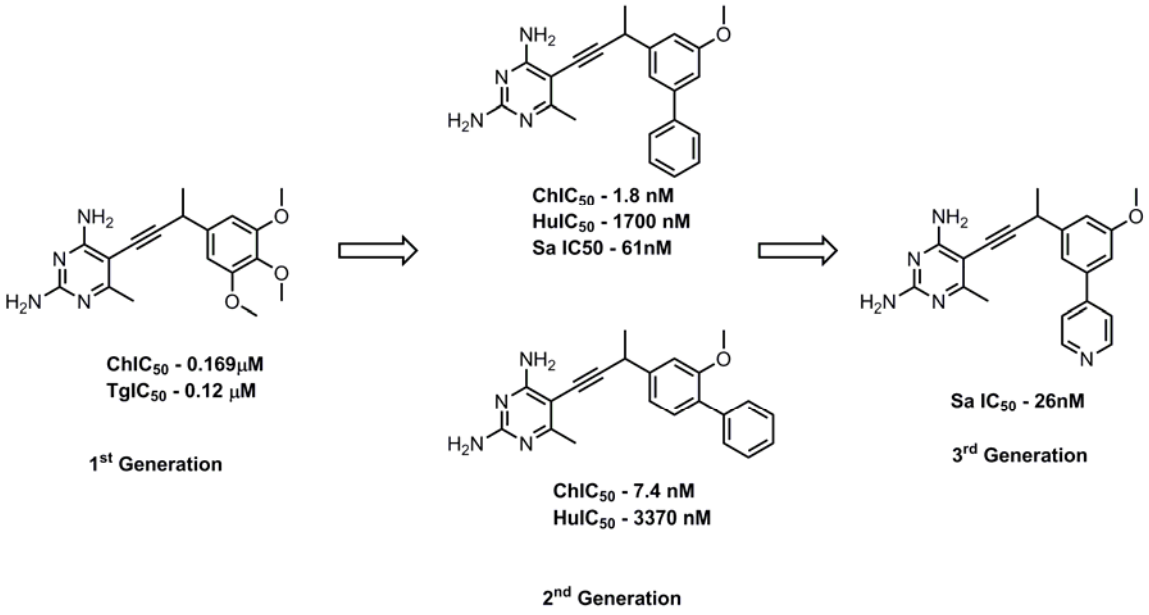

Figure 11. Antibacterial activity of antifolates of different generations

In order to gain potency against S.aureus organisms, the hydrophobic aromatic C-ring was changed to a heterocyclic pyridine14 ring[30]. The crystal structure (Fig.12& Fig.13) of a ligand with the heterocycle changed the orientation of the molecule and hence its interaction with the side chain residues. The enantiomer of the heterocycle ligand that crystallized preferentially was opposite in configuration to that of the hydrophobic C-ring. Also the pyridyl nitrogen interacts through hydrogen bonding with water molecules at the open end of the active site, contributing to the change in orientation of the C-ring. The 3rd generation heterocyclic ligand turned out to be potent inhibitor of S.aureus with increased solubility and permeability.

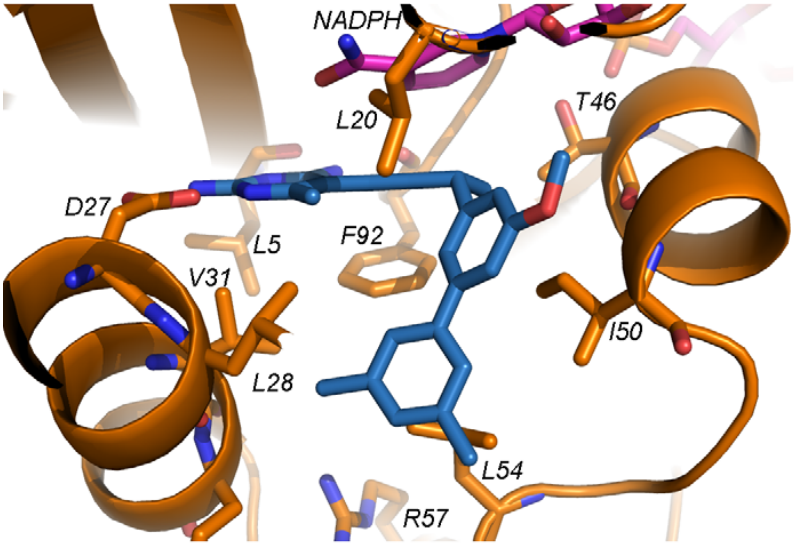

Figure 12. 2nd Generation UCP11D35M (blue) crystallized with Sa DHFR along with the cofactor NADPH

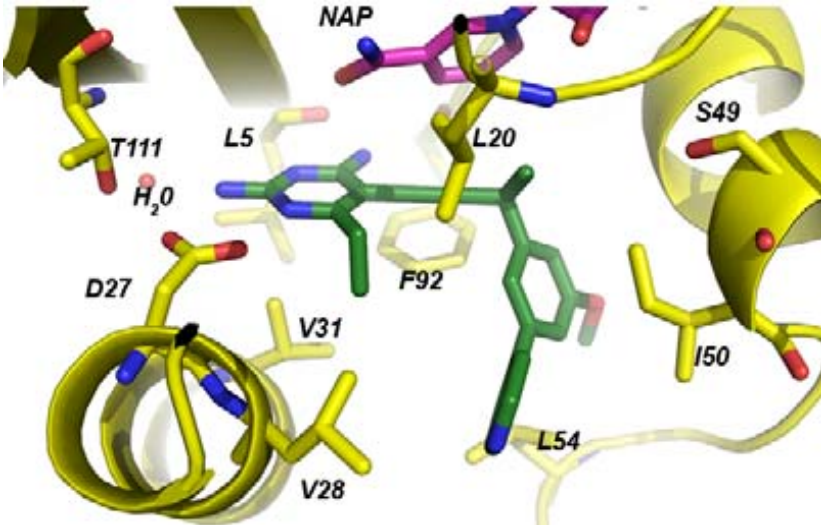

Figure 13. 3rd Generation UCP1006 (green) crystallized with Sa DHFR along with the cofactor NADPH

1.2 Conclusions

The different classes of antibiotics exhibit varying modes of resistance. The folate pathway is an essential metabolic process for the synthesis of nucleotides and amino acids. TMP targets the DHFR enzyme thereby inhibiting biological processes of the folate pathway. Resistance exhibited by TMP has engendered the design and synthesis of a new propargyl linked pharmacophore. Generational improvements by ligand optimization resulted in a potent inhibitor- **UCP1006** for MRSA.

References

1. http://www.who.int/mediacentre/factsheets/fs310/en/

2. http://www.nobelprize.org/nobel_prizes/medicine/laureates/1945/fleming-lecture.pdf.

3. Hollis, A.; Ahmed, Z. Preserving Antibiotics, Rationally. *New England Journal of Medicine* 2013,*369*, 2474-2476.

4. Fisher, J.; Meroueh, S.; Mobashery, S. Bacterial resistance to beta-lactam antibiotics: compelling opportunism, compelling opportunity*Chem. Rev.* 2005, *105*, 395-424.

5. Arthur, M.; Courvalin, P. Genetics and mechanisms of glycopeptide resistance in enterococci *Antimicrobial Agents and Chemotherapy* 1993, *37*, 1563-1571.

6. Walsh, C.; Fisher, S.; Park, I.; Prahalad, M.; Wu, Z. Bacterial resistance to vancomycin: five genes and one missing hydrogen bond tell the story. *Chemistry & Biology* 1996, *3*, 21-28.

7. Moazed, D.; Noller, H. Interaction of antibiotics with functional sites in 16S ribosomal RNA.*Nature* 1987, *327*, 389-394.

8. Andrew P. C.; William M. C.; Ditlev E. B.; Robert J. M.; Brian T. W.; Ramakrishnan, V., Functional insights from the structure of the 30S ribosomal subunit and its interactions with antibiotics, *Nature*, 2000, 407, 340-348.

9. Makosky, P.; Dahlberg, A. Spectinomycin resistance at site 1192 in 16S ribosomal RNA of E. coli: an analysis of three mutants. *Biochimie* 1987, *69*, 885-889.

10. Galimand, M.; Sabtcheva, S.; Courvalin, P.; Lambert, T. Worldwide Disseminated armA Aminoglycoside Resistance Methylase Gene Is Borne by Composite Transposon Tn1548. *Antimicrobial Agents and Chemotherapy* 2005, *49*, 2949-2953.

11. González-Zorn, B.; Teshager, T.; Casas, M.; Porrero, M.; Moreno, M.; Courvalin, P.; Domínguez, L. armA and Aminoglycoside Resistance in Escherichia coli. *Emerg. Infect. Dis.* 2005, *11*, 954-956.

12. Yamane, K.; Wachino, J.; Doi, Y.; Kurokawa, H.; Arakawa, Y. Global Spread of Multiple Aminoglycoside Resistance Genes. *Emerg. Infect. Dis.* 2005, *11*, 951-953.

13. Mitscher, L. Bacterial Topoisomerase Inhibitors: Quinolone and Pyridone Antibacterial Agents. *Chem. Rev.* 2005, *105*, 559-592.

14. Wang, J. Cellular roles of DNA topoisomerases: a molecular perspective. *Nature Reviews Molecular Cell Biology* 2002, *3*, 430-440.

15. Hooper, D. Mechanisms of fluoroquinolone resistance. *Drug Resistance Updates* 1999, *2*, 38-55.

16. Hooper, D. Emerging Mechanisms of Fluoroquinolone Resistance. *Emerg. Infect. Dis.* 2001, *7*, 337-341.

17. Brown, M.; Weisman, R.A.; Molnar, D.A. The Biosynthesis of Folic Acid. Substrate and cofactor requirements for enzymatic synthesis by cell-free extracts of Escherichia coli. *J Biol Chem 1961*, 236, 2534–2543.

18. Burg, A.; Brown, G. The biosynthesis of folic acidVI. Enzymatic conversion of carbon atom 8 of guanosine triphosphate to formic acid. *Biochimica et Biophysica Acta - General Subjects* 1966, *117*, 275-278.

19. Yim, J.J.; Brown, G.M. Characteristics of guanosine triphosphate cyclohydrolase I purified from Escherichia coli. *J Biol Chem* 1976, 251, 5087–5094.

20. Heine, M.C.; Brown, G.M. Enzymatic epimerization of D-erythro-dihydroneopterin triphosphate to L-threo-dihydroneopterin triphosphate. *Biochim Biophys Acta.* 1975, 411, 236–249.

21. Mathis, J.B.; Brown, G.M. The biosynthesis of folic acid. XI. Purification and properties of dihydroneopterin aldolase. *J. Biol. Chem* 1970, 245, 3015–3025.

22. Reynolds, J.J.; Brown, G.M. The Biosynthesis of Folic Acid. IV. Enzymatic synthesis of dihydrofolic acid from guanine and ribose compounds. *J Biol Chem* 1964, 239, 317–325.

23. Richey, D.P.; Brown, G.M. The biosynthesis of folic acid. IX. Purification and properties of the enzymes required for the formation of dihydropteroic acid. *J Biol Chem* 1969, 244, 1582–1592.

24. Suzuki, Y.; Brown, G.M. The biosynthesis of folic acid. XII. Purification and properties of dihydroneopterin triphosphate pyrophosphohydrolase. *J Biol Chem* 1974, 249, 2405–2410.

25. Bermingham, A.; Derrick,J.P. The folic acid biosynthesis pathway in bacteria: evaluation of potential for antibacterial drug discovery, *BioEssays,* 2002, 24, 637–648.

26. Woods, D.D. The relationship of p-aminobenzic acid to the mechanism o fthe action of sulphanilamide. *Br J Exp Pathol* 1940, 21, 74–90.

27. Sköld, O.Sulfonamide resistance: mechanisms and trends, *Drug Resistance Updates*, 2000, 3, 155–160.

28. Heaslet, H.; Harris, M.; Fahnoe, K.; Sarver, R.; Putz, H.; Chang, J.; Subramanyam, C.; Barreiro, G.; Miller, J. Structural Comparison Of Chromosomal And Exogenous Dihydrofolate Reductase From Staphylococcus Aureus In Complex With The Potent Inhibitor trimethoprim. *Proteins* 2009, *76*, 706-717.

29. Pelphrey, P.; Popov, V.; Joska, T.; Beierlein, J.; Bolstad, E.; Fillingham, Y.; Wright, D.; Anderson, A. Highly Efficient Ligands For Dihydrofolate Reductase From Cryptosporidium Hominis And Toxoplasma Gondii Inspired By Structural Analysis. *Journal of Medicinal Chemistry* 2007, *50*, 940-950.

30. Viswanathan, K.; Frey, K.; Scocchera, E.; Martin, B.; Swain III, P.; Alverson, J.; Priestley, N.; Anderson, A.; Wright, D. Toward New Therapeutics for Skin and Soft Tissue Infections: Propargyl-Linked Antifolates Are Potent Inhibitors of MRSA and *Streptococcus pyogenes PLoS ONE* 2012, *7*, e29434.

CHAPTER 2

New Synthetic Methodology for Propargyl Linked Antifolates

Introduction

Retrosynthetically, propargyl linked antifolates are synthesized in a convergent manner by Sonogashira coupling of two fragments – C6-substituted iodo-diaminopyrimidine **2** (Scheme.1) and biaryl/ aryl-heteroaryl propargylic alkyne **6**. Iodinated diamino pyrimidine **2** can be obtained from the tautomer of **3** - amino pyrimidinone in 3 steps: (1) by chlorination with $POCl_3$, (2) amination with ammonia in methanol and (3) iodination with ICl. The substitution at R_1 determines the starting precursor for fragment (2).

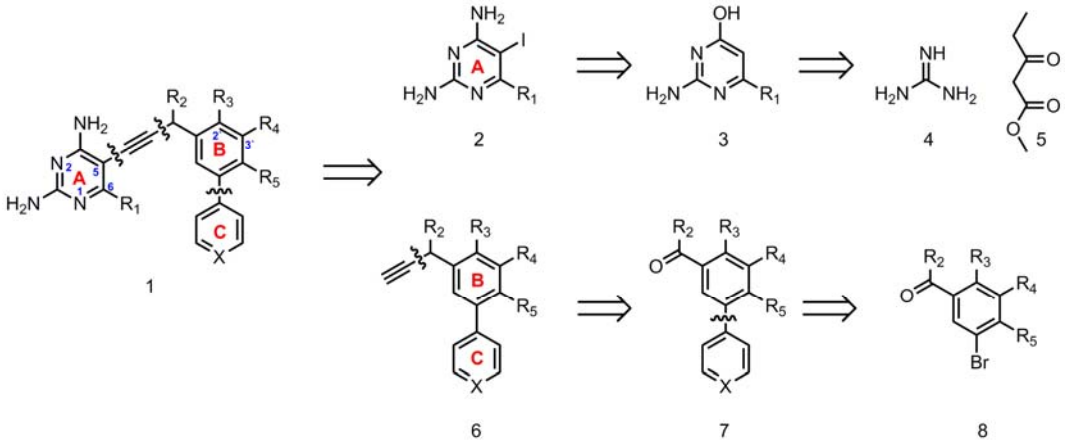

Scheme 1. Retrosynthesis of propargyl linked antifolates

For R_1 = H, CH_3, chlorinated analogs of **3** are commercially available, while for the ethyl group at C6 position, amino pyrimidinone **3** can be synthesized by the condensation of guanidine carbonate with methyl propionylacetate. The alkyne fragment

6 can be accessed through a series of homologation reactions from **7,** which is synthesized through Suzuki coupling of precursor **8** with suitable boronic acids.

2.1 Strategies to improve the synthesis of antifolates

Currently[1], a majority of our analogs are synthesized by changing the C-ring to probe for structure activity relatioships. A final step Suzuki coupling to the propargyl linked fragment **9**, as shown in Scheme 2, would be an ideal situation for screening an array of compounds at a rapid pace. But this strategy is limited by the base induced cyclization of aminopyrimidine onto the alkyne to form an indole derivative during Suzuki coupling. Even if protected amine can be used to prevent cyclization, debromination of ring B during palladium catalyzed Sonogashira coupling cannot be avoided.

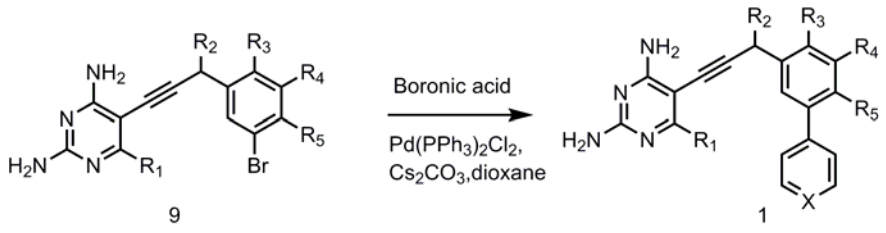

Scheme 2. Suzuki coupling to A B ring system

Another strategy to expedite the synthesis of antifolates was to access the fragment **6** in an economical way. Currently, the method involves the Suzuki coupling of rings B & C, followed by Wittig homologation to get the enol ether as shown in Scheme.3. The enol ether was hydrolyzed using either HCl or $Hg(OAc)_2$/KI. The resulting aldehyde was homologated by Ohira-Bestmann reagent to give the propargyl alkyne.

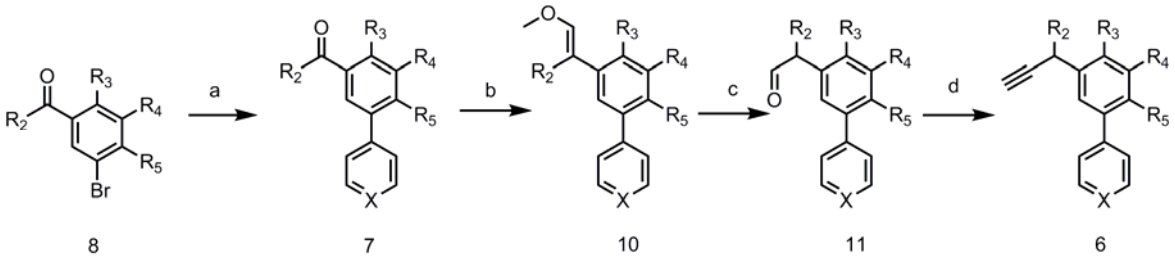

Scheme 3. Synthesis of Propargylic alkyne

Reactions and Conditions: (a) $Pd(PPh_3)_2Cl_2$, Cs_2CO_3, dioxane, 80°C; (b) Ph_3P=CHOMe, THF, NaOtBu; (c) $Hg(OAc)_2$, KI, THF/H_2O; (d) dimethyl(1-diazo-2-oxopropyl)phosphonate, K_2CO_3, MeOH; (e) $Pd(PPh_3)_2Cl_2$, CuI, Et_3N, DMF, 60°C.

The synthetic protocol above suffered from low yields, especially in the hydrolysis and condensation stage. The heterocycle based homologated aldehyde **11** is unstable upon exposure to atmospheric oxygen, reverting back to the starting aldehyde/ ketone **7**. This could be due to enolization of the benzylic position followed by reaction with oxygen and cleavage. In the next step of condensation with Ohira Bestmann reagent, a base induced isomerization of alkyne to give the thermodynamically stable allene was observed. The allene formation was more pronounced with compounds having no propargylic methyl (R_2 = H). Apart from low yields, the method entails repetitive procedure to synthesize compounds with varying substitution at the propargylic position, R_2 = H, CH_3, by starting with an aldehyde or a ketone respectively.

To overcome the iterative synthesis, a common precursor that can diverge to give substituted propargyl alkynes was required. From the literature, it was evident that propargyl alcohol could be the structural motif that can undergo substitution with

different nucleophiles. Substitution of alkynol with a hydride (deoxygenation) or a methyl nucleophile can engender the required alkynes.

2.2 Synthetic methodology I

Several methods are abound in the literature for the deoxygenation of propargylic alcohols. The propargylic alcohol consists of a hard basic site - lone electron pairs on oxygen of the alcohol and a soft Lewis basic site – π bonded electrons of alkyne. As a result, deoxygenation is catalyzed by bronsted acids, Lewis acids and transition metals.

A short account of the deoxygenation methods available in the literature are reviewed below.

2.2a Deoxygenation by Bronsted acids

Trifluoroacetic acid[2,3] is the most commonly used Bronsted acid for the deoxygenation with triethylsilane as the hydride source (Scheme.4). The isomerization between the propargyl and allenyl cation tends to decrease the yield of the deoxygenated product. The complex with cobalt carbonyl- Nicholas reaction[4-6] overcomes this limitation by stabilizing the propargyl cation. One of the disadvantages of Bronsted acid is over-stoichiometric use to counteract the poor leaving ability of hydroxyl moiety. Newer heteropolyacids[7] are used catalytically to deoxygenate both the secondary and tertiary alcohols.

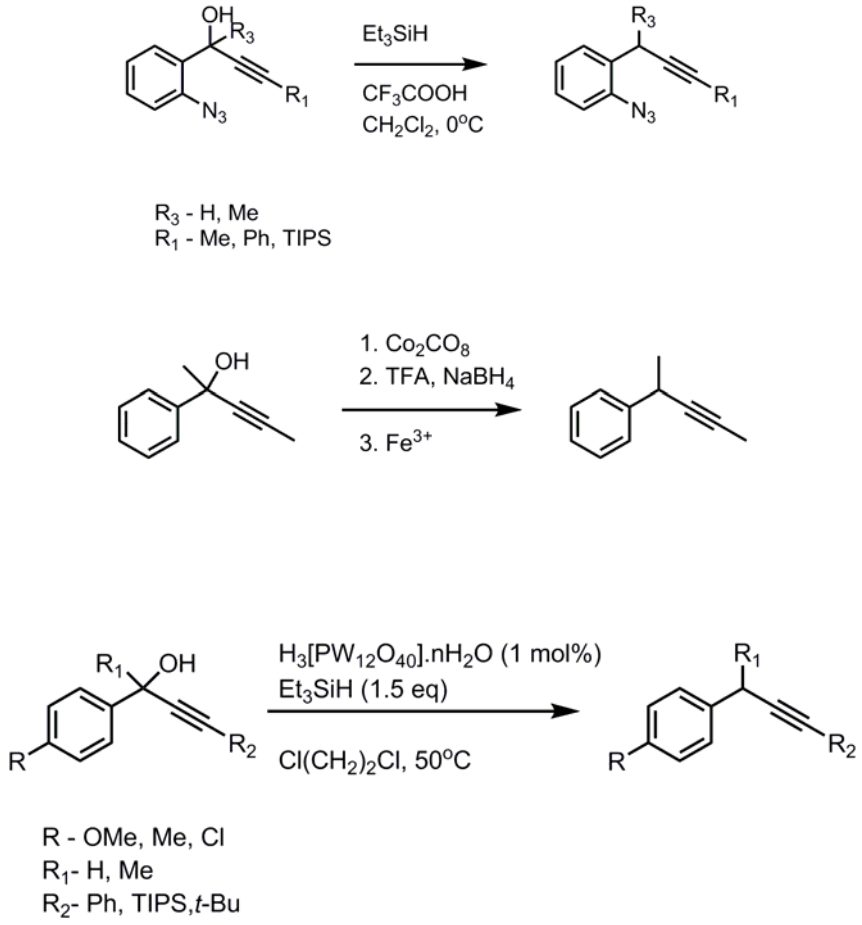

Scheme 4. Deoxygenation by a.Bronsted acid, b. Nicholas conditions, c. heteropolyacids

2.2b Deoxygenation by Lewis acids

Lewis acid - $BF_3.OEt_2$ in combination with triethylsilane[8] as the hydride source has been utilized for the deoxygenation of propargylic alcohols (Scheme.5). $Bi(OTf)_3$[9], $Ca(Ntf_2)_2$[10], $InBr_3$[11], $NaAuCl_4$[12] are examples of lewis acids that are available for hydrogenolysis. Except for $InBr_3$, all other lewis acid catalyze deoxygenation through a carbocationic mechanism. In the case of Indium tribromide, a radical mechanism involving $Br_2In^{\cdot}$ was proposed to be involved in the deacetoxylation of propargylic acetate.

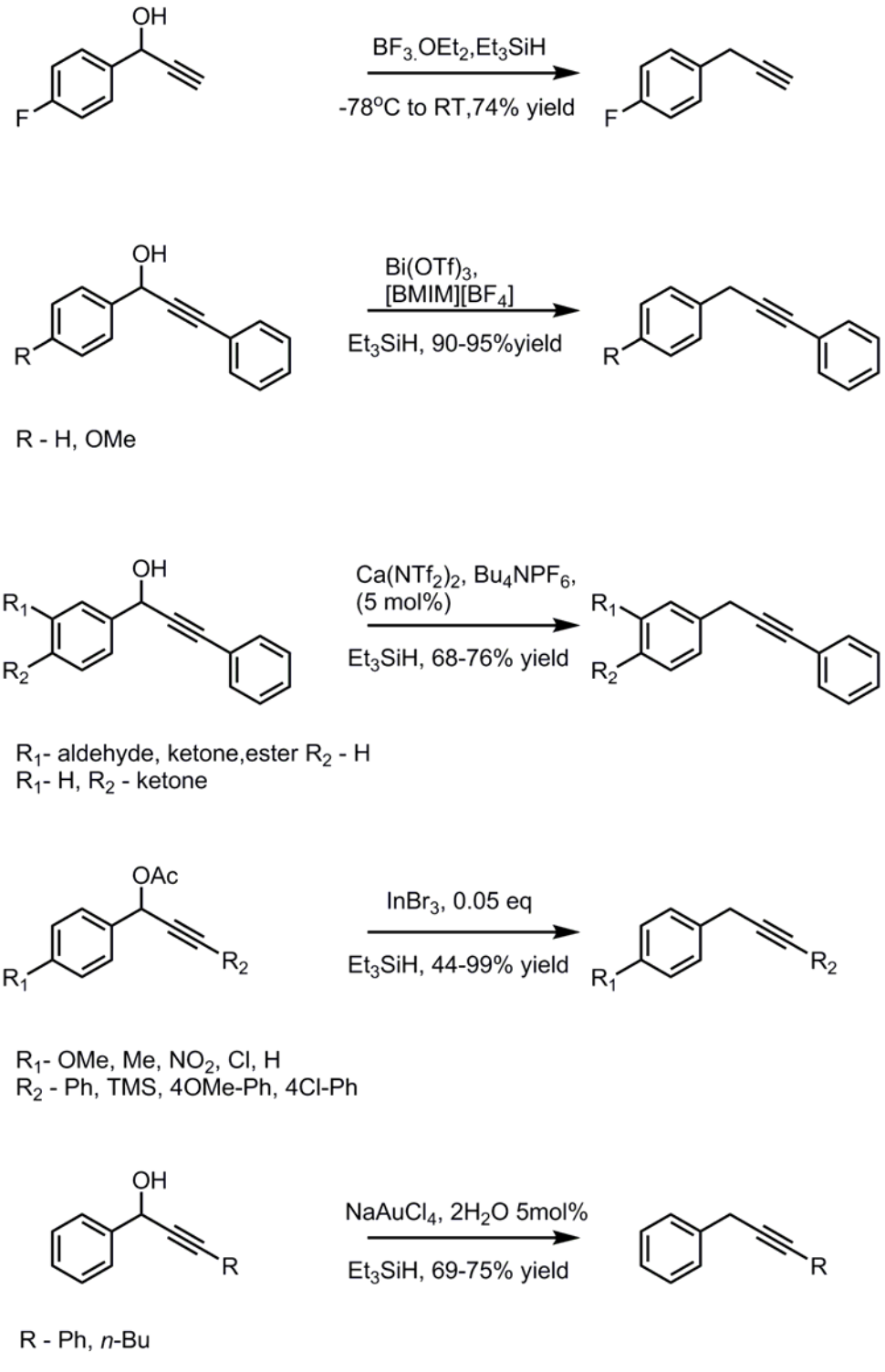

Scheme 5. Deoxygenation by Lewis acids

2.2c Deoxygenation by transition metals

Ruthenium[13,14] and a bimetallic Pd $^{2+}$ and $SnCl_2$[15] are known examples of transition metal catalyzed deoxygenation (Scheme.6). A carbocationic intermediate has been proposed with the ruthenium catalyst. As a result, substitutions with electron withdrawing groups (F, Cl, and CF_3) yield little to no product, while with electron donating substituents the yields exceed 90%. Moreover, both the transition metals have shown to be reactive against secondary propargylic alcohols.

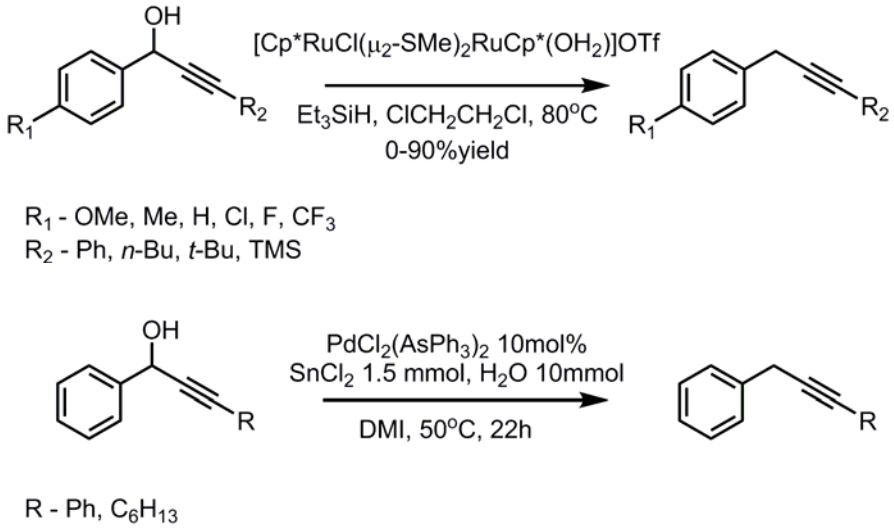

Scheme 6. Deoxygenation by transition metals

2.2d Deoxygenation for propargyl linked antifolates precursor

Although a plethora of examples exist for the deoxygenation of aryl propargylic alcohols, none of them have a heteroaromatic moiety. The presence of a heterocycle can complicate the hydrogenolysis, by complexing with the acids and transition metals. Since the antifolates are embedded with heteroaryls, a new methodology was required. The new method should be compatible with free or protected TMS alkyne, for which only a few

examples exist, as this intermediate will be the precursor for Sonogashira coupling. The synthesis of propargylic alcohol was carried out by Suzuki coupling of heteroaryls with substituted benzaldehyde derivative (Scheme.7). The alkynol precursor was obtained by a nucleophilic addition of ethynyl trimethylsilyl Grignard, generated in situ, to the aldehyde.

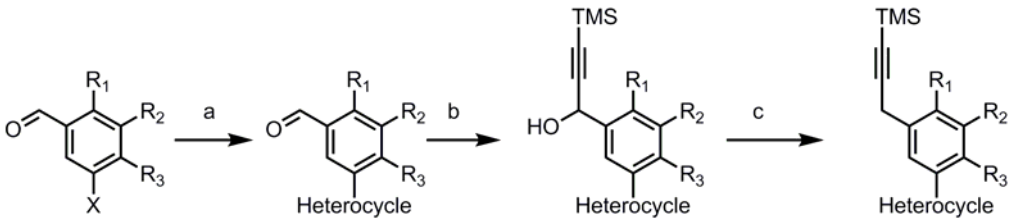

R_1,R_2,R_3,R_4 - H or OMe or dioxolane or dioxane

X - bromide or boronic acid

a. bromo or boronic acid of heterocycle, $Pd(PPh_3)_2Cl_2$, Cs_2CO_3, dioxane, 80 - 100°C. (b) TMS-alkyne, iPrMgCl THF, 0°C, (c) deoxygenation, deprotection of TMS

Scheme 7. Synthesis of Alkynol precursor

Alkynol of 2'OMe benzaldehyde coupled to pyridine was evaluated for deoxygenation under different conditions. With $Ca(Ntf_2)_2$ catalyzed reduction, starting material was recovered. Cobalt complex based Nicholas chemistry was carried out next. Apart from the extra steps arising from the complexation with cobalt carbonyl, during the oxidative removal of the complex with cerium ammonium nitrate, the pyridine heterocyle was oxidized. The reduction of the N-oxide added another step to the synthetic scheme and the yields suffered. Since the deoxygenated product was obtained using Nicholas conditions, optimization of reaction conditions ensued. The reaction was carried out without cobalt carbonyl to avoid the unnecessary steps. The reasoning behind this

approach was that the 2' OMe can serve as a carbocation stabilizer. So the alkynol precursor was subjected to deoxygenation using $BF_3.OEt_2$ and triethylsilane initially at 0°C followed by heating the reaction mixture to 41°C for 2h. Deoxygenated mixture of TMS, TES and free alkyne were obtained. Deprotection of alkyne mixture was carried out by hydrolyzing with $AgNO_3$/KCN to give the free alkyne in 74% yield over 2 steps. In order to avoid the toxic usage of KCN, the deprotection was also done with an equimolar mixture of acetic acid and tetrabutyl ammonium fluoride. Longer reaction time with lower yield due to the formation of allene favored the hydrolysis procedure of silver nitrate and KCN.

To understand the versatility of this deoxygenation method, substitutions were varied on the top B ring while maintaining pyridine as the C-ring. Table.1. A drop in yield for compound **35** was observed compared to **34**. This is could be attributed to the lack of carbocation stabilization from the 3'OMe. When an additional methoxy group was added to **35** as in compound **36** increase in yields were observed. Good yields were also obtained when methoxy groups were replaced by dioxolane ring **37**. Satisfactory results were obtained when the aryl top ring was replaced by an electron rich heteroaromatic thiophene ring. The relative low yield was due to the formation of allene during the deprotection of TES and TMS alkyne.

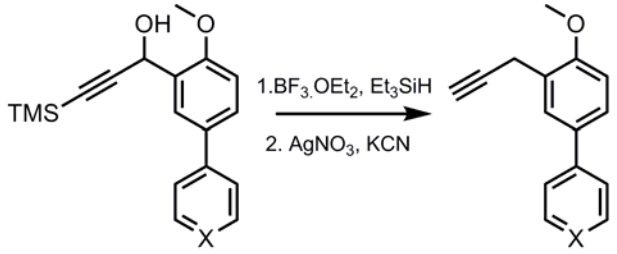

B RING		C RING	YIELDS %
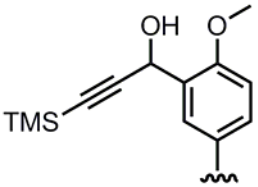	(34)	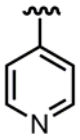	**74**
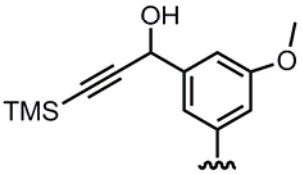	(35)	,,	**67**
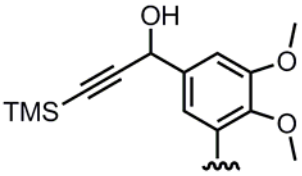	(36)	,,	**76**
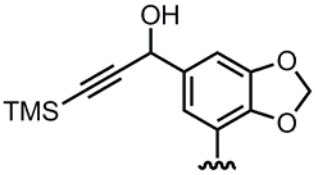	(37)	,,	**74**
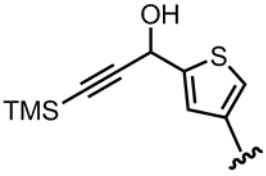	(38)	,,	**66**

Table 1. Deoxygenation with Pyridine as the C ring

B RING	C RING		YIELDS %
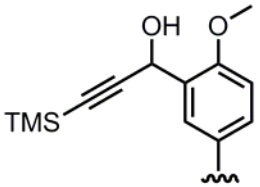	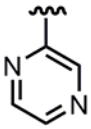	(39)	**76**
,,	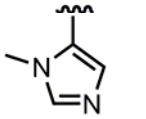	(40)	**70**
,,	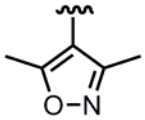	(41)	**74**
,,	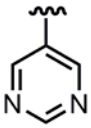	(42)	**5**
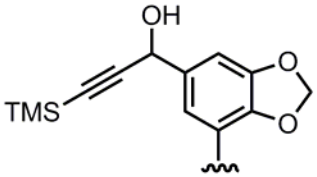	,,	(43)	**2**

Table 2. Deoxygenation with different heteroaromatics as the C-ring

Efforts were also directed towards screening for different heteroaromatics on the C-ring as shown below in Table.2. Yields ranging from 70-76% were obtained for

pyrazine **39**, N-methyl imidazole **40** and isoxazole **41**. In the case of **42**, **43** reduction of pyrimidine was observed for the deoxygenated compound in low yields.

In all of the above examples, a mixture of TES, TMS and a small percentage of free alkyne were obtained after the deoxygenation. Though they can be deprotected by hydrolysis, this intriguing insertion of triethylsilane is not reported in the literature. Further experiments were carried out to understand the mechanism of TES insertion during deoxygenation.

2.2e Mechanistic investigation of TES insertion

In order to understand the mechanism of insertion, screening of silane reagents as well as Lewis and Bronsted acids were carried out. Bulkier silane reagents – trisopropylsilane, triphenylsilane, 1,1,3,3 - tetramethyldisiloxane were screened against alkynol **34**.

SILANE	% DEOXYGENATED TERMINAL ALKYNE	% DEOXYGENATED TMS ALKYNE	% DEOXYGENATED Si-INSERTED ALKYNE
Triethylsilane	5	70	25
Triisopropylsilane	26	38	36
Triphenylsilane	67	19	14
1,1,3,3 tetramethyl disiloxane	2	98	0

Table 3. Distribution of products of deoxygenation

Based on the NMR, relative percentages of alkynes are shown below in Table.3. Relative to triethylsilane, a gradual increase in the amount of free alkyne was observed except for tetramethyldisiloxane (TMDS) where a majority of deoxygenated compound exists as TMS-alkyne. But a mixture of internal alkynes was observed when 1eq of TMDS was used.

Acids	Products
$MgCl_2$	No reaction
$Yb(OTf)_3$	No reaction
$Zn(OTf)_2$	No reaction
$B(C_6F_6)_3$	Unidentifiable complex
Silver trifluoroacetate	No reaction
Trifluoroacetic acid	Starting material TES & TMS deoxygenated alkyne
ZnBr	deoxygenated TMS & TES alkyne
$AlCl_3$	deoxygenated terminal alkyne (major) TES & TMS deoxygenated alkyne
$InCl_3$	deoxygenated terminal alkyne (major) TES & TMS deoxygenated alkyne
$In(OTf)_3$	deoxygenated terminal alkyne (major) allene

Table 4. Screening of Lewis acids

Since insertion of the silane reagent was observed even with increased steric bulk, except for substituted disiloxane, it became imperative to screen for lewis acids (Table.4). It could be postulated that F^- or HF was being formed during deoxygenation with $BF_3.OEt_2$. This could in turn deprotect the TMS alkyne generating an anion. The alkynyl anion can react with triethylsilyl cation to give TES alkyne. The Bronsted acid – trifluoroacetic acid along with Lewis acids such as $MgCl_2$, $B(C_6F_6)_3$, $AlCl_3$, $Yb(OTf)_3$, silver trifluoroacetate, $Zn(OTf)_2$, ZnBr, $InCl_3$, $In(OTf)_3$ were used for the deoxygenation of alkynol **34**.

The screening of lewis acids also gave a mixture of all three products in varying proportions. But it also gave a glimpse of tailoring the reaction to specific outcomes. When ZnBr is used, deoxygenated internal alkynes could be obtained exclusively, while $In(OTf)_3$ provides the the terminal alkyne with a small percentage of allene formation. One interesting feature observed with lewis acid screening was that the percentage of TES insertion was lower compared to $BF_3.OEt_2$ by NMR. It is also worthy to note that Br^- and Cl^- counterions of the lewis acids acts similar to F^- in deprotecting the TMS alkyne.

After screening for silane and lewis acids, the only remaining variable is the substrate. A simple aryl system **44**, **45** (Fig.14) were chosen to study the deoxygenation with $BF_3.OEt_2$ and triethylsilane.

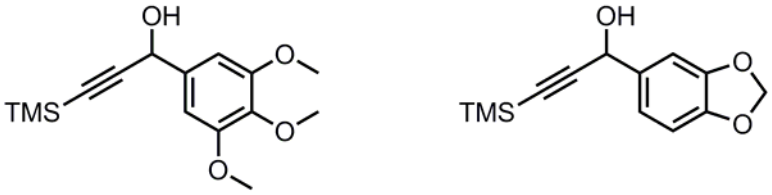

44 **45**

Figure 14. Alkynols without heteroaromatic C-ring

As soon as the $BF_3.OEt_2$ was added to the substrate maintained at 0°C, a dark brownish black color developed forming a complex. A mild color change normally occurs with all of the heteroaromatic substrates **34 - 43**, but changes into pale yellow color on addition of triethylsilane. Such reversal of color change did not occur with **44** or **45** even after addition of the reducing agent. NMR revealed neither the presence of starting material nor the product. So the experiment was repeated again, but before the addition of $BF_3.OEt_2$, pyridine was added to the substrate in the ratio of 1:1. The addition of Lewis acid did not lead to drastic color change as observed earlier and deoxygenation worked efficiently leading to the formation of reduced TES and TMS alkyne.

It appears that the heteroaromatic moiety plays a dominant role for the deoxygenation to take place. Further experiments have to be carried out to elucidate the formation of TES internal alkyne and the role of heterocycles in mediating the deoxygenation reaction.

2.3 Alkylation

Propargylic alcohols constitute an important structural motif which can undergo useful transformations in chemical synthesis. A wide variety of alkylations[16] catalyzed by

transition metals, Bronsted acids and Lewis acids are summarized here. A novel way to generate substituted allene was carried out using allylindium reagents[17] and alkylmercury halides by radical mechanism.[18] Gold catalyzed Friedel crafts based arylation of propargylic alcohol [19], allylation, etherification, thiolation with $NaAuCl_4$ [20] were synthesized by Campagne *et al*. Studies by Toste *et al*., on acetylenic alcohols showed that rhenium can catalyze addition of amine [21], alcohol [22], heteraromatics like furan, and thiophene [23]. Combined catalysis by gold and rhenium[24] were utilized for the synthesis of diethynes with aldehyde as the starting material. C-, O-, S-, N- based nucleophilic addition to the electrophilic propargylic alcohol were catalyzed by $BiCl_3$[25], $Bi(OTf)_3$[26], $FeCl_3$[27], $InCl_3$[28].

Nucleophilic addition of 1,3 dicarbonyl derivatives to propargyl alcohols catalyzed by $FeCl_3$, $Yb(OTf)_3$[29], and p-TSA monohydrate[30] served as precursors which underwent cycloisomerization to substituted furans. p-TSA[31] also catalyzed the addition of alcohol, sulfur and amine nucleophiles. Copper has been an invaluable catalysts for amination[32], thiolation[33] and allylation.[34] Interstingly, copper has been utilized in asymmetric addition reactions of amines[35,36]to propargylic acetates, while Indium (III) chloride[29] and $TiCl_4$[37,38] generated a racemate in displacing the ester.

Yadav *et al*., have worked on different catalysts – $InBr_3$[39], Iodine[40], phosphomolybdic acid-SiO_2[41], $Sc(OTf)_3$[42] to understand the propargylic substitution. Conversely Nishibayashi *et al*., made an in-depth study[43] of thiolate based ruthenium catalysts and exploited its versatility in functionalizing the propargylic alcohol and cyclopropyl-2-propyn-1-ols[44] with indoles[45], aromatics[46], ketones[47], alcohols, amines, and

phosphates. Several reviews[48-52] also exist, emphasizing the role of acetylenic carbinols as a valuable intermediate in organic synthesis.

2.3a Methylation

In spite of all the references and reviews found in the literature, no single procedure has been found for the functionalization of aryl propargyl alcohol with methyl as the nucleophile. Macdonald[53] et al., evaluated the role of organocopper species with propargylic substrates. Soft base – methyl cuprate engendered a wide distribution of products consisting of the required substituted acetylene and isomeric allenes. Using higher order cuprates, they were able to tilt the distribution in favor of the required acetylenic product. Apart from the copper mediated substitution, methylated propargyl can be obtained as racemate by deoxygenation of tertiary alcohol[10]. Enantioselectivity was achieved by nickel catalyzed[54] Negishi coupling between alkyl substituted propargylic halides and aryl zinc. Another cross coupling between substituted tosyl hydrozones [55] and trialkylsilylethynes provides alkyl linked propargyl compounds as shown in Scheme.8.

In search of a methyl carbanion to synthesize the propargyl antifolates from a common alkynol precursor, Reetz chemistry came to the rescue. Reetz had shown that geminal dimethylation of ketones can be done with $(CH_3)_2TiCl_2$[56] or sequentially in one pot by adding MeLi to the ketone and treating the resultant lithium alcoholide with CH_3TiCl_3.[57] Examples also exist for chemoselective methylation of *t*-alkyl halides with methyltitanium (IV) chlorides.[58]

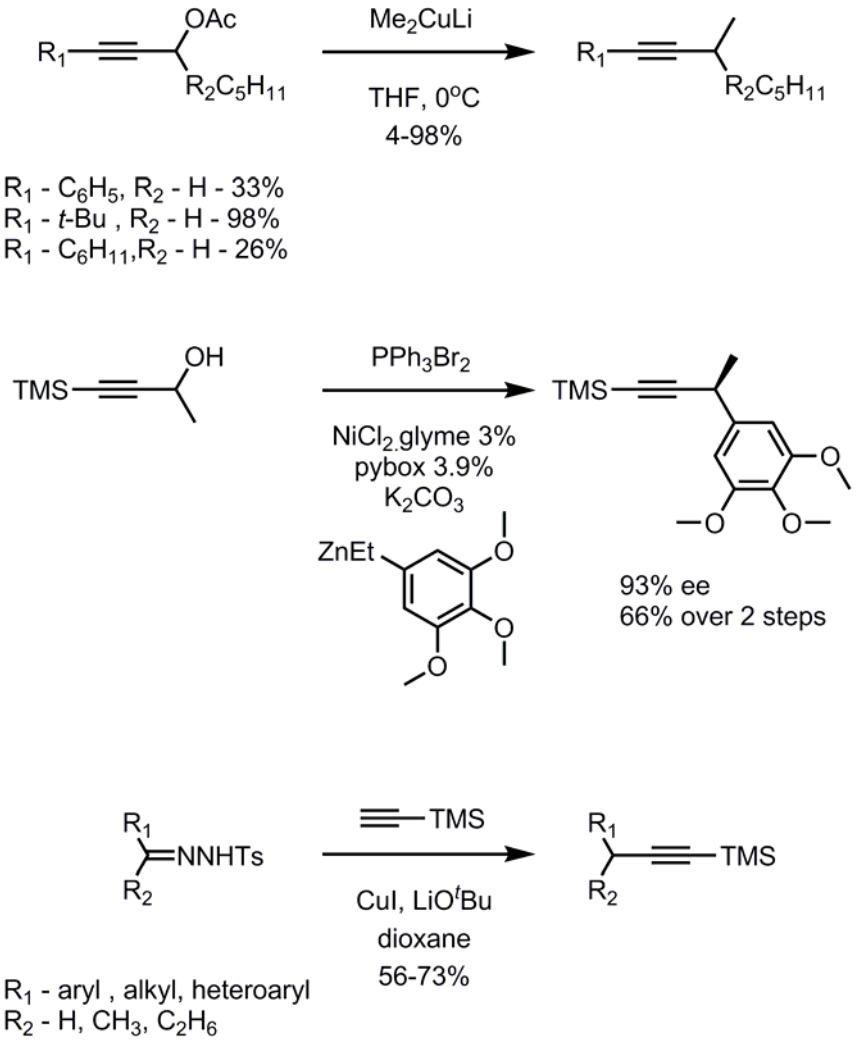

Scheme 8. Synthesis of methylated propargyl alkyne

2.3b Methylation of propargyl linked antifolate precursor

It was reasoned that since deoxygenation proceeds through a carbocationic intermediate, Reetz chemistry should comply with our substrates. Similar to deoxygenation, methylation was performed on the same set of 10 compounds (Table 5&6) to understand its versatility.

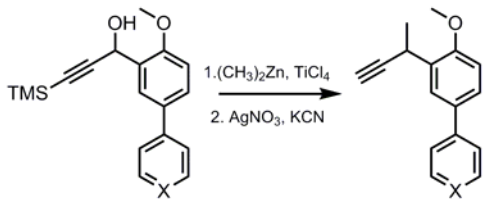

B RING		C RING	YIELDS %
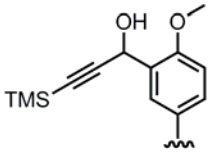	(34)	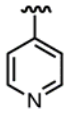	**66**
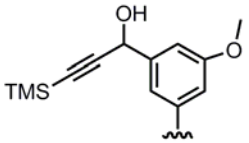	(35)	,,	**mixture of allene& methylated**
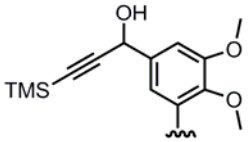	(36)	,,	**65**
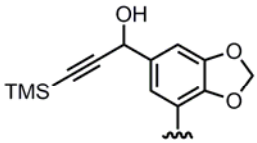	(37)	,,	**62**
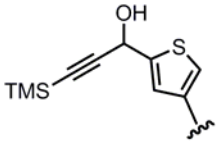	(38)	,,	**65**

Table 5. Methylation with Pyridine as the C-ring

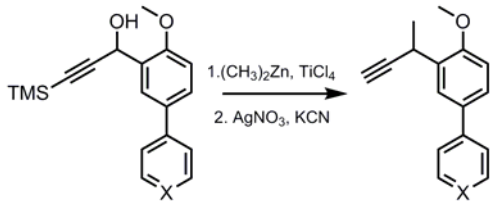

B RING	C RING		YIELDS %
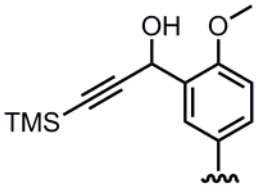	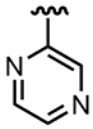	(39)	**60**
,,	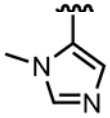	(40)	**62**
,,	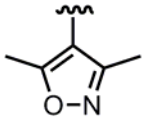	(41)	**65**
,,	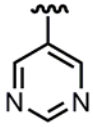	(42)	**60**
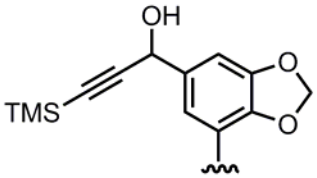	,,	(43)	**56**

Table 6. Methylation with different heteroaromatics as the C-ring

The yields of the methylation reaction varied between 56-66% over two steps after deprotection. As expected allene formation was observed in the case of **35** due to lack of carbocation stabilization. Thiophene substrate **38** generated allene during the deprotection step.

Thus a very simple procedure for deoxygenation and methylation have been devised to achieve a divergent synthesis of substituted propargylic antifolate precursor from a common alkynol intermediate.

2.4 Fluorination

In spite of the simplicity of deoxygenation and methylation, both reactions suffer from isomerization of alkyne to allene. Thus the reaction is limited only to substrates where the intermediate carbocation is stabilized by functional groups on the B-ring. In order to overcome the formation of allene, the scope of fluorinating the propargylic alcohol was tested. So the strategy was to install either a geminal difluoride at the propargylic position or substitute a tertiary alcohol with fluorine as shown in Scheme.9 so that the isomerization to allene is arrested. Also the fluorine atoms impart metabolic stability to labile sites in ligands and increases the lipophilicity.

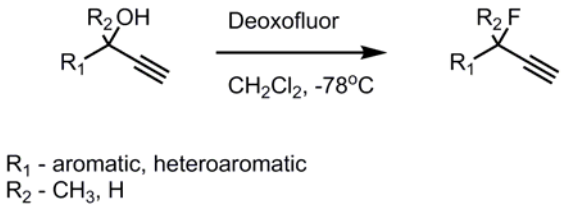

Scheme 9. Fluorination using Deoxofluor

Early reports of enantioselective α-fluorination of aldehydes using silylated prolinol catalyst was reported by Jorgensen[59] et al., while MacMillan[60] et al., reported an ee of 93-99% with an overall yield of 54-96% using an imidazolidinone catalyst. Since the fluorinated aldehdyes are unstable and obtained as the alcohol in the above cases, Jorgensen[61] group did a one-pot conversion to the alkyne using the Ohira-Bestmann homologation procedure. Direct fluorination of enantioenriched tertiary propargylic alcohol was carried out by Gree[62,63] et al., while Carroll et al., showed that enantioenriched fluorides can be obtained from tertiary propargylic alcohols through allenyl intermediates.[64] Reports also exist for the difluorinated propargyl synthesized by Suzuki coupling of aromatic boronic acids with gem-difluoropropargyl bromides.[65]

As a proof of concept, mono fluorination was done on a substrate that underwent deoxygenation and methylation. When substrate **37** (Scheme.10) was treated with Deoxofluor® mono-fluorinated alkyne was obtained in 60% yield. Another substrate with isoxazole as the B-ring **56** isomerizes to 100% allene when Ohira-Bestmann homologation route was carried out. This substrate would be an ideal target for fluorination on a tertiary alcohol. The fluorinated analog **59** was obtained in 55% yield which was subjected to Sonogashira coupling. Both substrates **55** and **59** did not undergo Sonogashira coupling. It is quite understandable in the case of **55**, since the acidic proton can isomerize to allene easily. Optimization of Sonogashira conditions might enable the coupling of substrate **59** with iodinated diamino ethylpyrimidine.

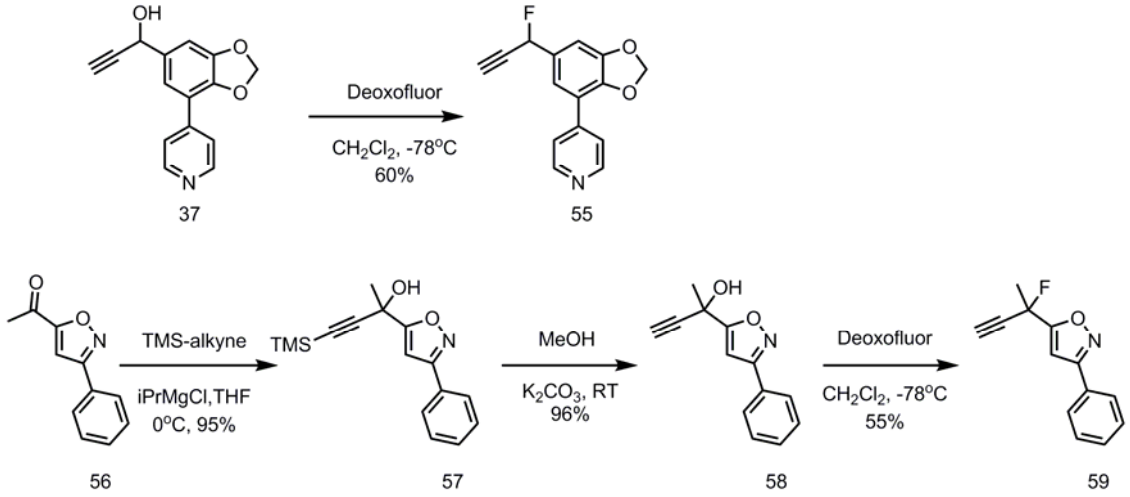

Scheme 10.Fluorination of 1,3 benzodioxole and isoxazole alkynol

2.5 Synthetic methodology II

One important feature of drug discovery program is that the lead compunds undergoes a series of refinement to achieve potency, selectivity and also to alleviate toxicity. Refinement in terms of functional groups or new ring systems is inevitable. As a result the homologation route or the nucleophilic substitution method may not suit certain substrates. Newer substrates demand novel synthons for building the molecule or synthetic scheme has to be changed depending on the availability of starting materials. For the metabolism project, a new difluoro benzodioxolane (Fig.15) as the B-ring **60** was required to overcome the CYP inhibition. The commercially available starting materials **61** & **62** lacks the functionality to attach the C-ring by Suzuki coupling.

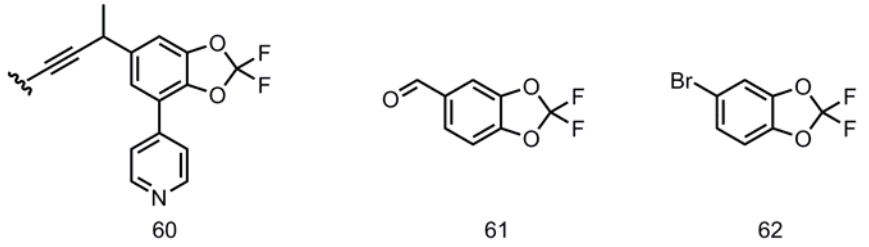

Figure 15. Diflurodioxolane ligand and available starting material

Since further substitution of **61**, **62** can give rise to multiple products [66,67] because of the pronounced reactivity at postions 4,7 (ortho to difluorodioxolane ring), synthesis of difluorinated ring from vanillin was considered the best option. Two methods were reported in the literature to synthesize the difluoro compound involving thiocarbonates from catechol as the intermediate (Scheme.11). Extremely unstable and difficult to handle BrF_3 reagent by Rozen[68] et al., was not pursued. Instead a milder fluorinating agent n-$Bu_4NH_2F_3$ involving oxidative desulfurization[69] and fluorination was attempted as shown in Scheme 2.11. Unfortunately the thiocarbonate **66** turned out to be very unstable on the column and efforts to do a one pot reaction proved futile.

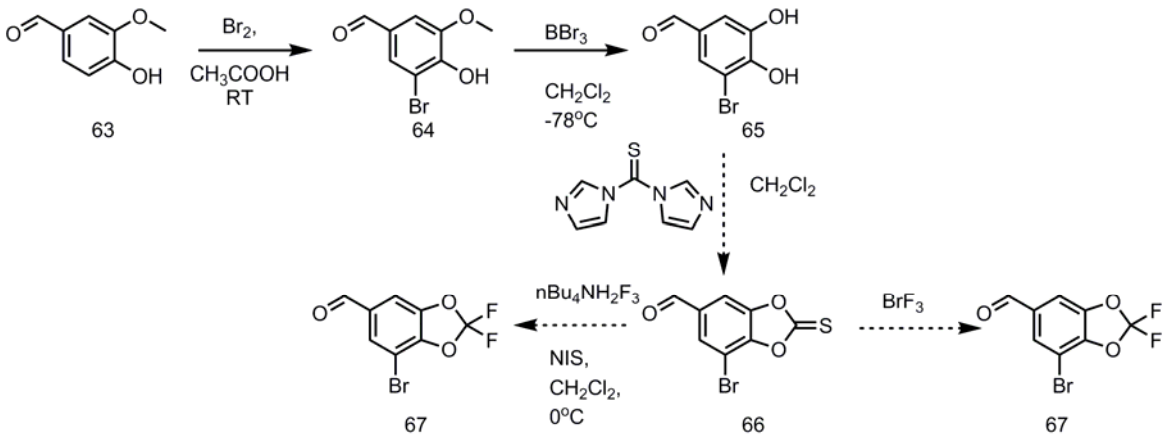

Scheme 11. Difluorination of thiocarbonate

Apart from the lithium mediated functionalization[66] of the difluoro benzodioxolane, a regiospecific Iridium catalyzed ortho borylation of benzodioxolane[70] is the other available strategy. It was reasoned that the greater reactivity of difluorodioxolane at the ortho position will engender a regiospecific borylation. From the knowledge that sterics, along with electronics, play a dominant role in the regiospecificity of Iridium catalyzed C-H activation, it was inferred that substate **62** as would be an ideal substrate for C-H activation.

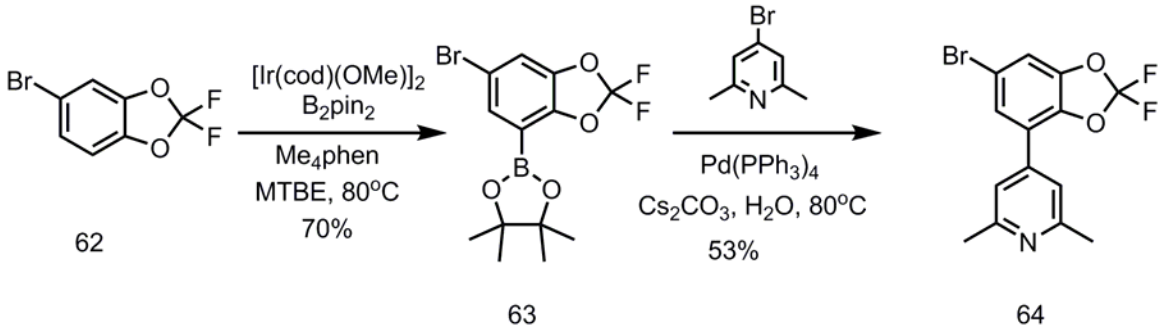

Scheme 12. Functionalization of bromo-1,1difluoro-benzodioxole

With the doubly functionalized difluorobenzodioxolane, Suzuki coupling was attempted with an excess equivalence of 4-bromo-2,6 dimethylpyridine (Scheme.12). Quite excitedly, a mono coupled product was obtained with the bromine moiety still intact. Similarly, Suzuki coupling was carried out on a benzoxazole derivative (Scheme.13), which was borylated by literature procedure.[71]

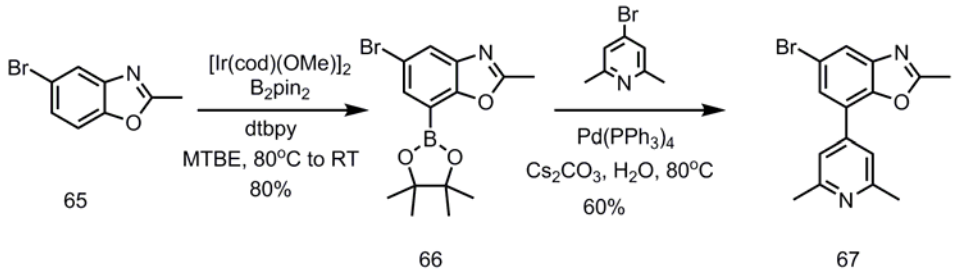

Scheme 13. Functionalization of benzoxazole

With both 64 and 67 available, it was reasoned that lithiation followed by nucleophilic addition to 3-(trimethylsilyl)-2-propynal would generate the alkynol precursor necessary for deoxygenation and methylation (Scheme.14). But unfortunately, with 64 a mixture of ortho lithiated product along with lithium halogen exchange product was obtained. With benzoxazole derivative 70 was obtained. Since the previous methods of deoxygenation and methylation could not be applied to these substrates, a cross coupling strategy was envisioned.

Stille coupling[72] was carried out for both substrates with vinyl ester stannane (Scheme.15) - obtained from Pd catalyzed coupling of tributyltin hydride and methyl propiolate.[73] The α,β unsaturated ester was subjected to hydrogenation, DIBAL-H reduction and Ohira Bestmann homologation to give the propargyl alkyne **73**, **74**. Allene formation was observed with difluoro benzodioxolane, while the isomerization was not observed in the case of benzoxazole derivative.

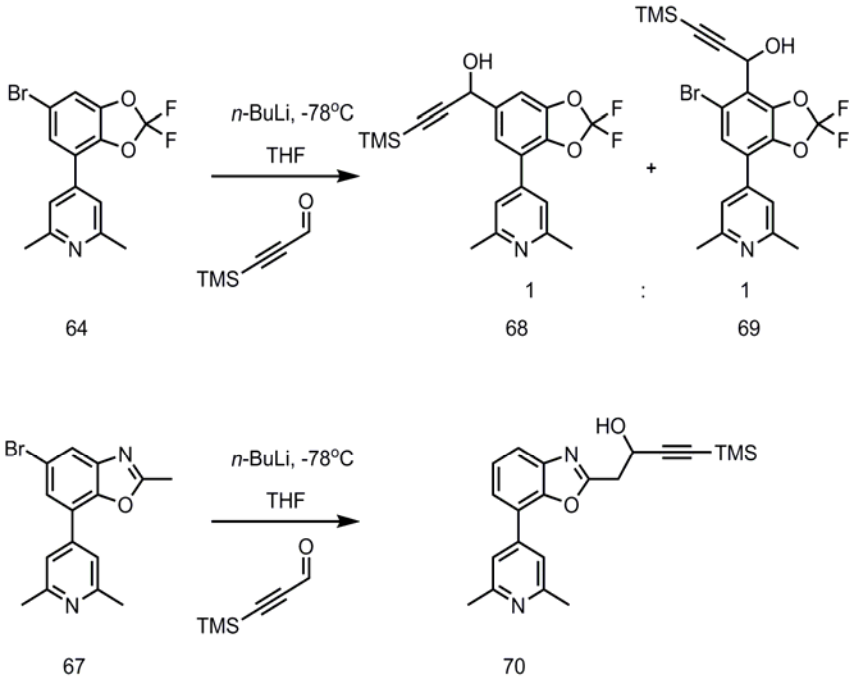

Scheme 14. Synthesis of alkynol

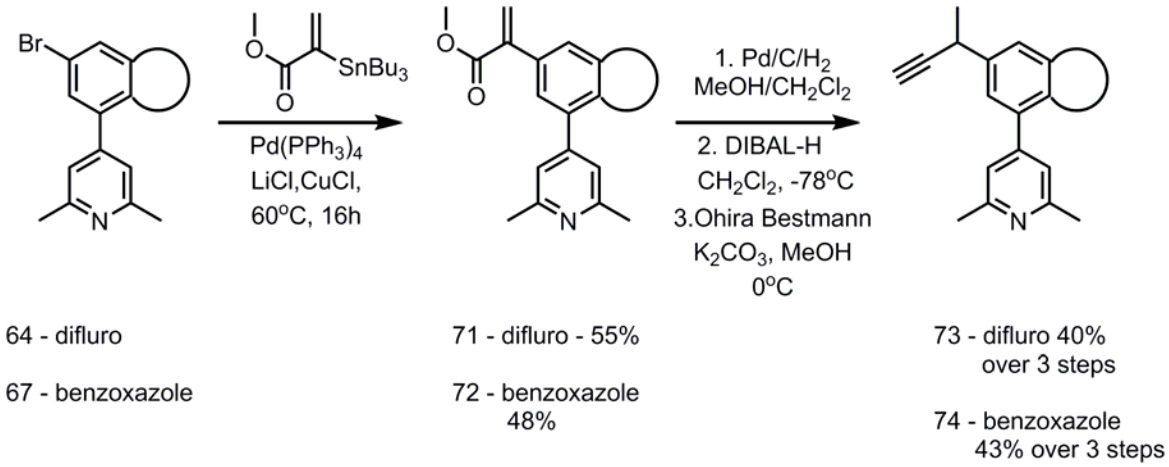

Scheme 15. Stille coupling and homologation to propargyl alkyne

The reasoning behind choosing vinyl ester stannane as a synthon for installing the propargyl alkyne because the method can be altered for enantioselective synthesis of propargylic methyl.

2.6 Conclusion

The synthetic protocol of propargylic antifolates by the homologation route was limited in its utility for certain substrates. New methods of nucleophilic substitution with hydride, a methyl carbanion and a fluoride source was utilized to overcome some of the limitations. A stille coupling method was devised for diflurodioxolane and benzimidazole substrates to generate the terminal alkyne.

2.7 Acknowledgements

Methylation of compound **35** was done by Dr. Santosh Keshipeddy. Methylation of compound **38** was designed and carried out by Eric W. Scocherra.

References

1. Viswanathan, K.; Frey, K.; Scocchera, E.; Martin, B.; Swain III, P.; Alverson, J.; Priestley, N.; Anderson, A.; Wright, D. Toward New Therapeutics for Skin and Soft Tissue Infections: Propargyl-Linked Antifolates Are Potent Inhibitors of MRSA and *Streptococcus pyogenes PLoS ONE* 2012, *7*, e29434.

2. Saito. T.; Furukawa. N.; Otani.T. A facile synthesis of pyrrolo[2,3-*b*]quinolines *via* a Rh(I)-catalyzedcarbodiimide-Pauson–Khand-type reaction. *Org. Biomol. Chem.*, 2010, *8*, 1126–1132.

3. Trost, B.M.; Michael T. R.; Ruthenium-Catalyzed Cycloisomerizations of Diynols, *J. Am. Chem. Soc*. 2005, 127, 4763-4776.

4. Nicholas.K.M. Chemistry and Synthetic Utility of Cobalt-Complexed Propargyl Cations. *Acc. Chem.Res*. 1987, 20, 6, 208-214.

5. McComsey, D.; Reitz, A.; Maryanoff, C.; Maryanoff, B. Deoxygenation Of Acetylenic Carbinols. Reduction Of Cobalt Carbonyl Adducts With Borane-Methyl Sulfide And Trifluoroacetic Acid.*Synthetic Communications* 1986, *16*, 1535-1549.

6. Teobald, B.J. The Nicholas reaction: the use of dicobalt hexacarbonyl- stabilized propargylic cations in synthesis, *Tetrahedron*, 58, 2002, 4133-4170.

7. Egi, M.; Kawai, T.; Umemura, M.; Akai, S. Heteropolyacid-Catalyzed Direct Deoxygenation Of Propargyl And Allyl Alcohols. *J. Org. Chem.* 2012, *77*, 7092-7097.

8. Gaudilliere, B.; Jacobelli, H.; Michael W.; Joseph A. Preparation of new alkynylated quinazoline compounds as MMP-13 inhibitors, 2004, WO 2004007469.

9. Narayana Kumar, G.; Laali, K. Facile Coupling Of Propargylic, Allylic And Benzylic Alcohols With Allylsilane And Alkynylsilane, And Their Deoxygenation With Et_3SiH, Catalyzed By Bi(Otf)3 In [BMIM][BF4] Ionic Liquid (IL), With Recycling And Reuse Of The IL. *Org. Biomol. Chem.* 2012, *10*, 7347.

10. Meyer, V.; Niggemann, M. Highly Chemoselective Calcium-Catalyzed Propargylic Deoxygenation. *Chemistry - A European Journal* 2012, *18*, 4687-4691.

11. Sakai, N.; Hirasawa, M.; Konakahara, T. Indium Tribromide-Catalyzed Deacetoxylation Of Propargylic Acetate With Triethylsilane. *Tetrahedron Letters* 2005, *46*, 6407-6409.

12. Georgy, M.; Boucard, V.; Debleds, O.; Zotto, C.; Campagne, J. Gold(III)-Catalyzed Direct Nucleophilic Substitution Of Propargylic Alcohols. *Tetrahedron* 2009, *65*, 1758-1766.

13. Nishibayashi, Y.; Shinoda, A.; Miyake, Y.; Matsuzawa, H.; Sato, M. Ruthenium-Catalyzed Propargylic Reduction Of Propargylic Alcohols With Silanes. *Angew. Chem. Int. Ed.* 2006, *45*, 4835-4839.

14. Yuki, M.; Miyake, Y.; Nishibayashi, Y. Preparation Of Thiolate-Bridged Dinuclear Ruthenium Complexes Bearing A Phosphine Ligand And Application To Propargylic Reduction Of Propargylic Alcohols With 2-Propanol. *Organometallics* 2010, *29*, 5994-6001.

15. Masuyama, Y.; Takahara, J.; Hashimoto, K.; Kurusu, Y. Palladium-Catalysed Dehydration Of Propynyl Alcohols With Tin(II) Chloride. *Journal of the Chemical Society, Chemical Communications* 1993, 1219-1220.

16. Liu, J.; Muth, E.; Flörke, U.; Henkel, G.; Merz, K.; Sauvageau, J.; Schwake, E.; Dyker, G. Alkylation Of Arenes With Benzylic And Propargylic Alcohols – Classicalversus Fancy Catalysts. *Advanced Synthesis & Catalysis* 2006, *348*, 456-462.

17. Lee, K.; Lee, P. Efficient Synthetic Method Of Multisubstituted Allenes From The Reactions Of Allylindium Reagents With 3°-Propargyl Alcohols. *Organic Letters* 2008, *10*, 2441-2444.

18. Russell, G.; Ngoviwatchai, P.; Wu, Y. Electron-transfer processes. 46. Allylic and propargylic substitution reactions involving radicals generated from alkylmercury halides. *J. Am. Chem. Soc.* 1989, *111*, 4921-4927.

19. Debleds, O.; Gayon, E.; Vrancken, E.; Campagne, J. Gold-catalyzed propargylic substitutions: Scope and synthetic developments. *Beilstein J. Org. Chem.* 2011, *7*, 866-877.

20. Georgy, M.; Boucard, V.; Debleds, O.; Zotto, C.; Campagne, J. Gold (III)-Catalyzed Direct Nucleophilic Substitution Of Propargylic Alcohols. *Tetrahedron* 2009, *65*, 1758-1766.

21. Kennedy-Smith, J.; Young, L.; Toste, F. Rhenium-Catalyzed Aromatic Propargylation. *Org. Lett.* 2004, *6*, 1325-1327.

22. Ohri, R.; Radosevich, A.; Hrovat, K.; Musich, C.; Huang, D.; Holman, T.; Toste, F. A Re(V)-Catalyzed C−N Bond-Forming Route to Human Lipoxygenase Inhibitors. *Org. Lett.* 2005, *7*, 2501-2504.

23. Sherry, B.; Radosevich, A.; Toste, F. A Mild C−O Bond Formation Catalyzed by a Rhenium-Oxo Complex. *J. Am. Chem. Soc.* 2003, *125*, 6076-6077.

24. Kuninobu, Y.; Ishii, E.; Takai, K. Rhenium- and Gold-Catalyzed Coupling of Aromatic Aldehydes with Trimethyl(phenylethynyl)silane: Synthesis of Diethynylmethanes. *Angew. Chem.* 2007, *119*, 3360-3363.

25. Zhan, Z.; Yang, W.; Yang, R.; Yu, J.; Li, J.; Liu, H. Bicl3-Catalyzed Propargylic Substitution Reaction Of Propargylic Alcohols With C-, O-, S- And N-Centered Nucleophiles. *Chem. Commun.* 2006, 3352-3354.

26. Qin, H.; Yamagiwa, N.; Matsunaga, S.; Shibasaki, M. Bismuth-Catalyzed Direct Substitution Of The Hydroxy Group In Alcohols With Sulfonamides, Carbamates, And Carboxamides. *Angew. Chem. Int. Ed.* 2007, *46*, 409-413.

27. Ji, W.; Pan, Y.; Zhao, S.; Zhan, Z. Fecl 3 -Catalyzed Propargylation-Cycloisomerization Tandem Reaction: A Facile One-Pot Synthesis Of Substituted Furans. *Synlett* 2008, *2008*, 3046-3052.

28. Lin, M.; Hao, L.; Liu, X.; Chen, Q.; Wu, F.; Yan, P.; Xu, S.; Chen, X.; Wen, J.; Zhan, Z. Nucleophilic Substitution Of Secondary Alkyl-Substituted Propargyl

Acetates: An Economic And Practical Indium Trichloride Catalyzed Access. *Synlett* 2011, 665-670.

29. Huang, W.; Wang, J.; Shen, Q.; Zhou, X. $Yb(OTf)_3$-catalyzed propargylation and allenylation of 1,3-dicarbonyl derivatives with propargylic alcohols: one-pot synthesis of multi-substituted furocoumarin.*Tetrahedron* 2007, *63*, 11636-11643.

30. Sanz, R.; Miguel, D.; Martínez, A.; Álvarez-Gutiérrez, J.; Rodríguez, F. Brønsted Acid Catalyzed Propargylation Of 1,3-Dicarbonyl Derivatives. Synthesis Of Tetrasubstituted Furans. *Org. Lett.*, 2007, *9*, 727-730.

31. Sanz, R.; Martínez, A.; Álvarez-Gutiérrez, J.; Rodríguez, F. Metal-Free Catalytic Nucleophilic Substitution of Propargylic Alcohols. *Eur. J. Org. Chem.* 2006, 1383-1386.

32. Imada, Y.; Yuasa, M.; Nakamura, I.; Murahashi, S. Copper (I)-Catalyzed Amination of Propargyl Esters. Selective Synthesis of Propargylamines, l-Alken-3-ylamines, and (2)-Allylamines, J. Org. Chem. 1994, 59, 2282-2284.

33. Hui, H.; Zhao, Q.; Yang, M.; She, D.; Chen, M.; Huang, G. Copper(II) Bromide Catalyzed Novel Preparation Of Propargylic Ethers And Sulfides By S N 1-Type Substitution Between Propargylic Alcohols And Alcohols Or Thiols. *Synthesis* 2008, *2008*, 191-196.

34. Yadav, J.; Subba Reddy, B.; Srinivasa Rao, T.; Raghavendra Rao, K. Copper(II)-Catalyzed Allylation Of Propargylic And Allylic Alcohols By Allylsilanes: A Facile Synthesis Of 1,5-Enynes. *Tetrahedron Letters* 2008, *49*, 614-618.

35. Hattori, G.; Matsuzawa, H.; Miyake, Y.; Nishibayashi, Y. Copper-Catalyzed Asymmetric Propargylic Substitution Reactions Of Propargylic Acetates With Amines. *Angew. Chem.* 2008, *120*, 3841-3843.

36. Detz, R.; Delville, M.; Hiemstra, H.; van Maarseveen, J. Enantioselective Copper-Catalyzed Propargylic Amination. *Angew. Chem.* 2008, *120*, 3837-3840.

37. Bartels, A.; Mahrwald, R.; Quint, S. Synthesis of propargylic ethers via Lewis-acid mediated nucleophilic substitution of propargylic esters. *Tet. Lett.* 1999, *40*, 5989-5990.

38. Mahrwald, R.; Quint, S. TiCl4-Mediated Nucleophilic Substitution of Propargylic Esters.*Tetrahedron* 2000, *56*, 7463-7468.

39. Yadav, J.; Reddy, B.; Rao, K.; Kumar, G. Indium(III) Bromide Catalyzed Rapid Propargylation Of Heteroaromatic Systems By A-Aryl-Substituted Propargyl Alcohols. *Synthesis* , 2007, 20 3205-3210.

40. Srihari, P.; Bhunia, D.; Sreedhar, P.; Mandal, S.; Reddy, J.; Yadav, J. Iodine-Catalyzed C- And O-Nucleophilic Substitution Reactions Of Aryl-Propargyl Methanols. *Tet. Lett.* 2007, *48*, 8120-8124.

41. Srihari, P.; Shyam Sunder Reddy, J.; Bhunia, D.; Mandal, S.; Yadav, J. PMA-SiO 2 : A Heterogenous Catalyst for O -, S -, and N -Nucleophilic Substitution Reactions of Aryl Propargyl Alcohols. *Syn. Comm.* 2008, *38*, 1448-1455.

42. Yadav, J.; Reddy, B.; Rao, K.; Kumar, G. Sc(OTf)3-catalyzed alkylation of indoles with propargyl alcohols: an expeditious synthesis of 3-substituted indoles. *Tet. Lett.* 2007, *48*, 5573-5576.

43. Ammal, S.; Yoshikai, N.; Inada, Y.; Nishibayashi, Y.; Nakamura, E. Synergistic Dimetallic Effects in Propargylic Substitution Reaction Catalyzed by Thiolate-Bridged Diruthenium Complex. *J. Am. Chem. Soc.* 2005, *127*, 9428-9438.

44. Yamauchi, Y.; Onodera, G.; Sakata, K.; Yuki, M.; Miyake, Y.; Uemura, S.; Nishibayashi, Y. Ruthenium-Catalyzed Reactions of 1-Cyclopropyl-2-propyn-1-ols with Anilines and Water via Allenylidene Intermediates: Selective Preparation of Tri- and Tetrasubstituted Conjugated Enynes. *J. Am. Chem. Soc.*2007, *129*, 5175-5179.

45. Matsuzawa, H.; Kanao, K.; Miyake, Y.; Nishibayashi, Y. Remarkable Effect of N -Substituent on Enantioselective Ruthenium-Catalyzed Propargylation of Indoles with Propargylic Alcohols. *Org. Lett.* 2007, *9*, 5561-5564.

46. Nishibayashi, Y.; Wakiji, I.; Ishii, Y.; Uemura, S.; Hidai, M. Ruthenium-Catalyzed Propargylic Alkylation of Propargylic Alcohols with Ketones: Straightforward Synthesis of γ-Keto Acetylenes. *J. Am. Chem. Soc.* 2001, *123*, 3393-3394.

47. Nishibayashi, Y.; Milton, M.D.; Inada, Y.; Yoshikawa, M.; Wakiji, I.; Hidai, M.; Uemura, S.; Ruthenium-Catalyzed Propargylic Substitution Reactions of Propargylic Alcohols with Oxygen-, Nitrogen-, and Phosphorus-Centered Nucleophiles, *Chem. Eur. J*. 2005, 11, 1433 – 1451.

48. Detz R.J.; Hiemstra.H.;Jvan Maarseveen.J.H. Catalyzed Propargylic Substitution, *Eur. J. Org. Chem.* 2009, 6263–6276.

49. Kabalka, G.; Yao, M. Direct Propargylic Substitution Of Hydroxyl Group In Propargylic Alcohols. *Curr.Org.Syn.* 2008, *5*, 28-32.

50. Bauer, E. Transition-Metal-Catalyzed Functionalization Of Propargylic Alcohols And Their Derivatives. *Synthesis* 2012, *44*, 1131-1151.

51. Ljungdahl, N.; Kann, N. Transition-Metal-Catalyzed Propargylic Substitution. *Angew. Chem. Int. Ed.* 2009, *48*, 642-644.

52. Nishibayashi, Y. Transition-Metal-Catalyzed Enantioselective Propargylic Substitution Reactions of Propargylic Alcohol Derivatives with Nucleophiles. *Synthesis* 2012, *2012*, 489-503.

53. Macdonald, T.; Reagan, D.; Brinkmeyer, R. Reaction Of Propargylic Substrates With Organocopper Species. Synthetic Aspects. *J. Org. Chem.* 1980, *45*, 4740-4747.

54. Smith, S.; Fu, G. Nickel-Catalyzed Asymmetric Cross-Couplings Of Racemic Propargylic Halides With Arylzinc Reagents. *J. Am. Chem. Soc.* 2008, *130*, 12645-12647.

55. Ye, F.; Ma, X.; Xiao, Q.; Li, H.; Zhang, Y.; Wang, J. C(sp)–C(sp 3) Bond Formation through Cu-Catalyzed Cross-Coupling of N -Tosylhydrazones and Trialkylsilylethynes. *J. Am. Chem. Soc.* 2012, *134*, 5742-5745.

56. Reetz, M.; Westermann, J.; Steinbach, R. Direct geminal dimethylation of ketones using dimethyltitanium dichloride. *J. Chem. Soc. Chem. Comm.* 1981, 237-239.

57. Reetz, M.; Westermann, J. Direct geminal dialkylation of ketones using organotitanium reagents. A simple entry into synthetic tetrahydrocannabinoids. *J. Org. Chem.* 1983, *48*, 254-255.

58. Reetz, M.; Westermann, J.; Steinbach, R. Chemoselective and Position Specific Methylation oftert-Alkyl Halides with Methyltitanium(IV) Chlorides. *Angew. Chem. Int. Ed. Engl.* 1980, *19*, 901-902.

59. Marigo, M.; Fielenbach, D.; Braunton, A.; Kjærsgaard, A.; Jørgensen, K. Enantioselective Formation of Stereogenic Carbon-Fluorine Centers by a Simple Catalytic Method. *Angew. Chem. Int. Ed.* 2005,*44*, 3703-3706.

60. Beeson, T.; MacMillan, D. Enantioselective Organocatalytic α-Fluorination of Aldehydes. *J. Am. Chem. Soc.* 2005, *127*, 8826-8828.

61. Jiang, H.; Falcicchio, A.; Jensen, K.; Paixão, M.; Bertelsen, S.; Jørgensen, K. Target-Directed Organocatalysis: A Direct Asymmetric Catalytic Approach to Chiral Propargylic and Allylic Fluorides. *J. Am. Chem. Soc.* 2009, *131*, 7153-7157.

62. Madiot, V.; Grée, D.; Gree, R.; Lesot, P.; Courtieu, J. Highly enantioselective propargylic monofluorination established by carbon-13 and fluorine-19 NMR in chiral liquid crystals. *Chem. Commun.*2000, 169-170.

63. Grée, D.; Madiot, V.; Grée, R. High regio-and stereocontrol in the dehydroxy — fluorination of propargylic alcohols and the corresponding Cobalt-carbonyl complexes. *Tet. Lett.* 1999, *40*, 6399-6402.

64. Carroll, L.; McCullough, S.; Rees, T.; Claridge, T.; Gouverneur, V. Stereospecific anti SE2′ fluorination of allenylsilanes: synthesis of enantioenriched propargylic fluorides. *Org. Biomol. Chem.* 2008, *6*, 1731-1733.

65. Yu, Y.; He, G.; Zhang, X. Synthesis of α,α-Difluoromethylene Alkynes by Palladium-Catalyzed gem -Difluoropropargylation of Aryl and Alkenyl Boron Reagents. *Angew. Chem. Int. Ed.* 2014, *53*, 10457-10461.

66. Schlosser, M.; Gorecka, J.; Castagnetti, E. A Homologous Series of O- andN-Functionalized 2,2-Difluoro1,3-benzodioxoles: an Exercise in Organometallic Methodology. *European Journal of Organic Chemistry* 2003, 452-462.

67. Castagnetti, E.; Schlosser, M. 2-, 3-, and 4-(Trifluoromethoxy)phenyllithiums: Versatile Intermediates Offering Access to a Variety of New Organofluorine Compounds. *European Journal of Organic Chemistry* 2001, *2001*, 691-695.

68. Hagooly, Y.; Welch, M.; Rozen, S. Synthesis of difluoroaryldioxoles using BrF3. *Org. Biomol. Chem.* 2011, *9*, 902.

69. Kuroboshi, M.; Hiyama, T. A Facile Synthesis of α,α-Difluoroalkyl Ethers and Carbonyl Fluoride Acetals by Oxidative Desulfurization-Fluorination. *Synlett* 1994, 251-252.

70. Vanchura, II, B.; Preshlock, S.; Roosen, P.; Kallepalli, V.; Staples, R.; Maleczka, Jr., R.; Singleton, D.; Smith, III, M. Electronic effects in iridium C–H borylations: insights from unencumbered substrates and variation of boryl ligand substituents. *Chem. Commun.* 2010, *46*, 7724.

71. Larsen, M.; Hartwig, J. Iridium-Catalyzed C–H Borylation of Heteroarenes: Scope, Regioselectivity, Application to Late-Stage Functionalization, and Mechanism. *J. Am. Chem. Soc.* 2014, *136*, 4287-4299.

72. Han, X.; Stoltz, B.; Corey, E. Cuprous Chloride Accelerated Stille Reactions. A General and Effective Coupling System for Sterically Congested Substrates and for Enantioselective Synthesis. *J. Am. Chem. Soc.* 1999, *121*, 7600-7605.

73. Nielsen, T.; Quement, S.; Juhl, M.; Tanner, D. Cu-mediated Stille reactions of sterically congested fragments: towards the total synthesis of zoanthamine. *Tetrahedron* 2005, *61*, 8013-8024.

CHAPTER 3

Optimization of Propargyl linked antifolates

Introduction

A series of generational improvements eventually led to lead compound **UCP 1006** and its derivatives. The lead compound[1] was based on the design that substitution of heteroaromatics as the B ring will impart solubility to the propargylic linked antifolates. As a result of the increased hydrophilicity (Table.7), **UCP1006** was more potent than the hydrophobic biphenyl series by > 60 fold. The next stage of drug development involves the investigation of metabolic stability of the lead compounds. The *in vitro* microsomal studies of the lead compounds gave a half-life of **34** and **31 mins**, for **UCP1006** and **UCP 1021** respectively.

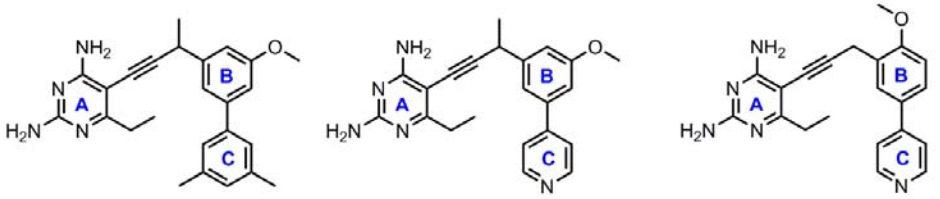

	UCP 111D35M	UCP 1006	UCP 1021
IC_{50} (nM)	42	19	20
MIC (μg/mL)	5.76	0.09	0.02
$t_{1/2}$ min *	NA	34	31
CYP 3A4 (μM)	NA	0.02	0.1
CYP 2D6 (μM)	NA	1.4	1.5

* higher concentration - 5 μg/mL

Table 7. Lead compounds for MRSA

3.1 Identification of Metbaolites

In order to achieve an ideal half – life of 1-2h, the need to identify the metabolites of the antifolates became imminent. Zhou[2] et al., carried out an in vitro studies by incubating UCP1006 (Scheme 3.1) with mouse liver microsomes in the presence of NADPH for one hour. The metabolites of the compound was identified and characterized by LC-MS.

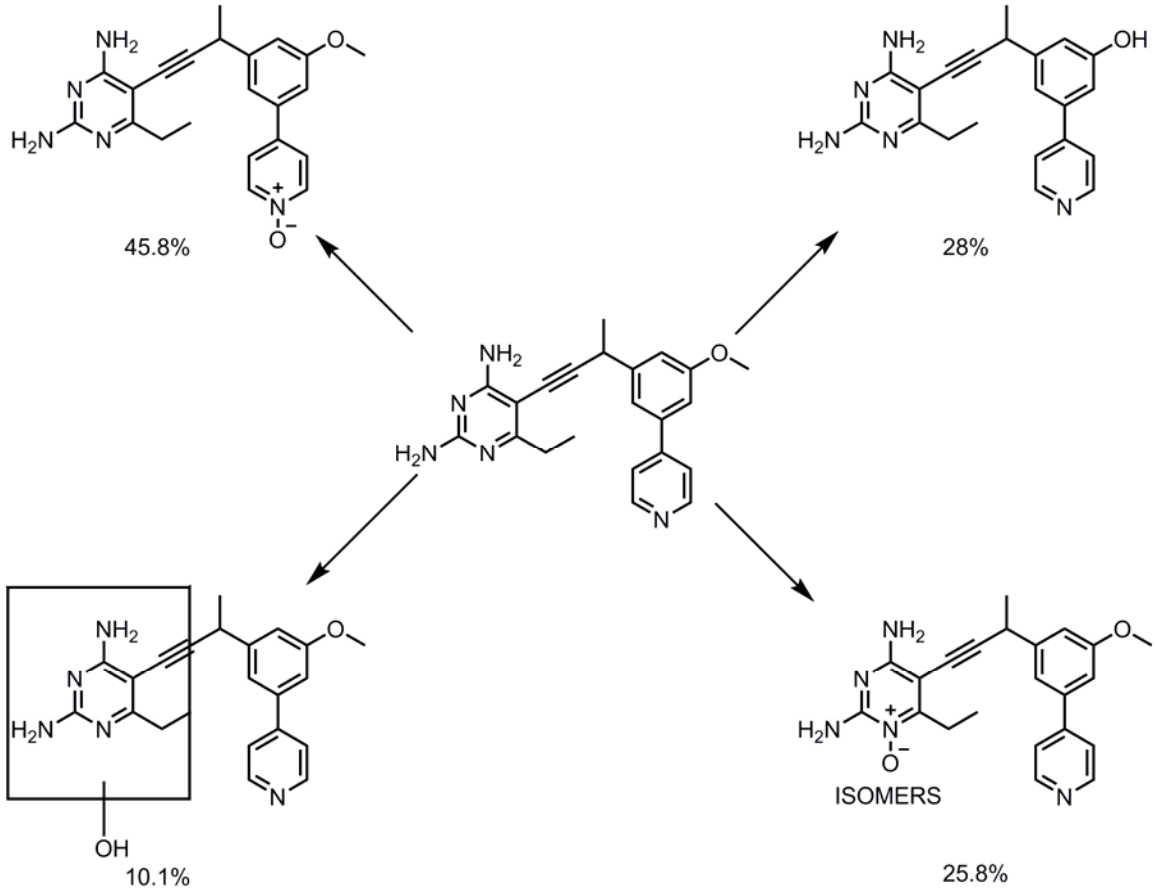

Scheme 16. Metabolites of UCP 1006

The two major metabolites of **UCP1006** are the N-oxidation of pyridine and demethylation accounting for 74% of all the metabolites. The remaining two metatolites are the N-oxidation of pyrimidinyl nitrogen (isomers) and the oxidation on the pyrimdine A-ring, ambiguously assigned as the C-6 oxidation at the benzylic position. It has been shown that propargyl methyl and the position of methoxy group have an effect on half-life and N-oxidation of pyridine ring. The presence of branching at the propargylic position with a methyl group increased the half-life and decreased the relative abundance of the pyridyl-N-oxide. Also shifting the methoxy from 3' to 2' position on the B-ring increases the half-life by decreasing the oxidation products of the amino pyrimidine A-ring. When a hybrid inhibitor was formed by combining the above two features – **UCP1040**, the half-life of the compound increased to 65 mins (Table.7)

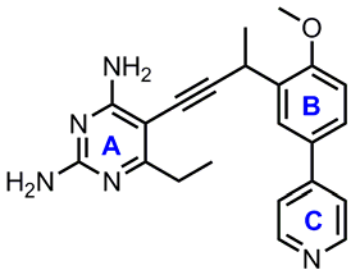

UCP 1040

IC_{50} -	0.03nM
MIC -	0.6mg/mL
$t_{1/2}$ -	65 mins
CYP3A4 -	0.02μM
CYP2D6 -	1.7μM

Table 8. Antibacterial and in-vitro metabolic profile of UCP1040

Though the half-life has been increased with **UCP1040**, CYP inhibition is in the low nanomolar range for CYP3A4, as is also the case with **UCP1006** and **UCP1021**. The

cytochrome P450 play a major role in the elimination of xenobiotics. CYP3A4, CYP2D6, and CYP2C9 constitute the major isoforms responsible for metabolism of pharmaceutical ligands. Inhibiting the CYPs can lead to drug-drug interactions and hence pose the risk of exposure to high concentrations of drug or formation of reactive intermediates leading to toxicity. The heterocyclic compounds – pyridine, imidazole are classified as type II ligands[3]. They interact with the heme of CYP450 through the lone pair of electrons on the nitrogen forming reversible inhibitor complexes. This inhibition can influence the half-life of the antifolates generating an artificially long $t_{1/2}$.

In order to be certain about the half-life value of **UCP1040**, the microsomal studies were carried out at a lower concentration (0.5µg/mL) of the ligand (Table.8). Unfortunately, the $t_{1/2}$ turned out to be 7 mins as against the 65 mins seen at a higher concentration (5µg/mL). Hence, optimization of lead compounds became necessary to overcome CYP inhibition and increase the half-life.

3.2 Minimizing CYP Inhibition

The strategies to overcome CYP inhibition involve reducing the pK_a of the heterocycle or by increasing the sterics around the nitrogen of pyridine. UCP1040 was taken as the template by retaining the top B-ring and changing the bottom C-ring.

3.2.1 Changing the C-ring

	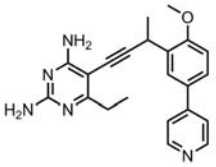	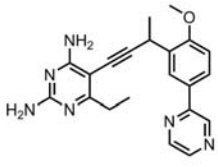	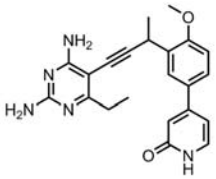	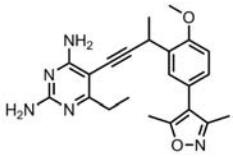
	UCP 1040	**UCP 1066**	**UCP 1104**	**UCP 1085**
IC_{50} (nM)	30	ND	ND	ND
MIC (μg/mL)	0.6	0.6	1.2	0.6
$t_{1/2}$ min	65*/7	24*	16	ND
CYP 3A4 (μM)	0.02	0.45	0.8	>50
CYP 2D6 (μM)	1.7	ND	34.6	>50

* higher concentration

Table 9. Changing the C-ring

Reduction of pK_a of the pyridine can be accomplished by introducing another nitrogen moiety into the pyridine rings. This was carried out by substituting the C-ring for pyrimidine, pyrazine, pyridone and an isoxazole heterocycle (Table.9).

Compared to the pK_a of pyridine ~ 5.2, the pK_a of pyrazine and pyrimidine are around 0.6 and 1.3 respectively. While the antibacterial activity of **UCP1066**, **UCP1067**, **UCP1085** have been maintained, great improvements in reducing the CYP inhibition occurred with the isoxazole ring. The pyrimidine, pyrazine and pyridone moieties show reduced inhibition of CYP2D6 while maintaining the inhibition of CYP3A4. The synthesis of the compounds followed method B, with a slight modification for pyridone.

Since the boronic acid of pyridone was not commercially available, the acid hydrolysis of 2 methoxy pyridine or diazotization reaction of 2-amino pyridine[4] were the

options available to access the pyridone. The commercially available 2-amino-4-bromo pyridine was subjected to diazotization (Scheme.17). Since the pyridone moiety has the propensity to form ligands with palladium catalysts, it necessitated the protection of N-pyridone. The pyridones are normally protected with benzyl group, but the presence of an alkyne moiety in the antifolate ligands precluded its use. Since the attempts to protect with a Boc group also failed, it was decided that acid hydrolysis of 2-methoxy pyridine after the final Sonogshira coupling could be employed.

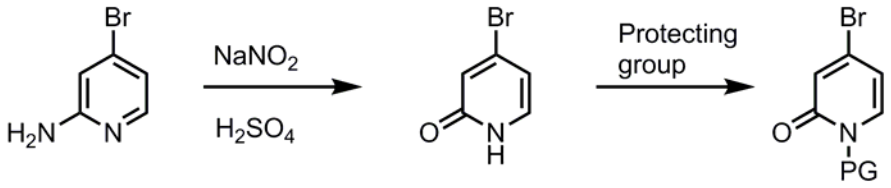

Scheme 17. Pyridone synthesis

The deprotection of 2 methoxy pyridine was carried out using BBr_3 (Scheme.18). The presence of 2'OMe in the B ring complicated the deprotection. NOESY experiments revealed that BBr_3 deprotected the top ring rather than methoxy next to pyridine. Increasing the equivalence of BBr_3 did not result in the formation of pyridone, since the deprotection of 2'OMe of the top B-ring resulted in precipitation of adduct.

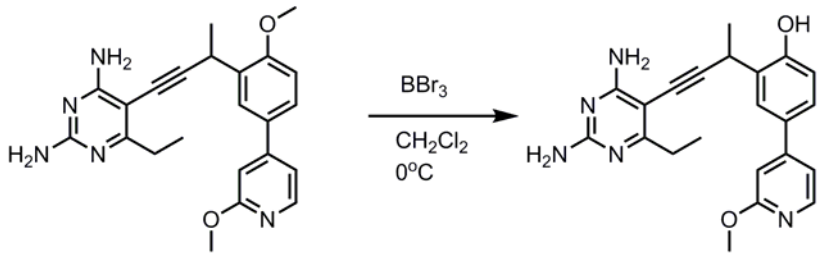

Scheme 18. Demethylation of UCP1077

A literature procedure[5] was found in which the deprotection of methoxy next to a heterocycle can be chemoselectively (Scheme.19) cleaved in the presence of other methoxy groups. Several byproducts coupled with increased polarity of the molecule necessitated an HPLC based separation with a 10% yield.

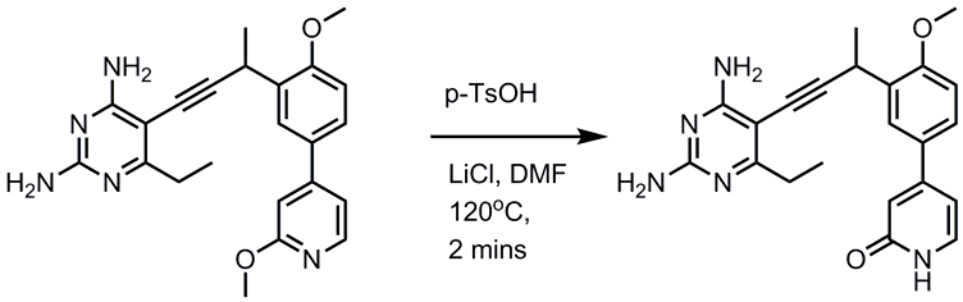

Scheme 19. Chemoselective demethylation of UCP1077

Although **UCP1085** with the isoxazole ring provided reduced CYP inhibition, the effect of sterics next to the pyridine nitrogen in reducing the CYP inhibition was also explored.

3.2.2 Steric Inhindrance around the pyridyl nitrogen

There are two ways of increasing the steric hindrance around the pyridine nitrogen. First method involves the substitution next to the pyridine and the other method is to move the nitrogen either a) ortho[6] to the biaryl linkage so that ring B can provide the necessary steric hindrance or b) flipping the two rings B&C so that pyridine now becomes B-ring (Table.10).

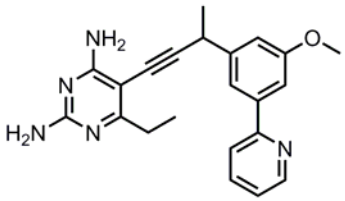
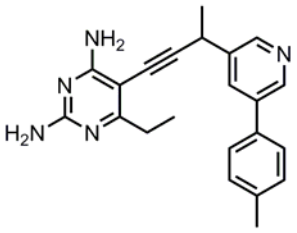

	UCP 1071	UCP 1047
IC_{50} (nM)	ND	ND
MIC (μg/mL)	0.6	2.5
$t_{1/2}$ min	15*	ND
CYP 3A4 (μM)	0.39	0.17
CYP 2D6 (μM)	28.3	ND

* higher concentration

Table 10. Changing the position of pyridyl nitrogen

Both compounds **UCP1071** and **UCP1047** did not show any reduction with the CYP3A4 inhibition. While antibacterial activity was maintained with **UCP1071**, it was lost with flipped pyridine ring- **UCP1047**. Possible reasons for the loss of activity with **UCP1047** could be due to electronegative pyridine on the top ring and also substantial loss of solubility. The other strategy to increase the steric bulk around pyridyl nitrogen by ortho substitution was carried out. The **UCP1040** was substituted with a methoxy and 2,6 dimethyl next to the pyridine. The sterically hindered pyridines – **UCP1076**, **UCP1077** (Table.11) seem to have better potency than **UCP1040** at 0.15μg/mL. Lowered CYP inhibition relative to **UCP1040** was also observed for both the analogs.

	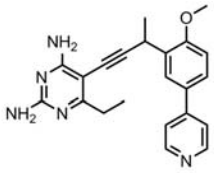 UCP 1040	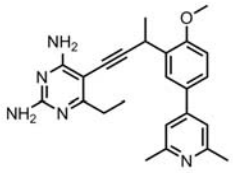 UCP 1076	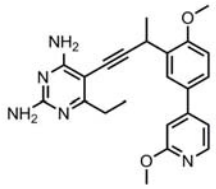 UCP 1077
IC_{50} (nM)	30	ND	ND
MIC (μg/mL)	0.6	0.15	0.15
$t_{1/2}$ min	7	8	ND
CYP 3A4 (μM)	0.02	3.7	2.7
CYP 2D6 (μM)	1.7	9.8	13.2

Table 11. Sterics around the pyridyl nitrogen

UCP1085 with the isoxazole ring and the sterically hindered pyridine analogs engendered reduced CYP inhibition. But still the half-life is very low at 8 mins for **UCP1076**. It could be argued that reduced half-life can arise from the demethylation of the 2'OMe of the B-ring.

3.3 Increasing Half-life

In order to synthesize analogs to increase the half-life, sterically hindered dimethylpyridine was chosen as the C-ring because of its potency compared to isoxazole and ease of its boronate ester synthesis[7]. Two routes of modification were planned for the top B-ring. One method involves variation of methoxy functionality and the second method involves replacing the methoxy with a different functional group.

3.3.1. Variations of O-Methoxy

The two common analogs to replace the methoxy group are the deuterated[8] and trifluoromethoxy groups. Both the analogs were proposed to slow down the rate of demethylation.

	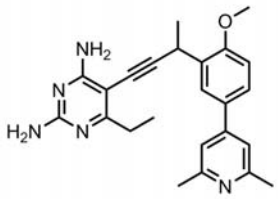 UCP 1076	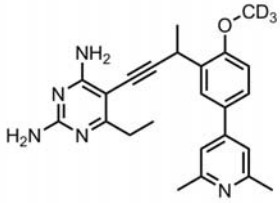 UCP 1077	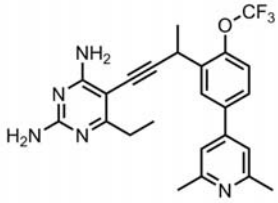 UCP 1129
IC_{50} (nM)	ND	ND	ND
MIC (μg/mL)	0.15	0.31	0.63
$t_{1/2}$ min	8	9	62
CYP 3A4 (μM)	3.7	11.0	> 50
CYP 2D6 (μM)	9.8	12.9	> 50

Table 12. Varying the methoxy group in B-ring

From the comparative table.12 above, it is evident that trifluoromethoxy has increased the half-life to 62 mins with minimal CYP inhibition. In terms of potency there is a 2-4 fold loss as the transition is made from a hydrogen bond donor (OCH_3) to a hydrogen bond acceptor (OCF_3). Substitution with OCD_3 had no effect on slowing down the rate of demethylation as evident from the low half-life values. With the fluorine of OCF_3 and dimethyl of pyridine, the hydrophobicity of the ligand has been increased. In order to further refine **UCP1129**, the need of methyl group at the propargylic position

and the effect of a single methyl around pyridine were probed. Quite satisfactorily, **UCP1125** without the propargylic methyl maintained the low inhibitory (Table.13) effect on CYPs while having a two fold increase in potency. This follows the pattern for MRSA in which compounds without the propargylic methyl are more potent. But the increased flexibility of the ligand has increased its CYP3A4 inhibition slightly, though within permissible limits. Similarly a single methyl around pyridine in **UCP1126** is well tolerated and does not show any CYP inhibitory activity. Based on the half-life data, it will prudent to further refine UCP1126 by removing the propargylic methyl and hence reducing the lipophilicity of the molecule further.

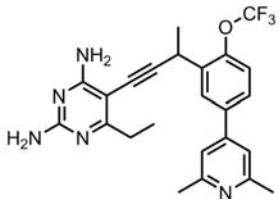
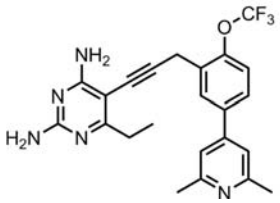
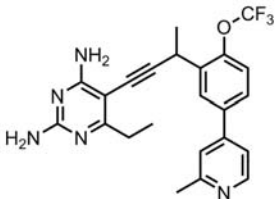

	UCP 1117	UCP 1125	UCP 1126
MIC (μg/mL)	0.6	0.31	ND
$t_{1/2}$ min	62	ND	ND
CYP 3A4 (μM)	>50	34.1	~50
CYP 2D6 (μM)	>50	>50	> 50

Table 13. Optimization of UCP1076

3.3.2. Changing substituents at 2'position of B-ring

To further probe the role of 2'OMe, substituents –H, Cl and –F at 3'position were studied (Table.14). No substitution at 2' position had an effect on increasing the potency of the ligand. The half-life though not optimal, has increased from 8 to 20 mins relative to **UCP1076**. The increase in half-life suggests that the rate of hydroxylation by CYP enzymes is slower than the rate of demethylation for the propargyl linked antifolates. In order to block the sites of hydroxylation, Cl was substituted at the 2' position and F at 3' position. A better half –life and reduced CYP inhibition was achieved for the chlorine analog, while the fluorine ligand shows inhibitory activity for CYP3A4 at 5.3 µg/mL.

	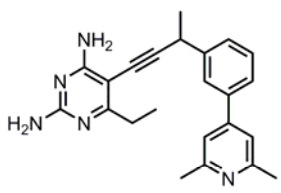	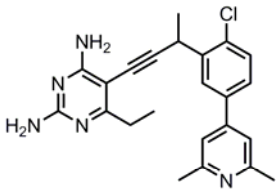	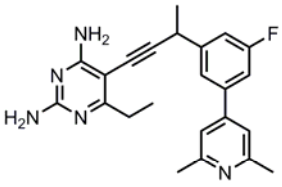
	UCP 1115	**UCP 1119**	**UCP 1120**
IC_{50} (nM)	ND	ND	ND
MIC (µg/mL)	0.16	0.31	0.63
$t_{1/2}$ min	20	56	50
CYP 3A4 (µM)	0.5	43.0	5.3
CYP 2D6 (µM)	27.4	>50	> 50

Table 14. Optimizing B-ring for potency

3.3.3. Blocking sites on the B-ring

From the above analogs, it became evident that the 2'methoxy is not required for maintaining the potency of ligands against MRSA. So the top ring was further probed for activity and pharmacokinetic behavior. To block the potential site of hydroxylation, a dioxolane ring was appended to the B-ring (Table.15). Since the benzodioxolane is a new pharmacophore, its potency was first tested with pyridine as the C-ring. Three new analogs were synthesized bearing a dioxolane ring at 2,3 and 3,4 positions.

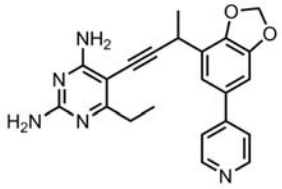
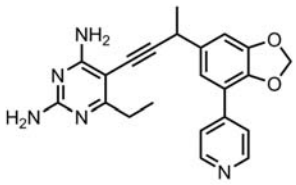
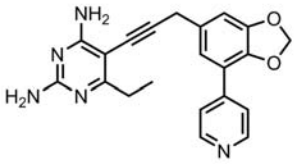

	UCP 1037	UCP 1038	UCP 1042
IC_{50} (nM)	17	17	19
MIC (μg/mL)	0.6	0.078	0.31
$t_{1/2}$ min*	63	79	33
CYP 3A4 (μM)	ND	0.02	ND
CYP 2D6 (μM)	ND	0.06	ND

* microsomal studies at 5μg/mL concentration

Table 15. 1,3 benzodioxole as the B ring

The new pharmacophore seems to maintain enzyme inhibition and good potency against MRSA. In the dioxolane series, UCP1038 exhibits potency similar to UCP1006. Again CYP inhibition are at an alarming low nanomolar levels and the half- life at 5μg/mL concentration is caused by pyridine. When the metabolite identification was

carried out, no metabolites were found. This is could be due to the Mechanism Based Inactivation[9] (MBI) of CYP enzymes. 1,3 benzodioxole moieties fall under the category of quasi-irreversible inactivators of CYP enzymes (Scheme.20). The reactive species of the benzodioxole bind to the heme of the CYP in a tight non-covalent interaction. Two paths can diverge from hydroxymethylene intermediate leading to carbene and catechol as shown below. In the case of UCP1038, it might be going through a carbene intermediate and forming an irreversible complex with the heme of the cytochrome. This could explain the lack of metabolite formation seen with dioxolane ligands.

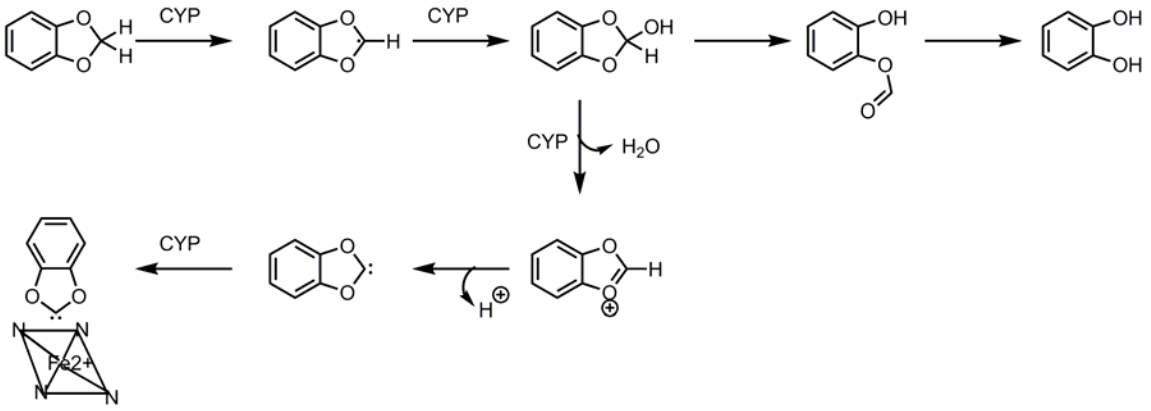

Scheme 20. Mechanism based inactivation of 1,3 benzodioxole moiety

Paroxetine by Concert pharmaceuticals [10] has a dioxolane moiety which undergoes carbene complex formation catalyzed by CYP2D6. CYP inhibition was reduced by slowing down the rate of carebene formation by deuteration of dioxolane moiety (Fig.16).

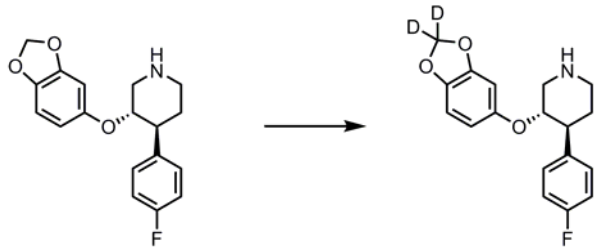

Figure 16. Deuterated paroxetine

Since the CYP numbers for both isoforms of UCP1038 were very low, it was decided to employ the same strategy of deuteration. Deuterated iodomethane (Scheme.21) was used to synthesize [11,12] **UCP1070** and **UCP1112**.

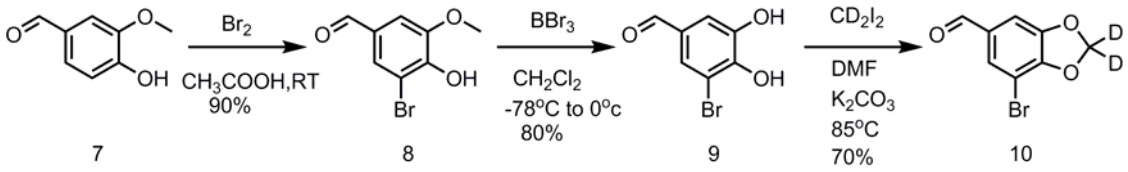

Scheme 21. Synthesis of deuterated dioxolane

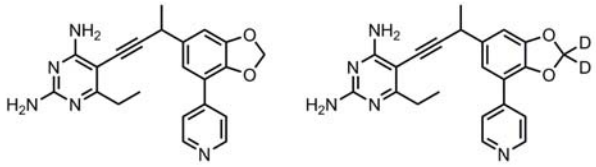

	UCP 1038	UCP 1070
IC_{50} (nM)	0.017	ND
MIC (μg/mL)	0.078	0.078
$t_{1/2}$ min	14	13
CYP 3A4 (μM)	0.02	0.04
CYP 2D6 (μM)	0.06	0.01

Table 16. Deuterated UCP1070

The effect of deuterium in reducing the CYP inhibition was not observed with **UCP1070** (Table.16). No improvements was seen in CYP2D6 as detected in the case of paroxetine. Only advantage of switching to d-dioxolane was the detection of metabolite formation by LC-MS. Though not quite proven without ambiguity, the metabolite appears to be formation of catechol. The CYP inhibition seen even with d-dioxolane could still be arising from the pyridine. Hence, to differentiate the effect of d-dioxolane from the H-dioxolane, the CYP inhibition by the pyridine moiety has to be stalled. So **UCP1112** (Table.17) was synthesized with dimethylpyridine as the C-ring. To further exploit the potency of bicyclic structures on the B-ring, bioisosteres of dioxolane were synthesized.

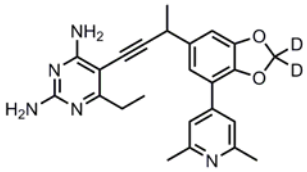

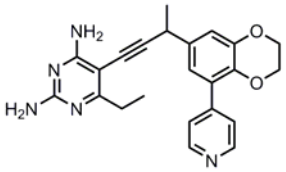

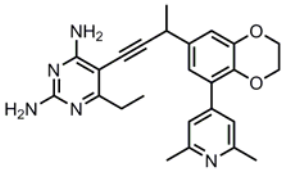

	UCP 1112	UCP 1113	UCP 1114
IC_{50} (nM)	ND	ND	ND
MIC (μg/mL)	0.15	0.15	0.31
$t_{1/2}$ min	16	ND	5
CYP 3A4 (μM)	0.01	ND	4.5
CYP 2D6 (μM)	0.54	ND	16.9

Table 17. Isosteres of 1,3 benzodioxole

Comparing **UCP1112** with **UCP1070**, potent CYP inhibition was still observed, except that the isoforms being inhibited extensively are reversed. A two-fold loss in

potency was observed with 2,6 lutidine as the C-ring. **UCP1114** analog shows moderate CYP inhibition relative to the dioxolane series, but suffers from rapid biotransformation by the microsomes. The low half-life value reflects the microsomal instability of 2' or 3' methoxy analogs.

To capitalize on the antibacterial activity of dioxolanes, a fluorinated analog[13] was conceived. Similar to OCF_3, it was hypothesized that the substitution of electronegative fluorine in the dioxolane moiety would overcome the CYP inhibition and low metabolic profile. Since it was anticipated that the fluorinated analog might increase the lipophilicity of the ligand, another bicyclic B-ring – benzimidazole was synthesized (Fig.17). It will be an interesting study to explore the effect of a restricted benzimidazole moiety on the antibacterial activity and enzyme inhibition.

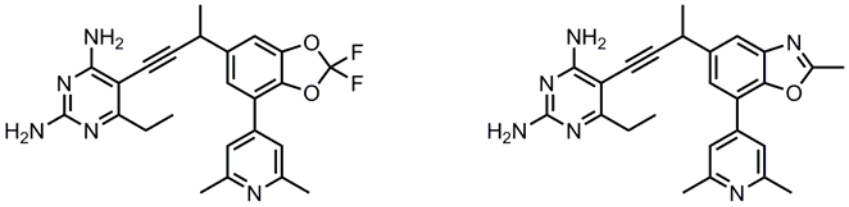

Figure 17. Fluorinated 1,3 benzodioxole and benzimidazole

3.4 Enzyme selectivity over human-DHFR

While improving the metabolic profile of propargyl linked antifolates, efforts were also directed towards gaining selectivity over human DHFR. Though the function of DHFR is conserved in evolutionary processes, small amino acid residue differences across species are exploited to achieve selective and potent antifolates. A study on the effect of propargyl linked antifolates towards the loop region in the active site revealed a

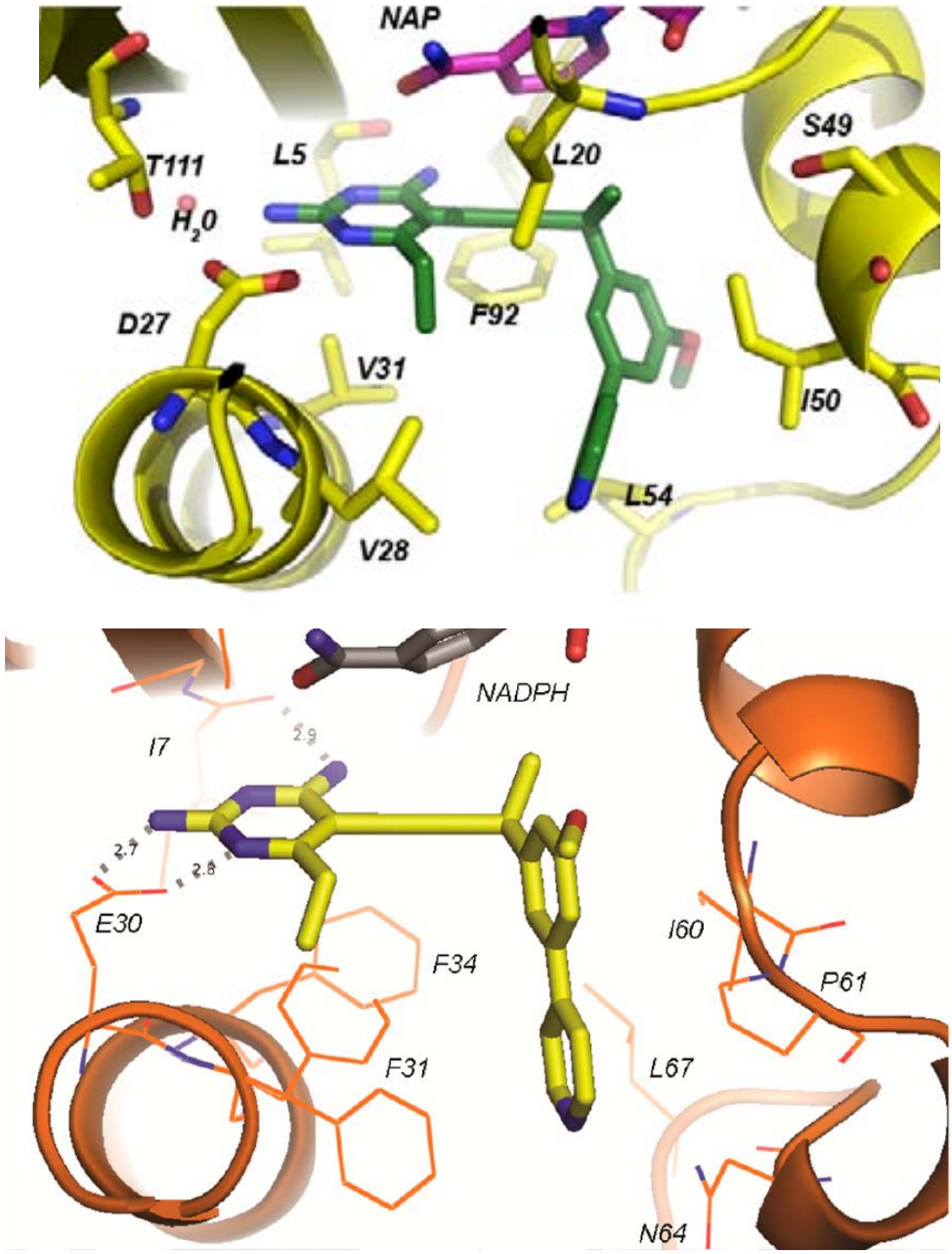

Figure 18. Crystal structures of UCP1006 in bacterial (green) and human (yellow) DHFR

ligand dependent conformational change that is prevalent across species[14]. The crystal structures of UCP1006 with h-DHFR revealed that interaction between the inhibitor and residues Phe 31, Phe 34 and Asn 64 increases the potency for h-DHFR.

Comparing the crystal structures of UCP1006 with bacterial and human DHFR (Fig.18), shows that the pyridine C-ring tends to adopt a perpendicular conformation with the B-ring in pathogenic DHFR while adopting a planar conformation with h-DHFR. To gain selectivity, a design wherein a methyl[15] group in the C-ring ortho to the biaryl linkage was conceived. The intended effect was to force the C-ring to adopt a perpendicular conformation thereby reducing its hydrophobic interaction with the Phe 31 and Phe 34 of h-DHFR.

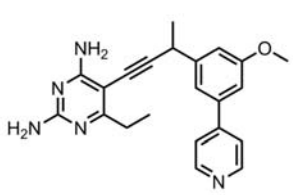
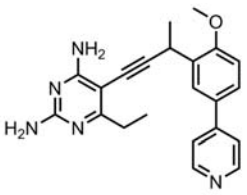
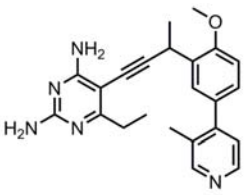

	UCP 1006	UCP 1040	UCP 1075
IC_{50} Sa DHFR(nM)	19	30	ND
MIC (μg/mL)	0.15	0.6	0.3
IC_{50} Hu DHFR(nM)	1300	164	2641

Table 18. Optimization for human selectivity

The newly designed **UCP1075** gave a 16-fold increase (Table.18) in selectivity compared to **UCP1040** while maintaining antibacterial activity at 0.3μg/mL.

3.5 Conclusions

Optimization of propargyl linked antifolates was carried out to overcome CYP inhibition, improve half-life and selectivity over human DHFR. The pyridine C-ring was replaced by isoxazole and 2,6 lutidine to overcome CYP inhibition. The B-ring was switched from methoxy to trifluoromethoxy to prevent demethylation and increase the half-life from 7 to >60 mins. Further changes in the B-ring were explored with benzodioxolane, d-benzodioxolane, fluorinated –benzodioxolane, benzodioxane and benzimidazole to gain potency and metabolic stability. Selectivity over human DHFR was also achieved with **UCP1075**.

3.6 Acknowlegments

Enzymatic assays for Sa DHFR were carried out by Stephanie Reeve of Dr. Anderson's lab. Microsomal half-life studies and CYP inhibition experiments were carried out by Dr. Wangda Zhou and Mike Lombardo of Dr. Anderson's lab. Crystal structures of antifolate ligands with human DHFR were done by Dr. Kristen Lamb also of Dr. Anderson's lab. Lead compounds **UCP1006**, **UCP1040** were synthesized by Dr. Kishore Viswanathan.

References

1. Viswanathan, K.; Frey, K.; Scocchera, E.; Martin, B.; Swain III, P.; Alverson, J.; Priestley, N.; Anderson, A.; Wright, D. Toward New Therapeutics for Skin and Soft Tissue Infections: Propargyl-Linked Antifolates Are Potent Inhibitors of MRSA and Streptococcus pyogenes. *PLoS ONE* 2012, *7*, e29434.

2. Zhou, W.; Viswanathan, K.; Hill, D.; Anderson, A.; Wright, D. Acetylenic Linkers in Lead Compounds: A Study of the Stability of the Propargyl-Linked Antifolates. *Drug Met. Dis.* 2012, *40*, 2002-2008.

3. Ahlström, M.; Zamora, I. Characterization of Type II Ligands in CYP2C9 and CYP3A4. *J. Med.Chem.* 2008, *51*, 1755-1763.

4. Li, J.; Zhang, X.; Zhang, Z.; Padakanti, P.; Jin, H.; Cui, J.; Li, A.; Zeng, D.; Rath, N.; Flores, H. et al. Heteroaromatic and Aniline Derivatives of Piperidines As Potent Ligands for Vesicular Acetylcholine Transporter. *J. Med. Chem.* 2013, *56*, 6216-6233.

5. Soni, A.; Dutt, A.; Sattigeri, V.; Cliffe, I. Efficient and Selective Demethylation of Heteroaryl Methyl Ethers in the Presence of Aryl Methyl Ethers. *Syn. Comm.* 2011, *41*, 1852-1857.

6. Marie M. Ahlström and Ismael Zamora, Characterization of Type II Ligands in CYP2C9 and CYP3A4, *J. Med. Chem.* 2008, *51,* 1755–1763.

7. Harrisson, P.; Morris, J.; Marder, T.; Steel, P. Microwave-Accelerated Iridium-Catalyzed Borylation of Aromatic C−H Bonds. *Org. Lett.* 2009, *11*, 3586-3589.

8. Gant, T. Using Deuterium in Drug Discovery: Leaving the Label in the Drug. *J. Med. Chem.* 2014, *57*, 3595-3611.

9. Orr, S.; Ripp, S.; Ballard, T.; Henderson, J.; Scott, D.; Obach, R.; Sun, H.; Kalgutkar, A. Mechanism-Based Inactivation (MBI) of Cytochrome P450 Enzymes: Structure–Activity Relationships and Discovery Strategies To Mitigate Drug–Drug Interaction Risks. *J. Med. Chem.* 2012, *55*, 4896-4933.

10. Yarnell.A. Heavy Hydrogen Turn heads, Again, *Chem. Eng. News*, 2009, *87* (25), pp 36–39.

11. Tadross, P.; Gilmore, C.; Bugga, P.; Virgil, S.; Stoltz, B. Regioselective Reactions of Highly Substituted Arynes. *Org. Lett.* 2010, *12*, 1224-1227.

12. Ellis, J.; Davis, E.; Dozeman, G.; Lenoir, E.; Belmont, D.; Brower, P. Development of a Scalable Process for CI-1020, A Novel Endothelin Antagonist 1. *Org. Process. Res. Develop.* 2001, *5*, 226-233.

13. Ruah, S.S.H.; Grootenhuis, P.D.J.; Van Goor, F.; Zhou, J.; Bear, B.; Miller, M.T.; McCartney, J.; Numa, M.M.D. Modulators of ATP-Binding Cassette transporters; Cystic Fibrosis Transmembrane Conductance Regulator; N-(5-hydroxy-2,4-ditert-butyl-phenyl)-4-oxo-1H-quinoline-3-carboxamide, US 7645789 B2.

14. Paulsen, J., Viswanathan, K., Wright, D., and Anderson, A. Structural analysis of the active sites of dihydrofolate reductase from two species of Candida uncovers ligand-induced conformationalchanges shared among species. Bioorg. Med. Chem. Lett. 2013, 23, 1279−1284.

15. Lamb, K.; G-Dayanandan, N.; Wright, D.; Anderson, A. Elucidating Features That Drive the Design of Selective Antifolates Using Crystal Structures of Human Dihydrofolate Reductase. *Biochem.* 2013, *52*, 7318-7326.

CHAPTER 4

Dual Inhibitors of Candida albicans and Candida glabrata

Introduction

Candida species constitute the fourth leading cause of blood stream infections after bacterial pathogens.[1-3] Of the *Candida* species, *glabrata* and *albicans* contribute to increasing prevalence of candidemia. While *C.albicans* remain susceptible to azoles, flucytosine and echinocandins, *C.glabrata* is losing its potency against azoles and gaining resistance to echinocandins.[4-6] This resistance necessitates the need for dual inhibition of both species since they are clinically indistinguishable from each other. Similar to the propargyl linked antifolates developed for MRSA, antifolates for the fungal species had undergone generational improvements (Table.19). The biaryl lead compound **UCP1023**[7,8] had good enzyme inhibition for *C.albicans* and *C.glabrata* at IC_{50} values of 30, 28nM respectively. Introduction of a heteroaromatic ring to increase the solubility of **UCP1006**[9] exhibited better antifungal activity compared to the hydrophobic **UCP1023** but does not correlate with the enzyme inhibition.

Lack of correlation between enyme inhibition and antifungal activity were also observed for *C.albicans* by two other research groups. Research by Glaxo[10] concluded the absence of relationship between activity and inhibitor size or hydrophobicity. Similarly a German company[11] also could not explain the lack of correlation after invalidating the role of efflux pumps. They speculated that the permeability of compounds against cell membranes might explain inconsistencies between IC_{50} and MIC.

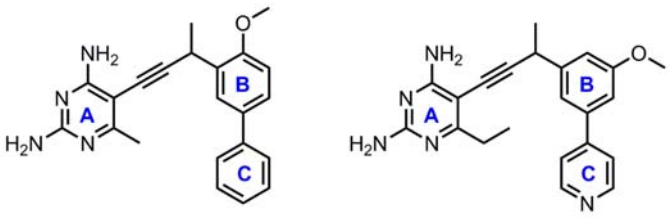

	UCP 1023	UCP 1006
CgDHFR IC_{50} (nM)	28	89
CaDHFR IC_{50} (nM)	30	60
CgMIC (μg/mL)	12.5	1.3
CaMIC (μg/mL)	>100	25

Table 19. Antifungal activity of propargyl linked antifolates

4.1 Dual Inhibitors for *C.glabrata* and *C.albicans*

In search of different chemotypes that might enable dual inhibition of both species of Candida, screening was performed on the library of propargyl linked antifolates. Interestingly, para isomers (Table.20) seem to exhibit dual inhibition with inconsistent enzyme inhibition as observed previously in literature.

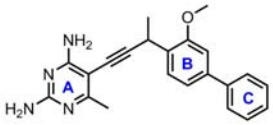
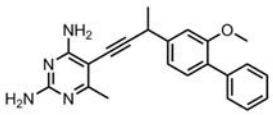
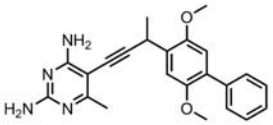

	UCP 111H	UCP 111F	UCP 111E
CgDHFR IC_{50} (nM)	5.5	9.1	8.2
CaDHFR IC_{50} (nM)	20	55	36
CgMIC (μg/mL)	0.39	0.78	1.6
CaMIC (μg/mL)	1.6	6.25	3.1

Table 20. Antifungal activity of para isomers

Apart from the enzyme inhibition – which is a good predictor for in vitro activity, the shape of the molecule also seems to influence the antifungal activity. To gain further understanding into the role of para isomers and their interaction with the active site, crystal structures of **UCP111H** with DHFR were grown in both species by Dr. Paulsen.

4.1.1 Crystal Structures of UCP111H with *Candida glabrata* and *C.albicans*

Crystallization with the racemate of **UCP111H** showed two molecules of the protein complexes in the asymmetric unit for the R enantiomer (Fig.19). The two molecules adopt different conformation in the active site. The difference lies in the orientation of the 3'methoxy. In one conformation, 3'OMe points down into the pocket enclosed by Phe 36, Leu 69 and Met 33 and the other points the methoxy toward Ser 61 to form a water mediated hydrogen bond. Except for the 3`OMe, all other interactions are conserved including the hydrogen bonds and hydrophobic interactions between the pyrimidine ring and Glu 32, Ile 9, Phe 36, Met/Ile 33 and Ile 121. The propargyl linker

forms van der Waals interactions with Ile 121 and Leu 25 as well as NADPH. The biphenyl moiety forms important hydrophobic contacts with Ile 62, Pro 63, and Phe 66. When **UCP111H** was co-crystallized with *C.albicans* DHFR, a conformation wherein 3'OMe was oriented towards Phe 36, Leu 69 and Met 33 was observed at 100% occupancy.

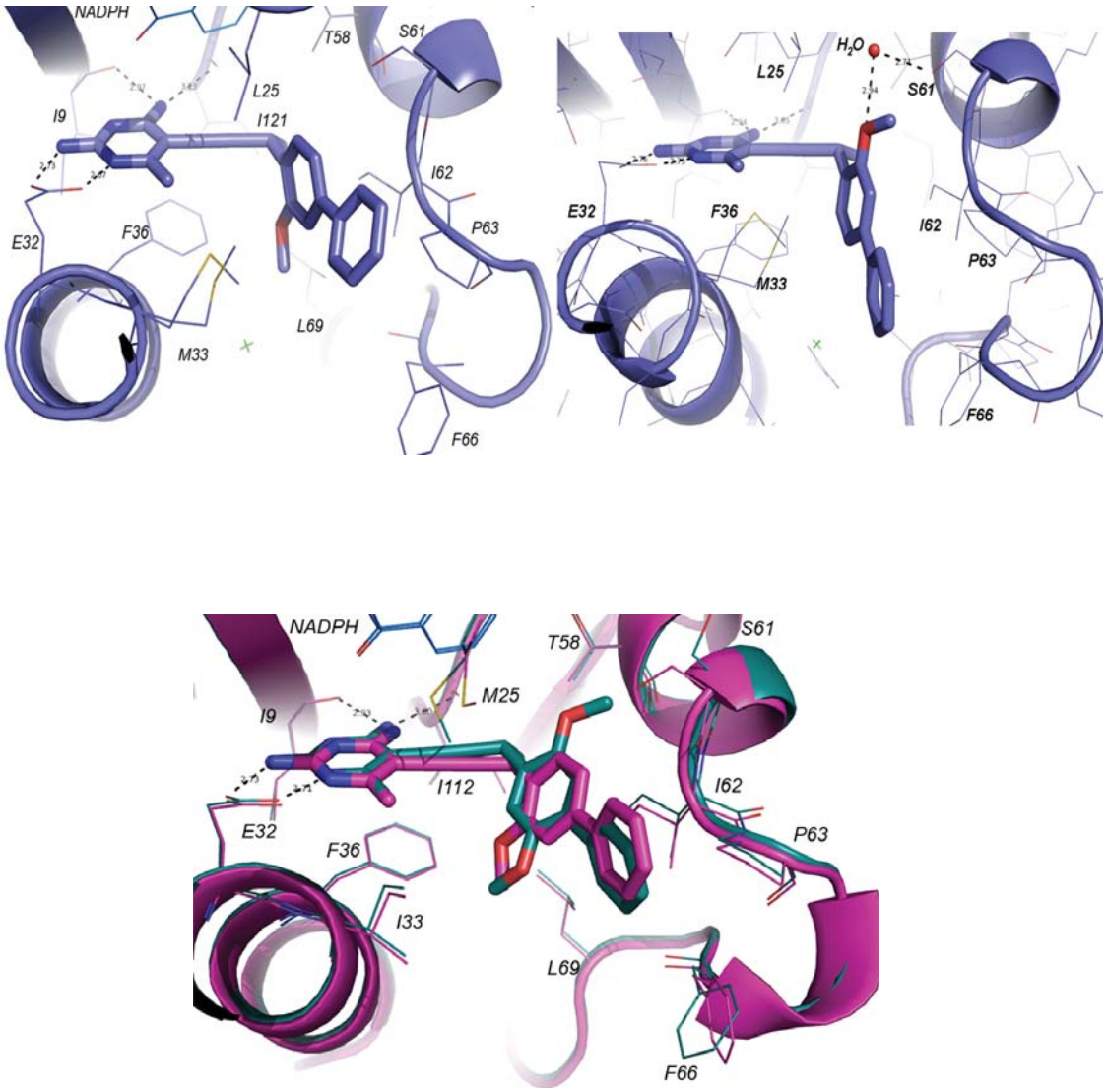

Figure 19. UCP111H crystalized with Cg DHFR in two conformations, b. Overlay of UCP111H and UCP111E in Ca DHFR

From the crystal structures of both species, it is evident that the ring C can be probed for better inhibition and potency without altering the conformations of the ligand.

4.1.2 SAR studies of para-linked antifolates

Using UCP111H as our lead compound, the C-ring was changed to reflect a variation in cLogP values. Ester, alcohol, carbamate, tolyl, pyridine, cyano derivatives were synthesized starting with the bromoketone1. Various boronic acids were coupled utilizing Suzuki coupling conditions (Scheme.22). Following the earlier route of Wittig, acid hydrolysis, Ohira Bestmann homologation and Sonogashira coupling the propargyl linked antifolates were obtained. Biological evaluation of these compounds show that the changes in the C-ring are well tolerated with the IC_{50} values of Cg DHFR varying between 6-31nm and for Ca DHFR aroung 18-64nM. Interestingly, compounds with lipophilic substitutions at C-ring

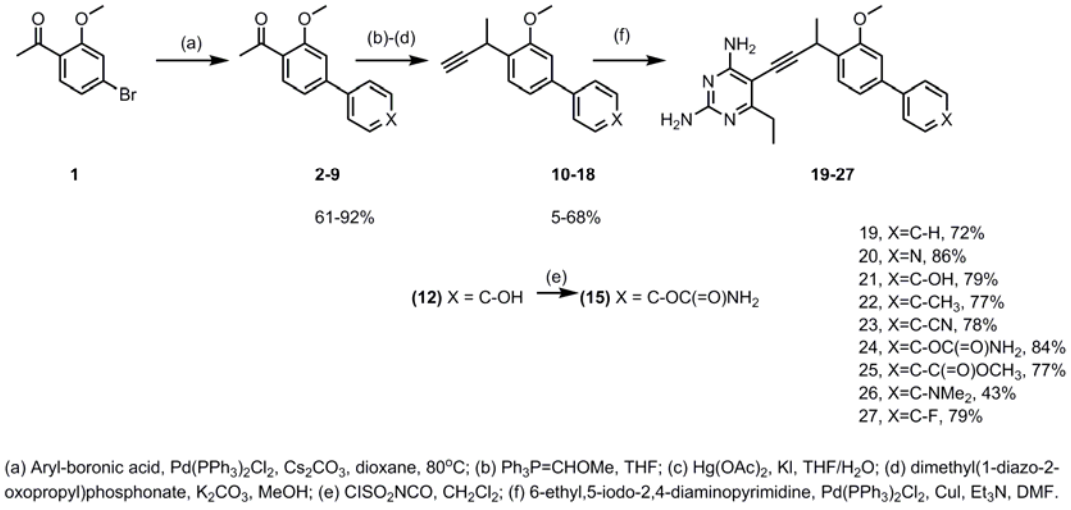

(a) Aryl-boronic acid, $Pd(PPh_3)_2Cl_2$, Cs_2CO_3, dioxane, 80°C; (b) Ph_3P=CHOMe, THF; (c) $Hg(OAc)_2$, KI, THF/H_2O; (d) dimethyl(1-diazo-2-oxopropyl)phosphonate, K_2CO_3, MeOH; (e) $ClSO_2NCO$, CH_2Cl_2; (f) 6-ethyl,5-iodo-2,4-diaminopyrimidine, $Pd(PPh_3)_2Cl_2$, CuI, Et_3N, DMF.

Scheme 22. Synthesis of para isomers of propargyl linked antifolates

exhibit significant antifungal activity against *C.albicans* with MIC values ranging from 1.8 – 7.5 µg/mL. Apart from the shape of the molecule, the hydrophobicity of the C-ring also influences the antifungal activity against *C.albicans.*

CMPD ID	COMPOUND	IC_{50} CgDHFR (nM)	IC_{50} CaDHFR (nM)	IC_{50} hDHFR (nM)	MIC *C. glabrata* (µg/mL)	MIC *C. albicans* (µg/mL)
UCP1058	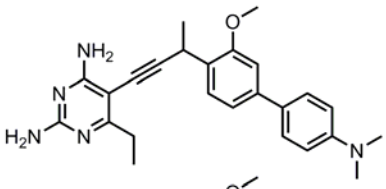	15	64	147	25	>100
UCP1045	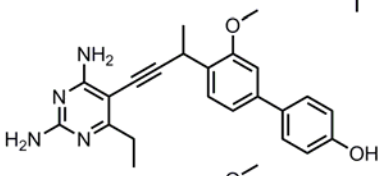	15	39	136	3.1	>100
UCP1054	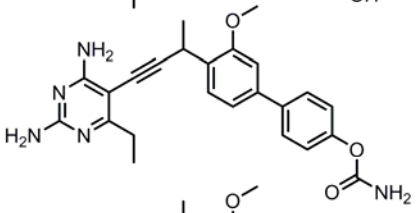	8	18	170	6.3	>100
UCP1044	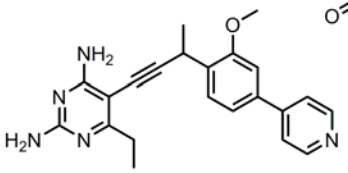	19	33	127	0.78	25

Table 21. Polar substituents in the C ring

The SAR studies also reveal two clusters of activity. In the first cluster of compounds with substituents NMe_2, endo-N, OH and CO_2NH_2, (Table.21) a significant differences in activity between the two species were observed. The compounds exhibited reasonable antifungal activity with *C.glabrata* but almost little to no activity was observed in the case of *C. albicans*, with an exception of heteroaromatic substituent **UCP1044**. Some pyridine and pyrimidine compounds were shown to exhibit antifungal

activity in efflux knockout strains[12] of *Candida albicans*. Their mechanism of action involves the inhibition of lanestrol demethylase of the pathogenic *C. albicans.*

In the second cluster of compounds consisting of hydrophobic and electron withdrawing groups, (Table.22) activity is maintained in both species.

CMPD ID	COMPOUND	IC_{50} CgDHFR (nM)	IC_{50} CaDHFR (nM)	IC_{50} hDHFR (nM)	MIC *C. glabrata* (μg/mL)	MIC *C. albicans* (μg/mL)
UCP1043	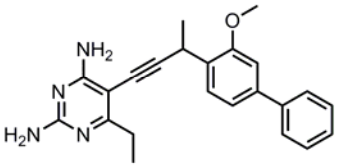	31	49	172	1.6	3.1
UCP1046	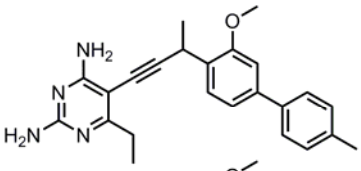	22	48	208	1.6	3.1
UCP1053	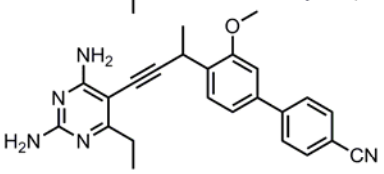	18	50	477	7.5	3.1
UCP1059	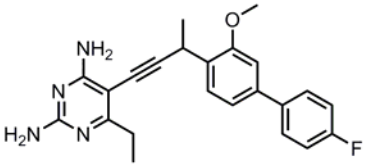	14	43	148	7.5	1.8
UCP1059	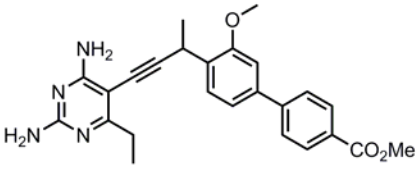	9	43	9	7.5	6.25

Table 22. Hydrophobic and electron withdrawing substituents

The hydrophobic phenyl and tolyl derivatives – **UCP1043** and **UCP1046** exhibit antifungal activity against *C.glabrata* that is relatively similar to the heteroaromatic derivative **UCP1044** belonging to the polar cluster. They suffer from a 6 fold loss in activity when electron withdrawing groups are substituted in the C-ring. Interestingly, no such drastic loss in activity is observed between hydrophobic and electron withdrawing substituents with *C.albicans* except in the case of ester derivative **UCP1059**. One of the drawbacks with the second cluster of molecules, which exhibit antifungal activity, is that their hydrophobic nature reduces the solubility of these ligands.

4.1.3 Case of META vs PARA substitution

A comparison of isomeric structures of the ligands depicts that the shape of the molecule influences the antifungal activity of both species of *Candida*. (Table.23)

CMPD ID	COMPOUND	MIC C. glabrata μg/mL	MIC C. albicans μg/mL
UCP1023	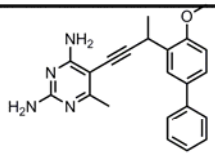	23	>100
UCP111D	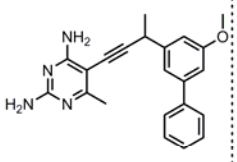	12.5	23
UCP1040	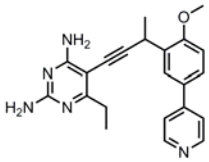	1.3	25
UCP1043	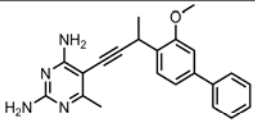	0.39	1.6
UCP111F	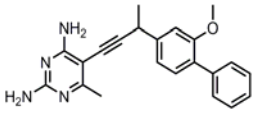	0.78	6.25
UCP1044	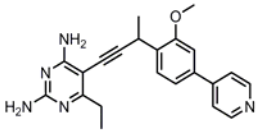	0.78	25

Table 23. Comparison of META vs PARA isomer

The para isomer seems to influence the penetrating ability of these propargyl linked antifolates. The permeability barrier of meta isomers was proven experimentally with Triton X-100 studies. Triton X- 100[13] is known to increase the membrane permeability without denaturation. When **UCP1023** or **UCP1044** were treated with 0.01% Triton X-100, the potency of the meta compounds were increased.

4.2 Lead Design and Synthesis for Dual Inhibition

The para compounds having dual inhibition are lipophilic in nature. **UCP1043** exhibited water solubility at 0.25 μg/mL in the presence of 0.02% hydroxypropyl cellulose.

CMPD ID	COMPOUND	IC_{50} CgDHFR (nM)	IC_{50} CaDHFR (nM)	IC_{50} hDHFR (nM)	MIC *C. glabrata* (μg/mL)	MIC *C. albicans* (μg/mL)
UCP1051	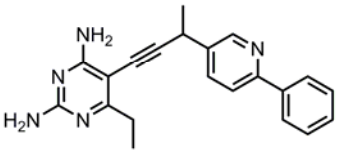	23	55	688	0.78	0.39
UCP1052	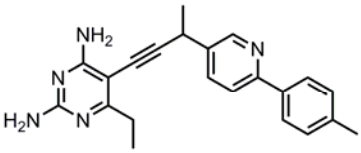	27	49	625	0.2	0.39
UCP1055	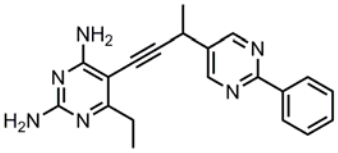	22	37	180	0.78	0.19
UCP1083	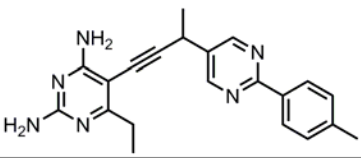	ND	ND	ND	0.6	ND

Table 24. Lead compounds with heterocyclic B-ring

To increase solubility, heteroaromatic rings (Table.24) can be incorporated into the ligands. From the SAR studies, it is evident that the C-ring has to be hydrophobic. So lead compounds were synthesized by changing the B-ring to pyridine and pyrimidine. A striking improvement in antifungal activity against both species (MIC = 0.2 – 0.78 μg/mL) was obtained. Triton X-100 experiments with **UCP1052** did not alter the antifungal activity. Compared to distal pyridines, incorporation of pyridine[14] in the B-ring did not improve the solubility of the compounds. But with the pyrimidine as the B-ring, solubility of 60 μg/mL was achieved.

4.3 Conclusions

The meta isomer of propargyl linked antifolates exhibit antifungal activity against *Candida glabrata*, while the para isomer has dual inbition for both species. Hydrophobic C-rings enhance the dual inhibition relative to the polar substitutions. Better enzyme inhibition and antifungal activity were achieved with pyridine and pyrimidine as the B-ring. The heterocyclic series also displayed better selectivity over h-DHFR along with improved solubility as in the case of **UCP1055**.

4.4 Acknowledgments

Cellular assays and enzyme inhibition studies were carried out by Dr. Janet Paulsen and Mike Lombardo of Dr. Anderson's lab. Human enzyme inhibition were evaluated by Dr. Kristen Lamb. Synthesis of compounds – **UCP1043, UCP1053,**

UCP1044 were done by Dr. Kishore Viswanathan, and **UCP1058** and **UCP1059** were done by Dr. Santosh Keshipeddy of Dr. Wright's lab.

References

1. Morrell, M.; Fraser, V.; Kollef, M. Delaying the empiric treatment of Candida bloodstream infections until positive blood culture results are obtained: a potential risk factor for hospital mortality. *Antimicrob. Agents Chemother*. 2005, 49, 3640−3645.

2. Pfaller, M.; Diekema, D. Epidemiology of invasive mycoses in North America. *Crit. Rev. Microbiol*. 2010, 36, 1−53.

3. Falagas, M.; Roussos, N.; Vardakas, K. Relative frequency of albicans and the various non-albicans Candida spp among candidemia isolates from inpatients in various parts of the world: a systematic review. *Int. J. Infect. Dis*. 2010, 14, e954−e966.

4. Borst, A.; Raimer, M.; Warnock, D.; Morrison, C.; Arthington- Skaggs, B. Rapid acquisition of stable azole resistance by Candida glabrata isolates obtained before the clinical introduction of fluconazole. *Antimicrob. Agents Chemother*. 2005, 49, 783−787.

5. Magill, S.; Shields, C.; Sears, C.; Choti, M.; Merz, W. Triazole cross-resistance among Candida spp.: case report, occurrence among bloodstream isolates, and implications for antifungal therapy. *J. Clin. Microbiol*. 2006, 44, 529−535.

6. Pfaller, M.; Castanheira, M.; Lockhart, S.; Ahlquist, A.; Messer, S.; Jones, R. Frequency of decreased susceptibility and resistance to echinocandins among fluconazole-resistant bloodstream isolates of Candida glabrata. *J. Clin. Microbiol*. 2012, 50, 1199−1203.

7. Liu, J.; Bolstad, D.; Smith, A.; Priestley, N.; Wright, D.; Anderson, A. Structure-guided development of efficacious antifungal agents targeting Candida glabrata dihydrofolate reductase. *Chem. Biol*. 2008, 15, 990−996.

8. Liu, J.; Bolstad, D.; Smith, A.; Priestley, N.; Wright, D.; Anderson, A. Probing the active site of Candida glabrata dihydrofolate reductase with high resolution crystal structures and the synthesis of new inhibitors. *Chem. Biol. Drug Des*. 2009, 73, 62−74.

9. Paulsen, J.; Viswanathan, K.; Wright, D.; Anderson, A. Structural analysis of the active sites of dihydrofolate reductase from two species of Candida uncovers ligand-induced conformational changes shared among species. *Bioorg. Med. Chem. Lett*. 2013, 23, 1279−1284.

10. Kuyper, L.; Baccanari, D.; Jones, M.; Hunter, R.; Tansik, R.; Joyner, S.; Boytos, C.; Rudolph, S.; Knick, V.; Wilson, H. R.; Caddell, J. M.; Friedman, H.; Comley, J.; Stables, J. High-affinity inhibitors of dihydrofolate reductase: antimicrobial and anticancer activities of 7,8- dialkyl-1,3-diaminopyrrolo[3,2-f]quinazolines with small molecular size. *J. Med. Chem*. 1996, 39, 892−903.

11. Otzen, T.; Wempe, E.; Kunz, B.; Bartels, R.; Lehwark-Yvetot, G.; Hansel, W.; Schaper, K.; Seydel, J. Folate-synthesizing enzyme system as target for development of inhibitors and inhibitors combinations against Candida albicans: Synthesis and biological activity of new 2,4-diaminopyrimidines and 4′-substituted 4-aminodiphenyl sulfones. *J. Med. Chem*. 2004, 47, 240−253.

12. Daniel Carcanague Ed T. Buurman, April E. Blodgett, Kenneth G. Hull and Daniel Carcanague, Pyridines and Pyrimidines Mediating Activity against an Efflux-Negative Strain of *Candida albicans* through Putative Inhibition of Lanosterol Demethylase, *Antimicrob. Agents Chemother.* 2004, 48(1):313.

13. Ziegelbauer, K.; Grusdat, G.; Schade, A.; Paffhausen, W. High throughput assay to detect compounds that enhance the proton permeability of Candida albicans membranes. *Biosci. Biotechnol. Biochem*. 1999, 63, 1246−1252.

14. G-Dayanandan, N.; Paulsen, J.; Viswanathan, K.; Keshipeddy, S.; Lombardo, M.; Zhou, W.; Lamb, K.; Sochia, A.; Alverson, J.; Priestley, N. et al. Propargyl-Linked Antifolates are Dual Inhibitors of Candida albicans and Candida glabrata. *J. Med. Chem.* 2014, *57*, 2643-2656.

CHAPTER 5

Antifolates for gram negative pathogens

Introduction

Resistance of antibiotics to gram negative pathogens is increasing at an alarming rate. The gram negative bacteria differ from the gram positive species by their specialized outer membrane. This is one of the manifestations of an intrinsic resistance apart from the efflux pumps. Intrinsic resistance is not brought about by drug pressure or horizontal gene transfer.

5.1 Outer membrane of gram negative species

In addition to the peptidoglycan layer – a constituent of gram positive bacteria, the gram negative species has an asymmetric bi-layered[1] outer membrane (Fig.20). It is made up of an outer leaflet of lipopolysaccharides (LPS) and an inner leaflet of phospholipids (PL).

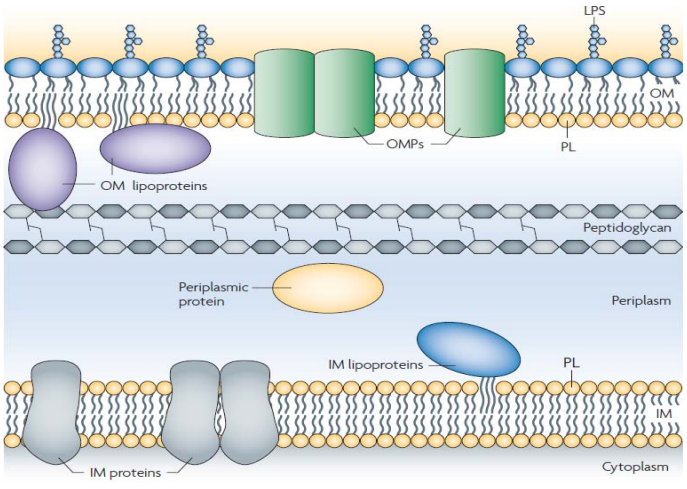

Figure 20. Outermembrane of gram negative bacteria

Reproduced from *Nat Rev Micro* 2009, *7*, 677-683

The LPS layer consists[2] of three domains – (1) lipid A connected to the (2) core oligosaccharide which is linked to (3) long polysaccharide - O-antigen (Fig.21). This layered arrangement makes it amphiphilic carrying a net negative charge. The fatty acid chain of the lipid A region acts as a secondary barrier to hydrophobic molecules. The saturated lipid chains originating from a single head group, and the phosphate groups are held together laterally by Mg^{2+}

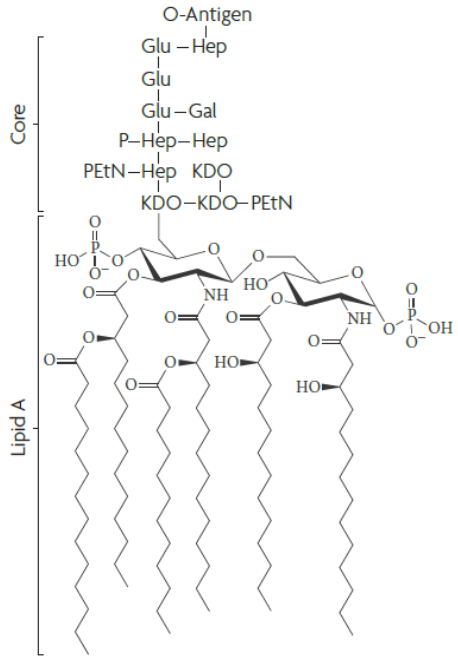

Figure 21. LPS layer of E.coli. Reproduced from *Nat Rev Micro* 2009, *7*, 677-683

and Ca^{2+} ions[3] enabling it to pack tightly and hence reduce fluidity. This prevents the hydrophobic molecules from partitioning into the inner core of the LPS layer and thereby slowing down the diffusion of lipophilic molecules into the cytoplasm. The membrane permeability also acts as a barrier for the pathogens to accumulate nutrients. They

overcome the permeability by having small outer membrane proteins called porins. Though the porins can serve as a conduit for hydrophilic antibiotics, then act as sieves filtering out drug molecules based on size[4], charge[5] and hydrophobicity. In response to influx of hydrophilic antibiotics, porins undergo mutation[6] differing in pore size, quantity and channel blockers, imparting resistance.

5.2 Efflux pumps

Another mode of intrinsic resistance exhibited by pathogenic bacteria is the presence of efflux pumps. Efflux pumps[7,8,9] tend to flush out the antibiotics utilizing a complex assembly of transporters.

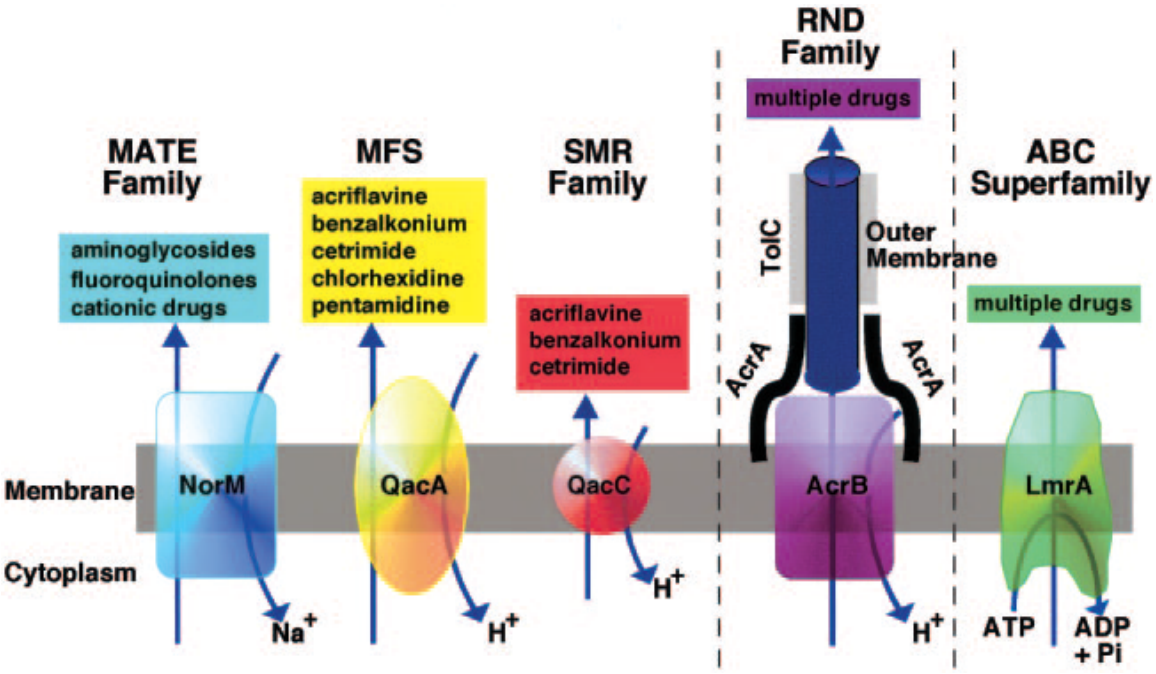

Figure 22. Different classes of efflux pumps. Reproduced from Clin. Microbio.Rev. 2006, 19, 382

Efflux reduces the accumulation of exogenous ligands inside the cell and thereby increases the survival of the pathogens. The efflux pumps can be encoded genetically or acquired through plasmids. Five families of efflux systems have been found: (Fig.22) (1) multidrug and toxic compound extrusion (MATE), (2) major facilitator superfamily (MFS), (3) staphylococcal multiresistance (SMR), (4) resistance nodulation divison (RND) and (5) ATP binding cassette (ABC) transporters.

The resistance nodulation division (RND) constitute major efflux systems imparting resistance and virulence to *Escherichia coli* and *Klebsiella pneumoniae*. The RND efflux pump is a tripartite system consisting of AcrA in the periplasmic space, AcrB in the cytoplasm region and TolC in the outer membrane. All the three components assemble together to pump out the antibiotics. The RND pumps use proton motive force (PMF) to establish efflux along a concentration gradient. They are also known as proton antiporters, exchanging one H^+ for one drug molecule. The RND efflux pump specificity is very broad extruding cationic, neutral and anionic species very efficiently. In order to overcome the efflux pump, two strategies can be employed – (1) design of antibiotics that are not substrates for the pump, (2) design of efflux pump inhibitors (EPI) [10] that can potentiate the activity of existing antibiotics. The examples of existing EPI (Fig 5.4) include phenylalanyl arginyl –β napthylamide (PAβN) [11], carbonyl cyanide m-chloropheylhydrazone (CCCP), quinolones and arylpiperzines. PAβN has been implicated to permeabilize the membrane at certain concentrations.[12]None of the EPI have been approved for clinical use yet.

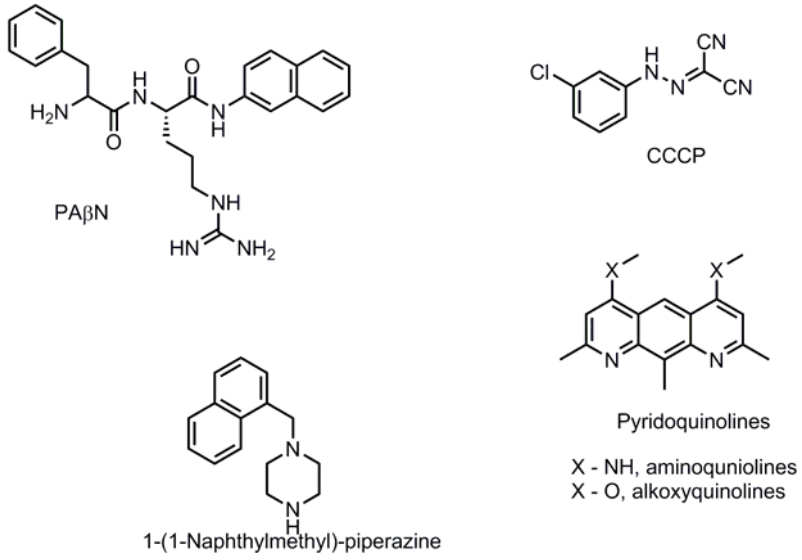

Figure 23. Efflux pump inhibitors

5.3 DHFR as drug target for gram negative pathogens

DHFR is a validated drug target for the treatment of gram negative infections. Trimethoprim-sulfamethaoxazole (TMP-SMX Bactrim) targeting the DHFR and dihydropteroate synthase DHPS enzymes is the only choice of clinically approved drugs of the folate pathway. A slow rise in resistance is observed for TMP-SMX[13-15] in Enterobacteriaceae strains. Resistance is normally acquired through the acquisition[16-18] of TMP-insensitive DHFR. This necessitated the need for potent compounds to overcome resistance.

5.3.1. Screening of antifolate libraries

Initially, existing library of compounds (Table.25) were screened to assess the potency and inhibition of antifolates for both *Klebsiella pneumoniae* and *Escherichia coli*.

CMPD ID	COMPOUND	*Klebsiella pneumoniae* Kp10031		*Escherichia coli* Ec25922	
		IC_{50} (nM)	MIC(μg/mL)	IC_{50} (nM)	MIC (μg/mL)
TMP	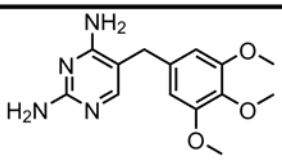	106	0.078	20	0.31
UCP 1113D5M	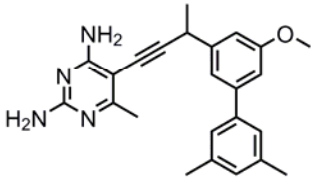	15	5	ND	15
UCP 1006	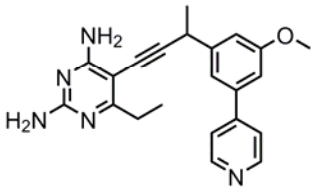	16	1.25	ND	16
UCP 1003	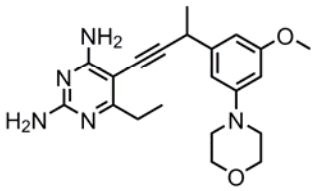	ND	10	ND	>20
UCP 1038	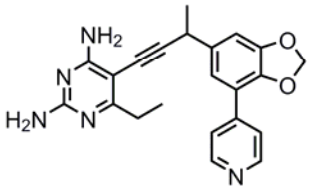	16	0.3	ND	3.1
UCP 1037	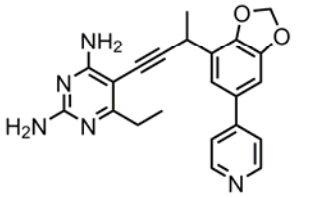	ND	2.5	ND	12.5

Table 25. Screening of antifolate library of compounds

CMPD ID	COMPOUND	*Klebsiella pneumoniae* Kp10031		*Escherichia coli* Ec25922	
		IC_{50} (nM)	MIC (μg/mL)	IC_{50} (nM)	MIC (μg/mL)
TMP	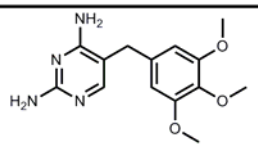	106	0.078	20	0.31
UCP 1045	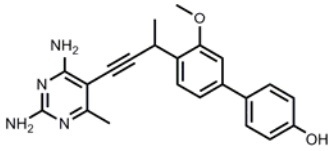	ND	5	ND	6.25
UCP 1054	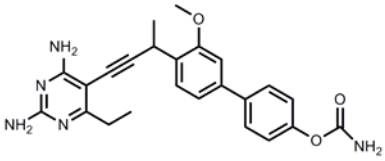	ND	1.25	ND	3.1
UCP 1044	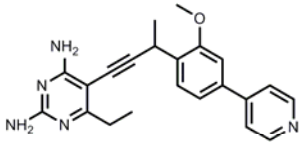	ND	10	ND	6.25
UCP 1043	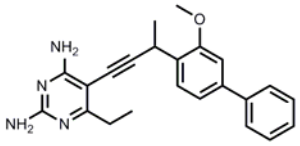	ND	ND	ND	>100
UCP 1051	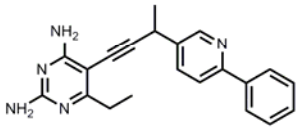	ND	ND	ND	25

Table 26. Influence of para isomers for antibacterial activity

It is evident from the comparison of **UCP1113D5M** and **UCP1006** that the heterocyclic moiety has better potency than the hydrophobic analog. Also the heteroaromatic analog exhibits a 10-fold greater potency over the saturated heterocycle **UCP1003**. **UCP1038** with the benzodioxole moiety shows good potency against *K.pneumoniae* and *E.coli* compared to other antifolate analogs except TMP, in spite of its low nanomolar enzyme inhibition of *K.pneumoniae.*

The other chemotype – para isomers of antifolates (Table.26), were also screened to see if they exhibit the membrane permeabilizing effect as observed with fungal pathogens. Similar to the meta isomer, the hydrophobic C-ring is not well tolerated. An interesting feature of para isomers is that the MIC values for both species are relatively close, compared to the meta isomer.

5.4 New inhibitors of antifolates for gram negative pathogens

Based on the screening, compounds were designed to utilize both chemotypes of meta and para isomer. Both the isomers were substituted with hydrophilic groups in the B and C-ring to exploit the presence of porins. Synthesis of compounds were carried out using the procedures described in chapter 2.

5.4.1 Para isomers

In the para series, the B-ring was switched to pyridine and pyrimidine (Table.27). The bottom C -ring was substituted with pyridine and piperazine to increase the polarity of the compounds. **UCP1087** with the piperazine C-ring was not active, consistent with the screening results. The para bipyridine analog showed good potency and enzyme

inhibiton against Kp but the activity did not translate to clinical strains with MIC values >50. Its activity was potentiated by the use of PaβN exhibiting a MIC value of 0.781 μg/mL, suggesting permeability or efflux issues.

CMPD ID	COMPOUND	*Klebsiella pneumoniae* Kp10031		*Escherichia coli* Ec25922	
		IC_{50} (nM)	MIC (μg/mL)	IC_{50} (nM)	MIC (μg/mL)
TMP	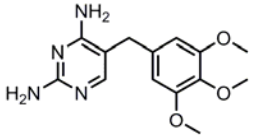	106	0.078	20	0.31
UCP 1087	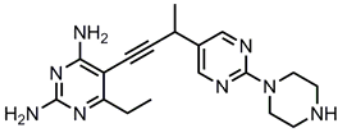	ND	>20	ND	>20
UCP 1093	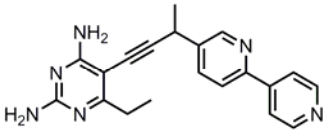	16	0.156	ND	20

Table 27. Antibacterial activity of polar para compounds

5.4.2 Meta isomers

Since the para isomers were exhibiting possible efflux activity, meta isomers were synthesized by changing the C-ring to more polar groups (Table.28). The anisole as the top B-ring was selected to impart hydrophobicity to the ligand, as the more hydrophilic ligands were extruded. When the C-ring was substituted with aminopyrimidine, activity of 1.25 μg/mL was achieved in the test strain, but these compounds lacked potency with the clinically resistant strain.

CMPD ID	COMPOUND	*Klebsiella pneumoniae*			
		Kp10031 MIC(μg/mL)	UCHC Kp3 MIC (μg/mL)	+ PAβN MIC (μg/mL)	Fold change
TMP	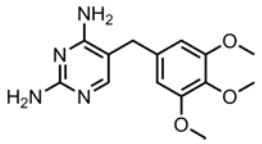	0.078	0.156	20	0.31
UCP 1090	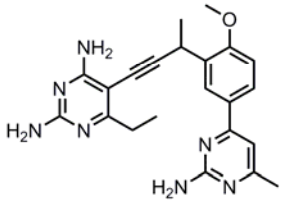	1.25	>50	20	>2.5
UCP 1084	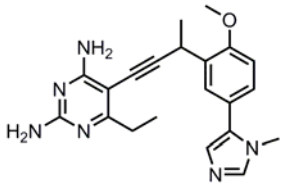	0.31	25	0.6	42
UCP 1091	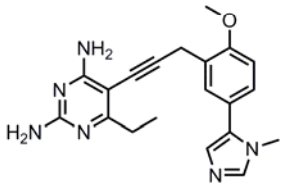	0.625	50	10	5
UCP 1092	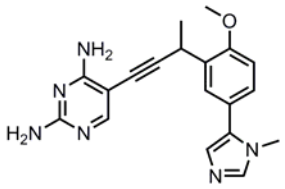	2.5	>50	20	>2.5
UCP 1101	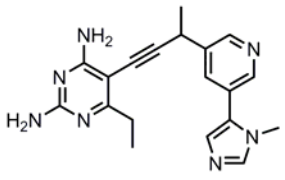	0.62	>50	20	>2.5

Table 28. Antibacterial activity of polar meta compounds

Another approach to increase the polarity of the C-ring was to reduce the ring size to 5-membered heteroaromatics. N-methylimidazole with a pKa of ~7 was chosen as the C-ring. **UCP1084** was potent against the test strain and also exhibited a reasonable potency against the clinical strains relative to other analogs. SAR was performed on **UCP1084** by removing some of the methyl groups to understand the effect on efflux. Though **UCP1091** without the propargylic methyl had the lowest fold change in terms of efflux activity, it lost its potency against the clinical strain. **UCP1092** and **UCP1101** were similar in activity to **UCP1090**. The efflux activity has been a recurring issue with both meta and para isomers. The benzodioxole scaffold **UCP1038** that exhibited potent activity against the test strain was screened against the resistant pathogenic strains. **UCP1038** turned out to be the best lead compound (Table.29) against the clinical isolates.

CMPD ID	COMPOUND	Kp IC50 (nM)	10031 MIC (μg/mL)	UCHC Kp1 MIC (μg/mL)	UCHC Kp2 MIC (μg/mL)	UCHC Kp3 MIC (μg/mL)	Ec25922 MIC (μg/mL)
TMP	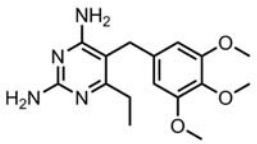	106	0.078	>20	2.5	0.156	0.31
UCP 1038	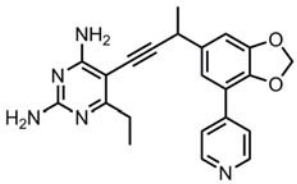	171	0.625	>20	5	6.25	3.125

Table 29. Influence of 1,3 benzodioxole on clinical isolates

5.4.3. Dioxolane series

Efforts were directed towards synthesizing more analogs of the dioxolane series to gain an understanding of the efflux pumps. Benzodioxole have been shown to exhibit efflux pump inhibitory activity against NOR efflux pumps of *Staphylococcus aureus*. With benzodioxole as the B-ring, the C-ring was substituted with heterocycles of varying pKa values for identifying any correlation with efflux activity (Table.30). Pyrimidine, N-methyl imidazole and thiazole were substituted for pyridine as the C-ring. The pKa value was calculated using Chemaxon software, while the logP and totat polar surface area (TPSA) were calculated using Molinspiration software. The cellular assay were carried out on *E.coli*. The control strain used is the ATCC Ec 25922, while JWO451 is an acrB efflux pump knock out strain, and BW25113 is the control stain for JW0451. Fold change was calculated from the ratio of BW25113 to JW0451. The pyrimidine substitution had the lowest pKa and lacked potency in both the control stains. Imidazole with a pKa of 2.7 had better activity in both the control strains relative to pyrimidine, but the efflux ratio was similar to pyrimidine. The thiazole moiety had the most potent activity in the series close to pyridine, but the efflux ratio was twice that of **UCP1038**. Efflux is still the dominant mode of resistance for the dioxolane series. More substrates in the dioxolane series are required to cull out the relationship between efflux pump and the ligand properties.

CMPD ID	COMPOUND	Ec25922 (μg/mL)	BW25113 (μg/mL)	JW0451 (μg/mL)	Fold change	pKa	TPSA	LogP
UCP 1038	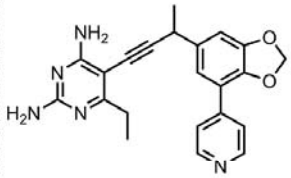	3.125	2.5	0.3125	8	4.55	109.19	3.5
UCP 1067	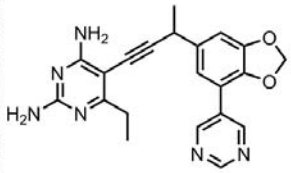	20	20	0.625	32	1.09	122.08	3.0
UCP 1102	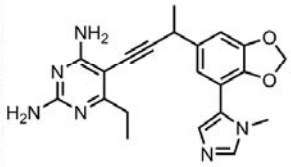	6.25	5	0.156	32	6.15	114.12	2.7
UCP 1137	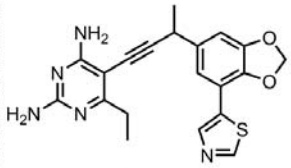	2.5	2.5	0.156	16	2.56	109.19	3.8

Table 30. Changing the C-ring in the dioxolane series

5.5 New pharmacophore

The propargyl linked antifolates were always built with B and C-rings coupled to the diaminopyrimidine through a propargylic linker. Though steady progress is being made to gain potency with the current pharmacophore, a new structural motif could provide the necessary breakthrough. The idea of using tropolones as the B-ring, while the diaminopyrimdine with the propargyl linker stays intact was conceived. The logic behind the use of tropolones is because of its metal chelating ability. The tropolone motif may

work by chelating the outer membrane ions Mg^{2+}/Ca^{2+}, and potentially gaining access to the periplasm. It could also potentiate the activity of the carbapenems by scavenging off the Zn^{2+} ions that are important for metallo-β lactamases to deactivate carbepenems. Finally with the diaminopyrimdine as the A-ring, it can anchor to the active site of DHFR, thereby acting as an antifolate.

5.5.1. Synthesis of tropolone antifolate

Tropolone was converted to methoxy under standard conitions (Scheme.23), followed by bromination with NBS. The next step was to synthesize the alkynol so that the methylation/ deoxygenation strategy can be utilized. Unfortunately, with Grignard and n-butyl-lithium reagents, ring contracted phenyl substituted products are obtained.

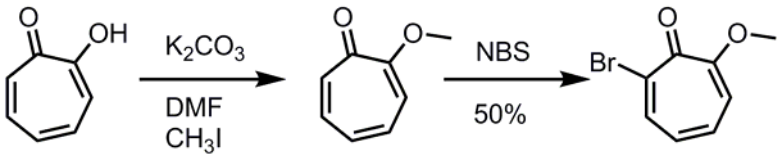

Scheme 23. Synthesis of bromo tropolones

So the coupling chemistry (Scheme.24) was utilized to overcome the limitations of metal exchange reactions. Stille coupling with vinyl ester stannane was carried out, followed by hydrogenation of the allyl ester.

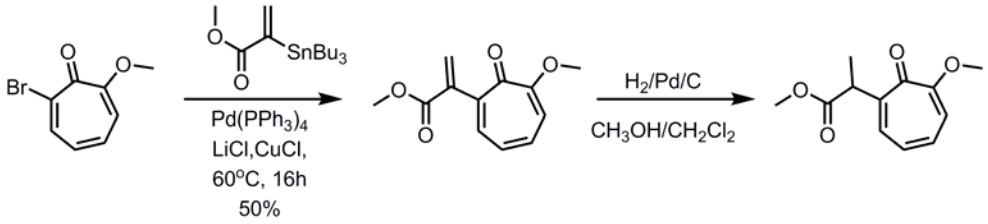

Scheme 24. Synthesis of homologated ester of tropolones

Further reactions of reduction, Ohira Bestmann homologation and Sonogshira coupling with diamino iodopyrimdine are to be carried out in the future.

5.6 Conclusions

Compounds that are active against the test strain for *Klebsiella* were designed and synthesized. Dioxolane series of compounds exhibit good potency against *Escherichia coli* strains. The benzodioxole moieties are less susceptible to efflux compared to the other pharmacophore. Efforts are directed towards reducing the efflux activity in dioxolane compounds and also new pharmacophores are being synthesized to gain activity with the gram negative pathogens.

5.7 Acknowledgements

The screening of antifolates and cellular assay for new compounds were carried out by Mike Lombardo of Dr. Anderson's lab.

References

1. Nikaido,H. Prevention of drug access to bacterial targets: permeability barrier and active efflux, *Science*, 1994, 264, 382 – 388.

2. Christian R. H. Raetz1 and Chris Whitfield, Lipopolysaccharide Endotoxins, *Annu.Rev.Biochem*, 2002, 71, 635-700.

3. Schindler, M.; Osborn, M.J. Interaction of Divalent Cations and Polymyxin B with Lipopolysaccharide, *Biochemistry*, 1979, 18, 20, 4425-4430.

4. Decad, G.M.; Nikaido, H. Outer membrane of gram-negative bacteria, XII. Molecular-sieving function of cell wall, *J. Bacteriol*. 1976, 128, 325–336

5. Nikaido, H., Rosenberg, E.Y., Foulds, J. Porin channels in Escherichia coli: studies with beta-lactams in intact cells, *J. Bacteriol*. 1983,153, 232–240.

6. Pagès, J.; James, C.; Winterhalter, M. The porin and the permeating antibiotic: a selective diffusion barrier in Gram-negative bacteria. *Nat Rev Micro* 2008, *6*, 893-903.

7. Laura J. V. Piddock, Clinically Relevant Chromosomally Encoded Multidrug Resistance Efflux Pumps in Bacteria, *Clin. Microbiol. Rev.* 2006, 19(2):382

8. Blair, J.; Piddock, L. Structure, function and inhibition of RND efflux pumps in Gram-negative bacteria: an update. *Curr. Opin. Microbiol.* 2009, *12*, 512-519.

9. Kourtesi, C. Microbial Efflux Systems and Inhibitors: Approaches to Drug Discovery and the Challenge of Clinical Implementation. *TOMICROJ* 2013, *7*, 34-52.

10. Pagès, J.; Masi, M.; Barbe, J. Inhibitors of efflux pumps in Gram-negative bacteria. *Trends Mol. Med.* 2005, *11*, 382-389.

11. Renau, T.; Léger, R.; Flamme, E.; Sangalang, J.; She, M.; Yen, R.; Gannon, C.; Griffith, D.; Chamberland, S.; Lomovskaya, O. et al. Inhibitors of Efflux Pumps in Pseudomonas a eruginosa Potentiate the Activity of the Fluoroquinolone Antibacterial Levofloxacin. *J. Med. Chem.* 1999, *42*, 4928-4931.

12. Lamers, R.; Cavallari, J.; Burrows, L. The Efflux Inhibitor Phenylalanine-Arginine Beta-Naphthylamide (PAβN) Permeabilizes the Outer Membrane of Gram-Negative Bacteria. *PLoS ONE* 2013, *8*, e60666.

13. Tsay, R.; Siu, L.; Fung, C.; Chang, F. Characteristics of bacteremia between community-acquired and nosocomial Klebsiella pneumoniae infection: risk factor for mortality and the impact of capsular serotypes as a herald for community-acquired infection. *Arch. Intern. Med*. 2002, 162, 1021-1027.

14. Zhanel, G.; Karlowsky, J.; Harding, G.; Carrie, A.; Mazzulli, T.; Low, D.; Group, T.; Hoban, D. A Canadian National Surveillance Study of Urinary Tract Isolates from Outpatients: Comparison of the Activities of Trimethoprim-sulfamethoxazole, ampicillin, mecillinam, nitrofurantoin and ciprofloxacin. *Antimicrob. Agents Chemother*. 2000, 44, 1089-1092.

15. García García, M.; Muñoz Bellido, J.; García Rodríguez, J. In Vitro Susceptibility of Community-Acquired Urinary Tract Pathogens to Commonly Used Antimicrobial Agents in Spain: a Comparative Multicenter Study (2002-2004). *J. Chemother.* 2007, *19*, 263-270.

16. Blahna, M. The role of horizontal gene transfer in the spread of trimethoprim-sulfamethoxazole resistance among uropathogenic Escherichia coli in Europe and Canada. *J.Antimicrob. Chemother.* 2006, *57*, 666-672.

17. Brolund, A.; Sundqvist, M.; Kahlmeter, G.; Grape, M. Molecular Characterisation of Trimethoprim Resistance in Escherichia coli and Klebsiella pneumoniae during a Two Year Intervention on Trimethoprim Use. *PLoS ONE* 2010, *5*, e9233.

18. Seputiene, V.; Povilonis, J.; Ruzauskas, M.; Pavilonis, A.; Suziedeliene, E. Prevalence of trimethoprim resistance genes in Escherichia coli isolates of human and animal origin in Lithuania. *J. Med. Microbiol.* 2009, *59*, 315-322.

CHAPTER 6

Tandem metathesis to synthesize the Spirocyclic core of Cylopamine

Introduction

Cyclopamine is a steroidal alkaloid extracted from corn lily (*Veratrum californicum*). When pregnant ewes grazed upon these corn lily, the offspring developed a condition[1-3] called cyclopia. Cyclopia is characterized by lack of differentiation of the brain frontal lobes into left and right hemishperes resulting in a fused nasal chamber with the eye in the middle. The other teratogenic alkaloids (Fig.24) include jervine and glucosylcyclopamine (cycloposine).

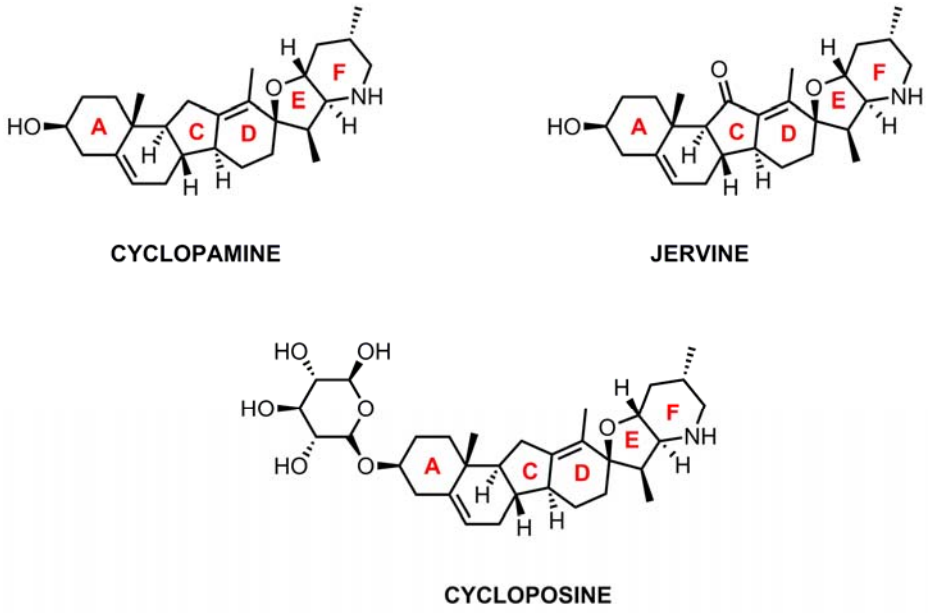

Figure 24. Teratogenic alkaloids

Beechey et al identified the seven transmembered receptor - Smoothened (Smo) of the Hedgehog (Hh) signaling pathway as the target[4] for cyclopamine. They also found that the binding of cyclopamine[5] to Smo effectively reverses the oncogenic mutations by balancing the active and inactive form of smoothened receptor.

6.1 Hedgehog Signaling Pathway

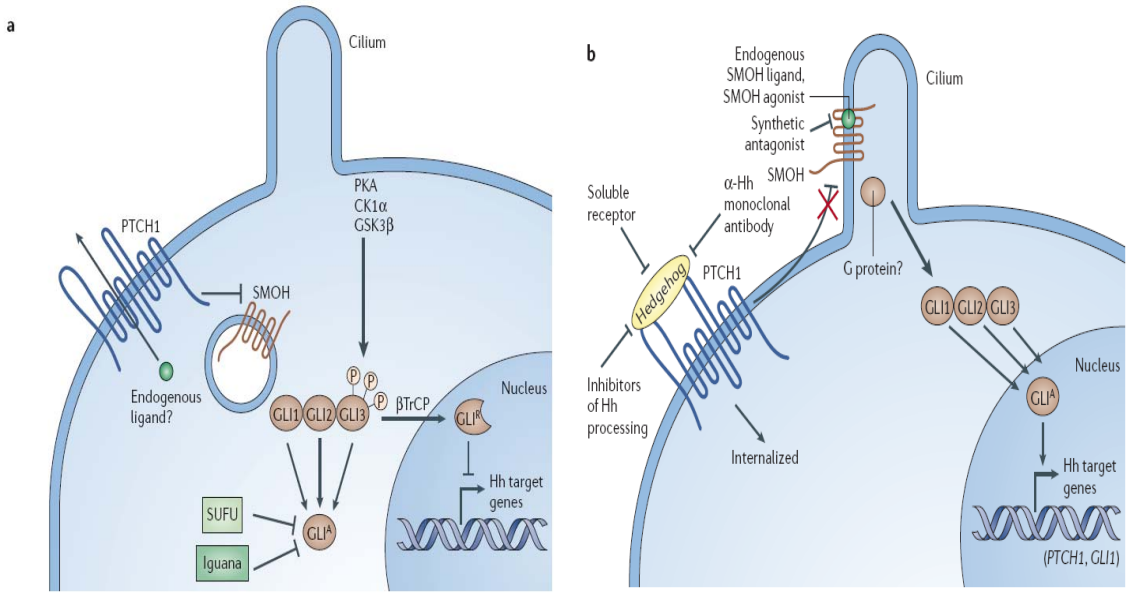

Figure 25. Hedgehog signaling pathway a. In the absence of Hedgehog ligand, b. In the presence of Hedgehog ligand

The components of the Hh signaling pathway consists[6] of Hh ligands (Fig.25) [Sonic Hh (SHh), Indian Hh(IHh) and Desert HH(DHh)], 12 transmembered patched (Ptch) receptor[7], transmembered Smoothened (Smo) receptor and glioma (Gli) associated oncogene family of zinc-finger transcription factors. The Hh signaling is activated by the

binding of the Hh ligands onto the Ptch membrane. The binding relieves the inhibition of Smo by Ptch, which translocate to the cell surface activated by an endogenous ligand. The translocation of Smo leads to downstream activation of Gli^A which in turn stimulates the production of Hh target genes in the nucleus. This cascade signaling pathway is usually active during embryogenesis for tissue growth and differentiation. In adults, the pathway is activated by tissue damage stimulating tissue repair, otherwise it remains dormant. The dormant state of the pathway is characterized by the absence of Hh ligand to activate the Ptch membrane. Inactivation of Ptch leads to internalization of Smo caused by the inhibition of Ptch. This leads to repressor form of Gli-G^R being active and hence the Hh gene activation is stalled.

6.2 Hedgehog signaling in cancer

The aberrant signaling of Hh pathway has been implicated in several forms of cancer7, most notably in basal cell carcinoma (BCC) and medulloblastoma. In the case of BCC, mutations in Ptch and Smo genes lead to cell proliferation. Mutation in Ptch relieves the suppression of Smo and alteration with Smo genes leads to decreased susceptibility towards Ptch.

Medullablastoma affecting the cerebellum of young adults is due to the mutation in Ptch gene accounting for 10% of the population while a majority of the mutation occurs in the REN gene responsible for neuroblast differentiation during embryonic stages. Apart from the above two malignancy, irregular Hh signaling is also responsible for Small Cell Lung Carcinoma (SCLC), colon, pancreatic and prostate cancer.

6.3 Synthesis of Cyclopamine and its derivatives

Even though the cyclopamine inhibits the Smo with an EC_{50} of 300 nm, the clinical use of the steroidal alkaloid has been hampered by its low availability. Keeler's extraction[9] from the roots of veratrum californicum yielded 320mg of cyclopamine per kg of dried roots. Cooper et al achieved an overall yield[10] of 0.13% by Soxhlet extraction from corn lily and recrystallization. Apart from the small molecule antognists[8] developed for Hh pathway, total synthesis of cyclopamine have always captured the imagination of organic chemists. Keeler synthesized cyclopamine from jervine9 by Wolf Kishner reduction, while a formal synthesis was carried out by Masamune[11] to build jervine and eventually using Keeler's protocol to get the cyclopamine. A semisynthetic total synthesis[12] was carried out by Giannis et al who achieved an overall yield of 1% over 20 steps.

Other limitations of cyclopamine are its low solubility – 5 µg/mL at pH, cytotoxic at concentrations greater than 10µM coupled with its instability in acidic medium (Scheme.25). At low pH, the tetrahydrofuran E ring opens up followed by aromatization of the D ring to form veratramine. Veratramine does not exhibit any antiproliferative activity against Smo.

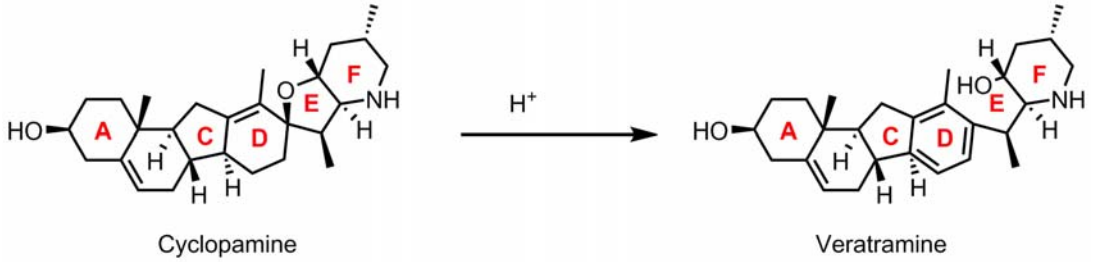

Scheme 25. Acid labile cyclopamine

To overcome the above constraints, several modifications to cyclopamine have been carried out. Taipale et al 5 synthesized 3-keto, N-aminoethyl aminocaproyl dihydrocinnamoyl cycloamine (KAAD – cyclopamine) which became more potent exhibiting an IC_{50} of 20 nm. Srinivas et al synthesized a targeted delivery of cyclopamine prodrug against prostate cancer, by functionalizing the amine of the alkaloid with a peptide specific to prostate[13] specific antigen. Similar functionalization of the secondary amine was carried out with carbohydrates[14] that had improved potency against lung cancer cell line.

In an effort to overcome the acid liability, researchers at Infinity pharmaceuticals[15] (Fig.26) developed an expanded seven membered D ring through a chemoselective cycloproponation and acid catalyzed rearrangement. This strategy reduces the hydrolysis of tetrahydrofuran ring mediated by allylic ether reactivity. With improved stability of the E-ring, they modified the A-ring to exhibit better pharmacokinetic properties[16] resulting in the synthesis of IPI-926. Another method to

improve the stability of cyclopamine at low pH was carried out by Giannis[17] et al who installed an exocyclic methylene group on the D-ring.

Efforts to improve the metabolic stability was also accomplished by Winkler et al who designed an estrone[18] based simplified analog of cyclopamine having potency similar to the natural product at 10 μM. SAR studies[19] were carried out on the estrone analog which was further refined from the aromatic pyridine to the saturated piperidine [20] analog.

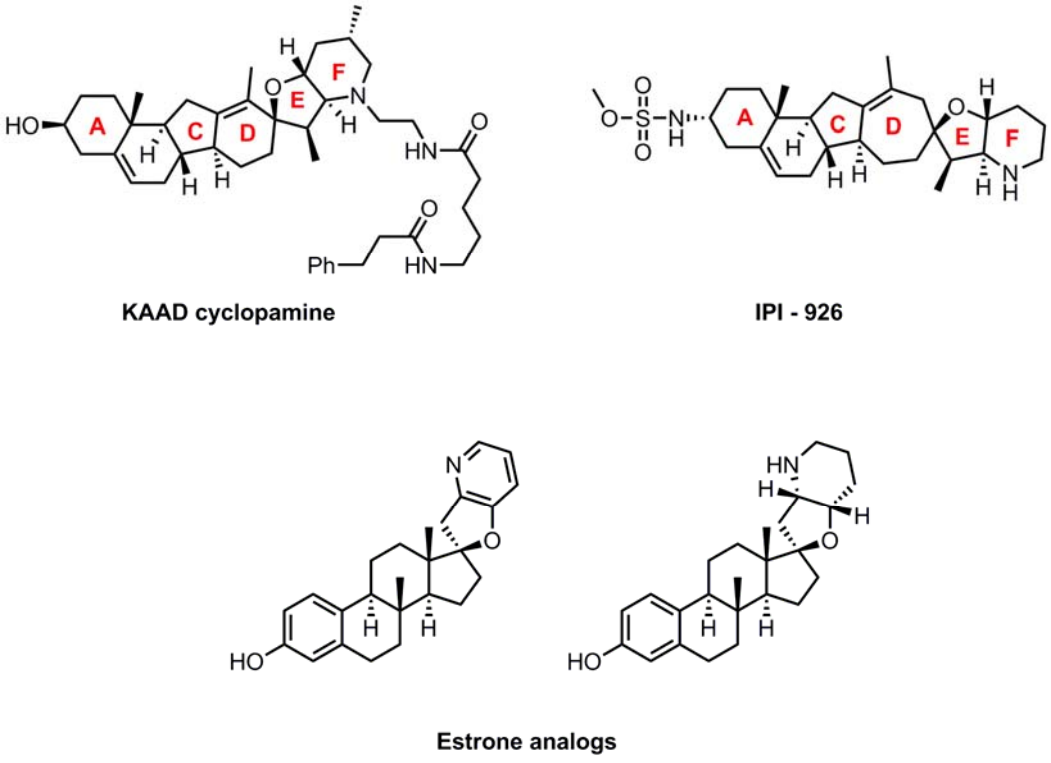

Figure 26. Analogs of cyclopamine

Encouraged by the potent inhibitory activity of the cyclopamine analogs, an attempt has been made to explore the synthesis of DEF-ring fragment of the alkaloid in the shortest possible route.

6.4 Retrosynthesis of Cylopamine

Cycloapamine can be assembled by convergent synthesis from the union of fragments 1 and 2 and eventual formation of cyclopentyl C-ring (Scheme.26). It was envisioned that the DEF-rings of fragment 2 can be built from a highly substituted oxabicyclic core through a tandem ring opening/closing metathesis reaction. The bicycloheptadiene moiety 3 can be obtained by Diels alder reaction between substituted furan 4 and an appropriate dienophile.

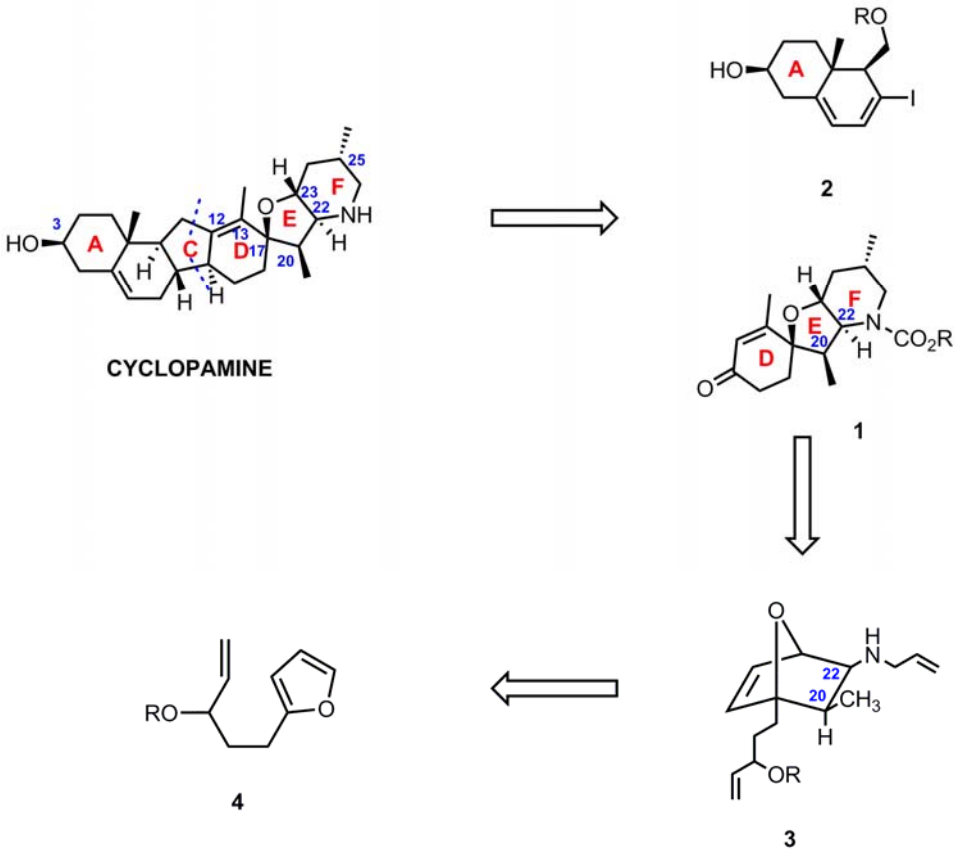

Scheme 26. Retrosynthesis of cyclopamine

6.5 Synthesis of DEF fragment

The starting precursor 5 was obtained by the lithiation of furan and quenching the reaction with 1-bromopentene to give 2-pentenyl furan. When the substituted furan was treated thermally with methylpropiolate, no Diels Alder product was obtained. But in the presence of Lewis acids[21] Me_2AlCl or $MeAlCl_2$, phenolic product 7 was obtained from the in-situ cleavage of bridged Diels Alder adduct 6. In order to increase the reactivity of Diels Alder reaction, a deactivated dienophile was required. Bromopropiolate was obtained by the NBS mediated bromination of methylpropiolate[22], catalyzed by $AgNO_3$. Subsequently, Diels Alder reaction between bromopropiolate (Scheme.27) and 2-methylfuran gave a highly selective oxabicyclo[2.2.1]heptadiene 8a in high yields with negligible amount of the undesired regioisomer 8b.

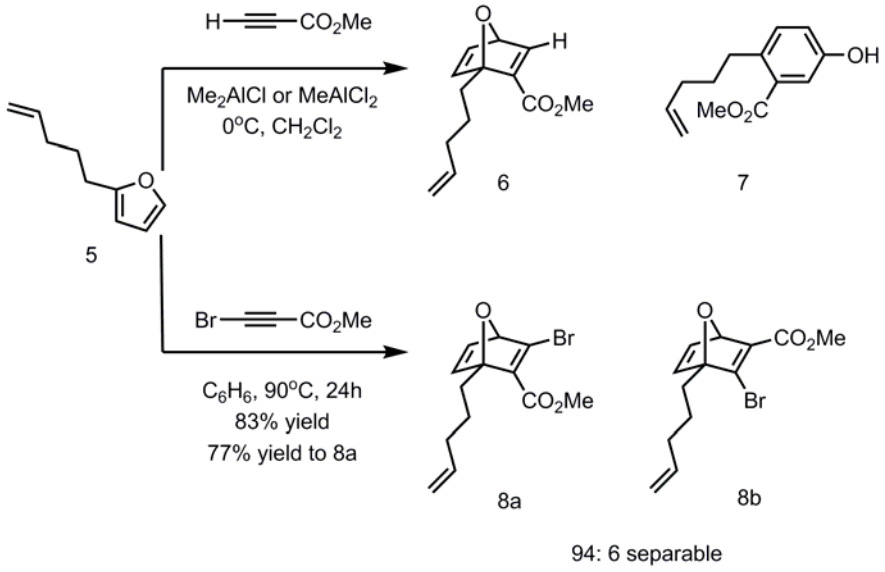

Scheme 27. Diels Alder reaction with 2-pentenyl furan

The oxabicyclo adduct 8a was subjected to substitution with amine nucleophiles to install the C-22 side chain. A double substitution of the amine was observed, possibly to relieve the strain of the two sp^2 centers of bromoenoate bicyclic adduct. To overcome the redundant double addition, reduction of β-bromide was investigated. The cyclic adduct 8b was subjected to zinc-silver couple[23,24] reduction reaction in a buffered solution (Scheme.28). This generated the Michael acceptor 6 which was very unstable.

Fortunately a one pot reaction was devised to carry out the Zn-Ag couple mediated dehalogenation followed by allylamine addition in situ to give the adduct 9 as a single diastereomer. It was found by NOE that the addition of allylamine had occurred exclusively from the exo position setting up the correct relative stereochemical relationships between C-23 and C-17/22. The protonation after the conjugate addition also occurred syn to the allylamine inverting the stereocenter at C-20. The substituted adduct 9 was protected with Boc anhydride to give the precursor 10.

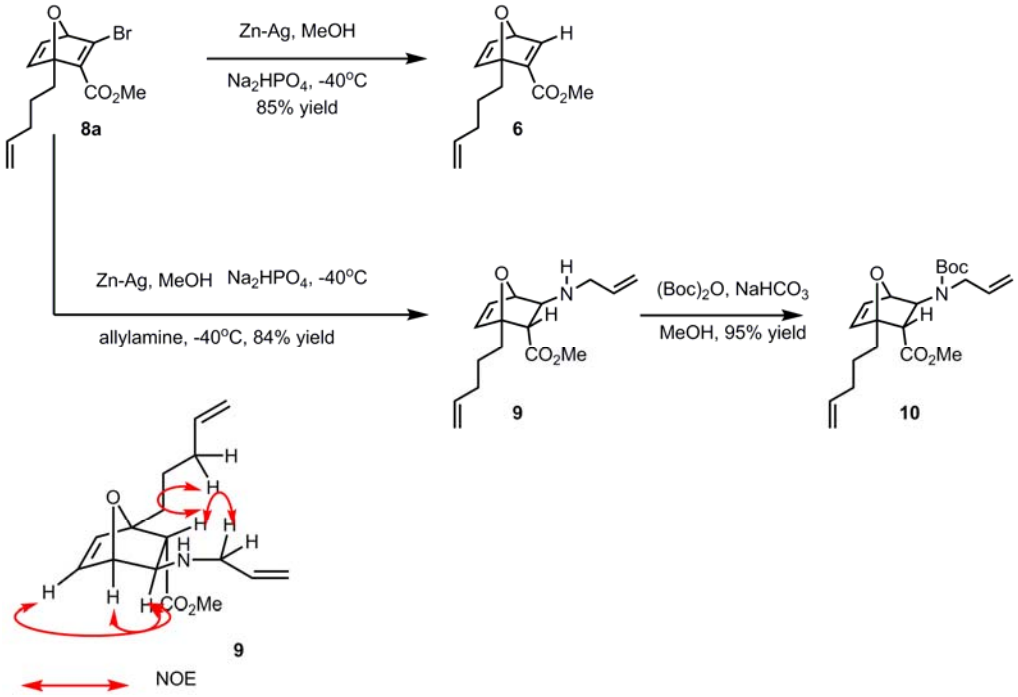

Scheme 28. One pot synthesis functionalization of oxabicyclic adduct

The precursor 10 was subjected to a cascade ring opening/closing metathesis (Scheme.29) reaction with second generation Grubbs catalyst. Quite excitedly, the reaction underwent metathesis mediated bond reorganization rapidly at room temperature to give the tricyclic DEF spiroannulated ring in excellent yield.

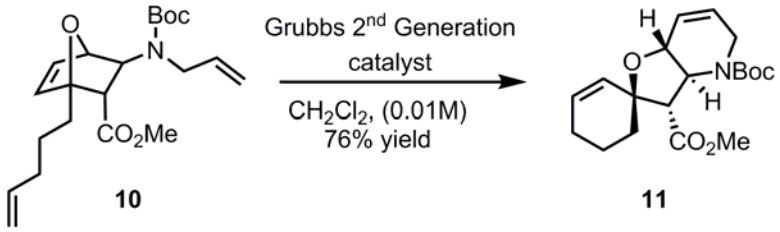

Scheme 29. Tandem metathesis to the spirocyclic core of cyclopamine

Based on the success of the metathesis reaction with 2-pentenyl furan, efforts were directed towards synthesizing the analog of IPI-926 using 2-hexenyl furan 12.

Tandem metathesis reaction was carried out for 13 which gave seven membered tricyclic analog 14 in good yields (Scheme.30).

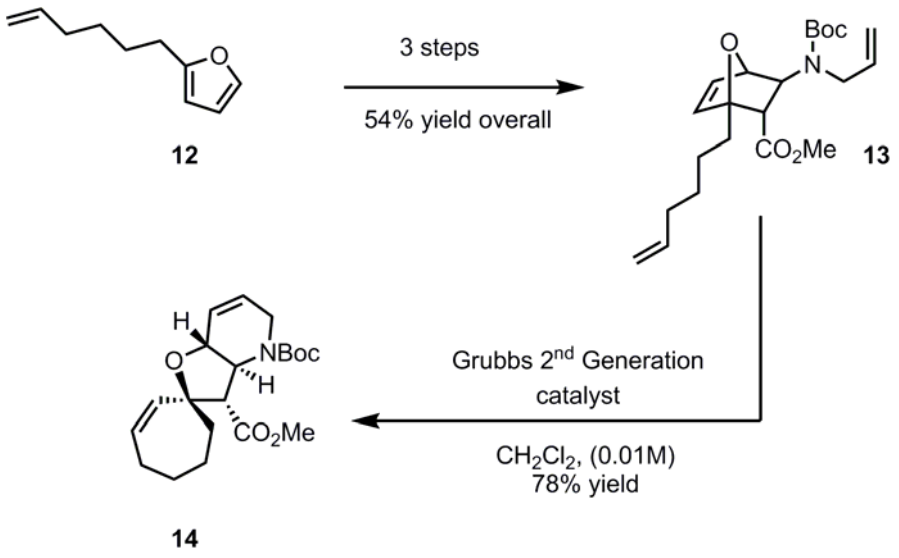

Scheme 30. Seven membered analog of cyclopamine

Although spirocyclic analogs were obtained in good yields for both the 6 and 7-membered ring system, the relative stereochemistry at C-20 is opposite to that of the natural product. In order to correct for the inversion at C-20 a new synthetic methodology was developed.

6.6 Inversion of methyl substitution at C-20

It was realized that the best way to set the methyl group at C-20 is by enolate based alkylation reaction. This methodology will utilize the geometry of the molecule for the electrophile to add from the exo face.

6.6.1 Retrosynthesis

While the tandem metathesis reaction forms the linchpin for accessing the spirocyclic tricycle, the intermediate 15 is envisioned to set the stereochemistry at C-21 and C-22. Alkylation of 15 with iodomethane followed by reduction of the ketone and Mitsunobu reaction with sodium azide was hypothesized to engender 3 with the right stereochemistry (Scheme.31).

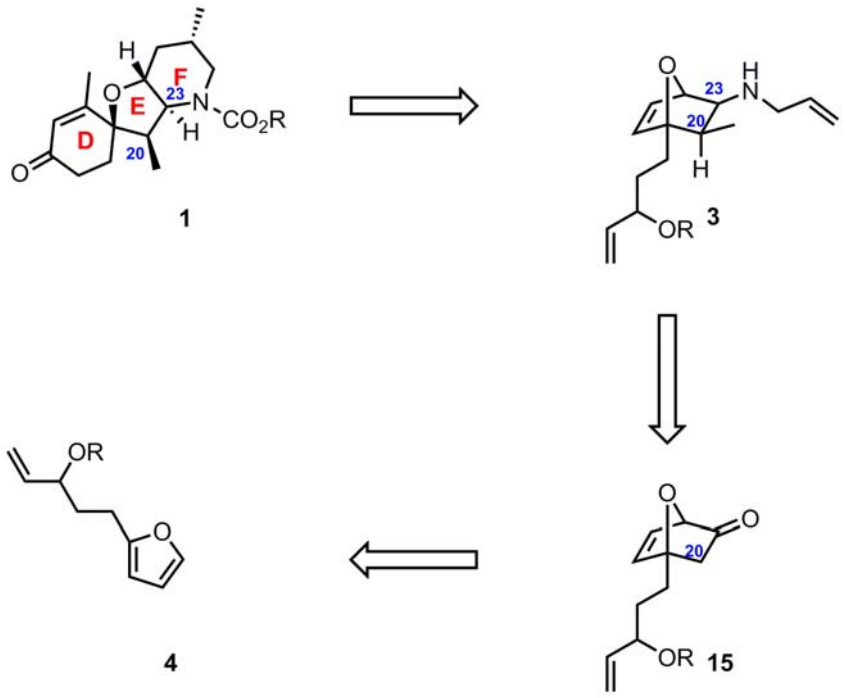

Scheme 31. Retrosynthesis 11 for the spirocyclic core of cyclopamine

6.6.2 Synthesis of Oxabicyclohepatadiene 15

To synthesize the bicyclic adduct 15 through the Diels Alder reaction, a new dienophile has to be utilized.

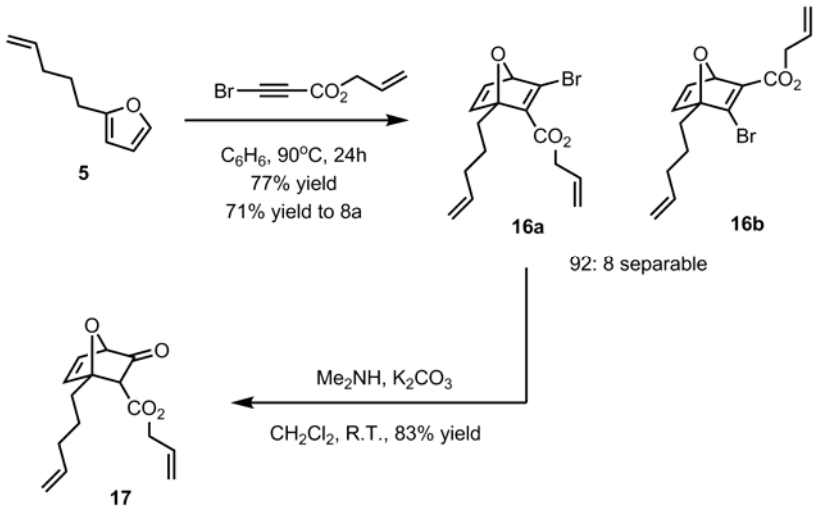

Scheme 32. Oxabicyclic adduct of β-keto allyl ester

The allyl 3-bromoprop-2-ynoate[25] underwent Diels Alder reaction with 2-pentenylfuran[5] to give the oxabicyclic compound 16a (Scheme.32).The double addition of amine nucleophile observed in the previous methodology was utilized to generate the aminal with dimethylamine. In situ hydrolysis of the aminal gave the β-keto ester 17.

6.6.3 Decarboxylation

The β-keto ester was subjected to Tsuji decaboxylation[26] catalyzed by $Pd(PPh_3)_4$ in the presence of morpholine as the allyl scavenger. The equivalence of morpholine used was found to be a critical parameter for improving the yields. Initially, when 5 eq of the scavenger was used, no product formation was observed. Instead a nucleophilic

substitution of morpholine to the ketone was observed resulting in a ring cleavage product (Scheme.33).

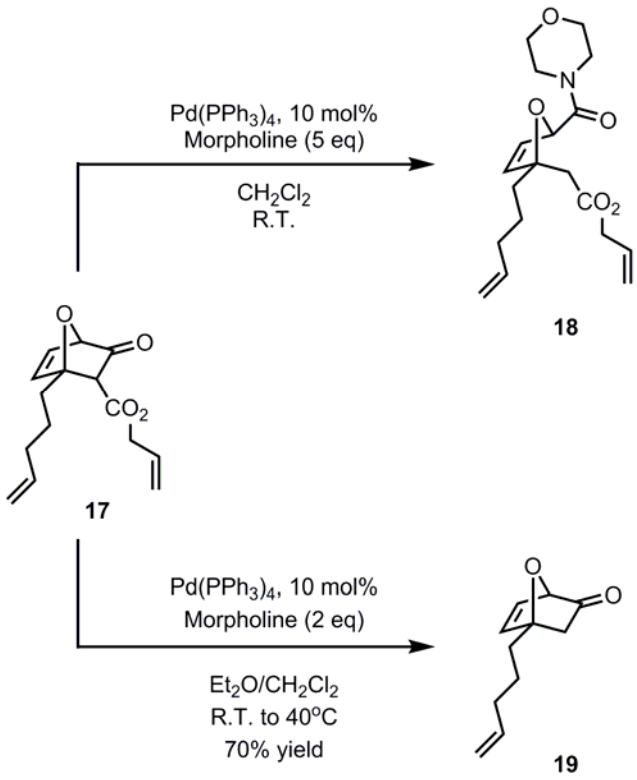

Scheme 33. Decarboxylation of β-keto allyl ester

After a series of optimization, it was found out that initially 1 eq of morpholine should be added to the mixture of β-keto ester and palladium in ether. Once the allyl group has been completely scavenged by the morpholine, as observed by the disappearance of starting material on the TLC, another 1eq of morpholine is added to trap the acid as the carboxylate salt. The precipitating solids were filtered, dissolved in dichloromethane and refluxed for 8h to get the decarboxylated ketone 19.

6.6.4 Methylation

The oxabicyclo heptenenone 19 was subjected to alkylation with LiHMDS and iodomethane. Low yields of the product were obtained along with starting material and concomitant formation of aldol product as observed in the literature[27]. A screening of the bases – NaHMDS, KHMDS, NaH, K-O*t*Bu provided better yields with KHMDS, but the formation of aldol product could not be eliminated.

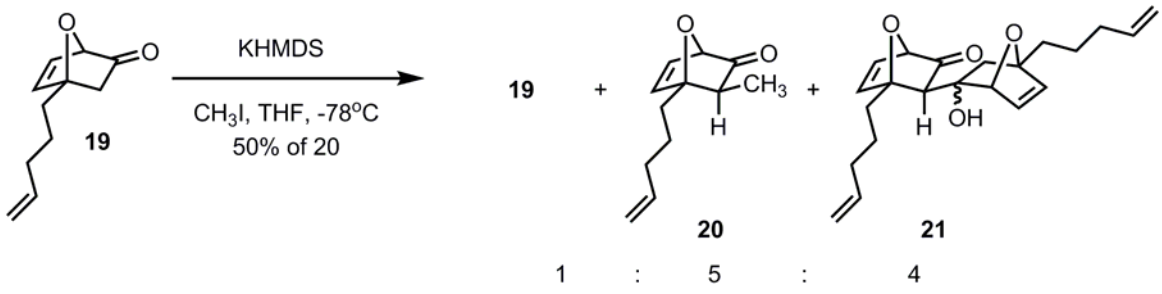

Scheme 34. Methylation of oxabicycloheptenone

With KHMDS as the base (Scheme.34), reaction conditions were optimized to overcome the self-condensation. Initially, when the temperature was lowered to -95 to -90°C, a greater proportion of the starting material with little to no product formation. When KHMDS was added to a precooled mixture of ketone and iodomethane in THF at -78°C, aldol product was still observed. Similar results were seen when ketone was added to a mixture of KHMDS and iodomethane. Alternatively, when ketone was added dropwise for 24 hrs at -60°C to the base and electrophile, starting material was recovered. It was decided to postpone further optimization until the viability of the substitution reaction with azide has been tested in the next step.

6.6.5. Nucleophilic substitution reaction

The methylated ketone 20 was reduced with $NaBH_4$ to obtain the endo alcohol 22 in 95% yield. When the alcohol was subjected to Mitsunobu conditions with diphenylphosphoryl azide a trace of azide formation (Scheme.35) was observed along with a cluster of non –separable side products. Nucleophilic substitution of tosylated 22 with sodium azide in DMF generated the starting material. Treatment of endo alcohol 22 with DPPA (Ref) and DBU generated the alkoxyphosphonium species that did not undergo displacement with the azide. The alkoxyphosphonium species was separated by column and subjected to displacement with sodium azide in DMF. No reaction was observed even after heating the reaction mixture to 92°C.

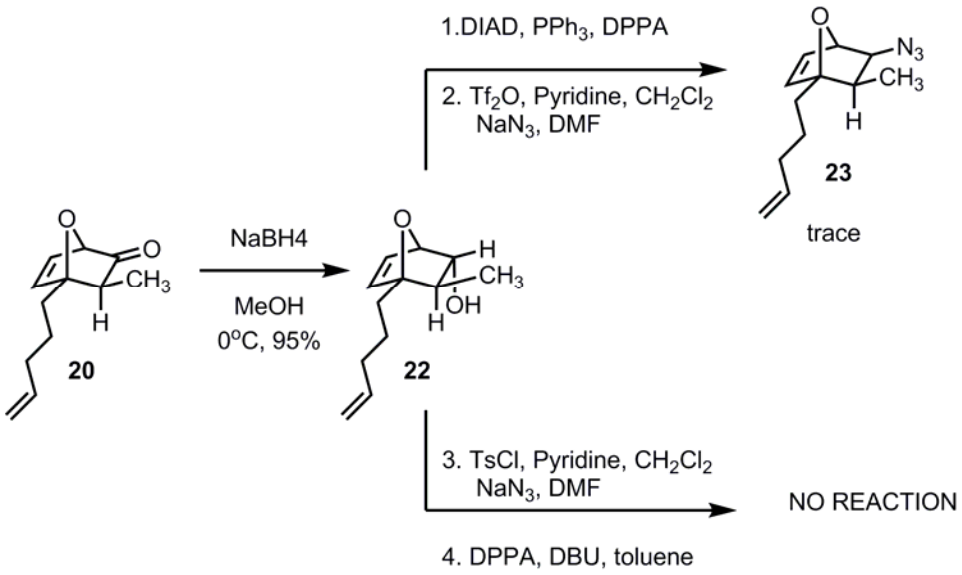

Scheme 35. S_N2 reaction with azide

Finally the leaving group was changed to a triflate and subjected to azide in DMF. A trace of product was observed along with several side products.

6.6.6 Reductive amination

Since the nucleophilic substitution did not provide the azide in reasonable yields, an alternate strategy was devised. The reductive amination was proposed as an alternate to azide substitution since it precludes the additional step of Staudinger reaction to convert the azide to an amine. The main limitation of the reductive amination is in setting up the relative stereocenter at C-23. In this case, the hydride will be delivered from the exo face, forcing the amine endo to the methyl group at C-20. But it could be overcome by utilizing a bulky reducing agent thereby forcing the hydride transfer from the endo face of the molecule.

The one pot reductive amination generated several products along with the reduced alcohol. Hence the reaction was carried out sequentially by the formation of imine followed by reduction with sodium triacetoxyborohydride(Scheme.36).

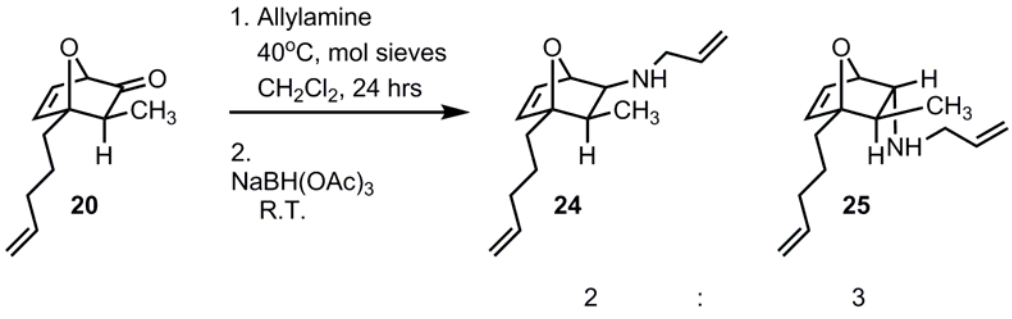

Scheme 36. Reductive amination of oxabicycloheptenone

The use of bulky $NaBH(OAc)_3$ generated the endo isomer more than the required exo isomer. Bulkier reducing agents were synthesized by treating NaBH4 with

ethylhexanoic acid, isobutyric acid, butyric acid. But no reaction was observed with these reagents. Further optimization of reductive amination is required to enhance the stereoselective reduction of the imine.

It is anticipated that the remaining steps of boc protection followed by metathesis reaction will engender the tricyclic DEF system efficiently.

6.7 Conclusion

A simplified analog of the cyclopamine was synthesized from the highly substituted oxabicyclic adduct using the tandem ring opening/closing metathesis reaction. The relative stereochemistry at C-20 was opposite to the natural product. Efforts to set the right stereocenter was achieved by a new methodology. But a series of bulky reducing agents have to be screened to favor the exo amine synthesis at C-23.

6.8 Acknowledgment

The first methodology was carried out jointly with Dr. Zachary E. Oblak of Dr. Wright's lab.

References

1. Keeler, R.; Binns, W. Chemical Compounds of Veratrum calif ornicum Related to Congenital Ovine Cyclopian Malformations: Extraction of Active Material. *Proc. Soc. Exp. Biol. Med.* 1964, 116, 123.

2. Keeler, R.; Binns, W. Teratogenic compounds ofVeratrum californicum (Durand). V. Comparison of cyclopian effects of steroidal alkaloids from the plant and structurally related compounds from other sources. *Teratology* 1968, *1*, 5-10.

3. Keeler, R. Toxic and teratogenic alkaloids of western range plants. *J. Agri. Food Chem.* 1969, *17*, 473-482.

4. Cooper, M. K.; Porter, J. A.; Young, K. E.; Beachy, P. A. Teratogen-Mediated Inhibition of Target Tissue Response to Shh Signaling *Science*, 1998, 280, 1603.

5. Taipale, J.; Chen, J.K.; Cooper, M.K.; Wang,B.; Mann, R.K.; Milenkovic, L.; Scott, M.P.; Beachy, P.A. Effects of oncogenic mutations in Smoothened and Patched can be reversed by cyclopamine, *Nature*, 406, 2000, 1005- 1009.

6. Lee L. Rubin* and Frederic J. de Sauvage, Targeting the Hedgehog pathwayin cancer, *Nat Rev Drug Discov*. 2006 , 5,12,1026-33.

7. Borzillo, G.V.; Lippa, B. The Hedgehog Signaling Pathway as a Target for Anticancer Drug Discovery, *Curr. Top. Med. Chem.* 2005, 5, 147-157.

8. Banerjee, U.; Hadden, M.K.; Recent advances in the design of Hedgehog pathway inhibitors for the treatment of malignancies, *Expert Opin. Drug Discov*. 2014, 9,7, 751-771.

9. Keeler, R. F. "Teratogenic Compounds of Veratrum Californicum (Durand) .4.First Isolation of Veratramine and Alkaloid Q and a Reliable Method for Isolation of Cyclopamine." *Phytochemistry* **1968**, *7*, 303.

10. Oatis, J.; Brunsfeld, P.; Rushing, J.; Moeller, P.; Bearden, D.; Gallien, T.; Cooper, G. Isolation, purification, and full NMR assignments of cyclopamine from Veratrum californicum. *Chemistry Central Journal* 2008, *2*, 12.

11. Masamune, T., Y. Mori, et al. "11-Deoxojervine a New Alkaloid from Veratrum Species." *Bull. Chem. Soc. Jpn.* **1965**, *38*, 1374.

12. Giannis, A.; Heretsch, P.; Sarli, V.; Stossel, A. Synthesis of Cyclopamine Using a Biomimetic and Diastereoselective Approach. *Angew. Chem., Int. Ed*. 2009, 48, 7911.

13. Kumar, S.; Roy, I.; Anchoori, R.; Fazli, S.; Maitra, A.; Beachy, P.; Khan, S. Targeted inhibition of hedgehog signaling by cyclopamine prodrugs for advanced prostate cancer. *Bioorg. Med. Chem.Lett.* 2008, *16*, 2764-2768.

14. Zhang, J.; Garrossian, M.; Gardner, D.; Garrossian, A.; Chang, Y.; Kim, Y.; Chang, C. Synthesis and anticancer activity studies of cyclopamine derivatives. *Bioorg. Med. Chem. Lett* 2008, *18*, 1359-1363.

15. Tremblay, M.; Nevalainen, M.; Nair, S.; Porter, J.; Castro, A.; Behnke, M.; Yu, L.; Hagel, M.; White, K.; Faia, K. et al. Semisynthetic Cyclopamine Analogues as Potent and Orally Bioavailable Hedgehog Pathway Antagonists. *J. Med. Chem.* 2008, *51*, 6646-6649.

16. Tremblay, M.; Lescarbeau, A.; Grogan, M.; Tan, E.; Lin, G.; Austad, B.; Yu, L.; Behnke, M.; Nair, S.; Hagel, M. et al. Discovery of a Potent and Orally Active Hedgehog Pathway Antagonist (IPI-926). *J. Med. Chem.* 2009, *52*, 4400-4418.

17. Moschner, J.; Chentsova, A.; Eilert, N.; Rovardi, I.; Heretsch, P.; Giannis, A. Cyclopamine analogs bearing exocyclic methylenes are highly potent and acid-stable inhibitors of hedgehog signaling. *Beilstein J. Org. Chem.* 2013, *9*, 2328-2335.

18. Winkler, J.; Isaacs, A.; Holderbaum, L.; Tatard, V.; Dahmane, N. Design and Synthesis of Inhibitors of Hedgehog Signaling Based on the Alkaloid Cyclopamine. *Org. Lett.* 2009, *11*, 2824-2827.

19. Isaacs, A.; Xiang, C.; Baubet, V.; Dahmane, N.; Winkler, J. Studies Directed toward the Elucidation of the Pharmacophore of Steroid-Based Sonic Hedgehog Signaling Inhibitors. *Org. Lett.* 2011, *13*, 5140-5143..

20. Zhang, Z.; Baubet, V.; Ventocilla, C.; Xiang, C.; Dahmane, N.; Winkler, J. Stereoselective Synthesis of F-Ring Saturated Estrone-Derived Inhibitors of Hedgehog Signaling Based on Cyclopamine. *Org. Lett.* 2011, *13*, 4786-4789.

21. Wright, D.; Robotham, C.; Aboud, K. Studies on the sequential multi-component coupling/Diels–Alder cycloaddition reaction. *Tet. Lett.* 2002, *43*, 943-946.

22. Leroy, J. Preparation of 3-bromopropiolic esters:methyl and tert-butyl 3-bromopropiolates, *Org. Synth*. 1997, 74, 212.

23. Clark, R. D.; Heathcock, C. H. Preparation and reactions of .beta.-chloro-.alpha.,.beta.-unsaturated ketones, *J. Org. Chem*. 1976, 41, 636.

24. Novak, L.; Baan, G.; Marosfalvi, J.; Szantay, C. Application of carbonyl umpolung to prostaglandin synthesis I. Synthesis of 11-deoxy prostaglandin intermediates *Tetrahedron Lett*. 1978, 19, 487.

25. Poulsen, T.; Bernardi, L.; Alemán, J.; Overgaard, J.; Jørgensen, K. Organocatalytic Asymmetric Direct α-Alkynylation of Cyclic β-Ketoesters. *J. Am. Chem. Soc.* 2007, *129*, 441-449.

26. Tsuji, J.; Nisar, M.; Shimizu, I. Facile palladium-catalyzed decarboxylation reaction of allylic .beta.-keto esters. *J. Org. Chem.* 1985, *50*, 3416-3417.

27. Mirsadeghi, S.; Rickborn, B. Trapping reactive intermediate carbanions generated by lithium tetramethylpiperidide treatment of 7-oxabicyclo[2.2.1]heptenes in the presence of trimethylsilyl chloride. *J. Org. Chem.* 1986, *51*, 986-992.

CHAPTER 7

Experimental Procedures

The ^{1}H and ^{13}C NMR spectra were recorded on Bruker instruments at 500 MHz. Chemical shifts are reported in ppm and are referenced to residual $CHCl_3$ solvent; 7.24 and 77.23 ppm for ^{1}H and ^{13}C, residual solvent MeOH; 4.78, 3.31 and 49.15 ppm respectively. Melting points were recorded on Mel-Temp 3.0 apparatus and are uncorrected. The high-resolution mass spectrometry was provided by the Notre Dame Mass Spectrometry Laboratory and University of Connecticut Mass Spectrometry Laboratory using AccuTOF mass spectrometer and/or using DART source. IR data were obtained using Alpha diamond ATR probe. TLC analyses were performed on Sorbent Technologies silica gel HL TLC plates. All glassware was oven-dried and allowed to cool under an argon atmosphere. Anhydrous dichloromethane, ether, and tetrahydrofuran were used directly from Baker Cycle-Tainers. Anhydrous Dimethylformamide was purchased from Acros and degassed by purging with argon. Anhydrous triethylamine was purchased from Aldrich and degassed by purging with argon. All reagents were used directly from commercial sources unless otherwise stated. Boronic acids for Suzuki coupling were purchased from Frontier Scientific, Inc.

General procedure for the Suzuki Coupling

An oven dried 100mL pressure vessel with stir bar was cooled to room temperature under argon. Bromo aldehyde, boronic acid and Cs_2CO_3 in mL anhydrous dioxane were stirred and purged under argon for 15 minutes. $Pd(PPh_3)_2Cl_2$ was then added and purging continued for further 10 minutes. The pressure vessel was sealed with a screw cap and placed in a preheated oil bath at 80 ^oC for 12 h. The dark colored reaction mixture was cooled, diluted with ether, filtered through celite and rinsed with ether. The filtered solution was concentrated, diluted with CH_2Cl_2, pre-absorbed onto silica gel and purified by column chromatography.

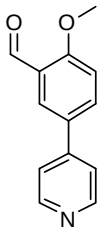

According to the general Suzuki coupling procedure Bromo aldehyde (3.50 g, 16.5 mmol), pyridine-4-boronic acid (4.05g, 32.94 mmol), Cs_2CO_3 (16.09 g, 4.93 mmol), $Pd(PPh_3)_2Cl_2$ (1.16 g, 1.65 mmol, 10% Pd) and anhydrous dioxane (16.5 mL) was heated at 80 ^oC for 12h (overnight). Following the general workup and flash chromatography (SiO_2, 60 g, 50% EtOAc/hexanes) biaryl aldehyde was obtained as a pale white solid (3.9 g, 85%): TLC R_f = 0.13 (50% EtOAc/hexanes); ^1H NMR (500 MHz, $CDCl_3$) δ 10.47 (s, 1H), 8.60 (d, J = 5.0 Hz, 2H), 8.09 (d, J = 5.0 Hz, 1H), 7.81 (dd, J =

15.0, 5.0 Hz, 1H), 7.44 (d, J = 10.0 Hz, 2H), 7.07 (d, J = 10.0 Hz, 1H), 3.95 (s, 3H); ^{13}C NMR (125 MHz, $CDCl_3$) δ 189.2, 162.3, 150.3, 146.5, 133.9, 130.4, 126.8, 125.1, 120.9, 112.5, 55.9; IR (neat cm^{-1}) 3063, 2976, 2896, 1677,1603, 1271, 804, 504; HRMS (DART, $M^+ + H$) *m/z* 214.0886 (calculated for $C_{13}H_{11}NO_2$, 214.0868).

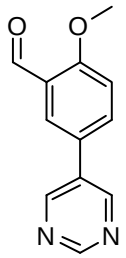

According to the general Suzuki coupling procedure Bromo aldehyde (1.50 g, 6.97 mmol), pyrimidine-5-boronic acid (1.73 g, 13.95 mmol), Cs_2CO_3 (6.81 g, 20.91 mmol), $Pd(PPh_3)_2Cl_2$ (0.49 g, 0.70 mmol, 10% Pd) and anhydrous dioxane (5 mL) was heated at 80 ^oC for 12h (overnight). Following the general workup and flash chromatography (SiO_2, 30 g, 50% EtOAc/hexanes) biaryl aldehyde was obtained as a pale white solid (1.04 g, 70%): TLC R_f = 0.2 (50% EtOAc/hexanes); ^{1}H NMR (500 MHz, $CDCl_3$) δ 10.51 (s, 1H), 9.18 (s, 1H), 8.93 (s, 2H), 8.06 (d, J = 2.0 Hz, 1H), 7.77 (dd, J = 8.5, 2.5 Hz, 1H), 7.15 (d, J = 9.0 Hz, 1H), 3.99(s, 3H); ^{13}C NMR (125 MHz, $CDCl_3$) δ 189.3, 162.5, 157.7, 154.7, 134.2, 133.2, 127.1, 127.0, 125.6, 113.1, 56.24; IR (neat cm^{-1}) 3035, 2849, 2760, 1742, 1606, 1498, 1414, 1387, 1186, 1014, 722; HRMS (DART, $M^+ + H$) *m/z* 215.0841 (calculated for $C_{12}H_{10}N_2O_2$, 215.0821).

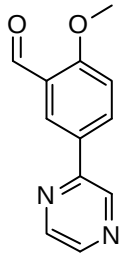

According to the general Suzuki coupling procedure Iodopyrazine (1.11 g, 5.39 mmol), 3-formyl-4-methoxyphenylboronic acid (1.94g, 10.78 mmol), Cs_2CO_3 (5.27 g, 16.17 mmol), $Pd(PPh_3)_2Cl_2$ (0.4 g, 0.54 mmol, 10% Pd) and anhydrous dioxane (6 mL) was heated at 80 ^oC for 12h (overnight). Following the general workup and flash chromatography (SiO_2, 30 g, 50% EtOAc/hexanes) biaryl aldehyde was obtained as a pale white solid (0.84 g, 73%): TLC R_f = 0.3 (50% EtOAc/hexanes); ^1H NMR (500 MHz, $CDCl_3$) δ 10.49 (s, 1H), 9.01 (s, 1H), 8.57 (s, 1H), 8.45 (dd, *J* = 9.5, 2.0 Hz, 2H), 8.29 (dd *J* = 8.5, 2.0 Hz, 1H) 7.12 (d, *J* = 8.5 Hz, 1H), 3.98 (s, 3H); ^{13}C NMR (125 MHz, $CDCl_3$) δ 189.4, 163.1, 151.5, 144.3, 143.0, 141.8, 134.5, 129.2, 127.1, 125.2, 112.7, 56.2; IR (neat cm^{-1}) 3055, 2980, 2884, 1675, 1604, 1454, 1414, 1392, 1272, 1256, 1112, 1010, 825, 512; HRMS (DART, M^+ + H) *m/z* 215.0831 (calculated for $C_{12}H_{10}N_2O_2$, 215.0821).

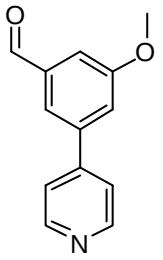

According to the general Suzuki coupling procedure Bromo aldehyde (1.7 g, 7.91 mmol), pyridine-4-boronic acid (1.94g, 15.81 mmol), Cs_2CO_3 (7.72g, 23.72 mmol), $Pd(PPh_3)_2Cl_2$ (0.55g, 23.72 mmol, 10% Pd) and anhydrous dioxane (8 mL) was heated at 80 ^oC for 12h (overnight). Following the general workup and flash chromatography (SiO_2, 20 g, 50% EtOAc/hexanes) biaryl aldehyde was obtained as a pale white solid (1.38 g, 82%): TLC R_f = 0.2 (50% EtOAc/hexanes); ^1H NMR (500 MHz, $CDCl_3$) δ 10.00 (s, 1H), 8.66 (d, J = 6.0 Hz, 2H), 7.67 (s, 1H), 7.48 (d, J = 9.5 Hz, 2H), 7.37 (d, J = 1.5 Hz, 1H), 3.89 (s, 3H); ^{13}C NMR (125 MHz, $CDCl_3$) δ 191.7, 160.9, 150.7, 146.9, 140.7, 138.7, 121.8, 119.9, 112.9, 100.1, 55.9; IR (neat cm^{-1}) 3013, 2972, 2834, 1693, 1586, 1468, 1217, 1151, 1046, 852, 816; HRMS (DART, $M^+ + H$) *m/z* 214.0897 (calculated for $C_{13}H_{11}NO_2$, 214.0868).

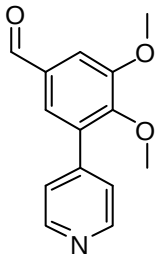

According to the general Suzuki coupling procedure Bromo aldehyde (1.06 g, 4.33 mmol), pyridine-4-boronic acid (1.06 g, 8.65 mmol), Cs_2CO_3 (4.22 g, 12.98 mmol),

$Pd(PPh_3)_2Cl_2$ (0.3 g, 0.43 mmol, 10% Pd) and anhydrous dioxane (4.3 mL) was heated at 80 °C for 12h (overnight). Following the general workup and flash chromatography (SiO_2, 30 g, 50% EtOAc/hexanes) biaryl aldehyde was obtained as a pale yellow solid (0.84 g, 80%): TLC R_f = 0.2 (50% EtOAc/hexanes); ^{1}H NMR (500 MHz, $CDCl_3$) δ 9.92 (s, 1H), 8.66 (d, J = 5.5 Hz, 2H), 7.49 (d, J = 2.0 Hz, 1H), 7.45 – 7.44 (comp, 3H), 3.96 (s, 3H), 3.73 (s, 3H); ^{13}C NMR (125 MHz, $CDCl_3$) δ 190.1, 154.0, 152.2, 150.1, 145.1, 133.5, 132.8, 126.4, 124.1, 111.2, 61.3, 56.4; IR (neat cm^{-1}) 3058, 3016, 2838, 2708, 1692, 1579, 1460, 1297, 1048, 816; HRMS (DART, M^+ + H) *m/z* 244.0999 (calculated for $C_{14}H_{13}NO_3$, 244.0974).

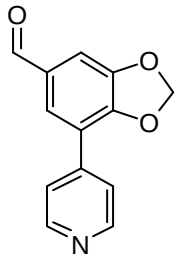

According to the general Suzuki coupling procedure Bromo aldehyde (3.04 g, 13.28 mmol), pyridine-4-boronic acid (3.26 g, 26.56 mmol), K_3PO_4 (4.8 g, 22.58 mmol), $Pd_2(dba)_3$ (1.21 g, 1.32 mmol, 10% Pd), $P(Cy)_3$ (1.11 g, 3.9 mmol) and anhydrous dioxane (35.9 mL), H_2O (17 mL) was heated at 100 °C for 12h (overnight). Following the general workup and flash chromatography (SiO_2, 60 g, 50% EtOAc/hexanes) biaryl ketone **10** was obtained as a pale white solid (2.41 g, 80%): TLC R_f = 0.2 (50% EtOAc/hexanes); ^{1}H NMR (500 MHz, $CDCl_3$) δ 9.87 (s, 1H), 8.69 (d, J = 6 Hz, 2H), 7.67 – 7.64 (comp, 3H), 7.36 (d, J = 1.5 Hz, 1H), 6.18 (s, 2H); ^{13}C NMR (125 MHz, $CDCl_3$) δ 190.1, 150.8, 150.6, 149.7, 142.0, 132.5, 127.0, 122.2, 120.0, 107.5, 102.8; IR

(neat cm^{-1}) 3337, 3062, 2915, 1685, 1594, 1402, 1097, 891; HRMS (DART, $M^+ + H$) *m/z* 228.0689 (calculated for $C_{13}H_9NO_3$, 228.0661).

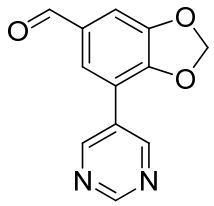

Bromo aldehyde (0.8 g, 3.49 mmol), pyrimidine-5-boronic acid (0.86 g, 6.99 mmol), K_3PO_4 (1.26 g, 5.94 mmol), $Pd_2(dba)_3$ (0.32 g, 0.35 mmol, 10% Pd), $P(Cy)_3$ (0.29 g, 1.05 mmol) anhydrous dioxane (9.4 mL), H_2O (4.7 mL) was heated at 100 ^oC for 12h (overnight). Following the general workup and flash chromatography (SiO_2, 20 g, 50% EtOAc/hexanes) biaryl aldehdye was obtained as a pale white solid (0.58 g, 73%): TLC R_f = 0.3 (50% EtOAc/hexanes); ^1H NMR (500 MHz, $CDCl_3$) δ 9.89 (s, 1H), 9.21 (s, 1H), 9.10 (s, 2H), 7.62 (d, *J* = 1.5 Hz, 1H), 7.39 (d, *J* = 1.5 Hz, 1H), 6.19 (s, 2H); ^{13}C NMR (125 MHz, $CDCl_3$) δ 189.8, 158.2, 155.6, 150.6, 149.7, 132.9, 128.8, 126.3, 116.2, 107.9, 102.9; IR (neat cm^{-1}) 3062, 2919, 2795, 1682, 1411, 1253, 1091, 933, 720; HRMS (DART, $M^+ + H$) *m/z* 229.0628 (calculated for $C_{12}H_8N_2O_3$, 229.0613).

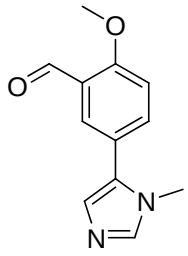

According to the general Suzuki coupling procedure 5-bromo-1-methyl-1H-imidazole (1.05 g, 6.5 mmol), 3-formyl-4-methoxyphenyl boronic acid (1.75 g, 9.75 mmol), sat.

Na_2CO_3 (3.25 mL), $PdCl_2dppf$ (0.095 g, 0.13 mmol, 2 mol% Pd) and anhydrous ethanol (30 mL), toluene (5 mL) was heated at 85 °C for 2h. Following the general workup and flash chromatography (SiO_2, 20 g, 3%MeOH/CH_2Cl_2) biaryl aldehyde was obtained as a orange solid (0.98 g, 70%): TLC R_f = 0.06 (3%MeOH/CH_2Cl_2); ^{1}H NMR (500 MHz, $CDCl_3$) δ 10.5 (s, 1H), 7.81 (d, J = 2.0 Hz, 1H), 7.56 (dd, J = 6.0, 2.0 Hz, 1H), 7.51 (b, 1H), 7.05 (d, J = 9.0 Hz, 2H), 3.96 (s, 3H), 3.62 (s, 3H); ^{13}C NMR (125 MHz, $CDCl_3$) δ 189.8, 158.2, 155.6, 150.6, 149.7, 132.9, 128.8, 126.3, 116.2, 107.9, 102.9; IR (neat cm^{-1}) 3101, 2971, 2945, 2860, 2768, 1681, 1614, 1482, 1245, 1114, 1017, 827; HRMS (DART, M^+ + H) *m/z* 217.0998 (calculated for $C_{12}H_{12}N_2O_2$, 217.0977).

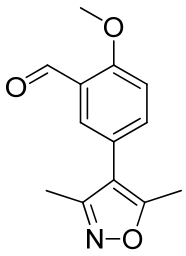

According to the general Suzuki coupling procedure 4-iodo-3,5-dimethylisoxazole (1.14 g, 5.1 mmol), 3-formyl-4-methoxyphenyl boronic acid (4.5 g, 25.5 mmol), Na_2CO_3 (3.5 g, 33.15 mmol), $Pd(PPh_3)_4$ (0.115 g, 0.10 mmol, 2% Pd), anhydrous dioxane (75 mL), H_2O (17 mL) was heated at 85 °C for 2h. Following the general workup and flash chromatography (SiO_2, 30 g, 50% EtOAc/hexanes) biaryl aldehyde was obtained as a pale white solid (1.04 g, 88%): TLC R_f = 0.6 (50% EtOAc/hexanes); ^{1}H NMR (500 MHz, $CDCl_3$) δ 10.5 (s, 1H), 7.68 (d, J = 2.0 Hz, 1H), 7.41 (dd, J = 8.5, 2.5 Hz, 1H), 7.05 (d, J = 8.5 Hz, 1H), 3.95 (s, 3H), 2.35 (s, 3H), 2.21 (s, 3H); ^{13}C NMR (125 MHz, $CDCl_3$) δ 189.5, 165.5, 161.3, 158.7, 137.0, 129.0, 125.2, 123.2, 115.5, 112.5, 56.1, 11.7, 10.9; IR

(neat cm^{-1}) 3038, 2923, 2862, 2724, 1682, 1601, 1268, 1120, 1014, 825; HRMS (DART, $M^+ + H$) *m/z* 232.0993 (calculated for $C_{13}H_{13}NO_3$, 232.0976).

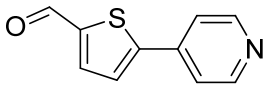

According to the general Suzuki coupling procedure Bromo aldehyde (0.56 g, 2.93 mmol), pyridine-4-boronic acid (0.72 g, 5.86 mmol), Cs_2CO_3 (2.86 g, 8.79 mmol), $Pd(PPh_3)_2Cl_2$ (0.21 g, 0.3 mmol, 10% Pd) and anhydrous dioxane (5 mL) was heated at 80 ^oC for 12h (overnight). Following the general workup and flash chromatography (SiO_2, 20 g, 50% EtOAc/hexanes) biaryl aldehyde was obtained as a pale white solid (0.44 g, 80%): TLC R_f = 0.2 (50% EtOAc/hexanes); ^1H NMR (500 MHz, $CDCl_3$) δ 9.91 (s, 1H), 8.66 (d, *J* = 4.5 Hz, 2H), 7.76 (d, *J* = 4.0, 1H), 7.55 (d, *J* = 3.5 Hz, 1H), 7.50 (d, *J* = 5.0 Hz, 2H); ^{13}C NMR (125 MHz, $CDCl_3$) δ 182.9, 151.0, 150.3, 144.4, 140.2, 137.1, 126.2, 120.4; IR (neat cm^{-1}) 3304, 3091, 1713, 1415, 1214, 1047, 799; HRMS (DART, $M^+ + H$) *m/z* 190.0351 (calculated for $C_{10}H_7NOS$, 190.0327).

Alkynol Synthesis

A 50 mL flask with stir bar was flame dried under argon. THF (0.1M) was added and temperature lowered to 0 ^oC. Ethynyltrimethyl silane was added and reaction mixture stirred for 2 minutes. Isopropyl magnesium chloride was added dropwise and stirred initially at 0 ^oC for 30 minutes followed by another 30 minutes at room temperature. The grey colored Grignard reagent was cooled to 0 ^oC and the aldehyde in THF was added

dropwise for 5 minutes. The reaction was followed by TLC quenched with water and sat. NH_4Cl. The organic layer was separated and water layer extracted 3 times with ether. The combined organic extracts were dried with MgSO4 filtered and rotoevaporated. The crude compound was preabsorbed onto silica gel and purified by column chromatography.

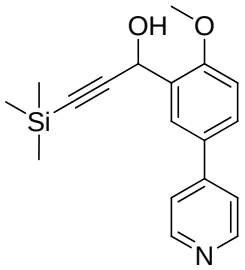

According to the general nucleophilic addition Ethynyltrimethyl silane (6.6mmol, 0.93mL) in THF (2M, 3.29mL) and isopropyl magnesium chloride (2M, 3.3mL) was stirred. At 0 ^oC was added the aldehyde (5.06mmol, 1.07g) in THF (0.1M, 50.6mL).Following the general workup and flash chromatography (SiO_2, 40 g, 3%MeOH/CH_2Cl_2) alkynol **10** was obtained as a white solid (1.48 g, 94%): TLC R_f = 0.1 (3%MeOH/CH_2Cl_2); ^1H NMR (500 MHz, $CDCl_3$) δ 8.58 (d, J = 5.7 Hz, 2H), 7.91 (d, J = 2.2 Hz, 1H), 7.58 (dd, J = 8.5, 2.2 Hz, 1H), 7.44 (d, J = 6.0 Hz, 2H), 6.98 (d, J = 8.5 Hz, 1H), 5.77 (s, 1H), 3.92 (s, 3H), 0.19 (s, 9H); ^{13}C NMR (125 MHz, $CDCl_3$) δ 158.0, 150.3, 148.0, 130.5, 129.8, 128.3, 127.0, 121.2, 111.6, 104.7, 91.5, 61.0, 56.0, 0.1.; IR (neat cm^{-1}) 3139, 2977, 2868, 2165, 1562, 1504, 1228, 1011; HRMS (DART, M^+ + H) *m/z* 312.1393 (calculated for $C_{18}H_{21}NO_2Si$, 312.1420).

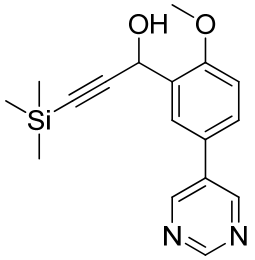

According to the general nucleophilic addition Ethynyltrimethyl silane (3.55mmol, 0.50mL) in THF (2M, 1.78mL) and isopropyl magnesium chloride (2M, 3.55mmol, 1.78mL) was stirred. At 0 ^{o}C was added the aldehyde (2.37mmol, 0.51g) in THF (0.1M, 23.6mL).Following the general workup and flash chromatography (SiO_2, 20 g, 3%MeOH/CH_2Cl_2) alkynol **10** was obtained as a white solid (0.7 g, 95%): TLC R_f = 0.1 (3%MeOH/CH_2Cl_2); ^{1}H NMR (500 MHz, $CDCl_3$) δ 9.14 (s, 1H), 8.90 (s, 2H), 7.85 (s, 1H), 7.52 (d, J = 10.7 Hz, 1H), 7.03 (d, J = 8.5 Hz, 1H), 5.77 (s, 1H), 3.93 (s, 3H), 0.18 (s, 9H); ^{13}C NMR (125 MHz, $CDCl_3$) δ 157.9, 157.2, 154.6, 134.0, 130.1, 128.4, 126.9, 126.9, 112.0, 104.2, 91.9, 61.1, 56.1, 0.1; IR (neat cm^{-1}) 3177, 3010, 2837, 2164, 1608, 1308, 1059; HRMS (DART, M^+ + H) *m/z* 313.1391 (calculated for $C_{17}H_{20}N_2O_2Si$, 312.1372).

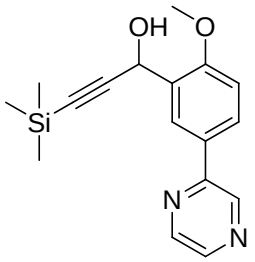

According to the general nucleophilic addition Ethynyltrimethyl silane (1.45mmol, 0.2mL) in THF (2M, 0.72mL) and isopropyl magnesium chloride (2M, 0.72mL) was

stirred. At 0 °C was added the aldehyde (0.9mmol, 0.2g) in THF (0.1M, 9.7mL).Following the general workup and flash chromatography (SiO_2, 10 g, 3%MeOH/CH_2Cl_2) alkynol **10** was obtained as a white solid (0.27 g, 95%): TLC R_f = 0.1 (3%MeOH/CH_2Cl_2); ^{1}H NMR (500 MHz, $CDCl_3$) δ 8.96 (s, 1H), 8.57 (s, 1H), 8.43 (d, *J* = 2.4 Hz, 1H), 8.28 (d, *J* = 2.2 Hz, 1H), 8.01 (dd, *J* = 8.6, 2.3, Hz, 1H), 7.01 (d, *J* = 8.6 Hz, 1H), 5.75 (s, 1H), 3.94 (s, 3H), 0.20 (s, 9H^{13}C NMR (125 MHz, $CDCl_3$) δ 158.6, 152.5, 144.3, 142.4, 141.7, 129.6, 129.1, 128.7, 127.0, 111.6, 104.5, 91.7, 61.5, 56.1, 0.1. IR (neat cm^{-1}) 3055, 2980, 2884, 2847, 1913, 1675, 1604, 1414, 1272, 1166, 1112, 1010, 825; HRMS (DART, M^+ + H) *m/z* 313.1394 (calculated for $C_{17}H_{20}N_2O_2Si$, 312.1372).

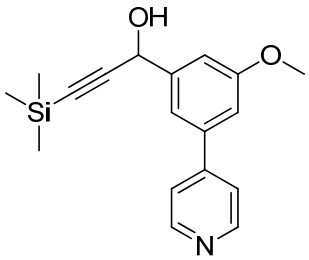

According to the general nucleophilic addition Ethynyltrimethyl silane (2.1mmol, 0.3mL) in THF (2M, 1.0mL) and isopropyl magnesium chloride (2M, 1.0mL) was stirred. At 0 °C was added the aldehyde (1.7mmol, 0.4g) in THF (0.1M, 17.4mL).Following the general workup and flash chromatography (SiO_2, 20 g, 3%MeOH/CH_2Cl_2) alkynol **10** was obtained as a bronish oil (0.51 g, 94%): TLC R_f = 0.1 (3%MeOH/CH_2Cl_2); ^{1}H NMR (500 MHz, $CDCl_3$) δ 8.59 (s, 2H), 7.46 (d, *J* = 4.5 Hz, 2H), 7.38 (s, 1H), 7.19 (s, 1H), 7.07 (s, 1H), 5.50 (s, 1H), 3.85 (s, 3H), 0.18 (s, 9H); ^{13}C NMR (125 MHz, $CDCl_3$) δ 160.5, 150.1, 148.5, 143.5, 139.7, 122.0, 118.0, 113.1, 112.7, 105.4, 91.7, 64.7, 55.7, 0.0;

IR (neat cm^{-1}) 3153, 2958, 2899, 2837, 2170, 1648, 1550, 1325, 1217, 1049; HRMS (DART, $M^+ + H$) *m/z* 312.1434 (calculated for $C_{18}H_{21}NO_2Si$, 312.1420).

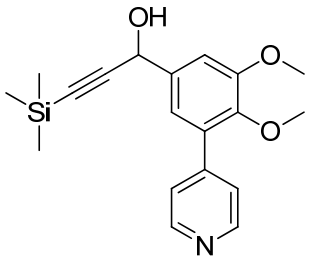

According to the general nucleophilic addition Ethynyltrimethyl silane (3.79mmol, 0.54 mL,) in THF (2M, 1.9mL) and isopropyl magnesium chloride (2M, 1.9mL) was stirred. At 0 ^oC was added the aldehyde (2.5mmol, 0.6g) in THF (0.1M, 25.2mL).Following the general workup and flash chromatography (SiO_2, 30 g, 50% 3%MeOH/CH_2Cl_2) alkynol **10** was obtained as a colorless oil (0.82g, 95%): TLC R_f = 0.1 (3%MeOH/CH_2Cl_2); ^1H NMR (500 MHz, $CDCl_3$) δ 8.57 (d, *J* = 4.9 Hz, 2H), 7.45 (d, *J* = 6.0 Hz, 2H), 7.21 (d, *J* = 1.75 Hz, 1H), 7.09 (d, *J* = 1.79 Hz, 1H), 5.45 (s, 1H), 3.91 (s, 3H), 3.59 (s, 3H), 0.18 (s, 9H); ^{13}C NMR (125 MHz, $CDCl_3$) δ 153.4, 149.5, 146.7, 146.4, 137.3, 132.6, 124.3, 120.4, 111.7, 105.5, 91.8, 64.6, 61.0, 56.2, 0.0; IR (neat cm^{-1}) 3085, 3009, 2964, 2821, 2162, 1642, 1410, 1241, 1134, 1049, 828; HRMS (DART, M^+ + H) *m/z* 342.1516 (calculated for $C_{19}H_{23}NO_3Si$, 342.1525).

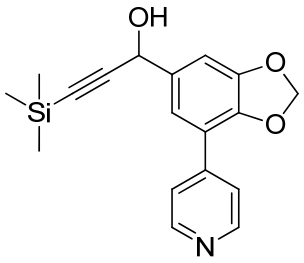

According to the general nucleophilic addition Ethynyltrimethyl silane (3.78mmol, 0.53mL) in THF (0.53mL) and isopropyl magnesium chloride (2M, 1.9mL) was stirred. At 0 ^{o}C was added the aldehyde (1.26mmol, 0.3g) in THF (0.1M, 12.6mL).Following the general workup and flash chromatography (SiO_2, 15 g, 3%MeOH/CH_2Cl_2) alkynol **10** was obtained as a yellow hygroscopic solid (0.41 g, 99%): TLC R_f = 0.1 (3%MeOH/CH_2Cl_2); ^{1}H NMR (500 MHz, $CDCl_3$) δ 8.58 (d, J = 4.3 Hz, 2H), 7.61 (d, J = 5.8 Hz, 2H), 7.28 (s, 1H), 7.09 (s, 1H), 6.05 (s, 2H), 5.42 (s, 1H), 0.18 (s, 9H); ^{13}C NMR (125 MHz, $CDCl_3$) δ 150.0, 148.8, 145.6, 143.6, 135.9, 122.3, 119.2, 119.0, 108.3, 105.4, 101.8, 91.6, 64.5, 0.0; IR (neat cm^{-1}) 3140, 2958, 2896, 2170, 1639, 1600, 1402, 1248, 1195, 1044, 1002, 824; HRMS (DART, M^+ + H) *m/z* 326.1223 (calculated for $C_{18}H_{19}NO_3Si$, 326.1212).

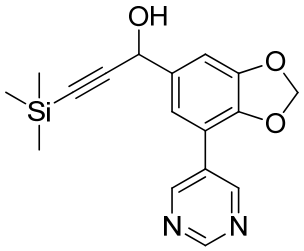

According to the general nucleophilic addition Ethynyltrimethyl silane (0.9mmol, 0.14mL) in THF (2M, 0.5mL) and isopropyl magnesium chloride (2M, 0.99mmol, 0.5mL was stirred. At 0 ^{o}C was added the aldehyde (0.66mmol, 0.15g) in THF (0.1M, 6.6mL).Following the general workup and flash chromatography (SiO_2, 10 g, 3%MeOH/CH_2Cl_2) alkynol **10** was obtained as a light yellow solid (0.21 g, 96%): TLC R_f

= 0.1 3%MeOH/CH_2Cl_2); ^{1}H NMR (500 MHz, $CDCl_3$) δ 9.14 (s, 1H), 9.05 (s, 2H), 7.24 (s, 1H), 7.10 (s, 1H), 6.07 (s, 2H), 5.42 (s, 1H), 0.20 (s, 9H); ^{13}C NMR (125 MHz, $CDCl_3$) δ 157.5, 155.5, 148.9, 145.5, 136.0, 129.8, 118.8, 115.3, 108.3, 104.8, 102.0, 92.3, 64.7, 0.0; IR (neat cm^{-1}) 3189, 2955, 2899, 2172, 1606, 1409, 1249, 1041, 1006, 837; HRMS (DART, $M^+ + H$) *m/z* 327.1190 (calculated for $C_{17}H_{18}N_2O_3Si$, 327.1165).

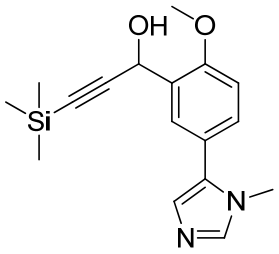

According to the general nucleophilic addition Ethynyltrimethyl silane (2.0mmol, 0.28mL) in THF (1.0mL) and isopropyl magnesium chloride (2M, 2.0mmol, 1.0mL) was stirred. At 0 ^oC was added the aldehyde (1.66mmol, 0.36g) in THF (0.1M, 16.6mL).Following the general workup and flash chromatography (SiO_2, 10 g, 3%MeOH/CH_2Cl_2) alkynol **10** was obtained as a light yellow solid (0.49 g, 94%): TLC R_f = 0.03 (3%MeOH/CH_2Cl_2); ^{1}H NMR (500 MHz, $CDCl_3$) δ 7.62 (d, J = 2.1 Hz, 1H), 7.45 (s, 1H), 7.27 (dd, J = 8.4, 2.2 Hz, 1H), 6.98 (s, 1H), 6.93 (d, J = 8.5 Hz, 1H), 5.76 (s, 1H), 3.88 (s, 3H), 3.60 (s, 3H), 0.15 (s, 9H); ^{13}C NMR (126 MHz, $CDCl_3$) δ 156.7, 138.8, 133.2, 129.9, 129.6, 128.5, 127.5, 122.3, 111.3, 105.0, 90.9, 60.5, 55.9, 32.6, 0.1; IR (neat cm^{-1}) 3113, 2957, 2899, 2837, 2167, 1488, 1279, 1040, 838; HRMS (DART, $M^+ + H$) *m/z* 315.1532 (calculated for $C_{17}H_{22}N_2O_2Si$, 315.1529).

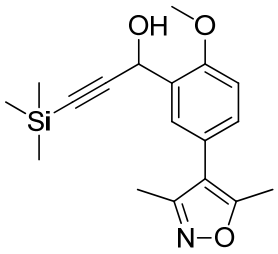

According to the general nucleophilic addition Ethynyltrimethyl silane (4.1mmol, 0.6mL) in THF (2M, 2.0mL) and isopropyl magnesium chloride (2M, 4.1mmol, 2.0mL) was stirred. At 0 ºC was added the aldehyde (2.72mmol, 0.63g) in THF (0.1M, 27.2mL). Following the general workup and flash chromatography (SiO_2, 20 g, 3%MeOH/CH_2Cl_2) alkynol **10** was obtained as a colorless oil (0.86 g, 96%): TLC R_f = 0.4 (3%MeOH/CH_2Cl_2); ^{1}H NMR (500 MHz, $CDCl_3$) δ 7.53 (s, 1H), 7.17 (d, J = 8.1 Hz, 1H), 6.95 (d, J = 8.1 Hz, 1H), 5.76 (d, J = 5.4 Hz, 1H), 3.90 (s, 3H), 2.38 (s, 3H), 2.24 (s, 3H), 0.18 (s, 9H); ^{13}C NMR (125 MHz, $CDCl_3$) δ 164.9, 158.7, 156.2, 130.2, 129.2, 128.9, 122.7, 116.1, 111.3, 104.6, 91.0, 60.5, 55.8, 11.5, 10.8, -0.1; IR (neat cm^{-1}) 3038, 2923, 2862, 2724, 1682, 1601, 1245, 1176, 1120, 1014, 825; HRMS (DART, M^+ + H) *m/z* 330.1528 (calculated for $C_{18}H_{23}NO_3Si$, 330.1525).

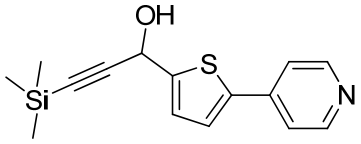

According to the general nucleophilic addition Ethynyltrimethyl silane (2.6mmol, 0.4mL) in THF (2M, 1.3mL) and isopropyl magnesium chloride (2M, 2.6mmol, 1.3mL) was stirred. At 0 ºC was added the aldehyde (2.2mmol, 0.41g) in THF (0.1M, 21.6mL).Following the general workup and flash chromatography (SiO_2, 20 g,

3%MeOH/CH_2Cl_2) alkynol **10** was obtained as a brown solid (0.6 g, 95%): TLC R_f = 0.2 (3%MeOH/CH_2Cl_2); ^{1}H NMR (500 MHz, $CDCl_3$) δ 8.49 (d, *J* = 6.2 Hz, 2H), 7.41 (d, *J* = 6.2 Hz, 2H), 7.33 (d, *J* = 3.7 Hz, 1H), 7.14 (d, *J* = 4.4 Hz, 1H), 5.65 (s, 1H), 0.19 (s, 9H); ^{13}C NMR (125 MHz, $CDCl_3$) δ 150.1, 147.7, 141.9, 141.1, 126.7, 125.3, 119.9, 104.4, 91.3, 60.6, -0.1; IR (neat cm^{-1}) 3181, 3017, 2112, 1592, 1494, 1414, 1219, 991.51, 800.26; HRMS (DART, M^+ + H) *m/z* 288.0901 (calculated for $C_{15}H_{17}NOSSi$, 288.0878).

Methylation.

To a 100 mL flame dried flask under argon was added CH_2Cl_2 (1M) at room temperature and cooled to 0 ºC. $TiCl_4$ (1M in toluene, 1 eq) was added followed by dimethyl zinc (1.2M in toluene, 2 eq) and stirred at 0 ºC for 30 minutes. To the yellow heterogeneous mixture, alkynol (1eq) dissolved in 0.1 M CH_2Cl_2 was added dropwise for 10 mins. TLC was performed on a small aliquot quenched with MeOH. After ~1hr, the reaction was stopped by a slow dropwise addition of MeOH. Care should be taken to avoid frothing and addition of MeOH continued until the reaction turns into a homogeneous yellow solution. The crude mixture was stirred at room temperature for 5 minutes and pushed through a plug of silica gel. Solvent was rotoevaporated and deprotection of TMS alkyne dissolved in 0.2M EtOH was carried out by stirring initially for 30min with $AgNO_3$ (3 eq) dissolved in 1.5M water. Then KCN (10 eq) dissolved in 10M H_2O was added slowly and stirred for 1hr. The reaction mixture was diluted with EtOAc, washed with water and

dried with $MgSO_4$. Solvent was rotoevaporated, the crude mixture was preabsorbed onto silica gel and column chromatography was carried out with 3% MeOH in CH_2Cl_2.

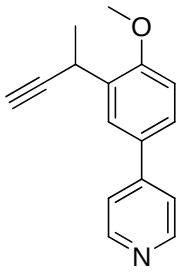

According to the general methylation protocol, alkynol (0.33mmol, 0.10g) in CH_2Cl_2 was added to the pre-mixed solution of $TiCl_4$ (0.33 mmol, 0.33mL) and dimethylzinc (0.66mmol, 0.5mL) in 1M CH_2Cl_2. Following the general workup and deprotection, the crude mixture was purified by flash chromatography (SiO_2, 5g, 3% MeOH in CH_2Cl_2) methylated alkyne was obtained as a yellow solid (51.6mg, 66%): TLC R_f = 0.2 (3% MeOH in CH_2Cl_2); ^{1}H NMR (500 MHz, $CDCl_3$) δ 8.60 (d, J = 5.1 Hz, 2H), 7.87 (d, J = 2.2 Hz, 1H), 7.63 – 7.32 (m, 3H), 6.93 (d, J = 8.5 Hz, 1H), 4.21 (qd, J = 7.0, 2.4 Hz, 1H), 3.87 (s, 3H), 2.25 (d, J = 2.4 Hz, 1H), 1.46 (d, J = 7.04 Hz, 3H); ^{13}C NMR (125 MHz, $CDCl_3$) δ 157.2, 150.2, 148.2, 132.0, 130.5, 126.7, 126.6, 121.4, 111.1, 87.3, 70.2, 55.8, 25.7, 22.9; IR (neat cm^{-1}) 3222, 3075, 2980, 2108, 1594, 1484, 1255, 803; HRMS (DART, $M^+ + H$) *m/z* 238.1256 (calculated for $C_{16}H_{15}NO$, 238.1232).

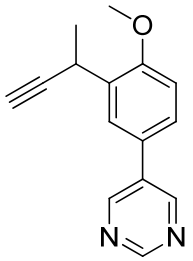

According to the general methylation protocol, alkynol (0.97mmol, 0.31g) in 0.1M CH_2Cl_2 was added to the pre-mixed solution of $TiCl_4$ (0.97mmol, 0.97mL)and dimethylzinc (1.94mmol, 1.62mL) in 1M CH_2Cl_2. Following the general workup and deprotection, the crude mixture was purified by flash chromatography (SiO_2, 10 g, 3% MeOH in CH_2Cl_2) methylated alkyne was obtained as a white solid (0.14 g, 60%): TLC R_f = 0.2 3% MeOH in CH_2Cl_2); ^{1}H NMR (500 MHz, $CDCl_3$) δ 9.13 (s, 1H), 8.91 (s, 2H), 7.79 (d, *J* = 2.3 Hz, 1H), 7.42 (dd, *J* = 8.4, 2.3, 1H), 6.96 (d, *J* = 8.4 Hz, 1H), 4.20 (qd, *J* = 7.0, 2.3 Hz, 1H), 3.88 (s, 3H), 2.24 (d, *J* = 2.5 Hz, 1H), 1.46 (d, *J* = 7.0 Hz, 3H); ^{13}C NMR (125 MHz, $CDCl_3$) δ 157.0, 157.0, 154.6, 134.2, 132.4, 126.7, 126.6, 126.5, 111.4, 87.0, 70.4, 55.8, 25.7, 22.8; IR (neat cm^{-1}) 3265, 3046, 2832, 1889, 1605, 1252, 724. HRMS (DART, $M^+ + H$) *m/z* 239.1207 (calculated for $C_{15}H_{114}N_2O$, 239.1184).

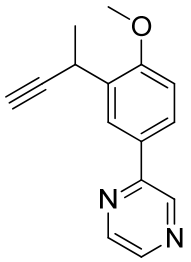

According to the general methylation protocol, alkynol (0.5mmol, 0.16g) in 0.1M CH_2Cl_2 was added to the pre-mixed solution of $TiCl_4$ (0.5mmol, 0.5mL) and dimethylzinc (1.0mmol, 0.9mL) in 0.1M CH_2Cl_2. Following the general workup and deprotection, the crude mixture was purified by flash chromatography (SiO_2, 10 g, 3% MeOH in CH_2Cl_2) methylated alkyne was obtained as a pale yellow solid (0.12 g, 60%): TLC R_f = 0.5 (3% MeOH in CH_2Cl_2); ^{1}H NMR (500 MHz, $CDCl_3$) δ 8.96 (s, 1H), 8.53 (s, 1H), 8.38 (s, 1H), 8.22 (d, *J* = 2.3 Hz, 1H), 7.86 (dd, *J* = 8.5, 2.3 Hz, 1H), 6.90 (d, *J* = 8.6 Hz, 1H), 4.18 (qd, *J* = 7.0, 2.5 Hz, 1H), 3.83 (s, 3H), 2.25 (d, *J* = 2.5 Hz, 1H), 1.45 (d, *J* = 7.0 Hz, 3H); ^{13}C NMR (125 MHz, $CDCl_3$) δ 157.7, 152.7, 144.1, 142.1, 141.8, 131.8, 128.9, 126.8, 126.5, 110.9, 87.1, 70.1, 55.7, 25.6, 22.6; IR(neat cm^{-1}) 3182, 3055, 2973, 2875, 2101, 1605, 1248, 1126, 1013, 812, 713; HRMS (DART, M^+ + H) *m/z* 239.1212 (calculated for $C_{17}H_{17}NO_2$, 239.1184).

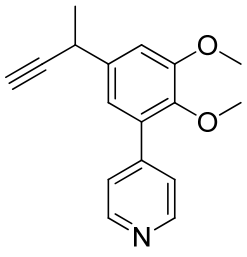

According to the general methylation protocol, alkynol (0.6mmol, 0.2g) in 0.1M CH_2Cl_2 was added to the pre-mixed solution of $TiCl_4$ (0.6mmol, 0.6mL) and dimethylzinc (1.2mmol, 1mL) in 0.1M CH_2Cl_2. Following the general workup and deprotection, the crude mixture was purified by flash chromatography (SiO_2, 15 g, 3% MeOH in CH_2Cl_2) methylated alkyne was obtained as a yellow oil (0.16 g, 65%): TLC R_f = 0.2 (3% MeOH in CH_2Cl_2); ^{1}H NMR (500 MHz, $CDCl_3$) δ 8.61 (s, 2H), 7.45 (d, J = 4.1 Hz, 2H), 7.00 (s, 1H), 6.92 (s, 1H), 3.90 (s, 3H), 3.74 (q, J = 6.7 Hz, 1H), 3.57 (s, 3H), 2.27 (s, 1H), 1.50 (d, J = 6.9 Hz, 3H); ^{13}C NMR (125 MHz, $CDCl_3$) δ 153.3, 149.8, 146.2, 145.6, 139.1, 133.0, 124.2, 120.2, 111.7, 86.9, 70.8, 61.0, 56.2, 31.7, 24.4; IR(neat cm^{-1}) 3299, 3050, 2975, 2933, 2873, 2837, 2003.75, 1586, 1406, 1264, 1139, 734; HRMS (DART, M^+ + H) *m/z* 268.1336 (calculated for $C_{17}H_{17}NO_2$, 268.1338).

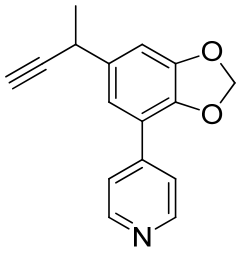

According to the general methylation protocol, alkynol (6.3mmol, 2.0g) in 0.1M CH_2Cl_2 was added to the pre-mixed solution of $TiCl_4$ (6.3mmol, 6.3mL)and dimethylzinc (12.6 mmol, 10.5mL) in 1M CH_2Cl_2. Following the general workup and deprotection, the crude

mixture was purified by flash chromatography (SiO_2, 20 g, 3% MeOH in CH_2Cl_2) methylated alkyne was obtained as a yellow oil (1.0 g, 62%): TLC R_f = 0.2 (3% MeOH in CH_2Cl_2); ^{1}H NMR (500 MHz, $CDCl_3$) δ 8.63 (d, J = 5.4 Hz, 2H), 7.62 (d, J = 6.1 Hz, 2H), 7.11 (d, J = 1.4 Hz, 1H), 6.93 (d, J = 1.6 Hz, 1H), 6.03 (d, J = 1.5 Hz, 2H), 3.73 (qd, J = 7.1, 2.4 Hz, 1H), 2.28 (d, J = 2.5 Hz, 1H), 1.50 (d, J = 7.1 Hz, 3H); ^{13}C NMR (125 MHz, $CDCl_3$) δ 150.3, 148.8, 144.5, 143.5, 137.6, 122.3, 119.5, 118.8, 108.2, 101.6, 86.9, 70.8, 31.7, 24.6; IR(neat cm^{-1}) 3200, 3026, 2929, 2786, 2106, 1737, 1596, 1402, 1197, 1040, 938, 823, 623; HRMS (DART, M^+ + H) *m/z* 257.1055 (calculated for $C_{16}H_{13}NO_2$, 257.1025).

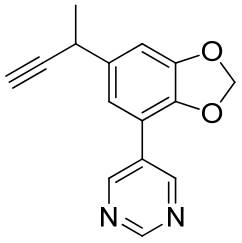

According to the general methylation protocol, alkynol (1.0mmol, 0.32g) in 0.1M CH_2Cl_2 was added to the pre-mixed solution of $TiCl_4$ (1.0mmol, 1mL) and dimethylzinc (2.0mmol, 1.6mL) in 1M CH_2Cl_2. Following the general workup and deprotection, the crude mixture was purified by flash chromatography (SiO_2, 15 g, 3% MeOH in CH_2Cl_2) methylated alkyne was obtained as a pale white solid (0.14 g, 56%): TLC R_f = 0.3 (3% MeOH in CH_2Cl_2); ^{1}H NMR (500 MHz, $CDCl_3$) δ 9.10 (s, 1H), 9.02 (s, 2H), 7.02 (s, 1H), 6.90 (s, 1H), 6.00 (s, 2H), 3.70 (qd, J = 7.1, 2.4 Hz, 1H), 2.27 (d, J = 2.5 Hz, 1H), 1.46 (d, J = 7.1 Hz, 3H); ^{13}C NMR (126 MHz, $CDCl_3$) δ 157.4, 155.4, 148.7, 144.2, 137.9,

129.8, 118.2, 115.4, 108.2, 101.7, 86.6, 70.9, 31.5, 24.4; IR(neat cm^{-1}) 3200, 2910, 2877, 2787, 1726, 1494, 1407, 1349, 1262, 1176, 1045, 940, 855, 718; HRMS (DART, $M^+ + H$) *m/z* 253.0968 (calculated for $C_{15}H_{12}N_2O_2$, 253.0977).

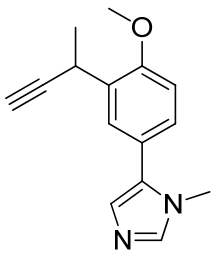

According to the general methylation protocol, alkynol (1.11mmol, 0.35g) in 0.1M CH_2Cl_2 was added to the pre-mixed solution of $TiCl_4$ (1.11mmol, 1.1mL) and dimethylzinc (2.22mmol, 1.9mL) in 1M CH_2Cl_2. Following the general workup and deprotection, the crude mixture was purified by flash chromatography (SiO_2, 15 g, 3% MeOH in CH_2Cl_2) methylated alkyne was obtained as a yellow oil (0.17 g, 62%): TLC R_f = 0.1 (3% MeOH in CH_2Cl_2); ^1H NMR (500 MHz, $CDCl_3$) δ 7.57 (s, 1H), 7.45 (s, 1H), 7.20 (d, *J* = 8.2 Hz, 1H), 7.02 (s, 1H), 6.87 (d, *J* = 8.4 Hz, 1H), 4.16 (q, *J* = 6.4 Hz, 1H), 3.83 (s, 3H), 3.60 (s, 3H), 2.18 (s, 1H), 1.42 (d, *J* = 7.0 Hz, 3H); ^{13}C NMR (125 MHz, $CDCl_3$) δ 156.0, 138.8, 133.5, 131.5, 128.3, 128.2, 127.6, 122.3, 110.7, 87.3, 70.0, 55.7, 32.5, 25.6, 22.8; IR(neat cm^{-1}) 3283, 2973, 2931, 2837, 1612, 1490, 1249, 1024, 813, 650; HRMS (DART, $M^+ + H$) *m/z* 241.1362 (calculated for $C_{15}H_{16}N_2O$, 241.1341).

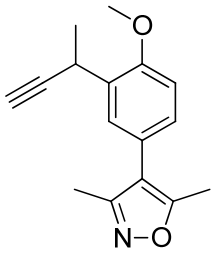

According to the general methylation protocol, alkynol (1.0mmol, 0.32g) in 0.1M CH_2Cl_2 was added to the pre-mixed solution of $TiCl_4$ (1.0mmol, 1.0mL) and dimethylzinc (2.0mmol, 1.6mL) in 1M CH_2Cl_2. Following the general workup and deprotection, the crude mixture was purified by flash chromatography (SiO_2, 20 g, 3% MeOH in CH_2Cl_2) methylated alkyne was obtained as a colorless oil (0.17 g, 65%): TLC R_f = 0.8 (3% MeOH in CH_2Cl_2); ^{1}H NMR (500 MHz, $CDCl_3$) δ 7.47 (s, 1H), 7.09 (d, J = 8.3 Hz, 1H), 6.89 (d, J = 8.3 Hz, 1H), 4.19 (q, J = 6.8 Hz, 1H), 3.85 (s, 3H), 2.38 (s, 3H), 2.25 (s, 1H), 2.20 (s, 0H), 1.44 (d, J = 6.9 Hz, 3H); ^{13}C NMR (125 MHz, $CDCl_3$) δ 165.0, 159.0, 155.5, 131.6, 128.8, 128.6, 122.9, 116.5, 110.8, 87.4, 69.9, 55.7, 25.6, 22.9, 11.7, 11.0; IR(neat cm^{-1}) 3292, 2973, 2931, 2837, 2125, 1606, 1505, 1246, 1130, 1026, 637; HRMS (DART, $M^+ + H$) *m/z* 256.1361 (calculated for $C_{16}H_{17}NO_2$, 256.1338).

Deoxygenation

To a 100mL flame dried flask was added the TMS- protected alkynol dissolved in anhydrous 0.1M CH_2Cl_2 and cooled to 0 ^{o}C. BF_3.OEt_2 was slowly added followed by Et_3SiH. Equivalence of lewis acid and triethylsilane ratio varies relative to the number of

heteroatoms present. After addition, the reaction mixture was brought to room temperature followed by heating to 41 ^{o}C for ~2hr. The reaction was quenched with sat.$NaHCO_3$, extracted with EtOAc and dried with the $MgSO_4$. After rotoevaporation, the crude products were subjected to deprotection as described in the methylation protocol.

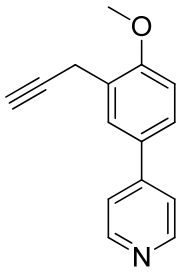

According to general deoxygenation protocol, alkynol (1.0mmol, 0.31g) dissolved in 0.1M CH_2Cl_2 was subjected to deoxygenation with $BF_3.OEt_2$ (4.0mmol, 1.3mL) and triethylsilane (2.0mmol, 0.32mL) at 41 ^{o}C. Following the general workup and deprotection, the crude mixture was purified by flash chromatography (SiO_2, 15 g, 50% EtOAc in Hexane) deoxygenated alkyne was obtained as a white solid (0.17 g, 74%): TLC R_f = 0.3 (50% EtOAc in Hexane); ^{1}H NMR (500 MHz, $CDCl_3$) δ 8.59 (d, J = 4.2 Hz, 2H), 7.80 (s, 1H), 7.50 (d, J = 8.2 Hz, 1H), 7.45 (d, J = 4.9 Hz, 2H), 6.90 (d, J = 8.4 Hz, 1H), 3.85 (s, 3H), 3.60 (s, 2H), 2.21 (s, 1H); ^{13}C NMR (125 MHz, $CDCl_3$) δ 157.8, 150.3, 148.0, 130.4, 127.6, 126.7, 125.5, 121.2, 110.6, 81.6, 71.2, 55.7, 19.5; IR(neat cm^{-1}) 3164, 2999, 2917, 2834, 2110, 1594, 1508, 1306, 804, 665; HRMS (DART, M^{+} + H) *m/z* 224.1071 (calculated for $C_{15}H_{13}NO$, 224.1075).

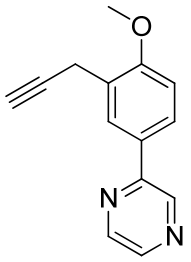

According to general deoxygenation protocol, alkynol (0.9mmol, 0.27g) dissolved in 0.1M CH_2Cl_2 was subjected to deoxygenation with $BF_3.OEt_2$ (4.3mmol, 1.3mL) and triethylsilane (2.1mmol, 0.34mL) at 41 ^oC. Following the general workup and deprotection, the crude mixture was purified by flash chromatography (SiO_2, 10 g, 50% EtOAc in Hexane) deoxygenated alkyne was obtained as a pale yellow solid (0.15 g, 76%): TLC R_f = 0.5 (50% EtOAc in Hexane); ^1H NMR (500 MHz, $CDCl_3$) δ 8.99 (s, 1H), 8.56 (s, 1H), 8.42 (s, 1H), 8.17 (s, 1H), 7.91 (d, J = 10.4 Hz, 1H), 6.95 (d, J = 8.5 Hz, 1H), 3.89 (s, 3H), 3.62 (d, J = 2.5 Hz, 2H), 2.21 (t, J = 2.5 Hz, 1H); ^{13}C NMR (125 MHz, $CDCl_3$) δ 158.3, 152.4, 143.9, 142.1, 141.6, 128.7, 127.4, 126.8, 125.2, 110.3, 81.5, 71.1, 55.5, 19.4; IR(neat cm^{-1}) 3201, 3071, 2975, 2933, 2842, 2205, 1607, 1276, 1116, 1018, 809, 697, 433; HRMS (DART, M^+ + H) *m/z* 225.1050 (calculated for $C_{14}H_{12}N_2O$, 225.1028).

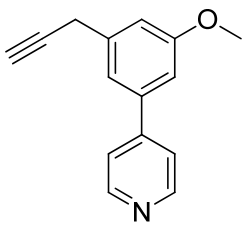

According to general deoxygenation protocol, alkynol (0.34mmol, 0.11g) dissolved in 0.1M CH_2Cl_2 was subjected to deoxygenation with $BF_3.OEt_2$ (1.4mmol, 0.17mL) and

triethylsilane (0.7mmol, 0.11mL) at 41 °C. Following the general workup and deprotection, the crude mixture was purified by flash chromatography (SiO_2, 7 g, 50% EtOAc in Hexane) deoxygenated alkyne was obtained as a brownish oil (0.05 g, 67%): TLC R_f = 0.3 (50% EtOAc in Hexane); ^{1}H NMR (500 MHz, $CDCl_3$) δ 8.62 (d, J = 5.6 Hz, 2H), 7.45 (d, J = 6.0 Hz, 2H), 7.18 (s, 1H), 7.00 (s, 1H), 6.96 (s, 1H), 3.84 (s, 3H), 3.63 (d, J = 2.4 Hz, 2H), 2.21 (t, J = 2.7 Hz, 1H); ^{13}C NMR (125 MHz, $CDCl_3$) δ 160.6, 150.4, 148.2, 140.0, 138.7, 121.9, 119.2, 114.2, 111.4, 81.5, 71.2, 55.6, 25.1; IR(neat cm^{-1}) 3288, 2959, 2931, 2837, 2113, 1592, 1406, 1217, 1049, 816, 627; HRMS (DART, M^+ + H) *m/z* 224.1100 (calculated for $C_{15}H_{13}NO$, 224.1075).

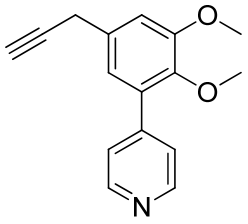

According to general deoxygenation protocol, alkynol (1.0mmol, 0.35g) dissolved in 0.1M CH_2Cl_2 was subjected to deoxygenation with $BF_3.OEt_2$ (5.0mmol, 1.7mL) and triethylsilane (2.5mmol, 0.41mL) at 41 °C. Following the general workup and deprotection, the crude mixture was purified by flash chromatography (SiO_2, 10 g, 50% EtOAc in Hexane) deoxygenated alkyne was obtained as a yellow brownish solid (0.2 g, 76%): TLC R_f = 0.3 (50% EtOAc in Hexane); ^{1}H NMR (500 MHz, $CDCl_3$) δ 8.62 (d, J =

6.1 Hz, 2H), 7.46 (d, J = 6.1 Hz, 2H), 6.97 (d, J = 1.9 Hz, 1H), 6.91 (d, J = 2.0 Hz, 1H), 3.91 (s, 3H), 3.60 (d, J = 2.7 Hz, 2H), 3.58 (s, 3H), 2.21 (t, J = 2.7 Hz, 1H); ^{13}C NMR (125 MHz, $CDCl_3$) δ 153.4, 149.6, 146.3, 145.7, 133.0, 132.6, 124.3, 121.3, 112.7, 81.8, 71.1, 61.1, 56.2, 24.9; IR(neat cm^{-1}) 3285, 3034, 2908, 2885, 2836, 2117, 1711, 1404, 1264, 1132, 994, 816, 627; HRMS (DART, M^+ + H) *m/z* 254.1196 (calculated for $C_{16}H_{15}NO_2$, 254.1181).

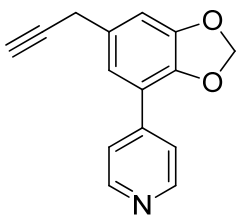

According to general deoxygenation protocol, alkynol (0.75mmol, 0.24g) dissolved in 0.1M CH_2Cl_2 was subjected to deoxygenation with $BF_3.OEt_2$ (3.7mmol, 1.2mL) and triethylsilane (1.9mmol, 0.30mL) at 41 °C. Following the general workup and deprotection, the crude mixture was purified by flash chromatography (SiO_2, 7 g, 50% EtOAc in Hexane) deoxygenated alkyne was obtained as a pale white solid (0.13 g, 74%): TLC R_f = 0.3 (50% EtOAc in Hexane); ^{1}H NMR (500 MHz, $CDCl_3$) δ 8.62 (d, J = 5.4 Hz, 2H), 7.60 (d, J = 5.9 Hz, 2H), 7.06 (s, 1H), 6.87 (s, 1H), 6.01 (s, 2H), 3.55 (d, J = 2.3 Hz, 2H), 2.20 (t, J = 2.6 Hz, 1H); ^{13}C NMR (125 MHz, $CDCl_3$) δ 150.3, 148.8, 144.5, 143.3, 130.8, 122.2, 119.7, 119.5, 109.2, 101.6, 81.8, 71.1, 24.8; IR(neat cm^{-1}) 3229, 3069, 3031, 2989, 2917, 2114, 1703, 1599, 1407, 1256, 1094, 944, 815, 652; HRMS (DART, M^+ + H) *m/z* 238.0883 (calculated for $C_{15}H_{11}NO_2$, 238.0868).

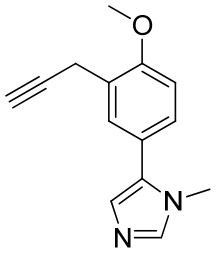

According to general deoxygenation protocol, alkynol (0.51mmol, 0.16g) dissolved in 0.1M CH_2Cl_2 was subjected to deoxygenation with $BF_3.OEt_2$ (2.0mmol, 0.26mL) and triethylsilane (1.0mmol, 0.16mL) at 41 °C. Following the general workup and deprotection, the crude mixture was purified by flash chromatography (SiO_2, 7 g, 3% MeOH in CH_2Cl_2) deoxygenated alkyne was obtained as a yellow oil (0.08 g, 70%): TLC R_f = 0.1 (50% EtOAc in Hexane); ^{1}H NMR (500 MHz, $CDCl_3$) δ 7.53 (d, J = 2.1 Hz, 1H), 7.48 (s, 1H), 7.24 – 7.21 (m, 1H), 7.02 (s, 1H), 6.88 (d, J = 8.4 Hz, 1H), 3.85 (s, 3H), 3.61 (s, 3H), 3.58 (d, J = 2.6 Hz, 2H), 2.17 (t, J = 2.7 Hz, 1H); ^{13}C NMR (125 MHz, $CDCl_3$) δ 156.8, 138.8, 133.5, 129.4, 128.5, 127.6, 125.1, 122.2, 110.3, 81.6, 71.1, 55.7, 32.6, 19.4; IR(neat cm^{-1}) 3215, 2969, 2930, 2884, 1658, 1466, 1127, 950, 816, 627; HRMS (DART, $M^+ + H$) *m/z* 227.1184 (calculated for $C_{14}H_{14}N_2O$, 227.1204).

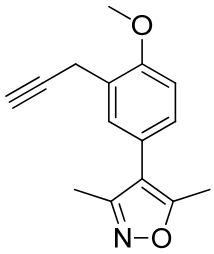

According to general deoxygenation protocol, alkynol (0.33mmol, 0.11g) dissolved in 0.1M CH_2Cl_2 was subjected to deoxygenation with $BF_3.OEt_2$ (1.7mmol, 0.21mL) and triethylsilane (0.8mmol, 0.13mL) at 41 °C. Following the general workup and deprotection, the crude mixture was purified by flash chromatography (SiO_2, 7g, 50% EtOAc in Hexane) deoxygenated alkyne was obtained as a white solid (0.06 g, 74%): TLC R_f = 0.7 (50% EtOAc in Hexane); ^{1}H NMR (500 MHz, $CDCl_3$) δ 7.42 (d, *J* = 2.1 Hz, 1H), 7.10 (dd, *J* = 8.3, 2.2 Hz, 1H), 6.89 (d, *J* = 8.3 Hz, 1H), 3.85 (s, 3H), 3.59 (d, *J* = 2.4 Hz, 2H), 2.38 (s, 3H), 2.25 (s, 3H), 2.18 (t, *J* = 2.7 Hz, 1H); ^{13}C NMR (125 MHz, $CDCl_3$) δ 165.0, 159.0, 156.3, 129.8, 128.7, 125.2, 122.7, 116.5, 110.4, 81.7, 71.0, 55.7, 19.4, 11.7, 11.0; IR(neat cm^{-1}) 3243, 3020, 2927, 2838, 2115, 1632, 1504, 1246, 1114, 1027, 815, 684; HRMS (DART, M^+ + H) *m/z* 242.1195 (calculated for $C_{15}H_{15}NO_2$, 242.1181).

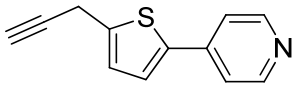

According to general deoxygenation protocol, alkynol (0.44mmol, 0.13g) dissolved in 0.1M CH_2Cl_2 was subjected to deoxygenation with $BF_3.OEt_2$ (1.8mmol, 0.22mL) and triethylsilane (0.9mmol, 0.14mL) at 41 ^oC. Following the general workup and deprotection, the crude mixture was purified by HPLC chromatogaraphy with 60% ACN in water; deoxygenated alkyne was obtained as a pale white solid (0.06 g, 66%): TLC R_f = 0.4 (50% EtOAc in Hexane); ^1H NMR (500 MHz, $CDCl_3$) δ 8.55 (d, *J* = 4.5 Hz, 1H), 7.40 (d, *J* = 5.0 Hz, 1H), 7.33 (d, *J* = 3.6 Hz, 0H), 6.98 (d, *J* = 3.2 Hz, 1H), 3.78 (d, *J* = 2.3 Hz, 2H), 2.24 (t, *J* = 2.4 Hz, 1H); ^{13}C NMR (125 MHz, $CDCl_3$) δ 150.6, 141.5, 141.2, 140.1, 126.8, 125.4, 119.7, 80.5, 71.1, 20.3; IR(neat cm^{-1}) 3181, 3072, 3040, 3017, 2112, 1592, 1414, 1219, 991, 800, 689, 463; HRMS (DART, $M^+ + H$) *m/z* 200.0556 (calculated for $C_{12}H_9NS$, 200.0534).

APPENDIX

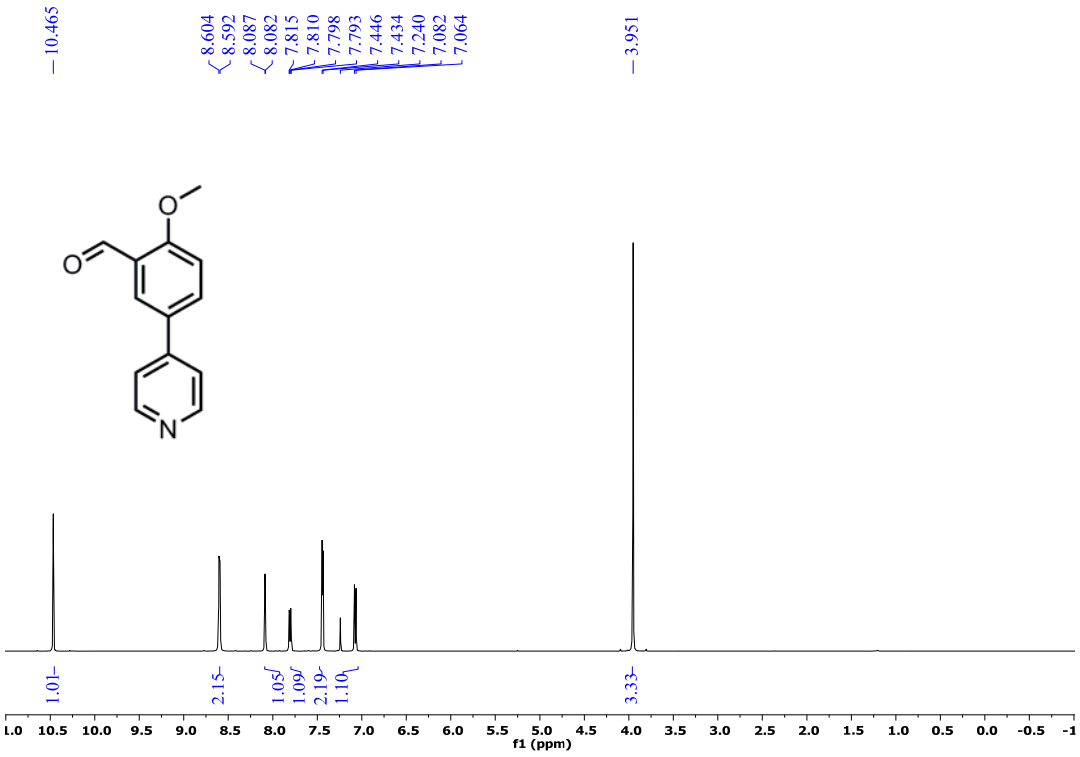
10.465
8.604
8.592
8.087
8.082
7.815
7.810
7.798
7.793
7.446
7.434
7.240
7.082
7.064
3.951
O
O
N
1.01
2.15
1.05
1.09
2.19
1.10
3.33
f1 (ppm)

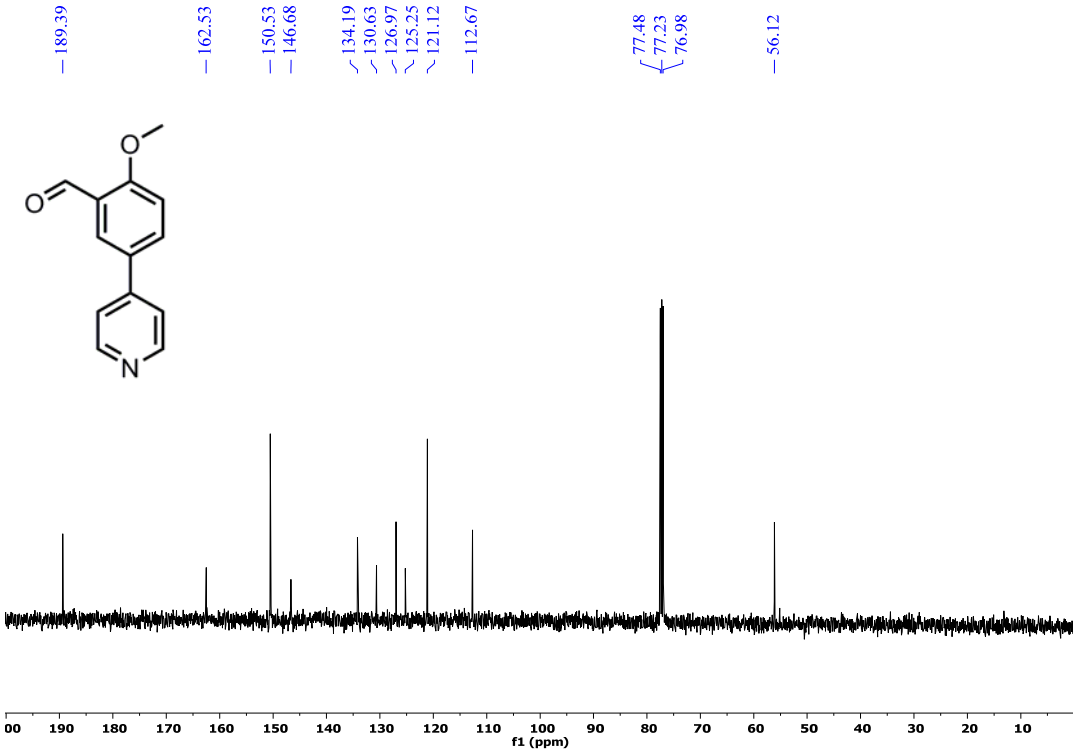
189.39
162.53
150.53
146.68
134.19
130.63
126.97
125.25
121.12
112.67
77.48
77.23
76.98
56.12
O
O
N
f1 (ppm)

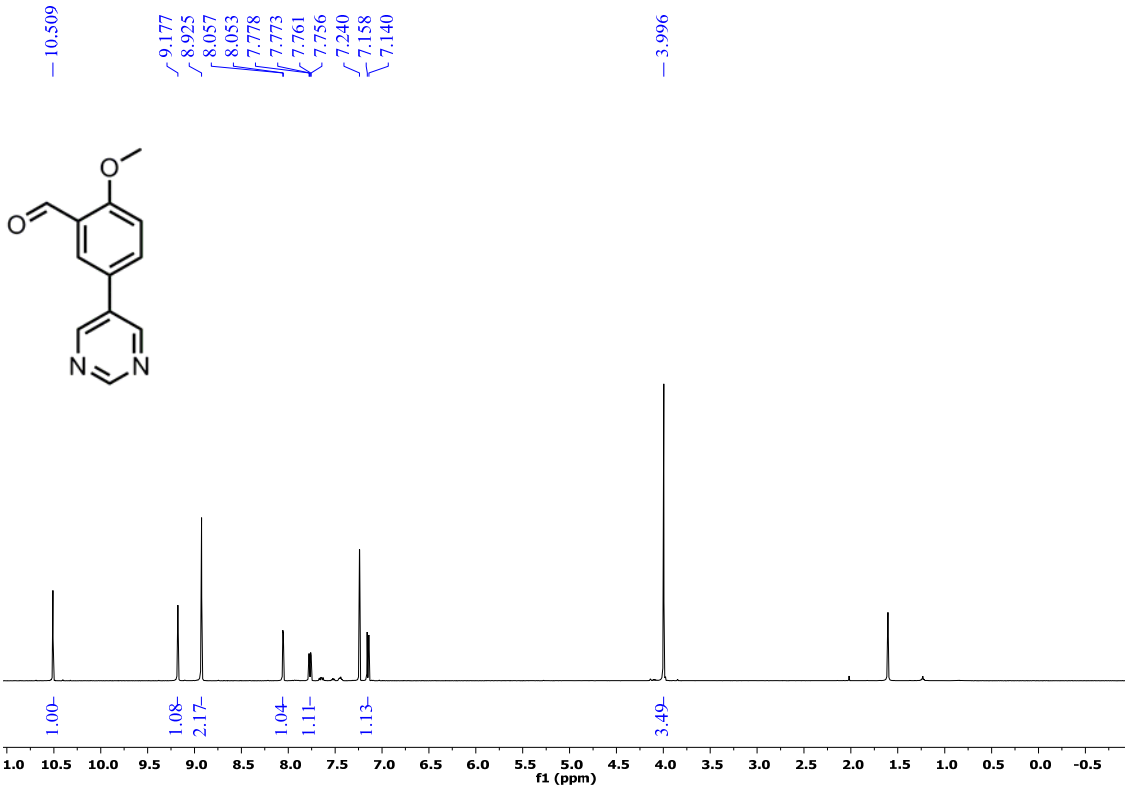
10.509
9.177
8.925
8.057
8.053
7.778
7.773
7.761
7.756
7.240
7.158
7.140
3.996
1.00
1.08
2.17
1.04
1.11
1.13
3.49
f1 (ppm)

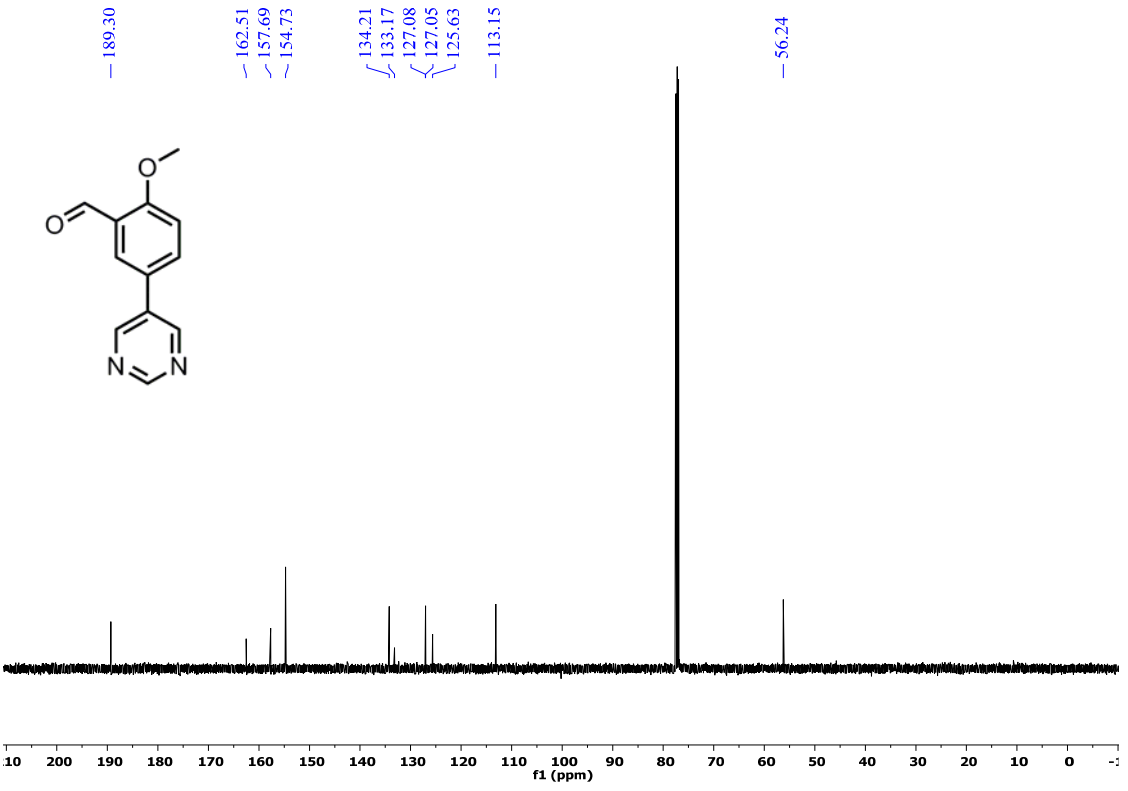
189.30
162.51
157.69
154.73
134.21
133.17
127.08
127.05
125.63
113.15
56.24
f1 (ppm)

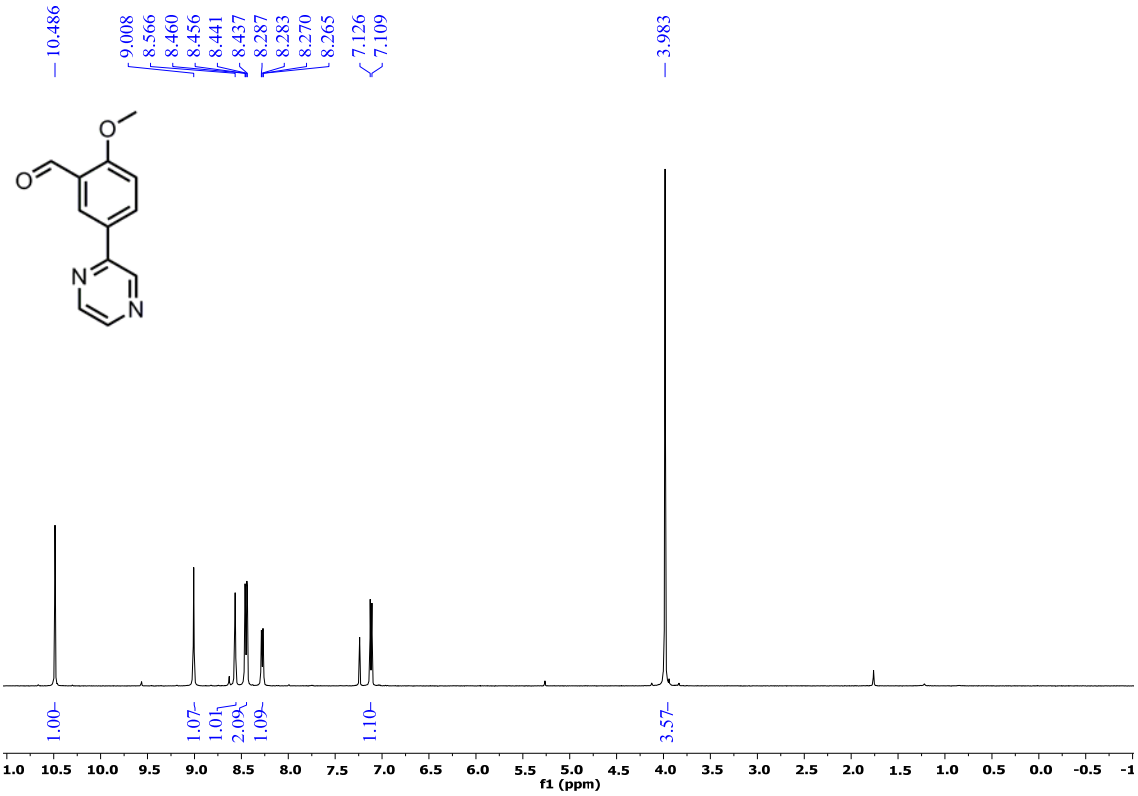
10.486
9.008
8.566
8.460
8.456
8.441
8.437
8.287
8.283
8.270
8.265
7.126
7.109
3.983
1.00
1.07
1.01
2.09
1.09
1.10
3.57
f1 (ppm)

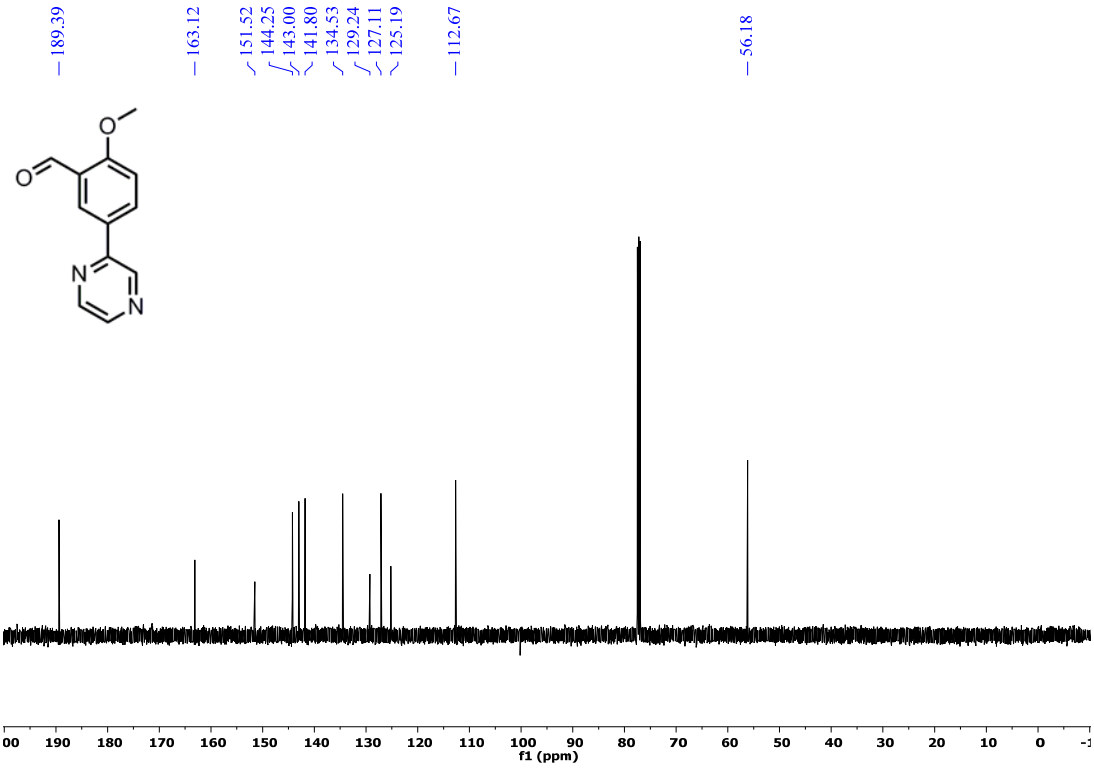
189.39
163.12
151.52
144.25
143.00
141.80
134.53
129.24
127.11
125.19
112.67
56.18
f1 (ppm)

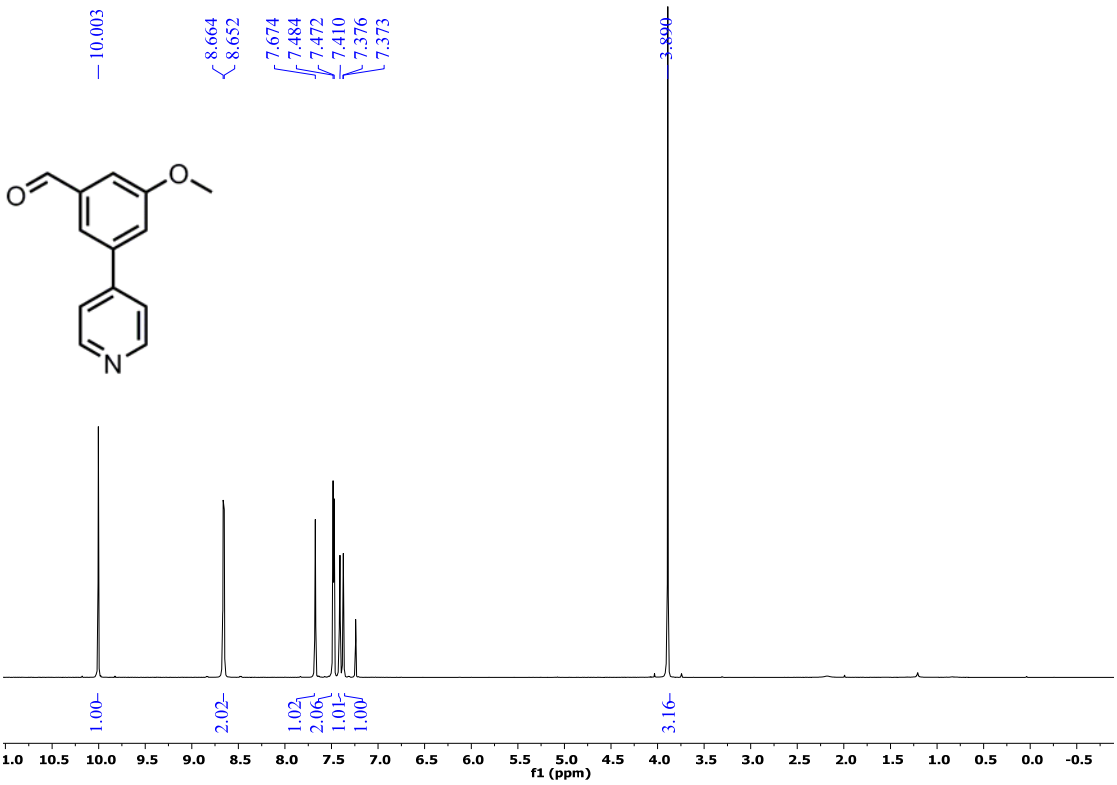
10.003
8.664
8.652
7.674
7.484
7.472
7.410
7.376
7.373
3.890
O
O
N
1.00
2.02
1.02
2.06
1.01
1.00
3.16
f1 (ppm)

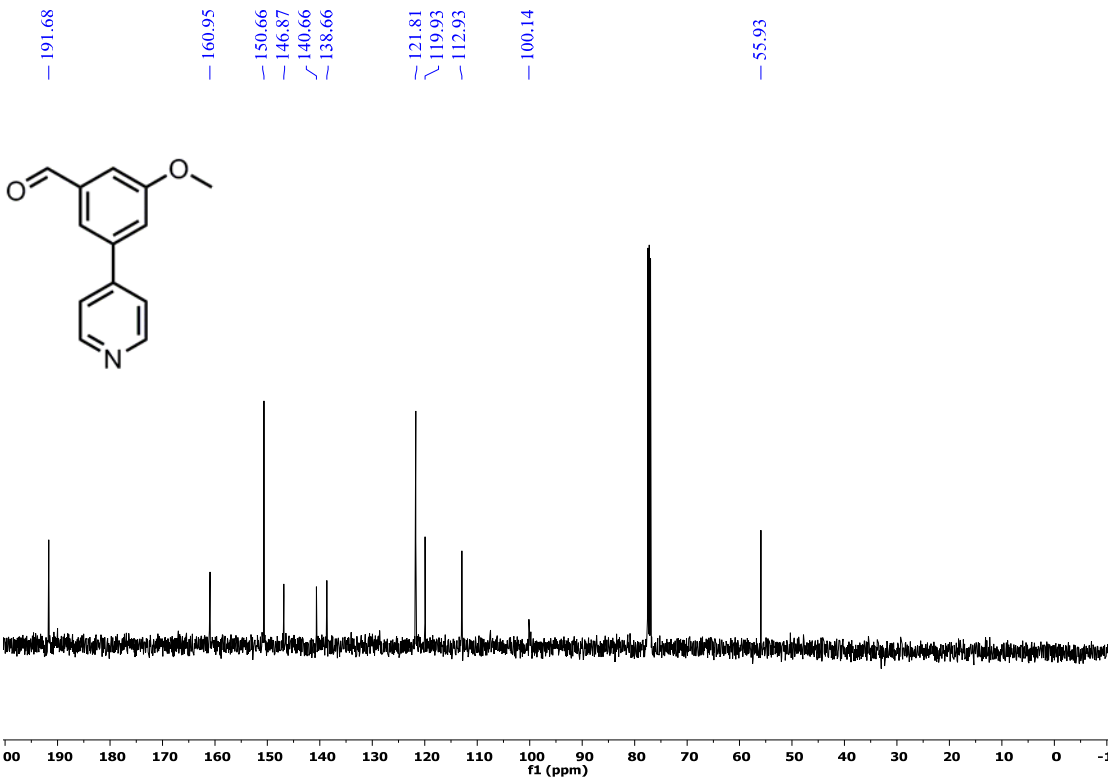
191.68
160.95
150.66
146.87
140.66
138.66
121.81
119.93
112.93
100.14
55.93
O
O
N
f1 (ppm)

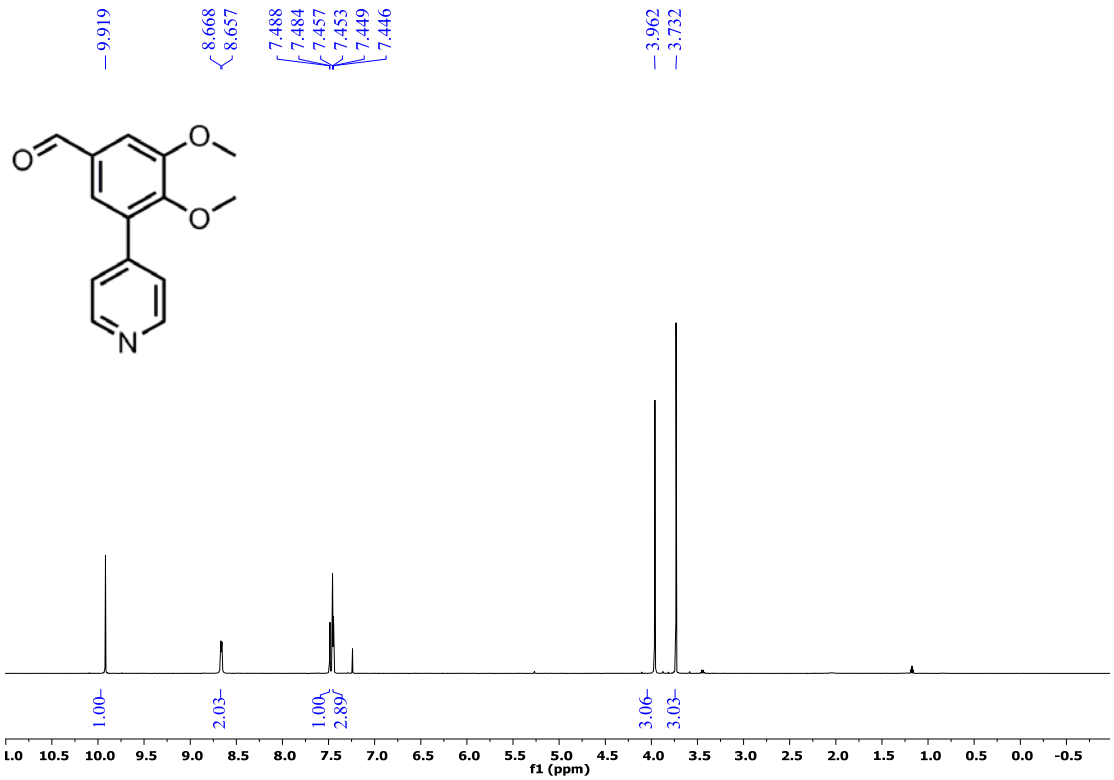
9.919
8.668
8.657
7.488
7.484
7.457
7.453
7.449
7.446
3.962
3.732
O
O
O
N
1.00
2.03
1.00
2.89
3.06
3.03
f1 (ppm)

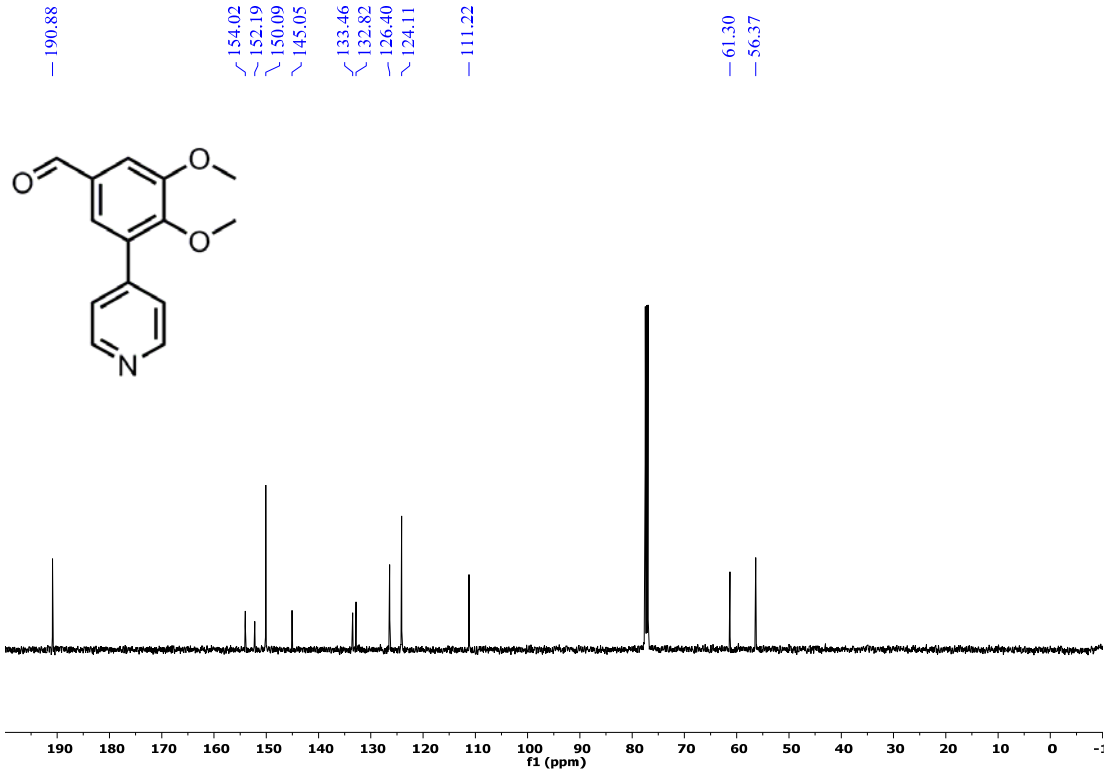
190.88
154.02
152.19
150.09
145.05
133.46
132.82
126.40
124.11
111.22
61.30
56.37
O
O
O
N
f1 (ppm)

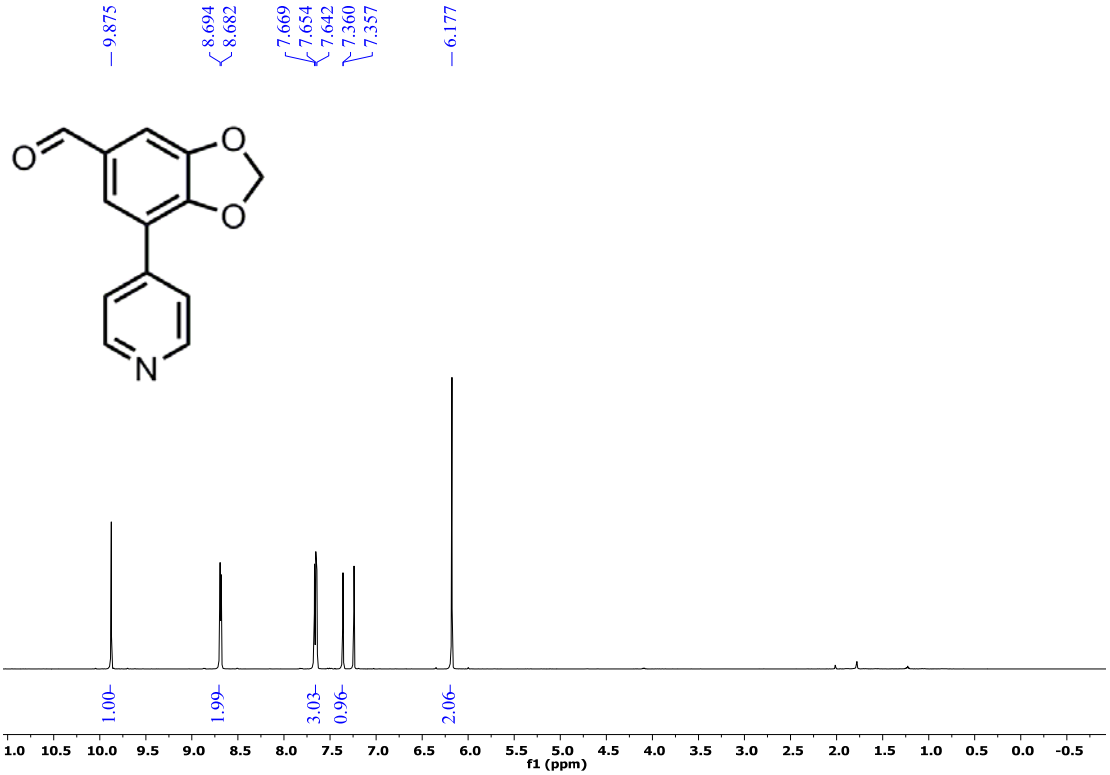
9.875
8.694
8.682
7.669
7.654
7.642
7.360
7.357
6.177
1.00
1.99
3.03
0.96
2.06
f1 (ppm)

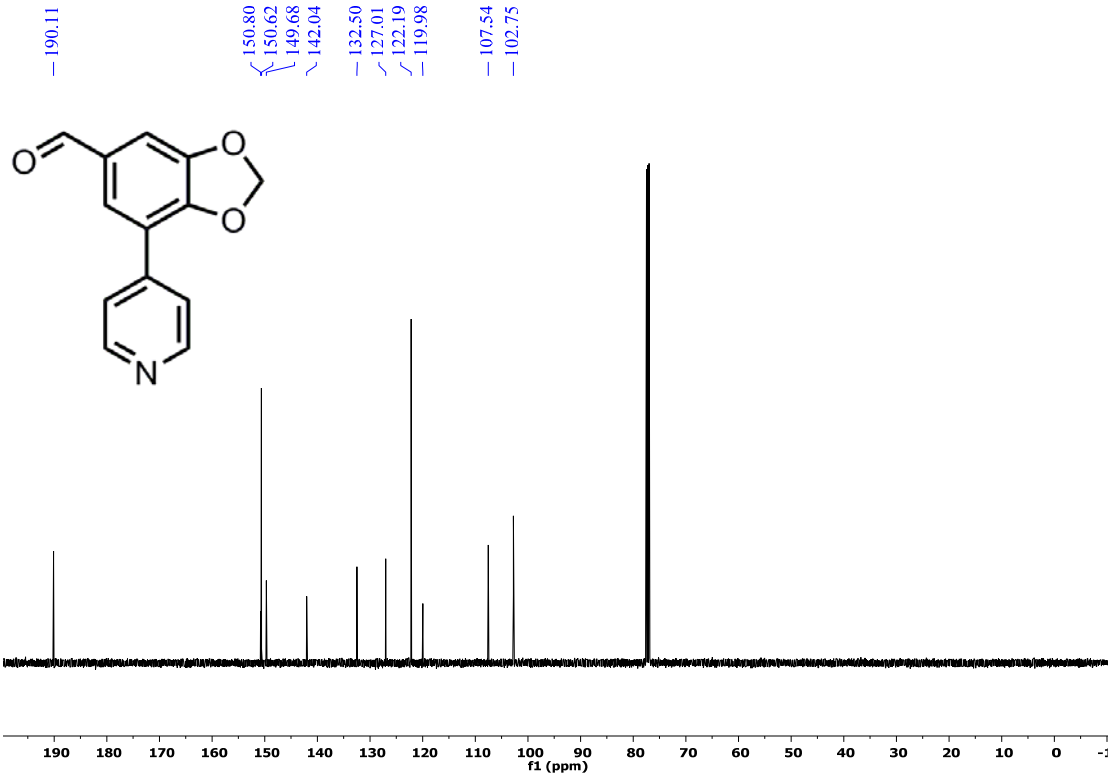
190.11
150.80
150.62
149.68
142.04
132.50
127.01
122.19
119.98
107.54
102.75
f1 (ppm)

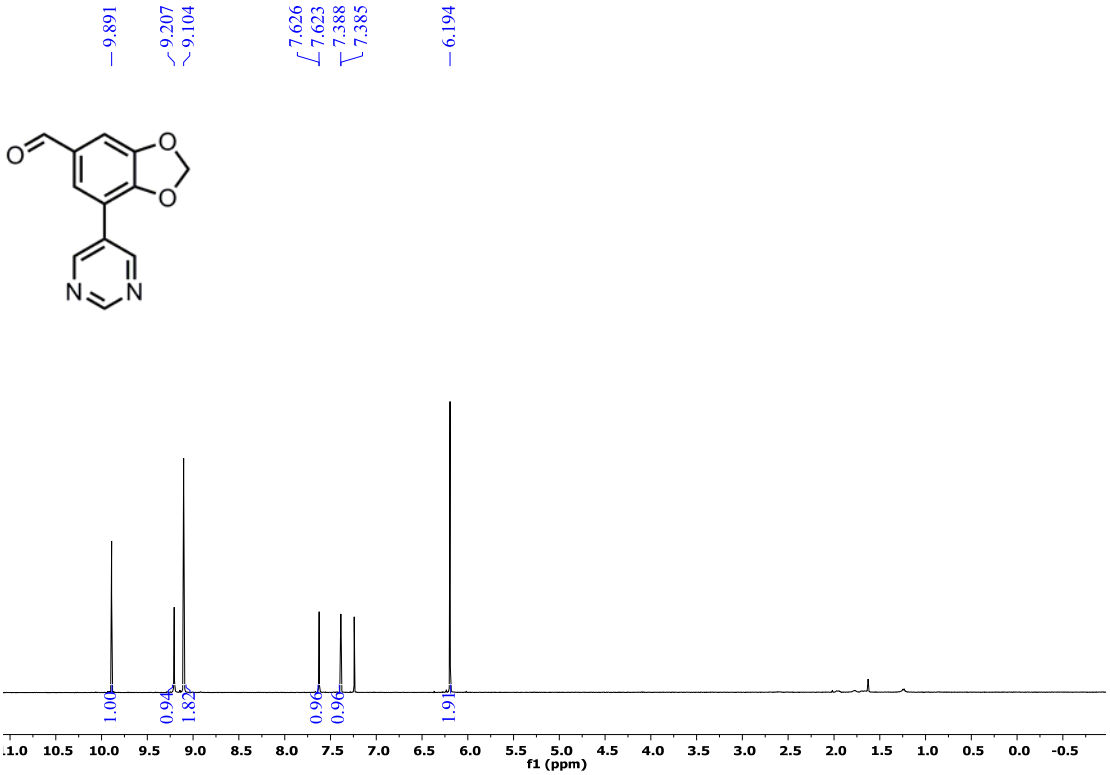
9.891
9.207
9.104
7.626
7.623
7.388
7.385
6.194
1.00
0.94
1.82
0.96
0.96
1.91
f1 (ppm)

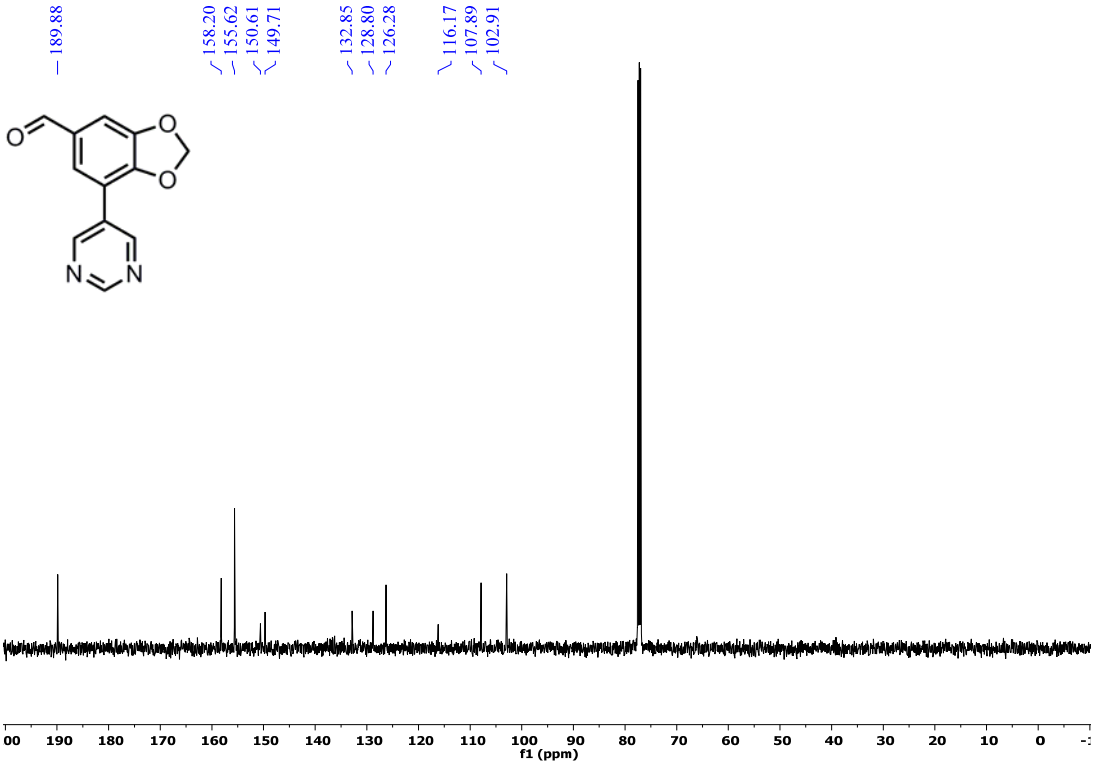
189.88
158.20
155.62
150.61
149.71
132.85
128.80
126.28
116.17
107.89
102.91
f1 (ppm)

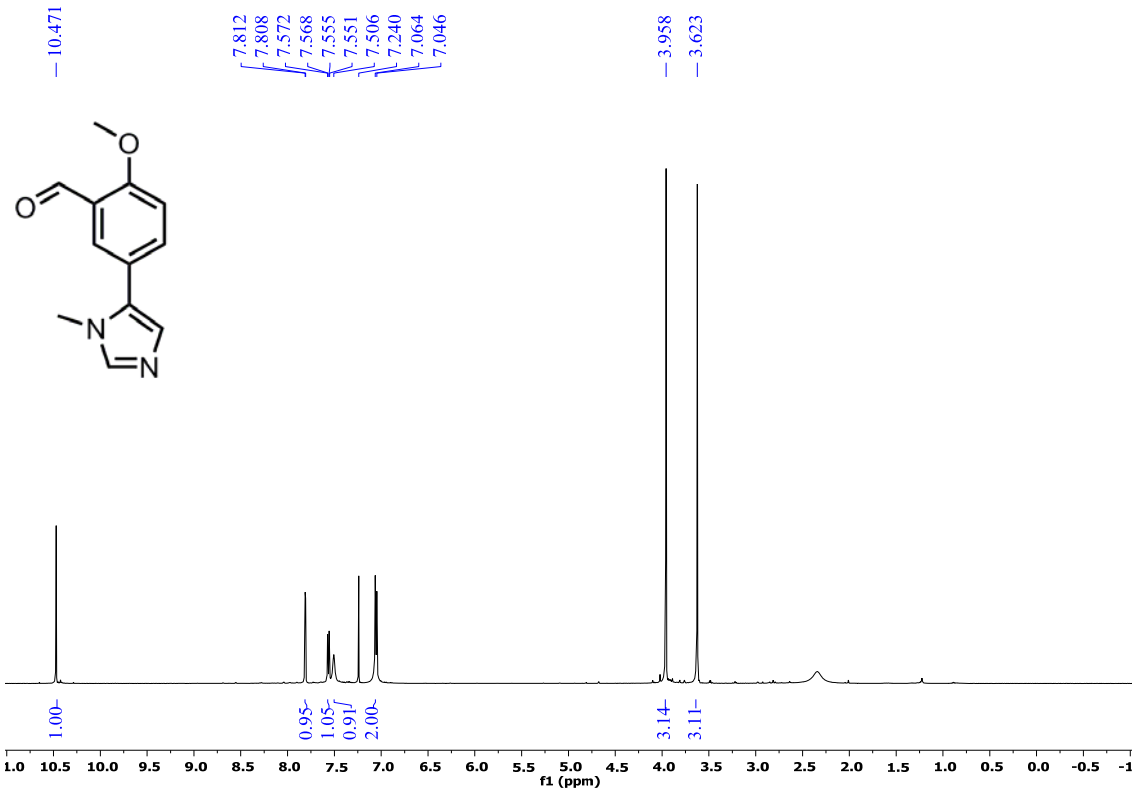
10.471
7.812
7.808
7.572
7.568
7.555
7.551
7.506
7.240
7.064
7.046
3.958
3.623
1.00
0.95
1.05
0.91
2.00
3.14
3.11
f1 (ppm)

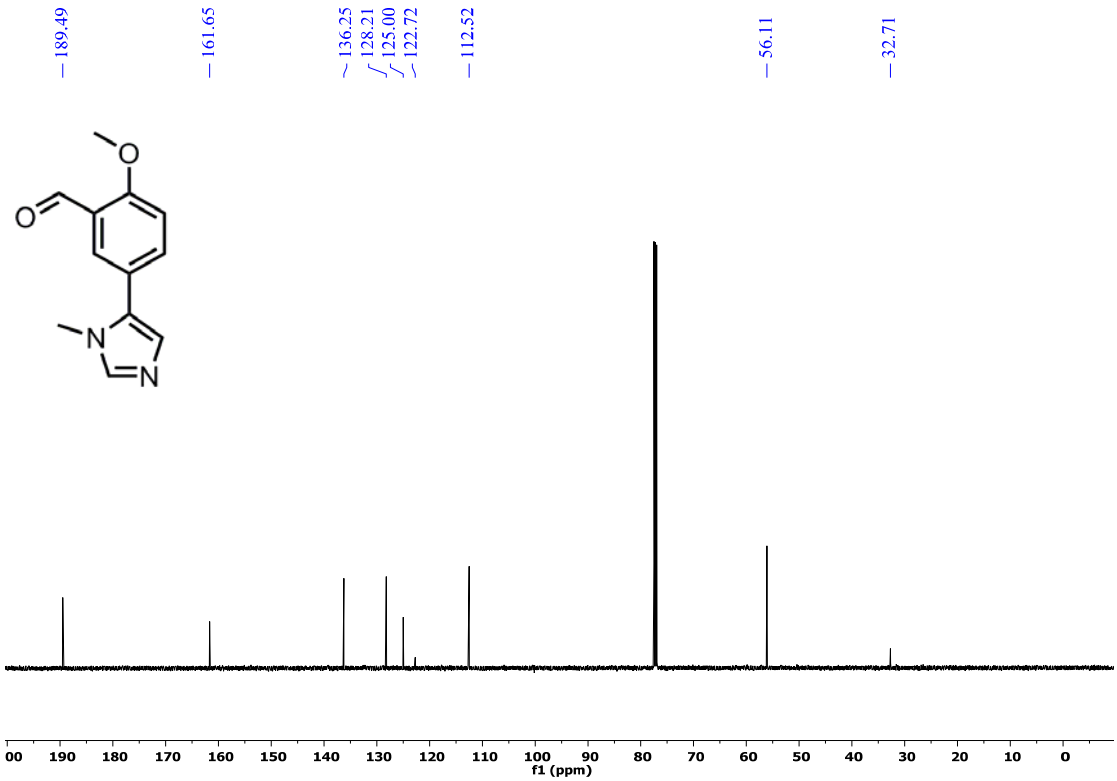
189.49
161.65
136.25
128.21
125.00
122.72
112.52
56.11
32.71
f1 (ppm)

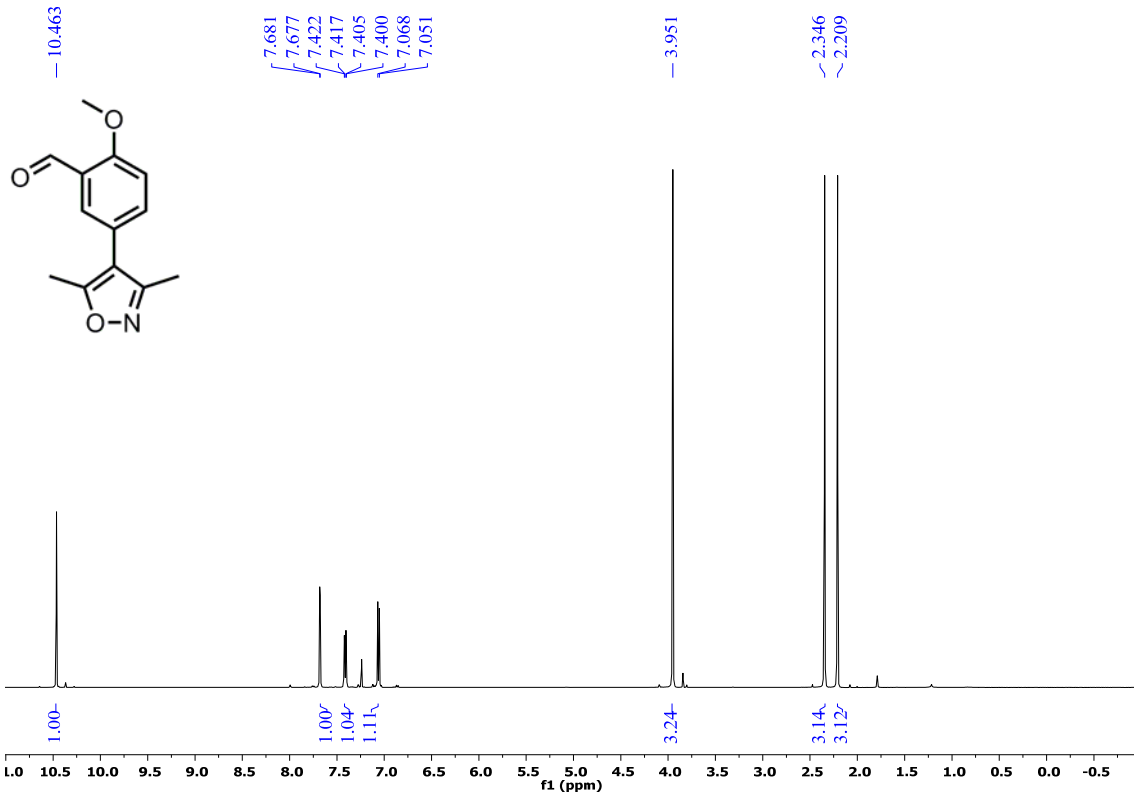
10.463
7.681
7.677
7.422
7.417
7.405
7.400
7.068
7.051
3.951
2.346
2.209
1.00
1.00
1.04
1.11
3.24
3.14
3.12
f1 (ppm)

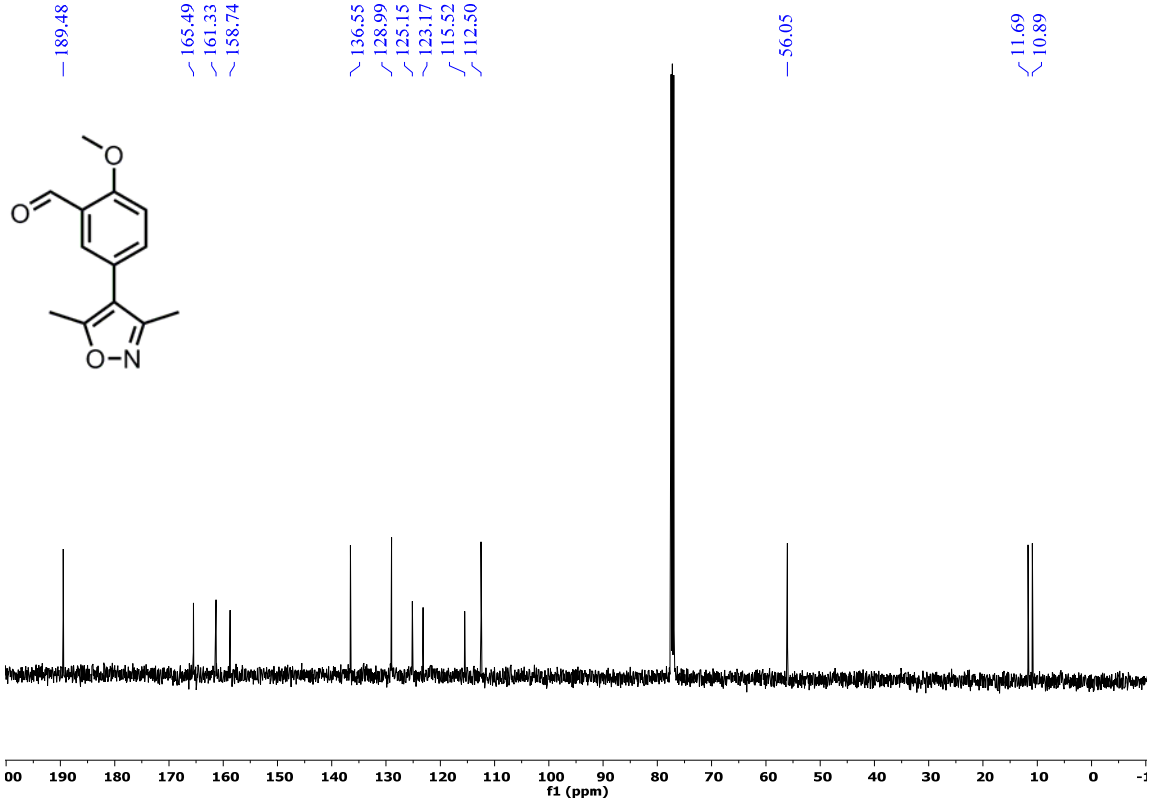
189.48
165.49
161.33
158.74
136.55
128.99
125.15
123.17
115.52
112.50
56.05
11.69
10.89
f1 (ppm)

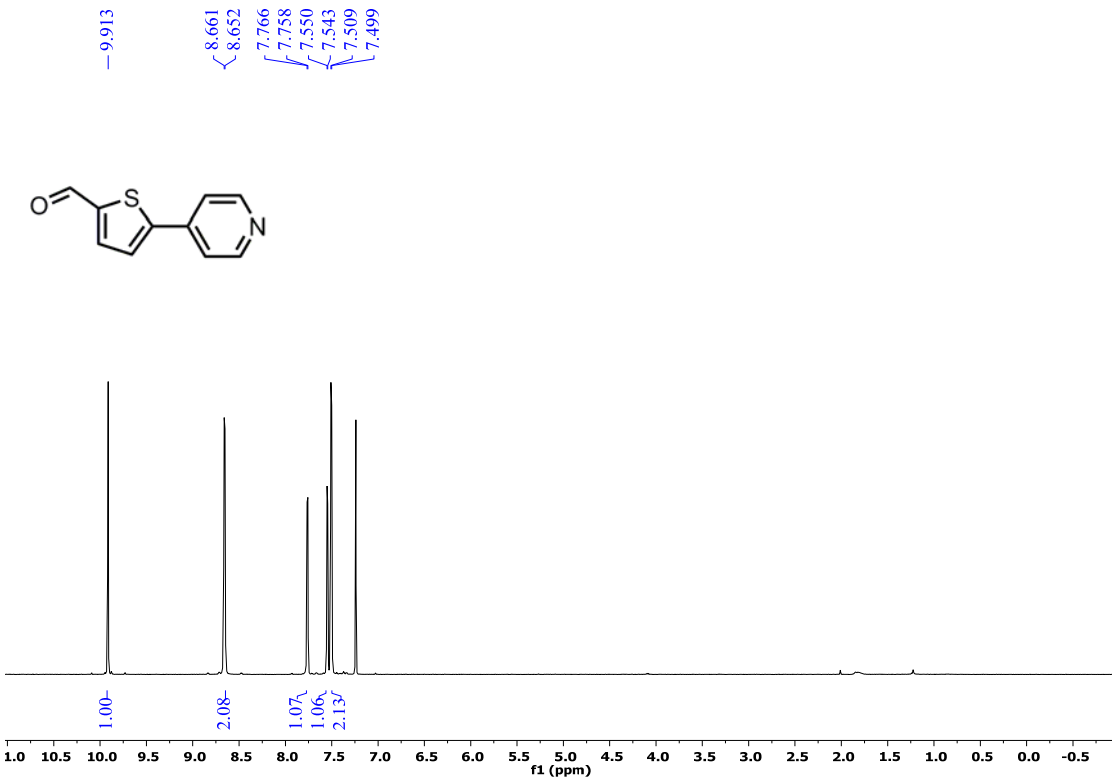
9.913
8.661
8.652
7.766
7.758
7.550
7.543
7.509
7.499
O
S
N
1.00
2.08
1.07
1.06
2.13
f1 (ppm)

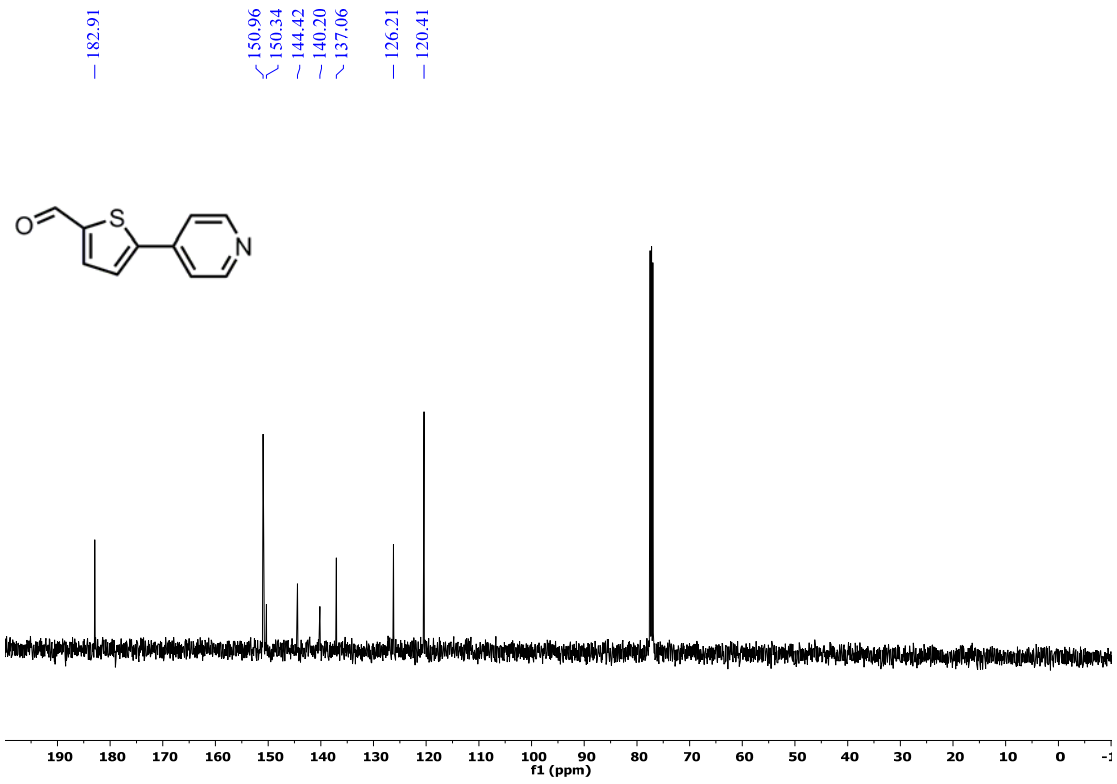
182.91
150.96
150.34
144.42
140.20
137.06
126.21
120.41
O
S
N
f1 (ppm)

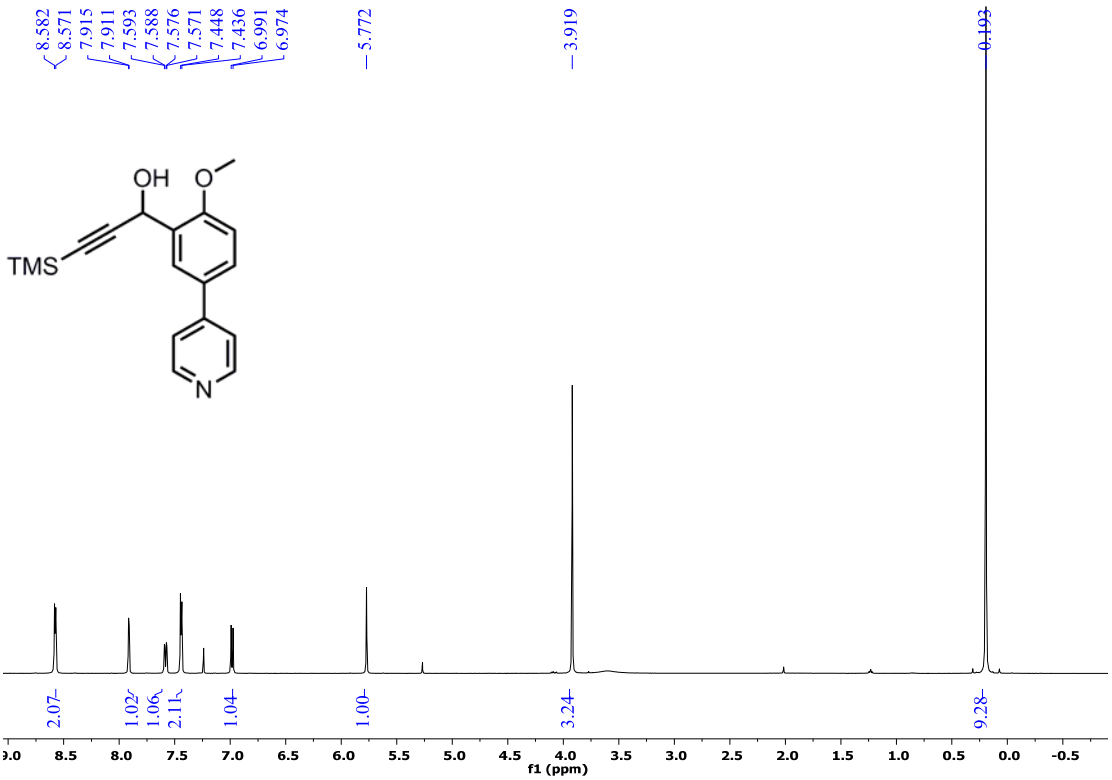
8.582
8.571
7.915
7.911
7.593
7.588
7.576
7.571
7.448
7.436
6.991
6.974
5.772
3.919
0.193
OH
O
TMS
N
2.07
1.02
1.06
2.11
1.04
1.00
3.24
9.28
f1 (ppm)

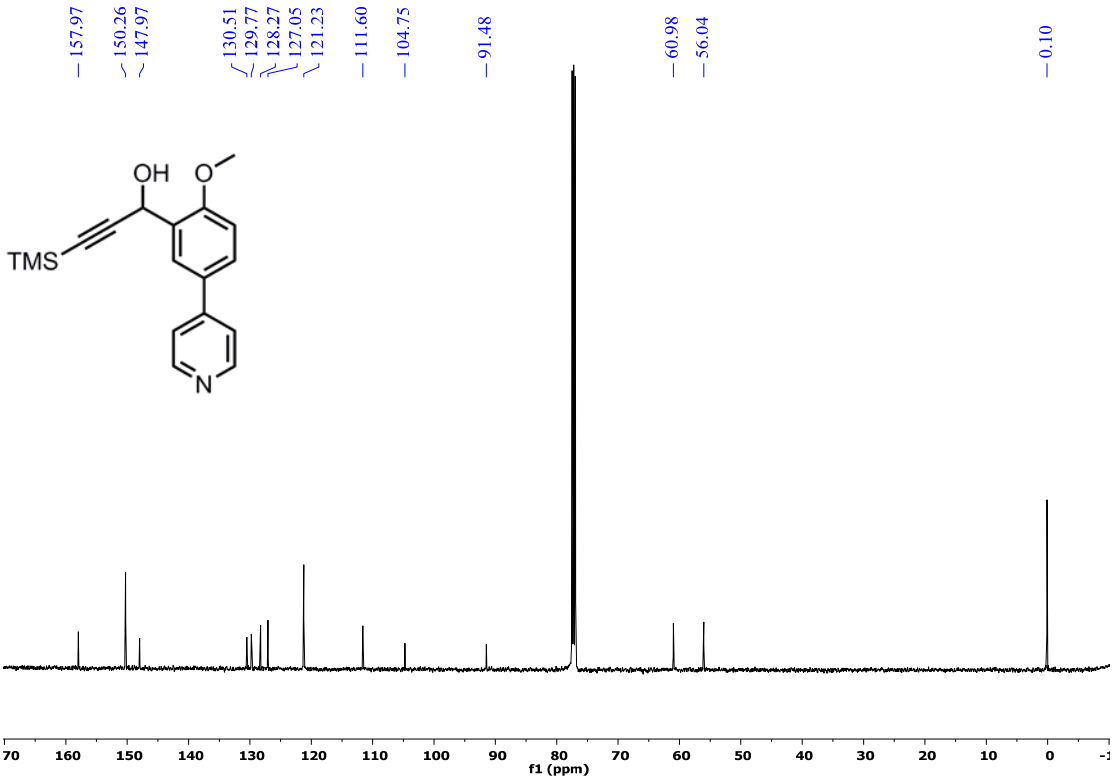
157.97
150.26
147.97
130.51
129.77
128.27
127.05
121.23
111.60
104.75
91.48
60.98
56.04
0.10
OH
O
TMS
N
f1 (ppm)

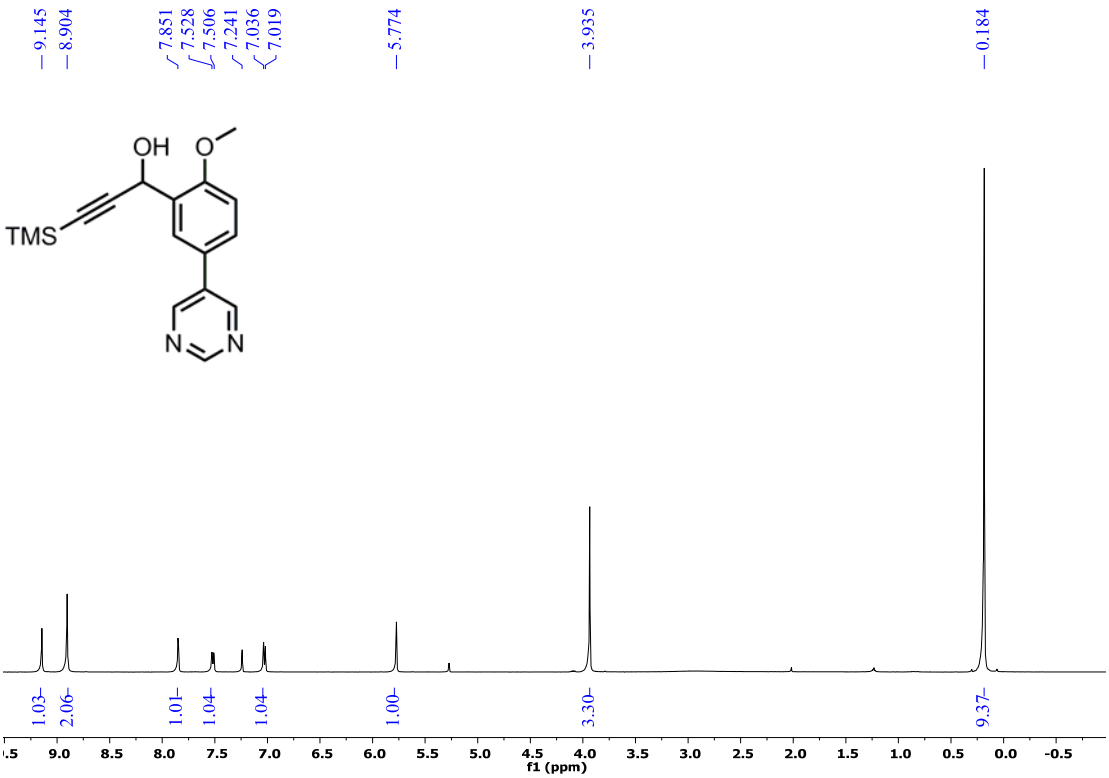
9.145
8.904
7.851
7.528
7.506
7.241
7.036
7.019
5.774
3.935
0.184
OH
O
TMS
N
N
1.03
2.06
1.01
1.04
1.04
1.00
3.30
9.37
f1 (ppm)

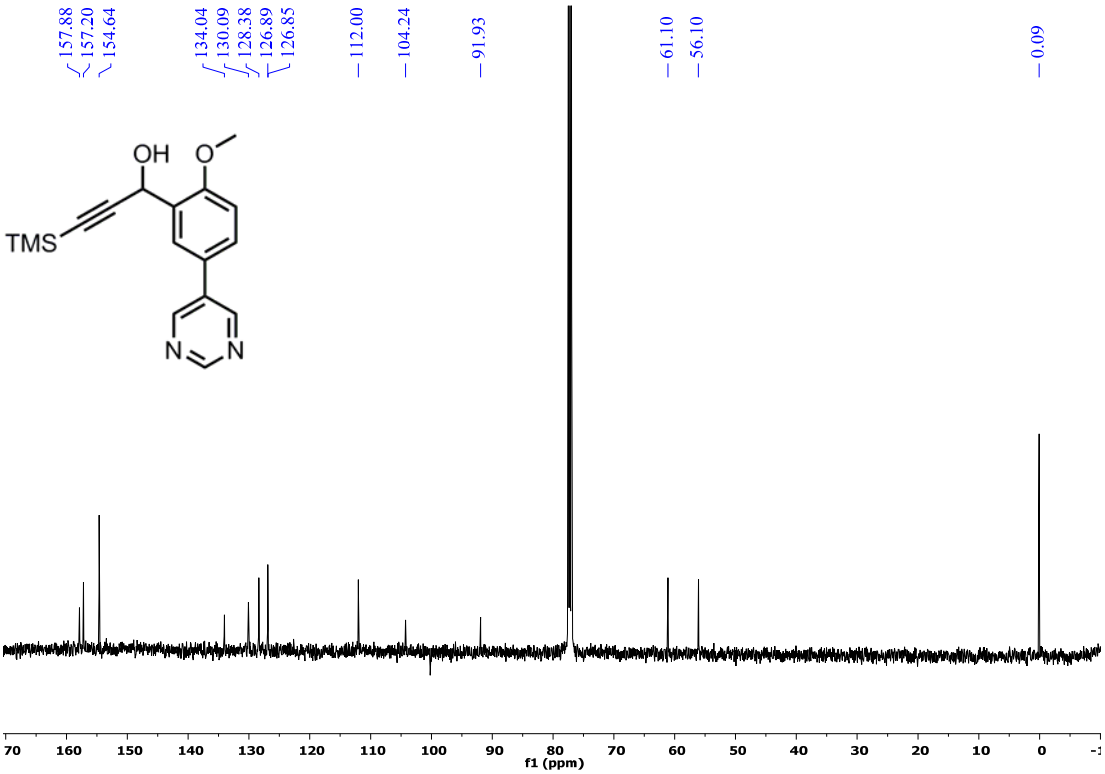
157.88
157.20
154.64
134.04
130.09
128.38
126.89
126.85
112.00
104.24
91.93
61.10
56.10
0.09
OH
O
TMS
N
N
f1 (ppm)

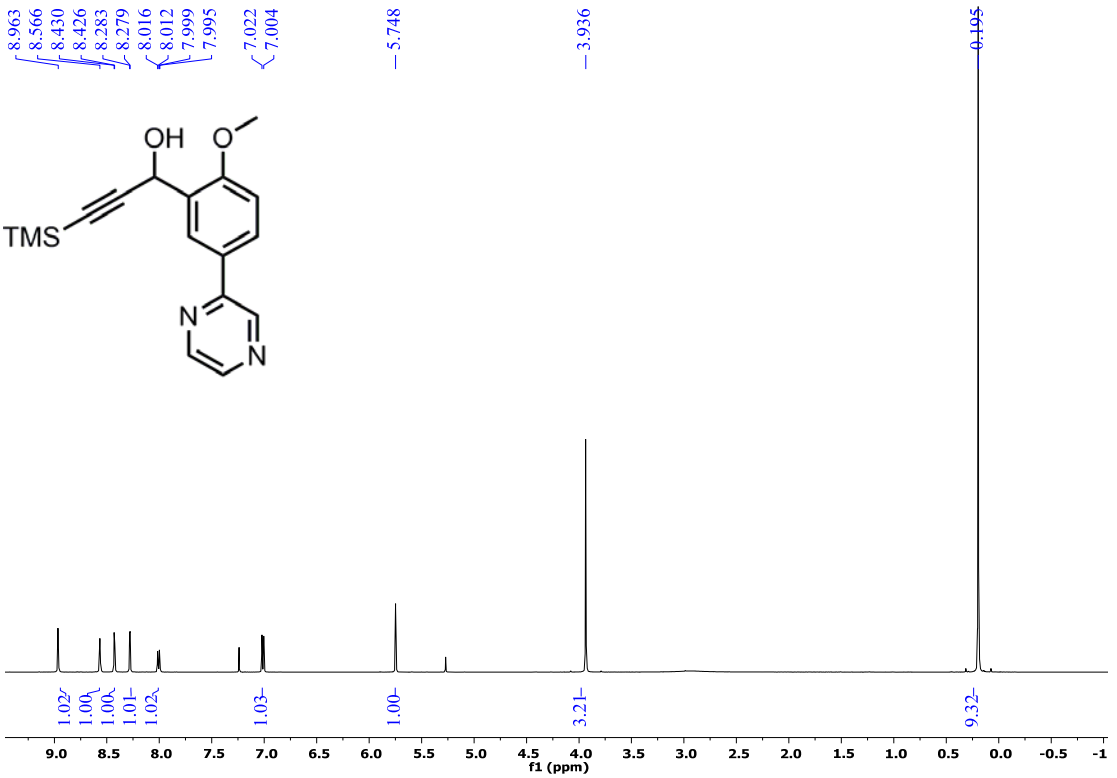
8.963
8.566
8.430
8.426
8.283
8.279
8.016
8.012
7.999
7.995
7.022
7.004
5.748
3.936
0.195
OH
O
TMS
N
N
1.02
1.00
1.00
1.01
1.02
1.03
1.00
3.21
9.32
f1 (ppm)

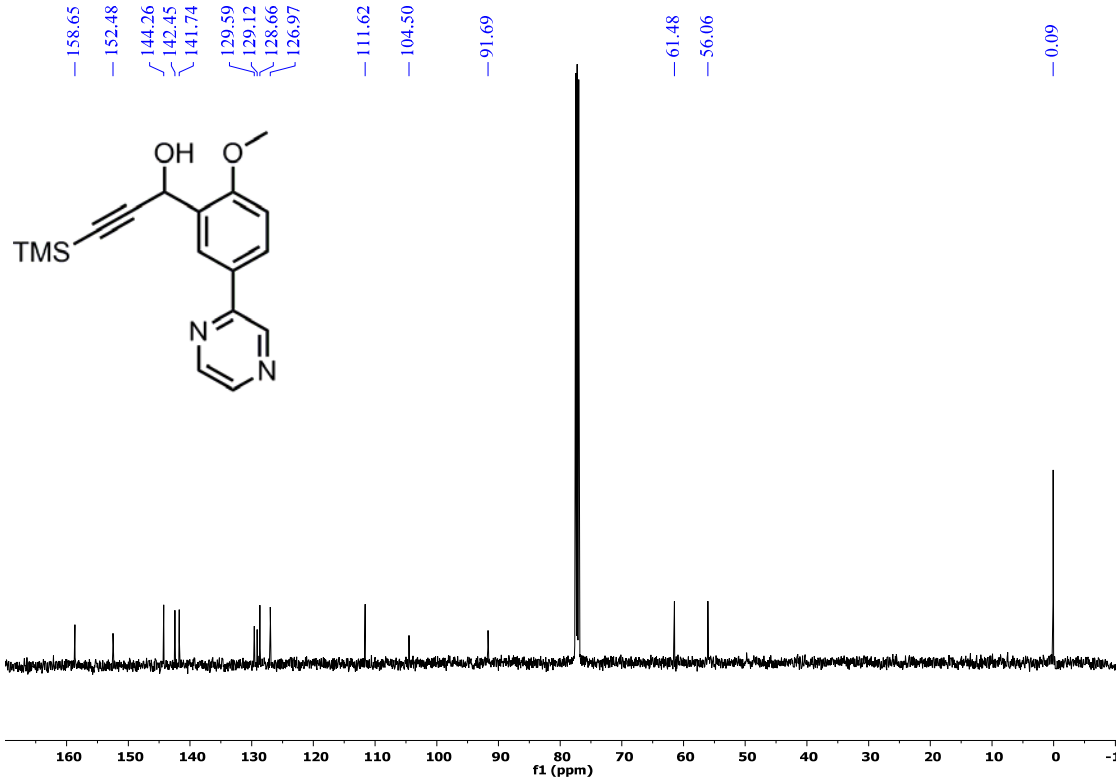
158.65
152.48
144.26
142.45
141.74
129.59
129.12
128.66
126.97
111.62
104.50
91.69
61.48
56.06
0.09
OH
O
TMS
N
N
f1 (ppm)

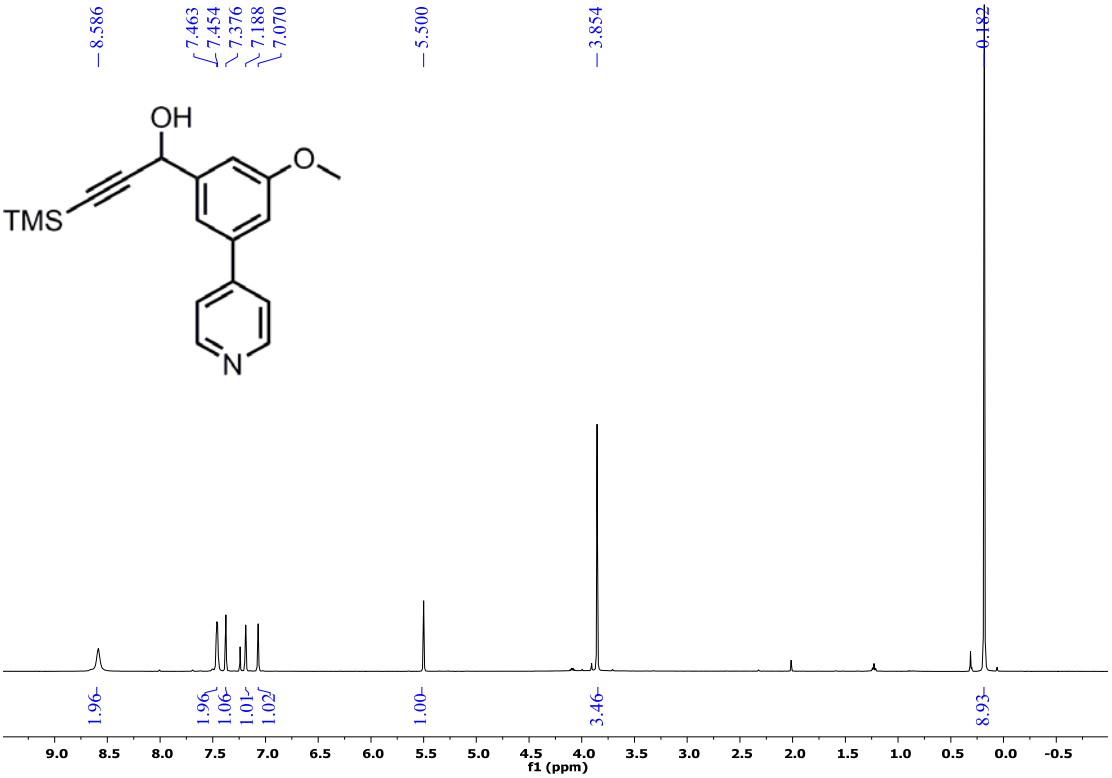
8.586
7.463
7.454
7.376
7.188
7.070
5.500
3.854
0.182
OH
O
TMS
N
1.96
1.96
1.06
1.01
1.02
1.00
3.46
8.93
f1 (ppm)

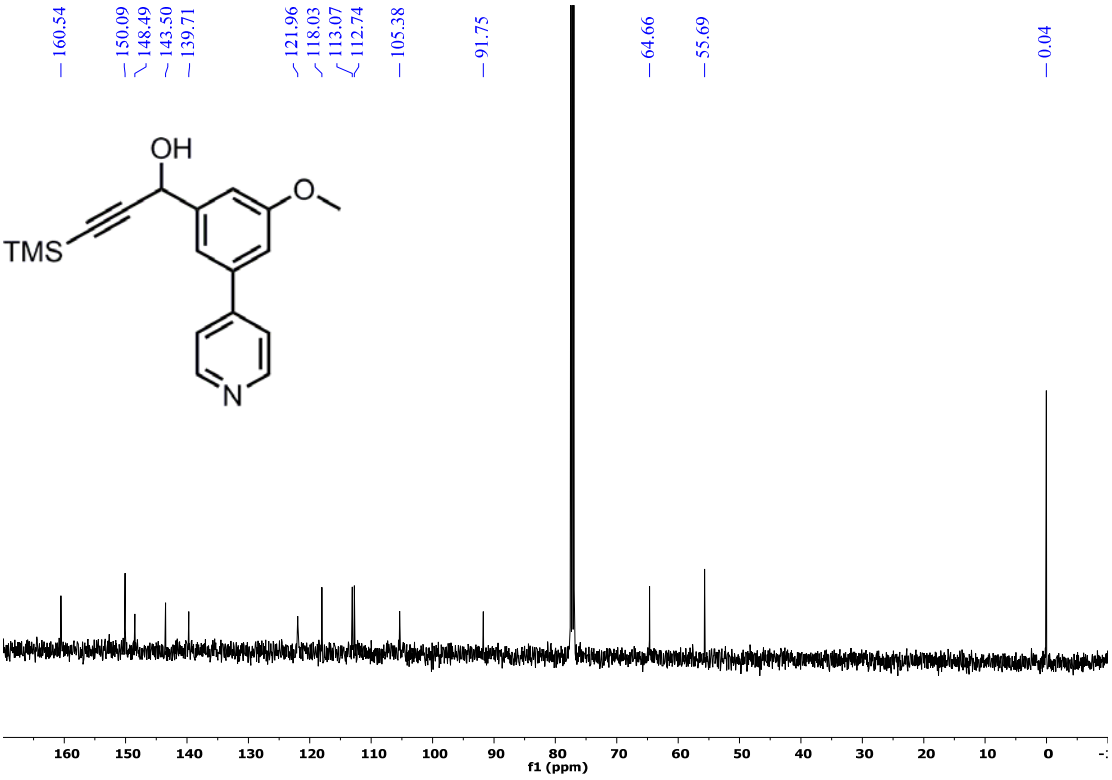
160.54
150.09
148.49
143.50
139.71
121.96
118.03
113.07
112.74
105.38
91.75
64.66
55.69
0.04
OH
O
TMS
N
f1 (ppm)

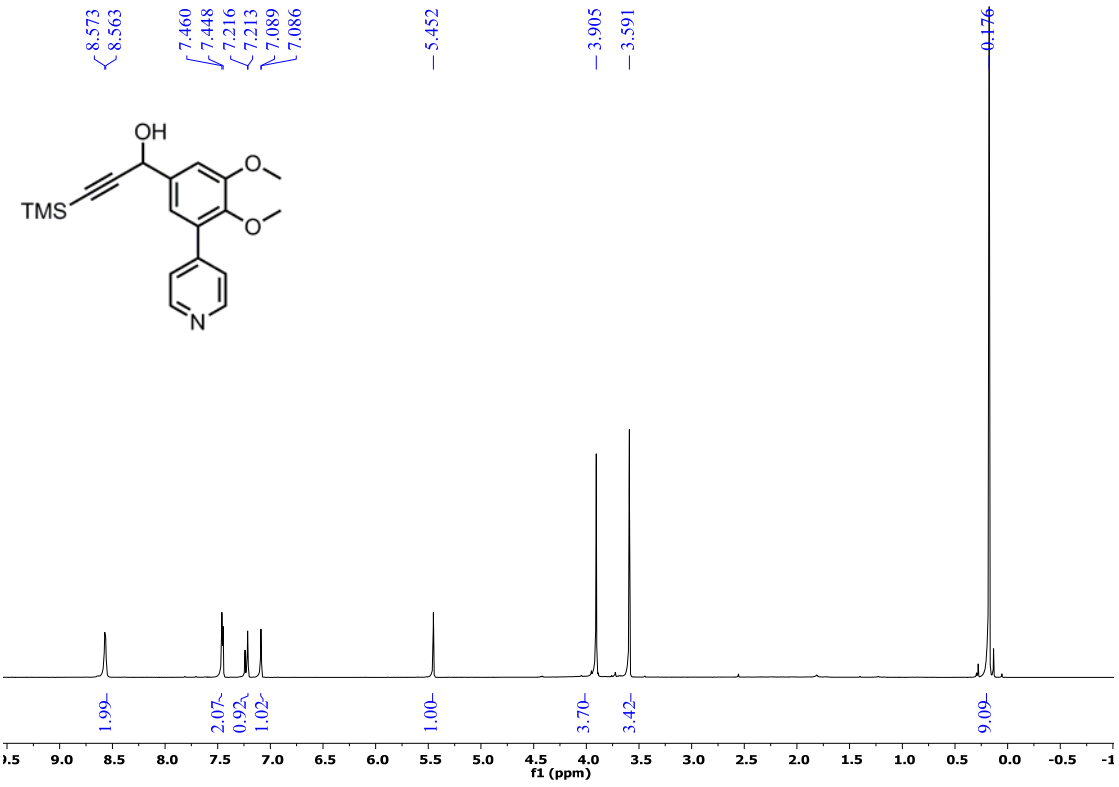
8.573
8.563
7.460
7.448
7.216
7.213
7.089
7.086
5.452
3.905
3.591
0.176
OH
TMS
O
O
N
1.99
2.07
0.92
1.02
1.00
3.70
3.42
9.09
f1 (ppm)

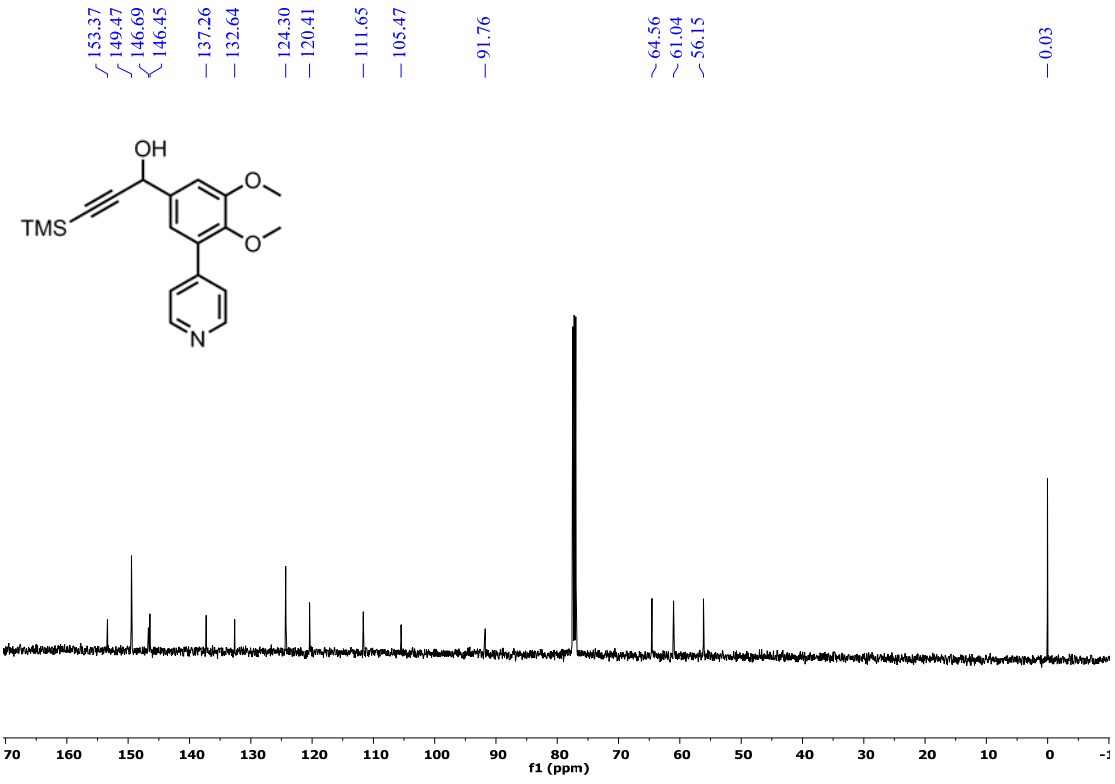
153.37
149.47
146.69
146.45
137.26
132.64
124.30
120.41
111.65
105.47
91.76
64.56
61.04
56.15
0.03
OH
TMS
O
O
N
f1 (ppm)

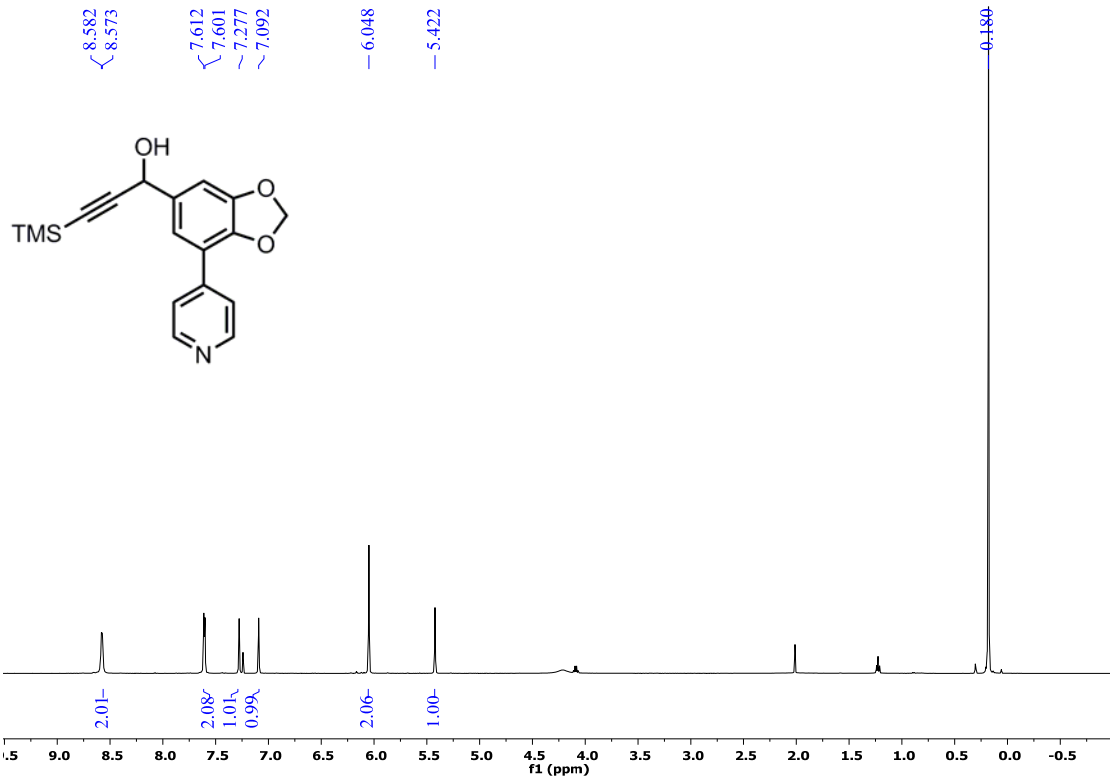
8.582
8.573
7.612
7.601
7.277
7.092
6.048
5.422
0.180
OH
TMS
O
O
N
2.01
2.08
1.01
0.99
2.06
1.00
f1 (ppm)

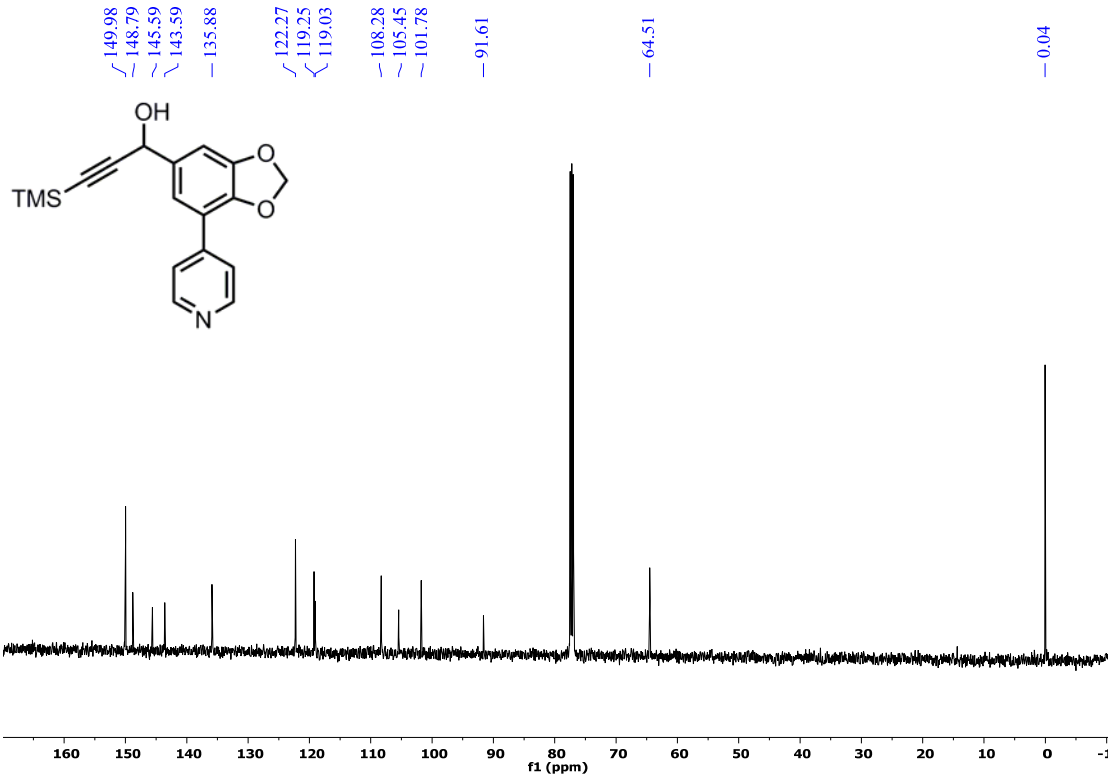
149.98
148.79
145.59
143.59
135.88
122.27
119.25
119.03
108.28
105.45
101.78
91.61
64.51
0.04
OH
TMS
O
O
N
f1 (ppm)

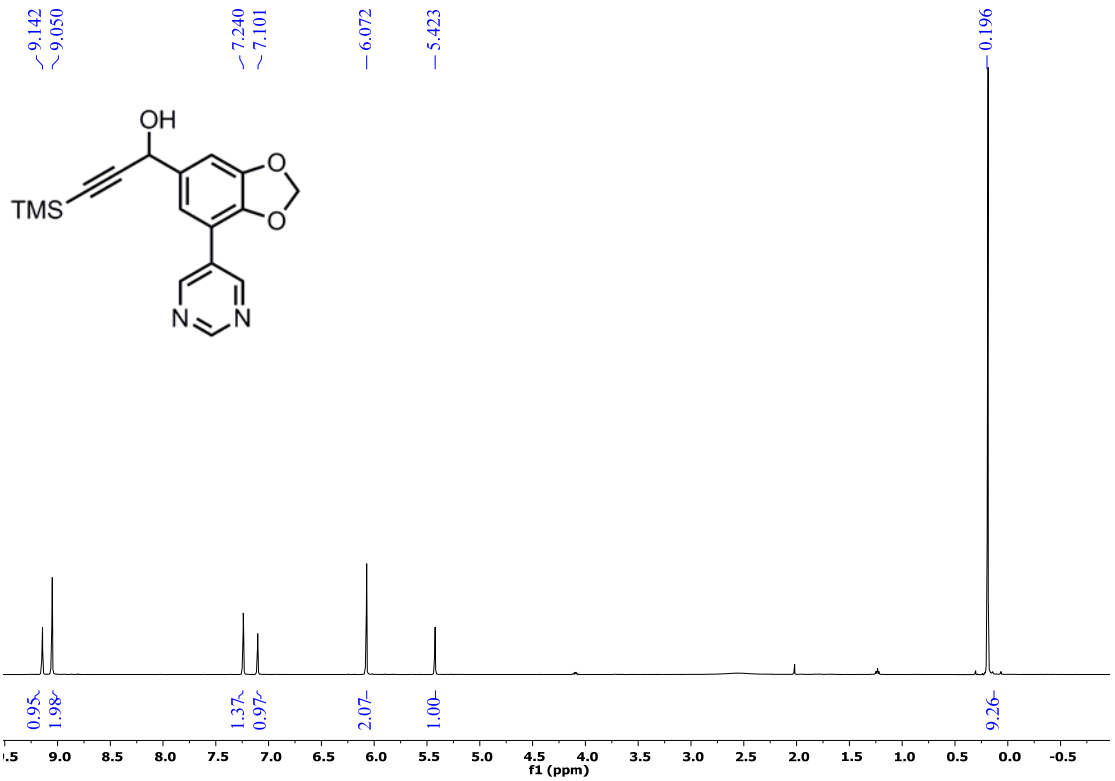
9.142
9.050
7.240
7.101
6.072
5.423
0.196
OH
TMS
O
O
N
N
0.95
1.98
1.37
0.97
2.07
1.00
9.26
f1 (ppm)

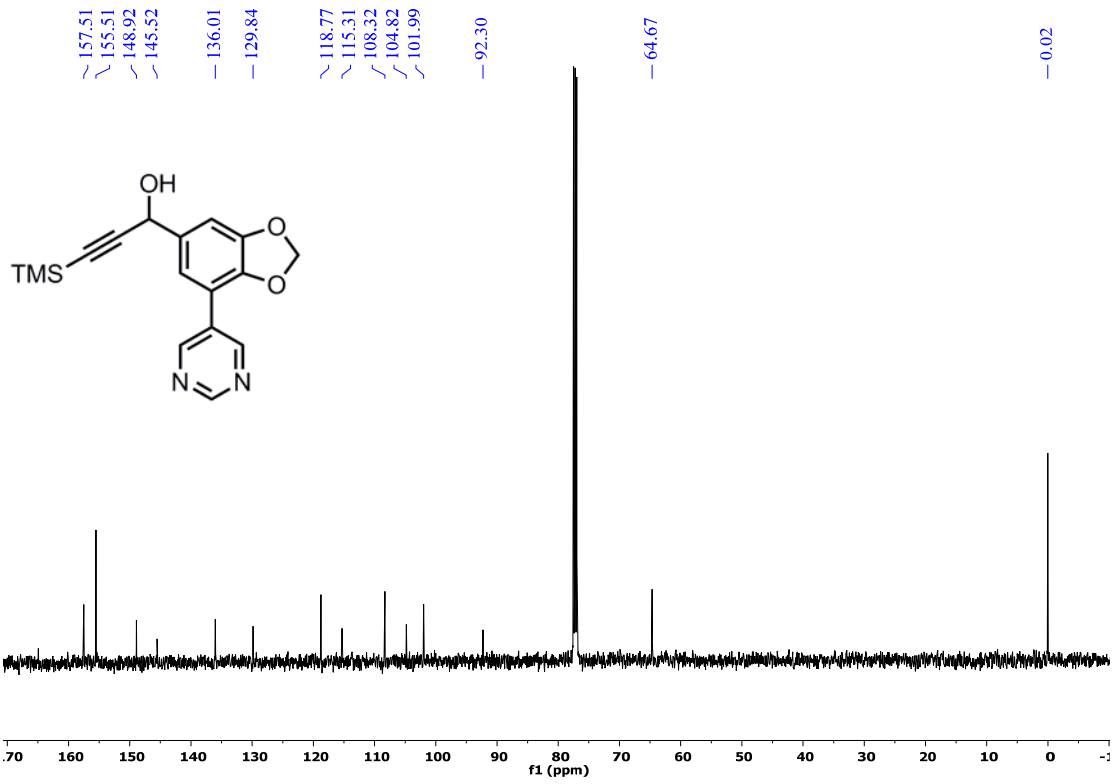
157.51
155.51
148.92
145.52
136.01
129.84
118.77
115.31
108.32
104.82
101.99
92.30
64.67
0.02
OH
TMS
O
O
N
N
f1 (ppm)

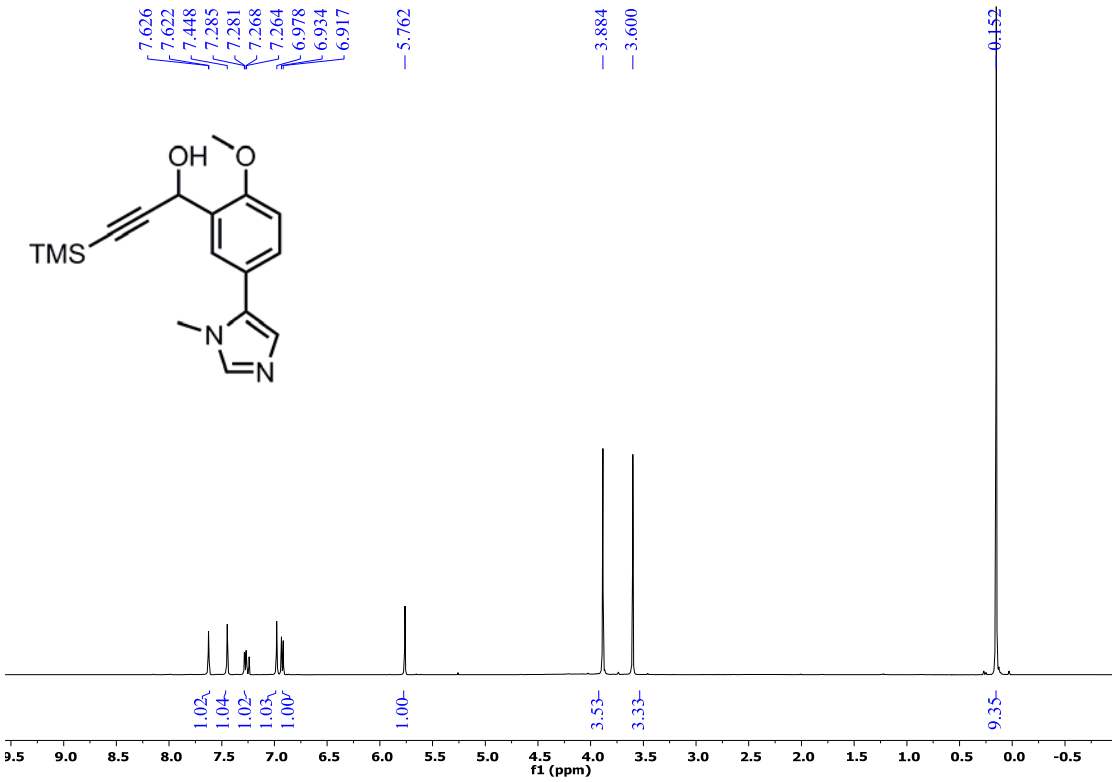
7.626
7.622
7.448
7.285
7.281
7.268
7.264
6.978
6.934
6.917
5.762
3.884
3.600
0.152
OH
O
TMS
N
N
1.02
1.04
1.02
1.03
1.00
1.00
3.53
3.33
9.35
f1 (ppm)

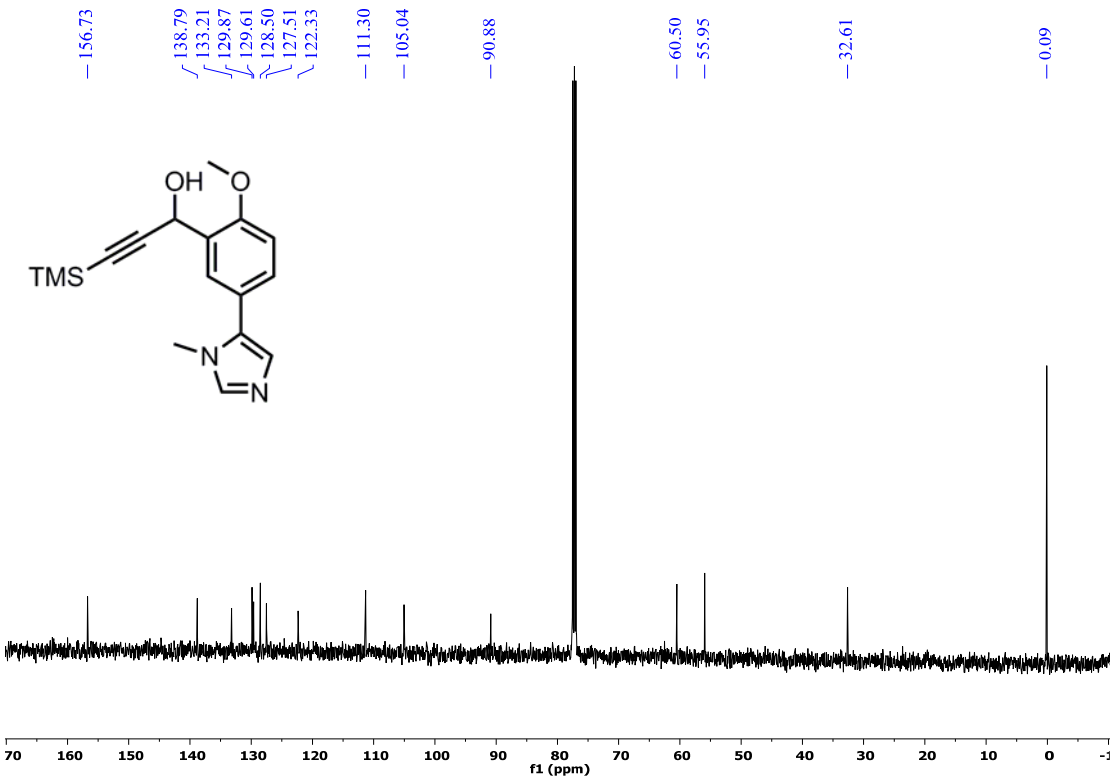
156.73
138.79
133.21
129.87
129.61
128.50
127.51
122.33
111.30
105.04
90.88
60.50
55.95
32.61
0.09
OH
O
TMS
N
N
f1 (ppm)

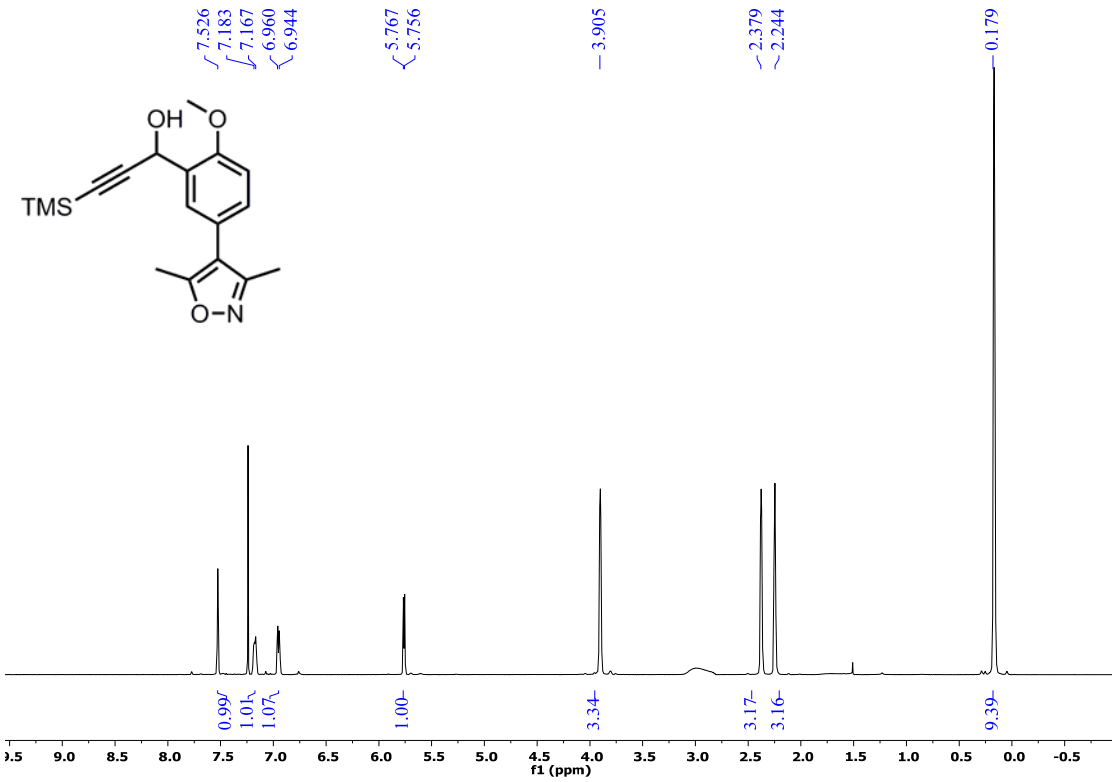
7.526
7.183
7.167
6.960
6.944
5.767
5.756
3.905
2.379
2.244
0.179
OH
O
TMS
O–N
0.99
1.01
1.07
1.00
3.34
3.17
3.16
9.39
f1 (ppm)

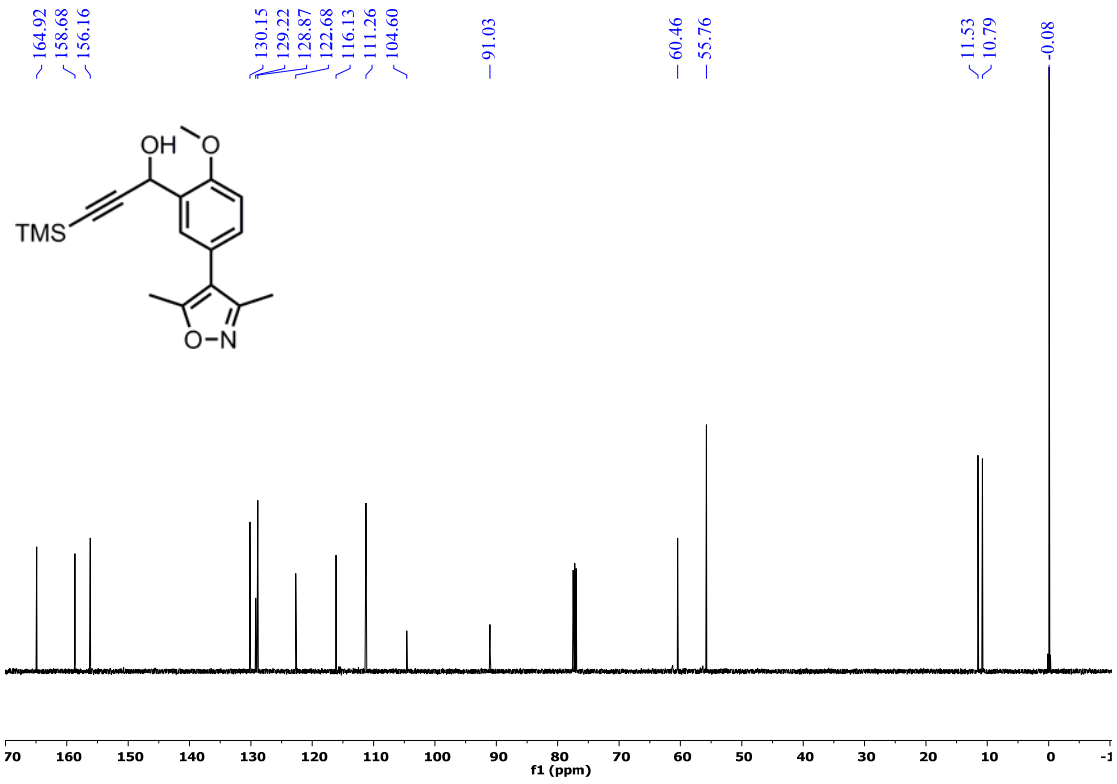
164.92
158.68
156.16
130.15
129.22
128.87
122.68
116.13
111.26
104.60
91.03
60.46
55.76
11.53
10.79
-0.08
OH
O
TMS
O–N
f1 (ppm)

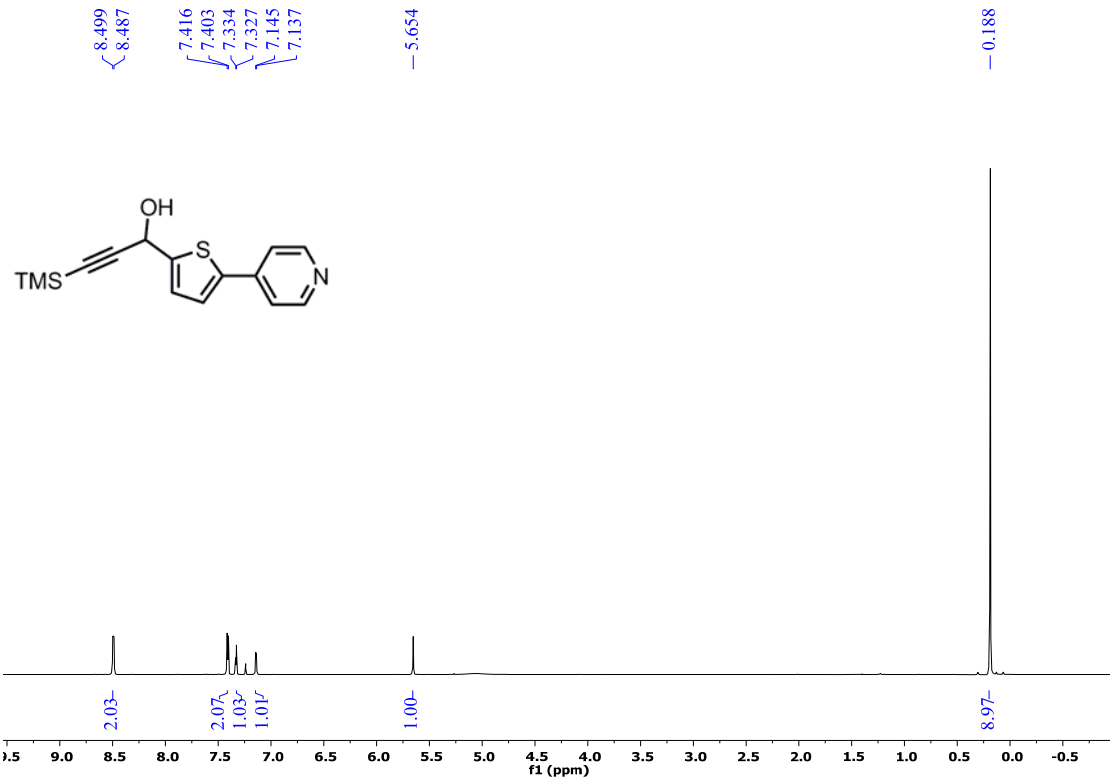
8.499
8.487
7.416
7.403
7.334
7.327
7.145
7.137
5.654
0.188
OH
TMS
S
N
2.03
2.07
1.03
1.01
1.00
8.97
f1 (ppm)

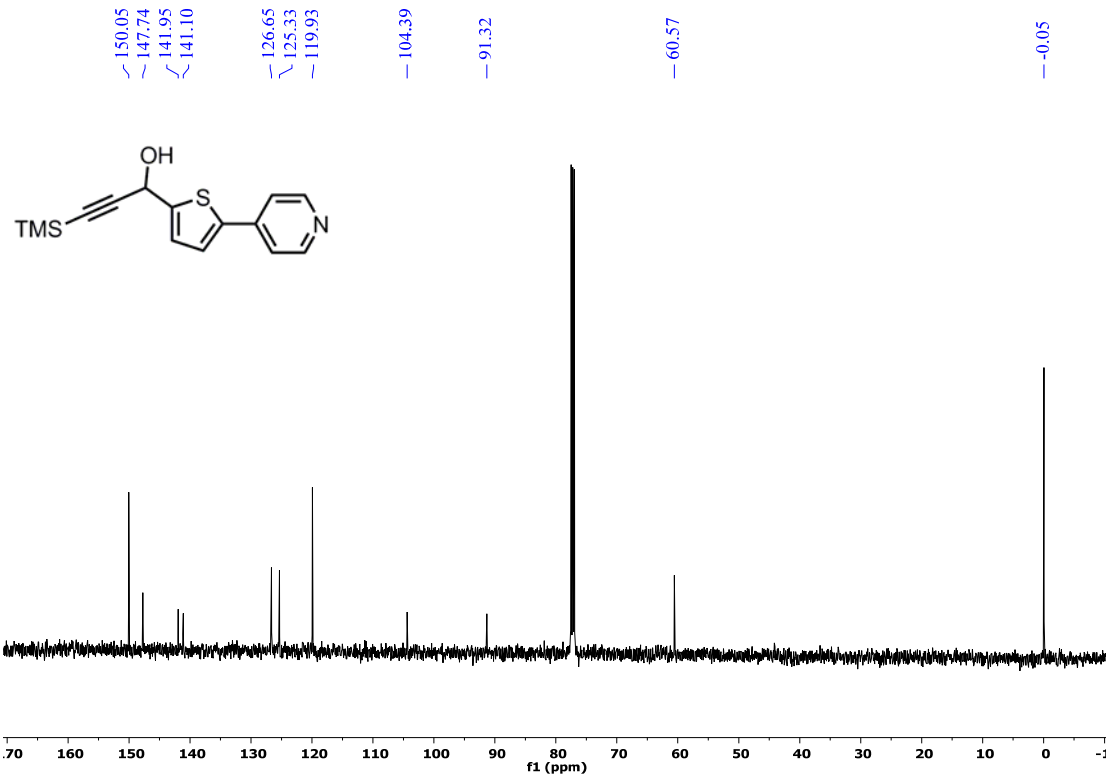
150.05
147.74
141.95
141.10
126.65
125.33
119.93
104.39
91.32
60.57
-0.05
OH
TMS
S
N
f1 (ppm)

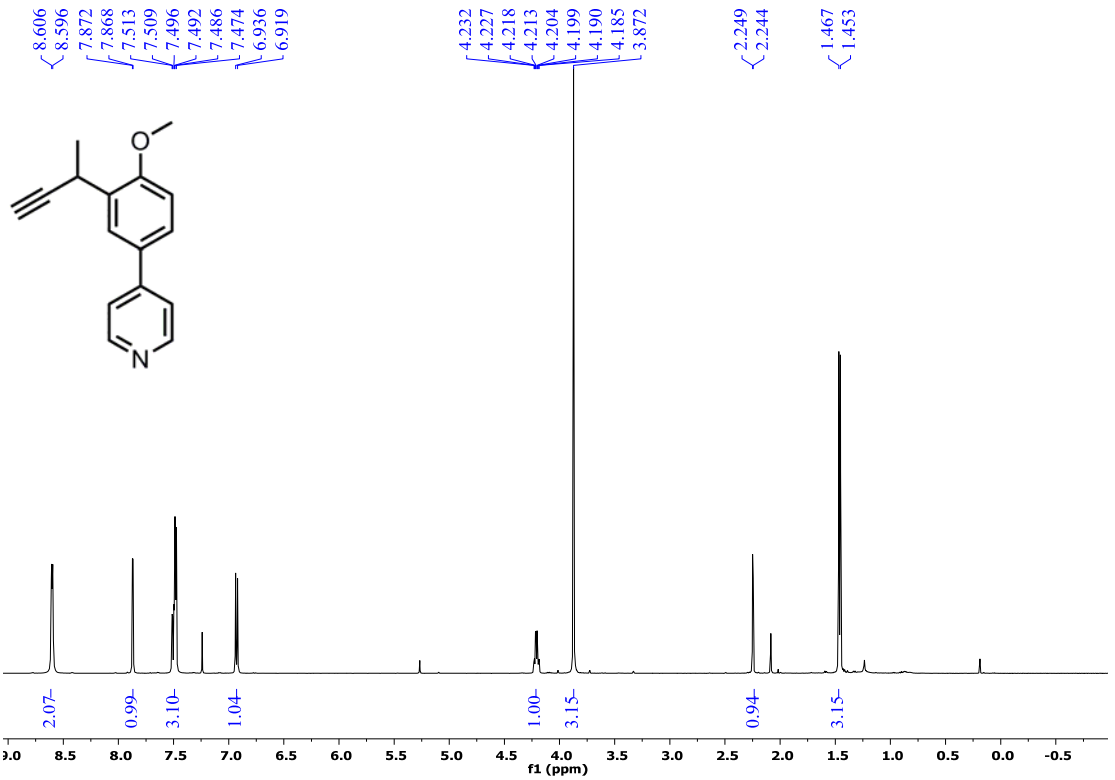
8.606
8.596
7.872
7.868
7.513
7.509
7.496
7.492
7.486
7.474
6.936
6.919
4.232
4.227
4.218
4.213
4.204
4.199
4.190
4.185
3.872
2.249
2.244
1.467
1.453
O
N
2.07
0.99
3.10
1.04
1.00
3.15
0.94
3.15
f1 (ppm)

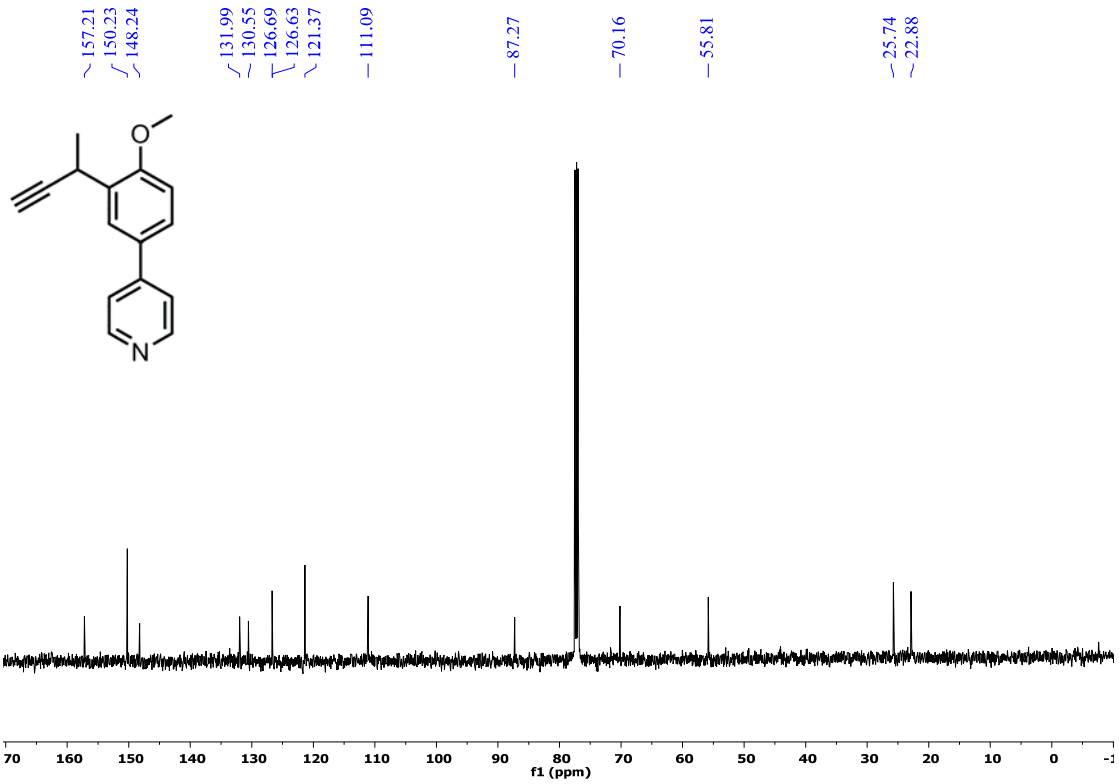
157.21
150.23
148.24
131.99
130.55
126.69
126.63
121.37
111.09
87.27
70.16
55.81
25.74
22.88
O
N
f1 (ppm)

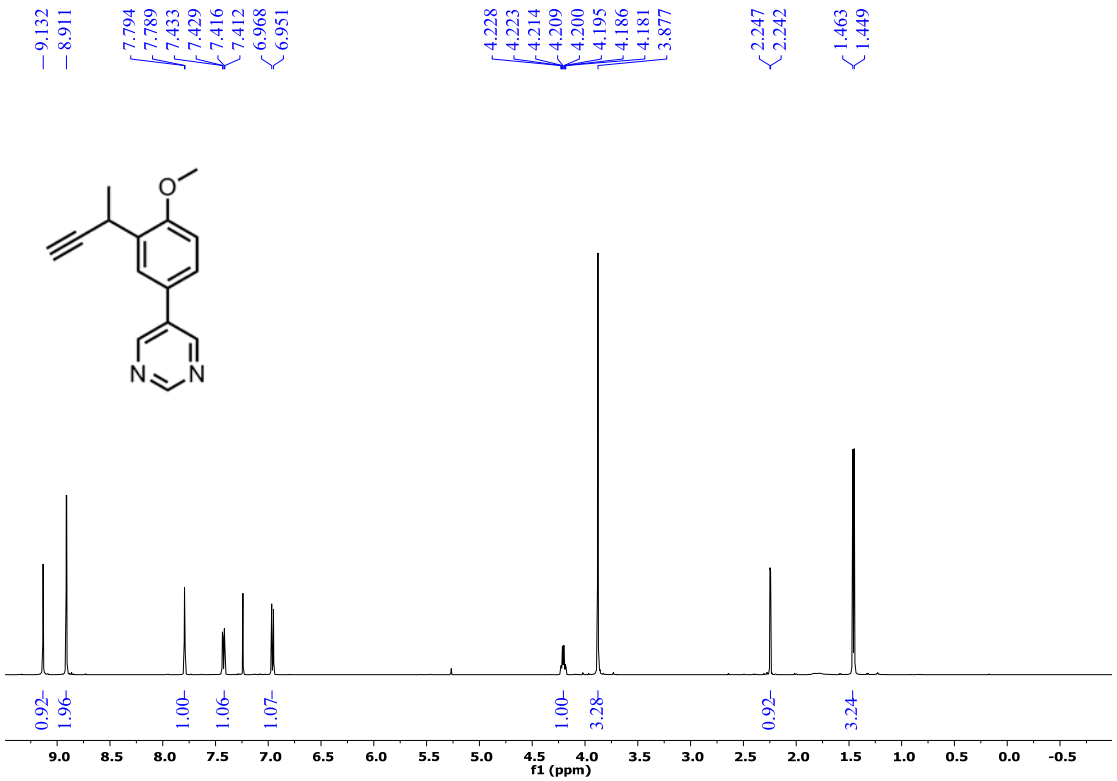
9.132
8.911
7.794
7.789
7.433
7.429
7.416
7.412
6.968
6.951
4.228
4.223
4.214
4.209
4.200
4.195
4.186
4.181
3.877
2.247
2.242
1.463
1.449
O
N
N
0.92
1.96
1.00
1.06
1.07
1.00
3.28
0.92
3.24
f1 (ppm)

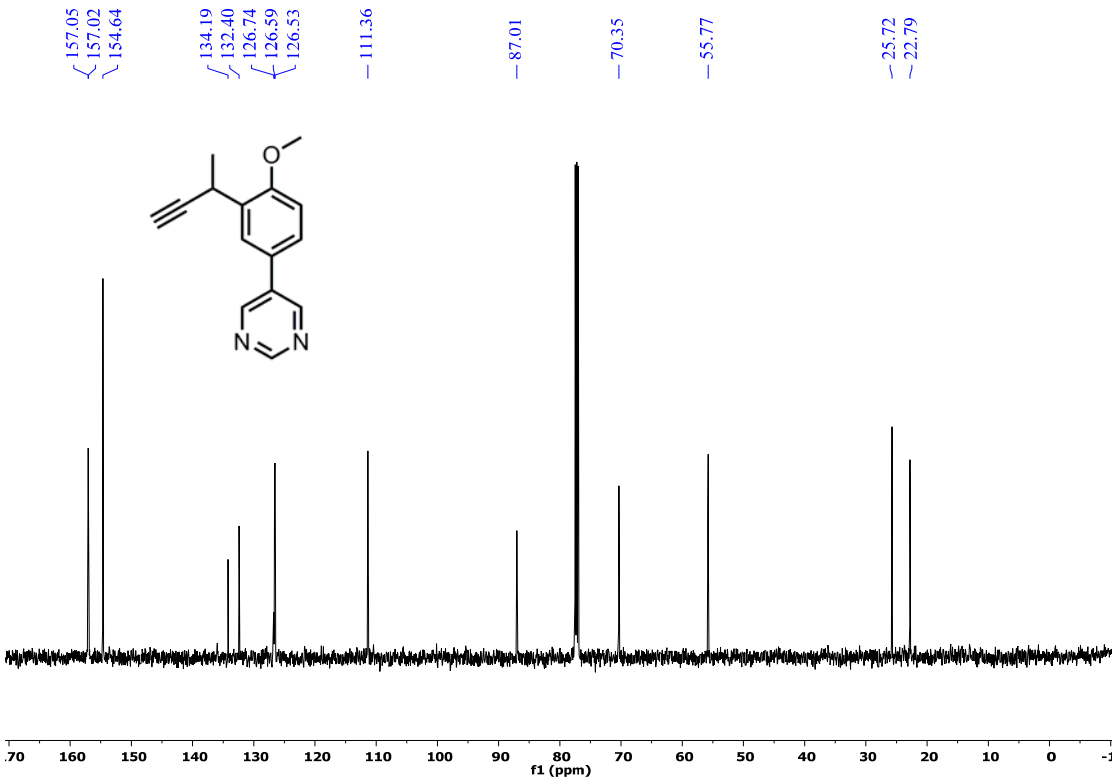
157.05
157.02
154.64
134.19
132.40
126.74
126.59
126.53
111.36
87.01
70.35
55.77
25.72
22.79
O
N
N
f1 (ppm)

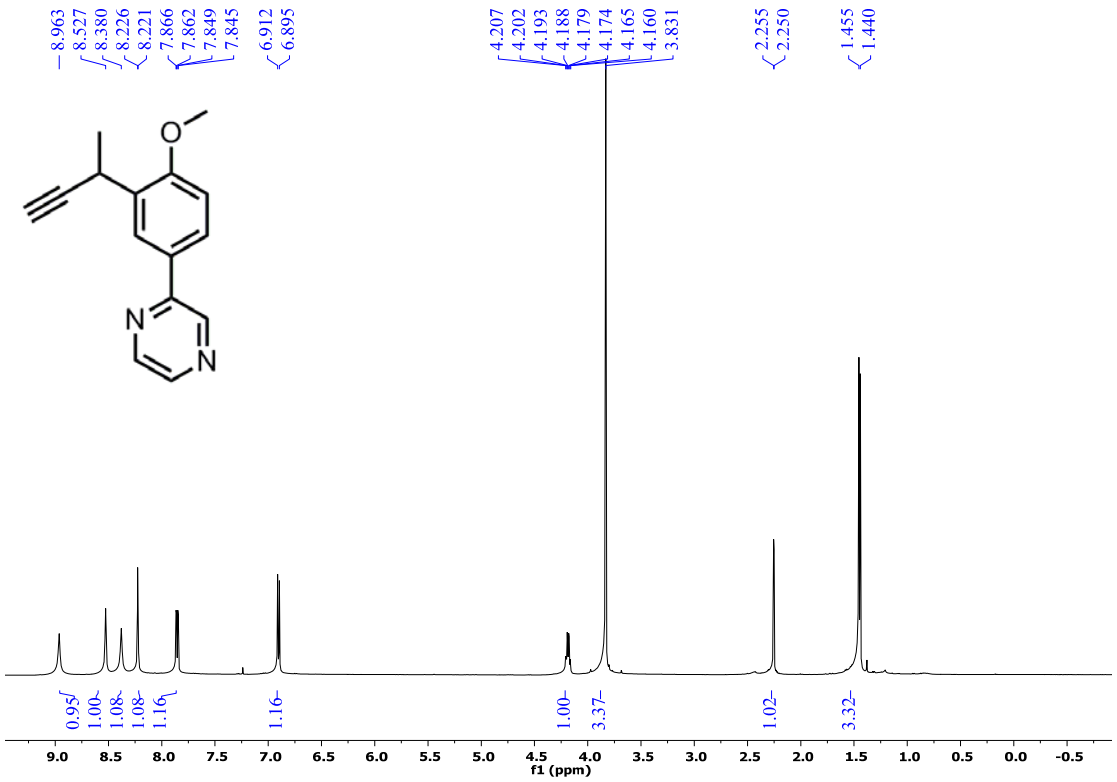
8.963
8.527
8.380
8.226
8.221
7.866
7.862
7.849
7.845
6.912
6.895
4.207
4.202
4.193
4.188
4.179
4.174
4.165
4.160
3.831
2.255
2.250
1.455
1.440
O
N
N
0.95
1.00
1.08
1.08
1.16
1.16
1.00
3.37
1.02
3.32
f1 (ppm)

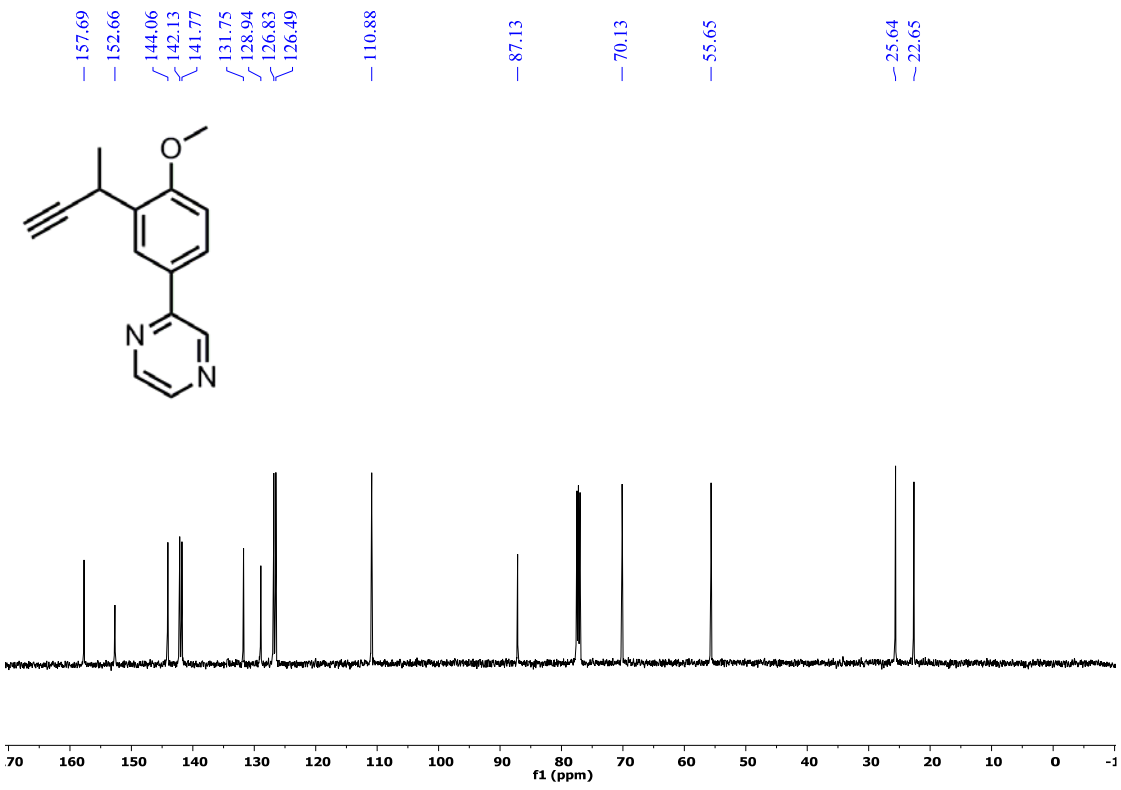
157.69
152.66
144.06
142.13
141.77
131.75
128.94
126.83
126.49
110.88
87.13
70.13
55.65
25.64
22.65
O
N
N
f1 (ppm)

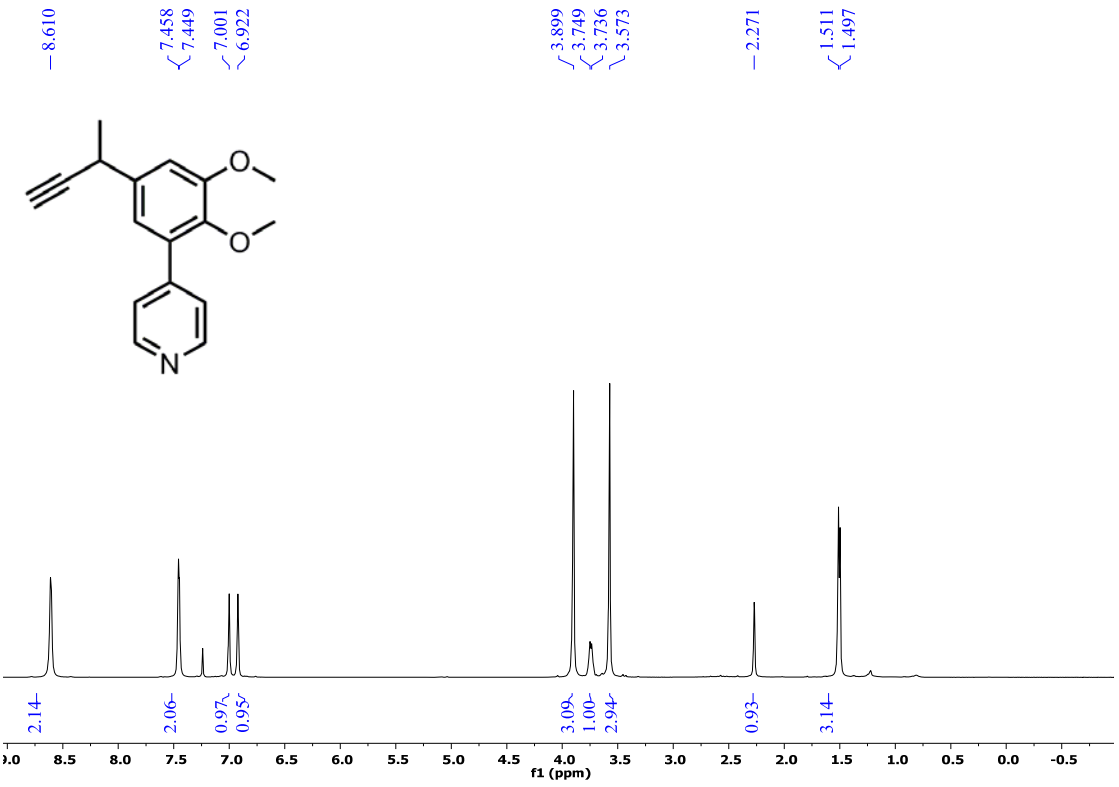
8.610
7.458
7.449
7.001
6.922
3.899
3.749
3.736
3.573
2.271
1.511
1.497
O
O
N
2.14
2.06
0.97
0.95
3.09
1.00
2.94
0.93
3.14
f1 (ppm)

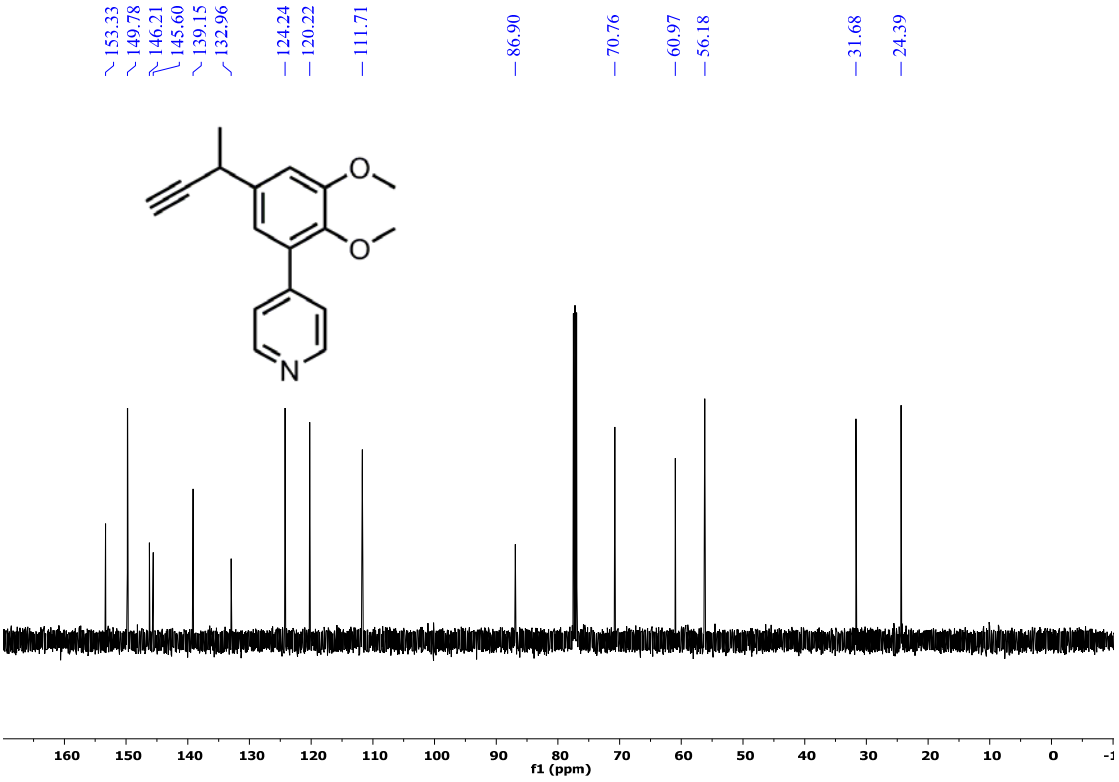
153.33
149.78
146.21
145.60
139.15
132.96
124.24
120.22
111.71
86.90
70.76
60.97
56.18
31.68
24.39
O
O
N
f1 (ppm)

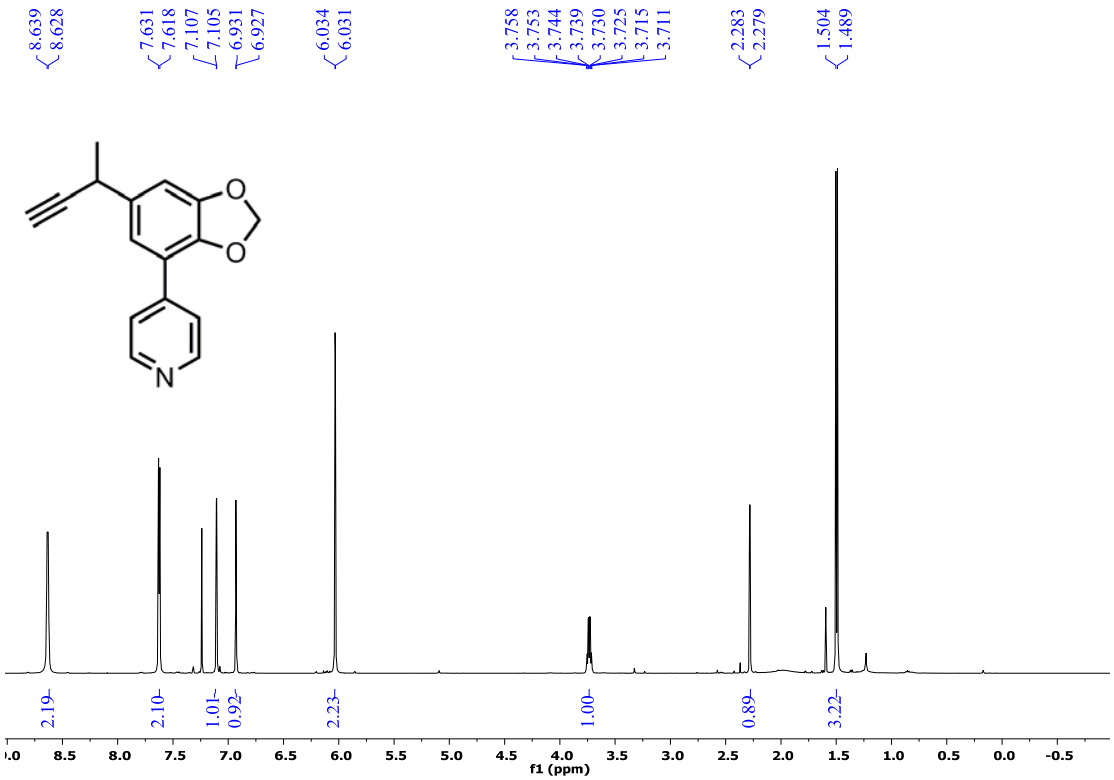
8.639
8.628
7.631
7.618
7.107
7.105
6.931
6.927
6.034
6.031
3.758
3.753
3.744
3.739
3.730
3.725
3.715
3.711
2.283
2.279
1.504
1.489
O
O
N
2.19
2.10
1.01
0.92
2.23
1.00
0.89
3.22
f1 (ppm)

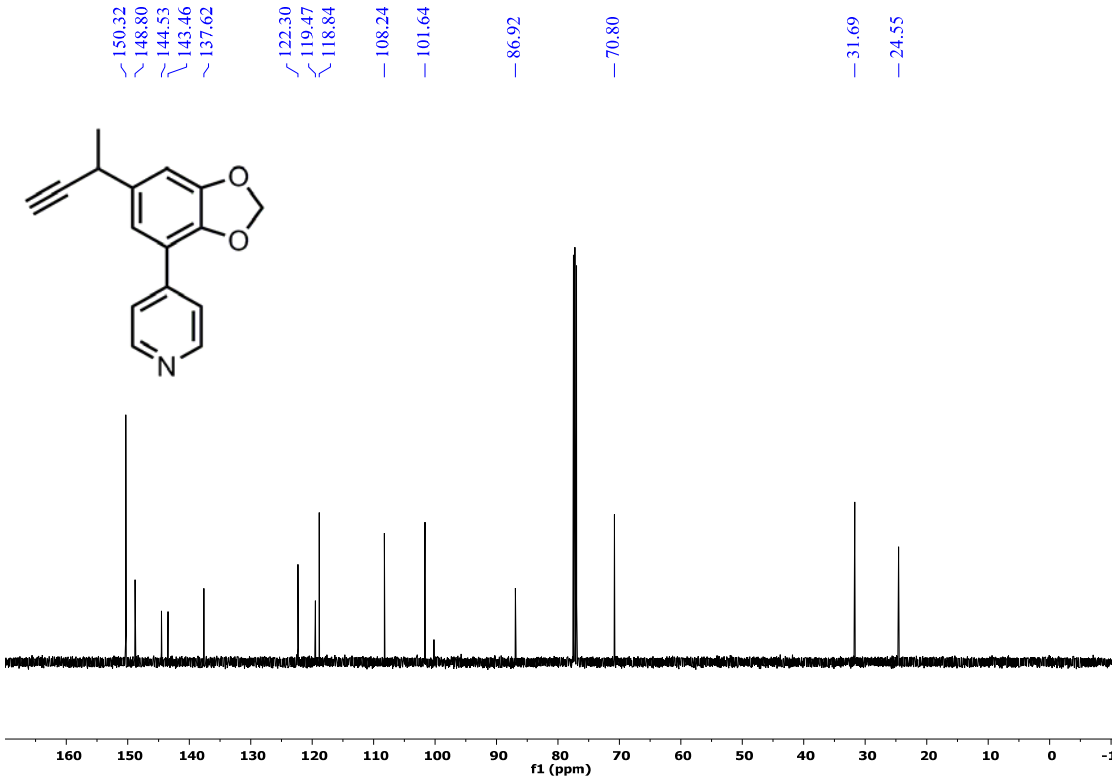
150.32
148.80
144.53
143.46
137.62
122.30
119.47
118.84
108.24
101.64
86.92
70.80
31.69
24.55
O
O
N
f1 (ppm)

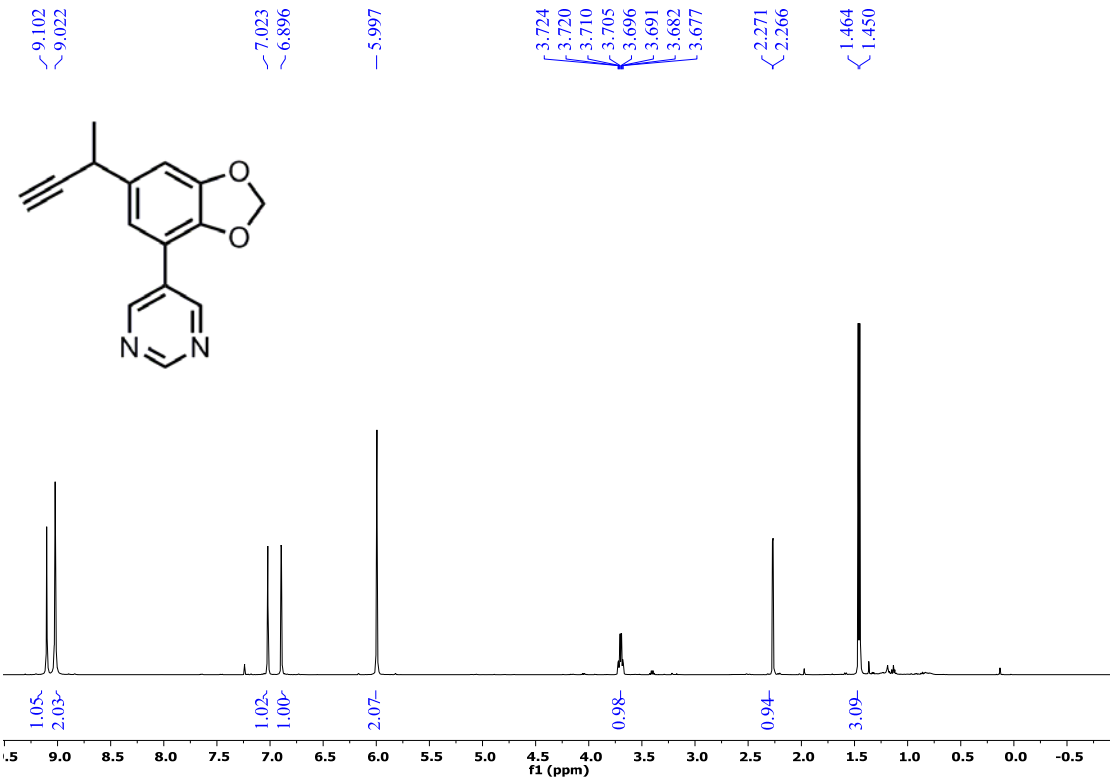
9.102
9.022
7.023
6.896
5.997
3.724
3.720
3.710
3.705
3.696
3.691
3.682
3.677
2.271
2.266
1.464
1.450
1.05
2.03
1.02
1.00
2.07
0.98
0.94
3.09
f1 (ppm)

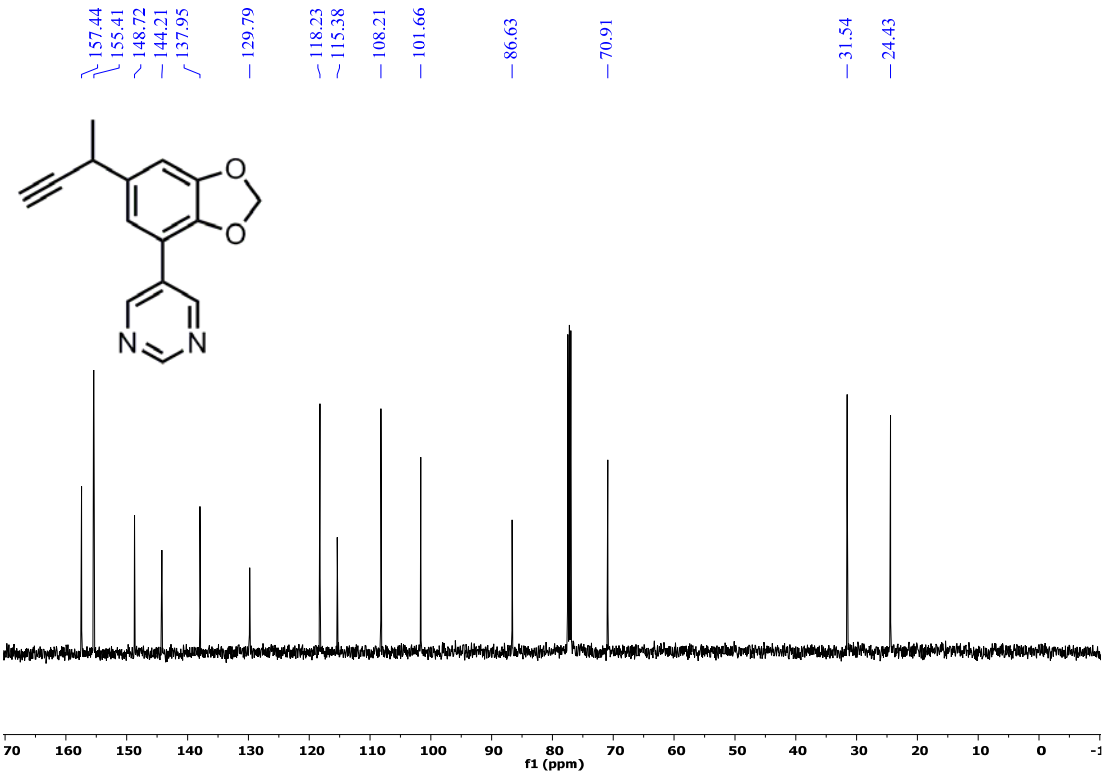
157.44
155.41
148.72
144.21
137.95
129.79
118.23
115.38
108.21
101.66
86.63
70.91
31.54
24.43
f1 (ppm)

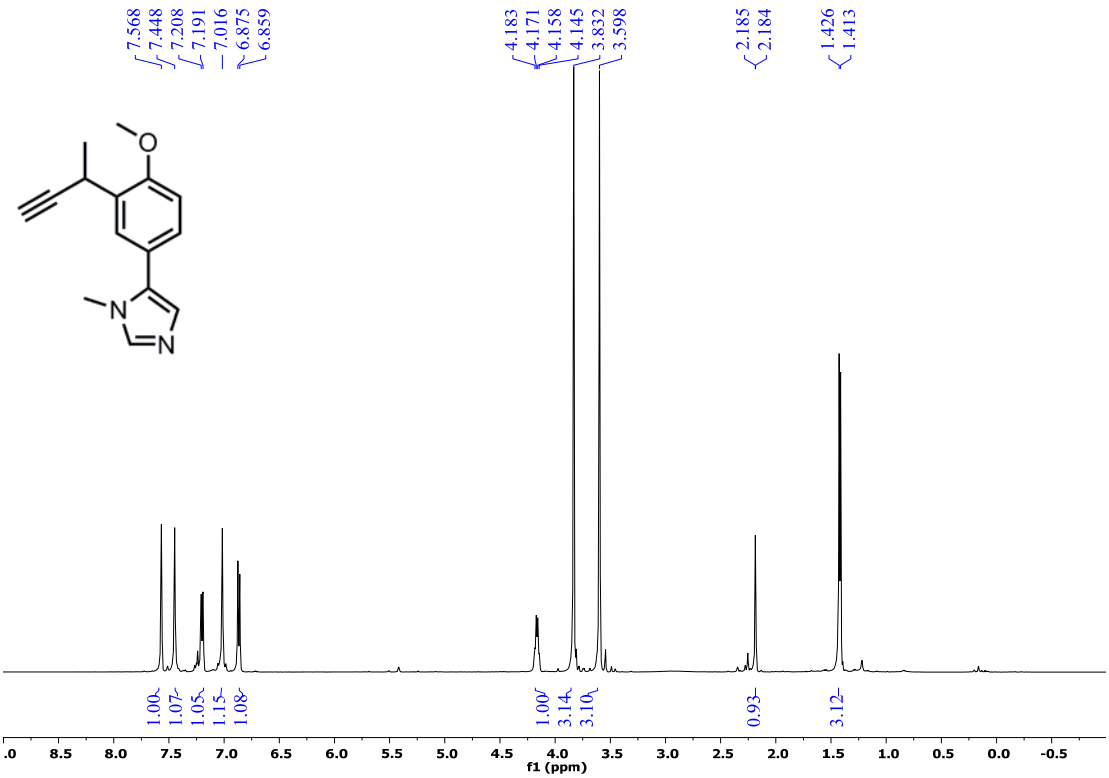
7.568
7.448
7.208
7.191
7.016
6.875
6.859
4.183
4.171
4.158
4.145
3.832
3.598
2.185
2.184
1.426
1.413
1.00
1.07
1.05
1.15
1.08
1.00
3.14
3.10
0.93
3.12
f1 (ppm)

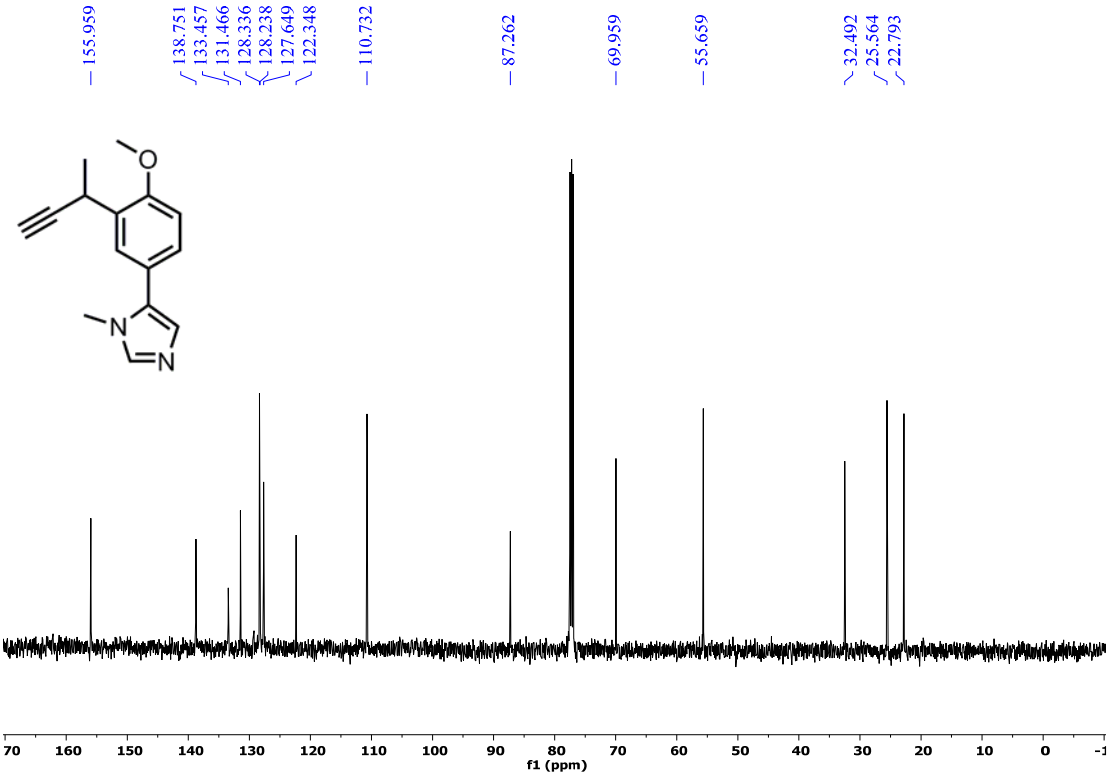
155.959
138.751
133.457
131.466
128.336
128.238
127.649
122.348
110.732
87.262
69.959
55.659
32.492
25.564
22.793
f1 (ppm)

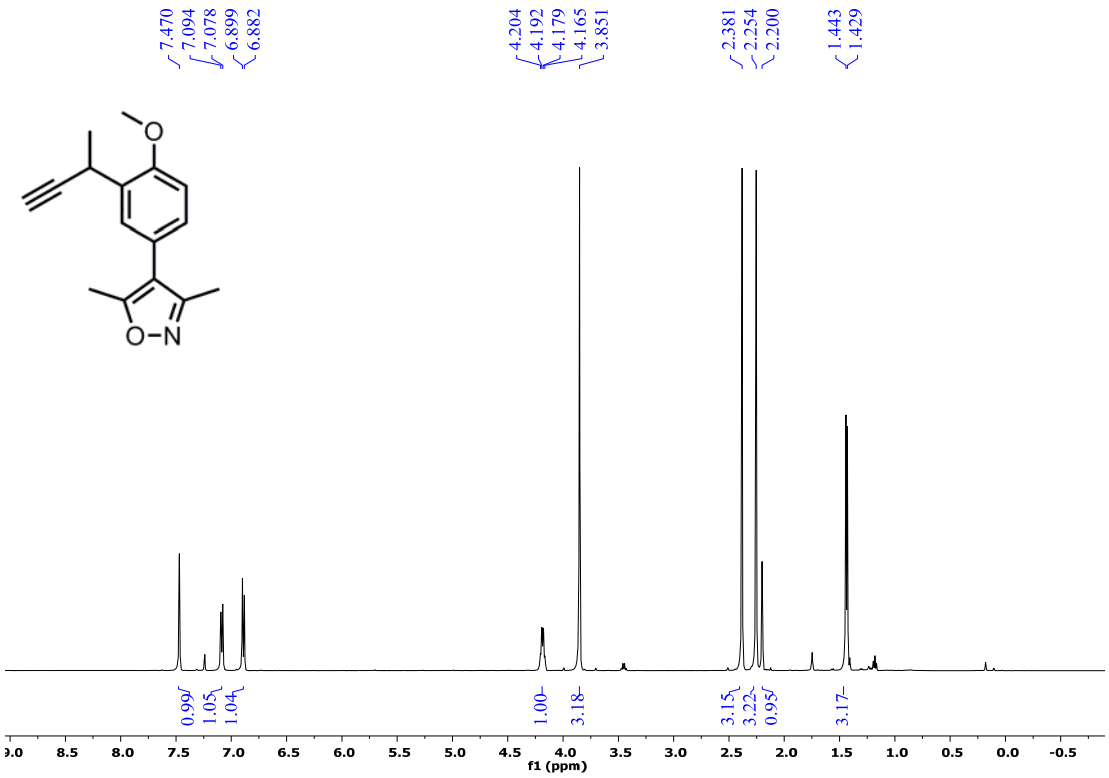
7.470
7.094
7.078
6.899
6.882
4.204
4.192
4.179
4.165
3.851
2.381
2.254
2.200
1.443
1.429
O
O–N
0.99
1.05
1.04
1.00
3.18
3.15
3.22
0.95
3.17
f1 (ppm)

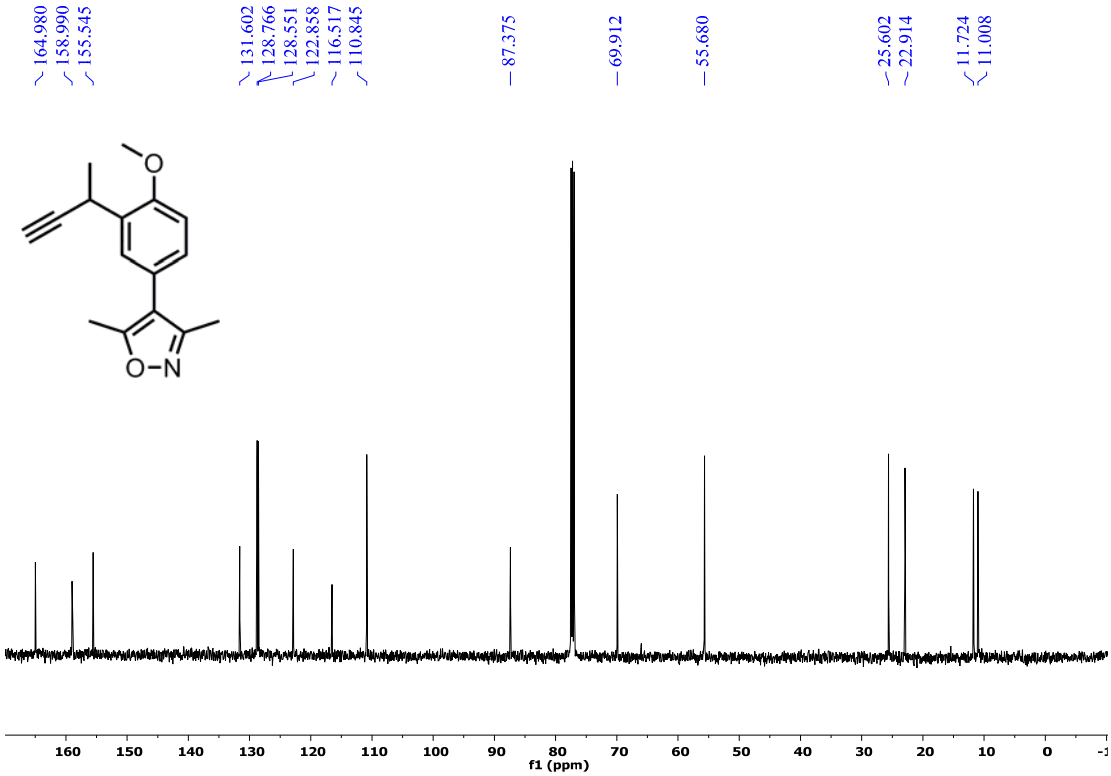
164.980
158.990
155.545
131.602
128.766
128.551
122.858
116.517
110.845
87.375
69.912
55.680
25.602
22.914
11.724
11.008
O
O–N
f1 (ppm)

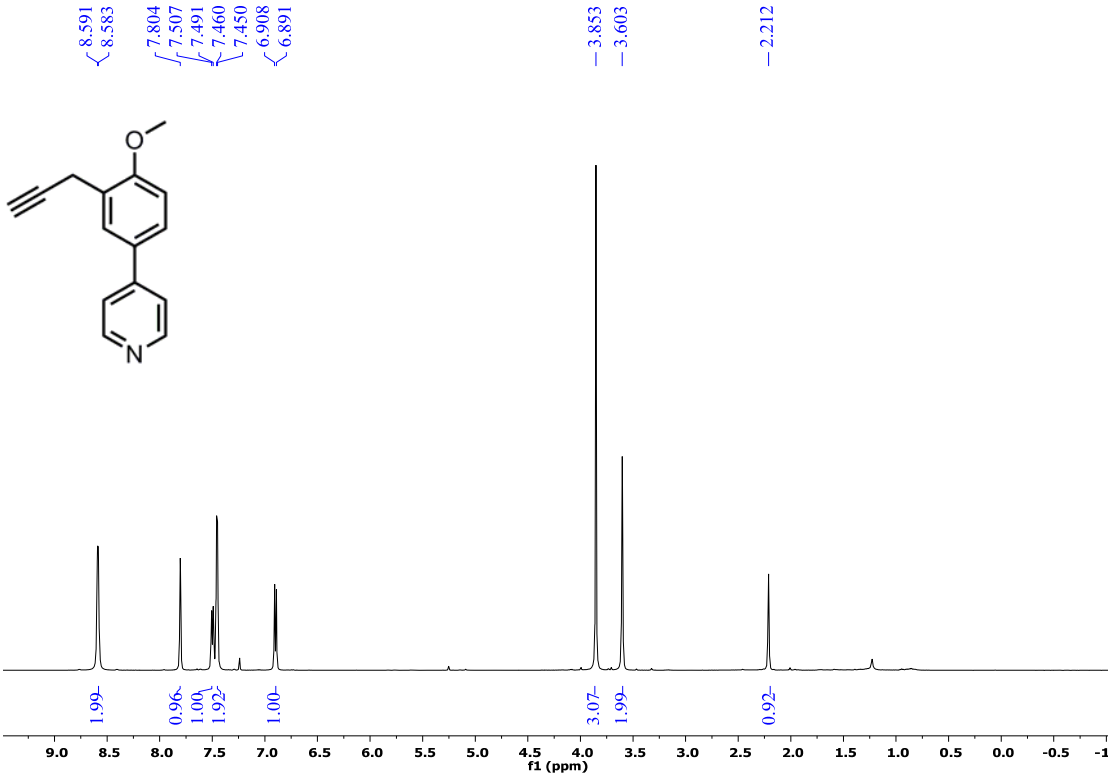
8.591
8.583
7.804
7.507
7.491
7.460
7.450
6.908
6.891
3.853
3.603
2.212
O
N
1.99
0.96
1.00
1.92
1.00
3.07
1.99
0.92
9.0 8.5 8.0 7.5 7.0 6.5 6.0 5.5 5.0 4.5 4.0 3.5 3.0 2.5 2.0 1.5 1.0 0.5 0.0 -0.5 -1
f1 (ppm)

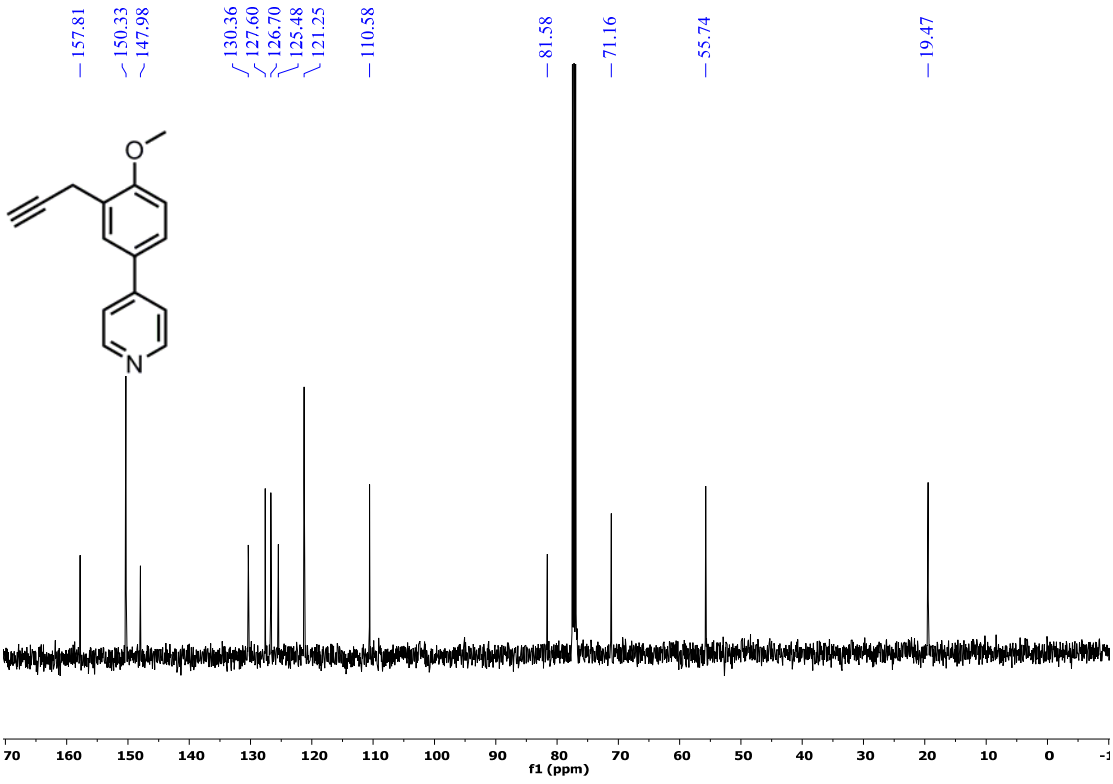
157.81
150.33
147.98
130.36
127.60
126.70
125.48
121.25
110.58
81.58
71.16
55.74
19.47
O
N
70 160 150 140 130 120 110 100 90 80 70 60 50 40 30 20 10 0 -1
f1 (ppm)

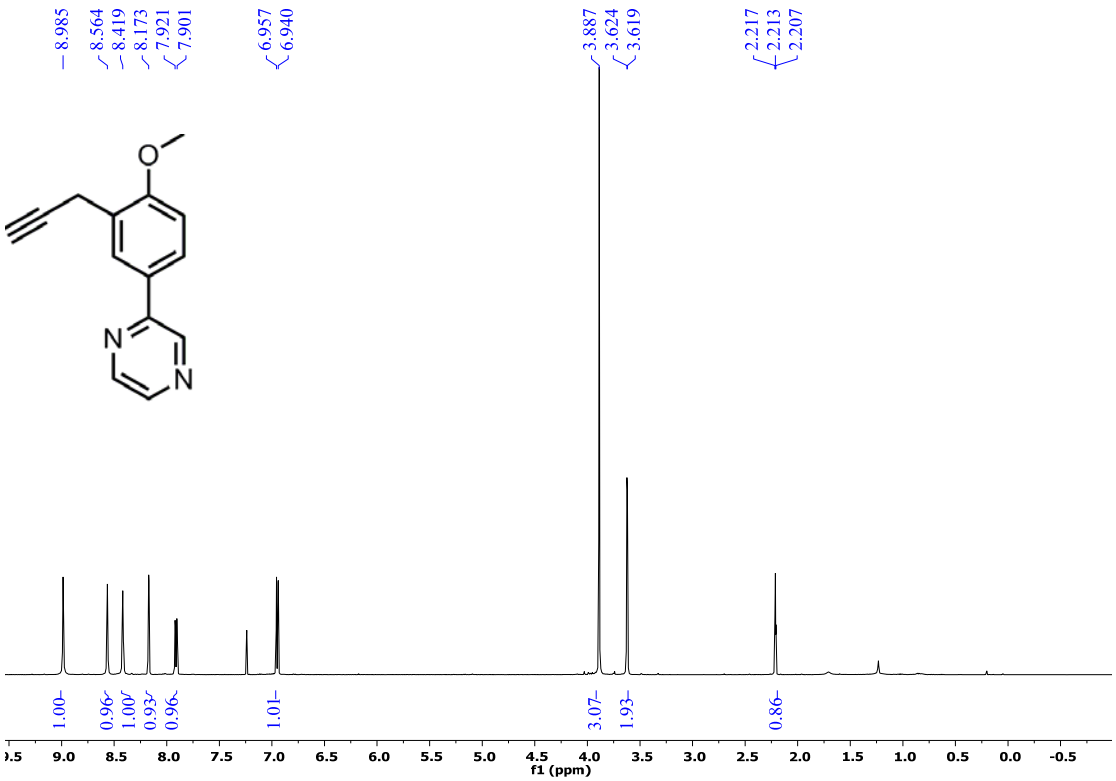
8.985
8.564
8.419
8.173
7.921
7.901
6.957
6.940
3.887
3.624
3.619
2.217
2.213
2.207
O
N
N
1.00
0.96
1.00
0.93
0.96
1.01
3.07
1.93
0.86
f1 (ppm)

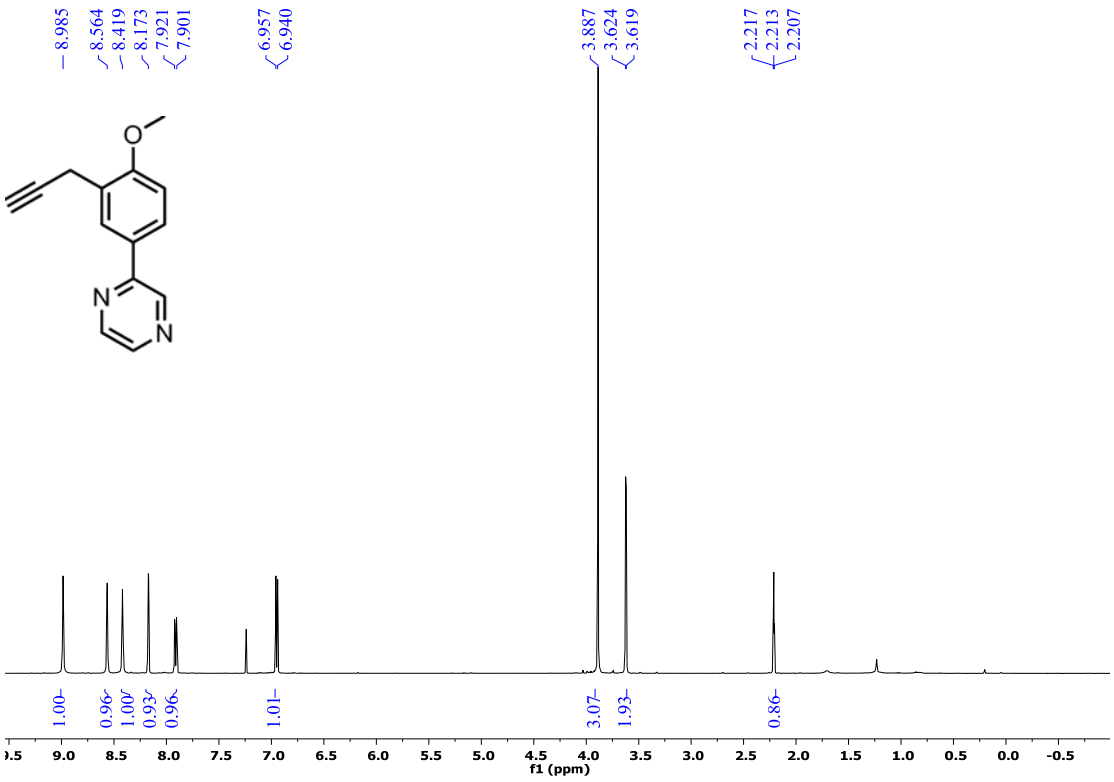
8.985
8.564
8.419
8.173
7.921
7.901
6.957
6.940
3.887
3.624
3.619
2.217
2.213
2.207
O
N
N
1.00
0.96
1.00
0.93
0.96
1.01
3.07
1.93
0.86
f1 (ppm)

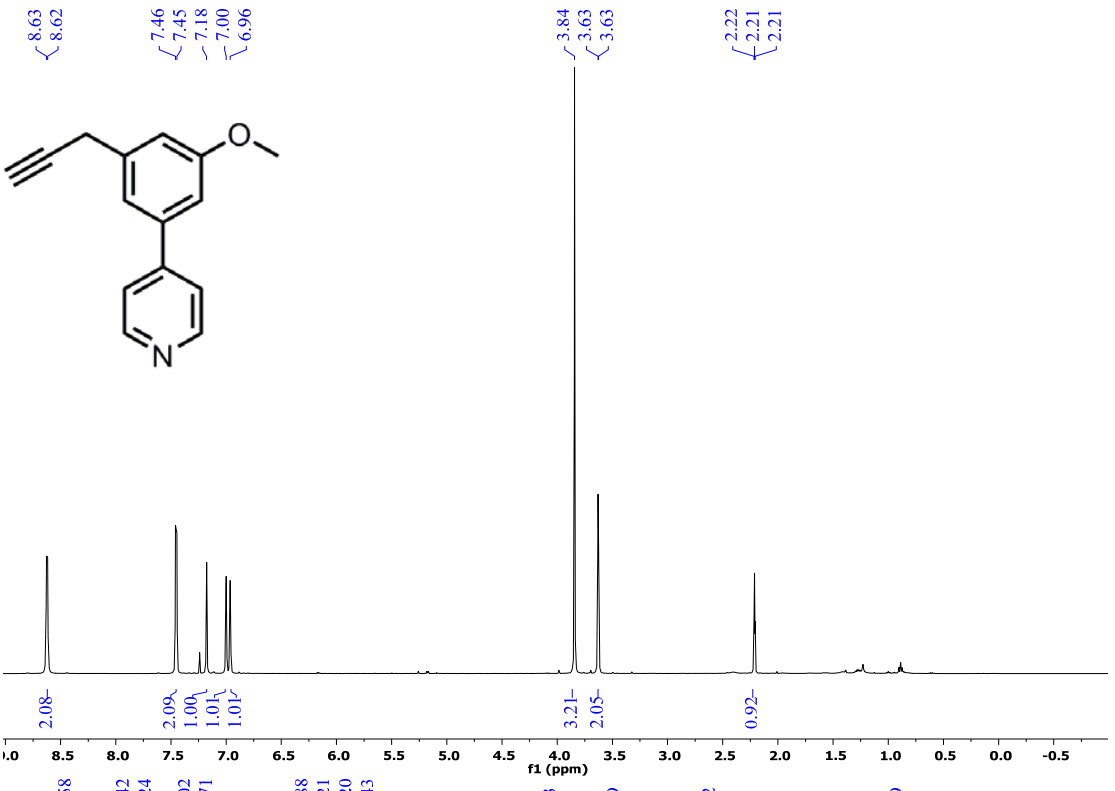
8.63
8.62
7.46
7.45
7.18
7.00
6.96
3.84
3.63
3.63
2.22
2.21
2.21
O
N
2.08
2.09
1.00
1.01
1.01
3.21
2.05
0.92
f1 (ppm)

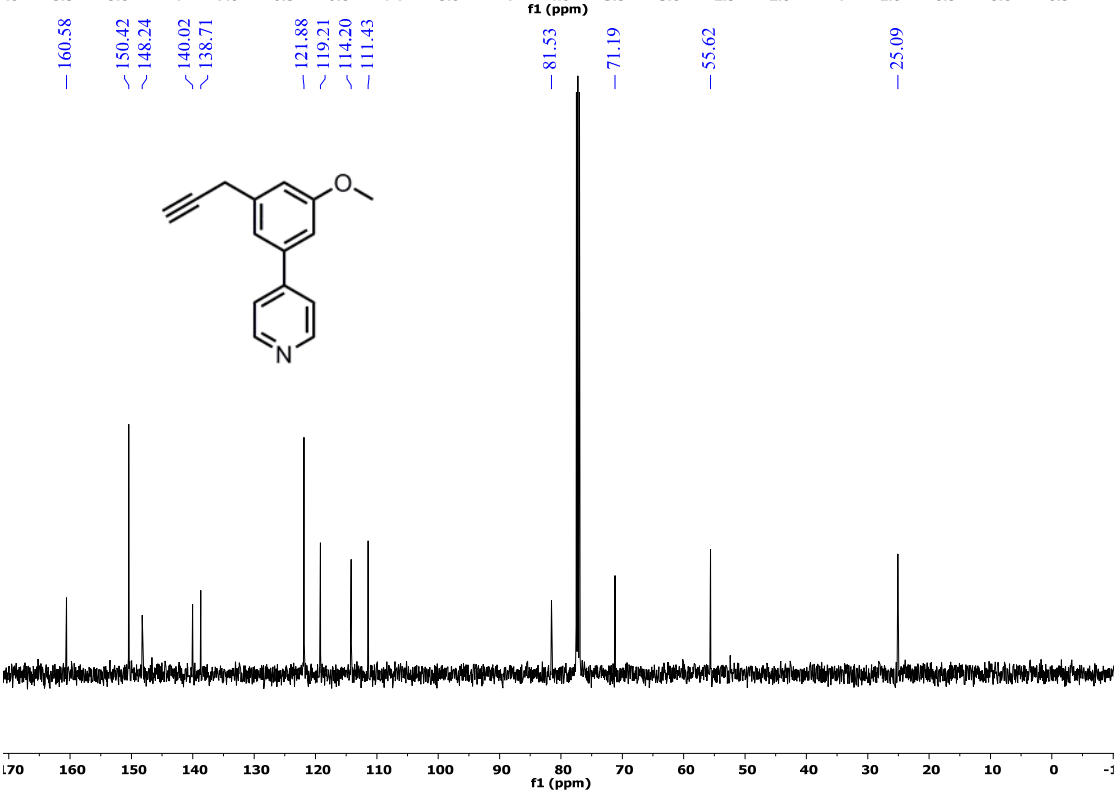
160.58
150.42
148.24
140.02
138.71
121.88
119.21
114.20
111.43
81.53
71.19
55.62
25.09
O
N
f1 (ppm)

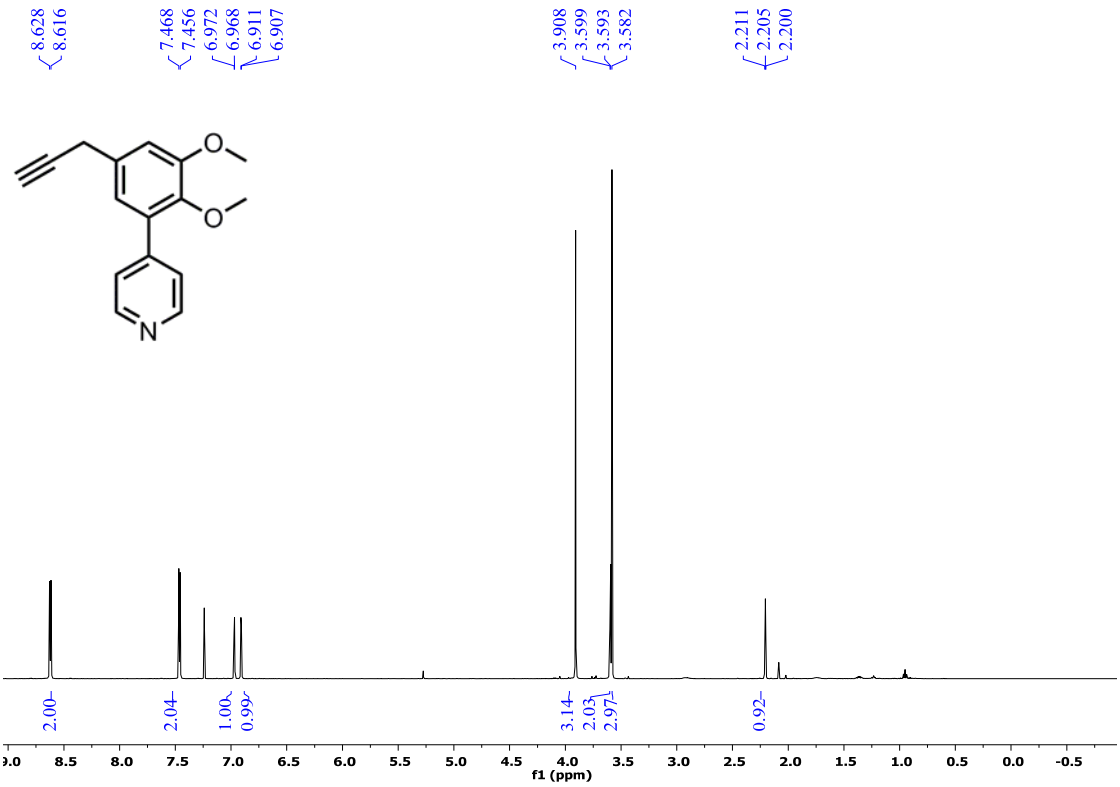
8.628
8.616
7.468
7.456
6.972
6.968
6.911
6.907
3.908
3.599
3.593
3.582
2.211
2.205
2.200
O
O
N
2.00
2.04
1.00
0.99
3.14
2.03
2.97
0.92
f1 (ppm)

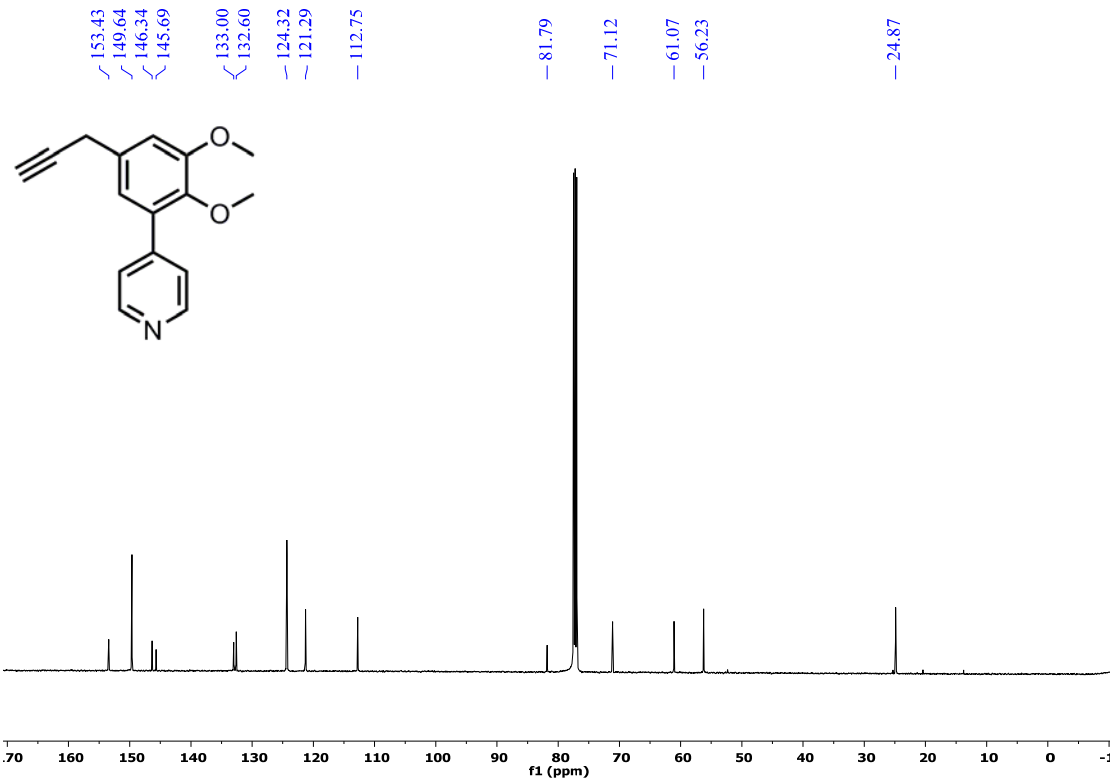
153.43
149.64
146.34
145.69
133.00
132.60
124.32
121.29
112.75
81.79
71.12
61.07
56.23
24.87
O
O
N
f1 (ppm)

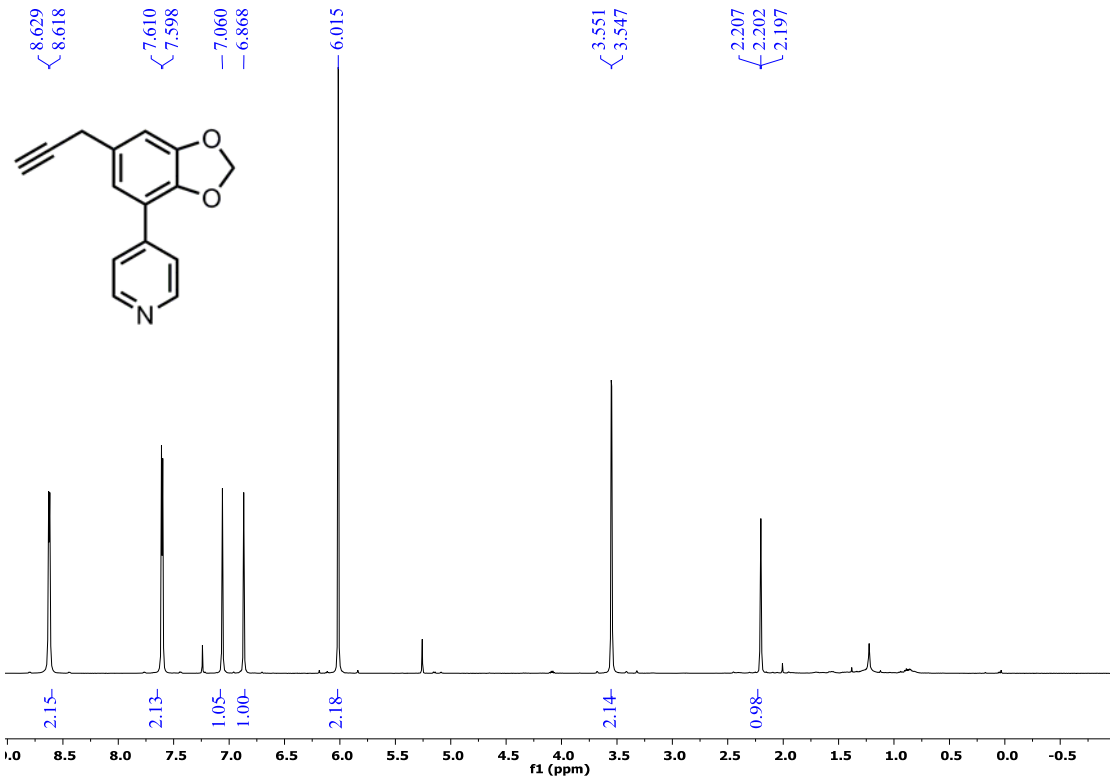
8.629
8.618
7.610
7.598
7.060
6.868
6.015
3.551
3.547
2.207
2.202
2.197
O
O
N
2.15
2.13
1.05
1.00
2.18
2.14
0.98
f1 (ppm)

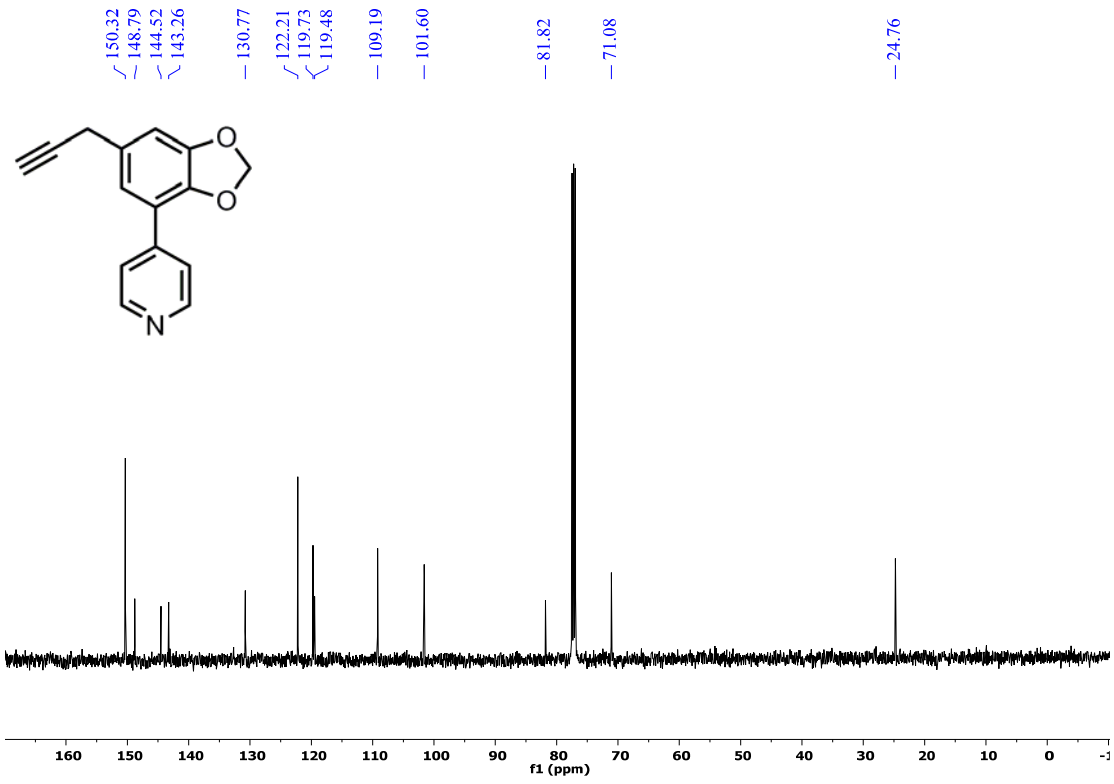
150.32
148.79
144.52
143.26
130.77
122.21
119.73
119.48
109.19
101.60
81.82
71.08
24.76
O
O
N
f1 (ppm)

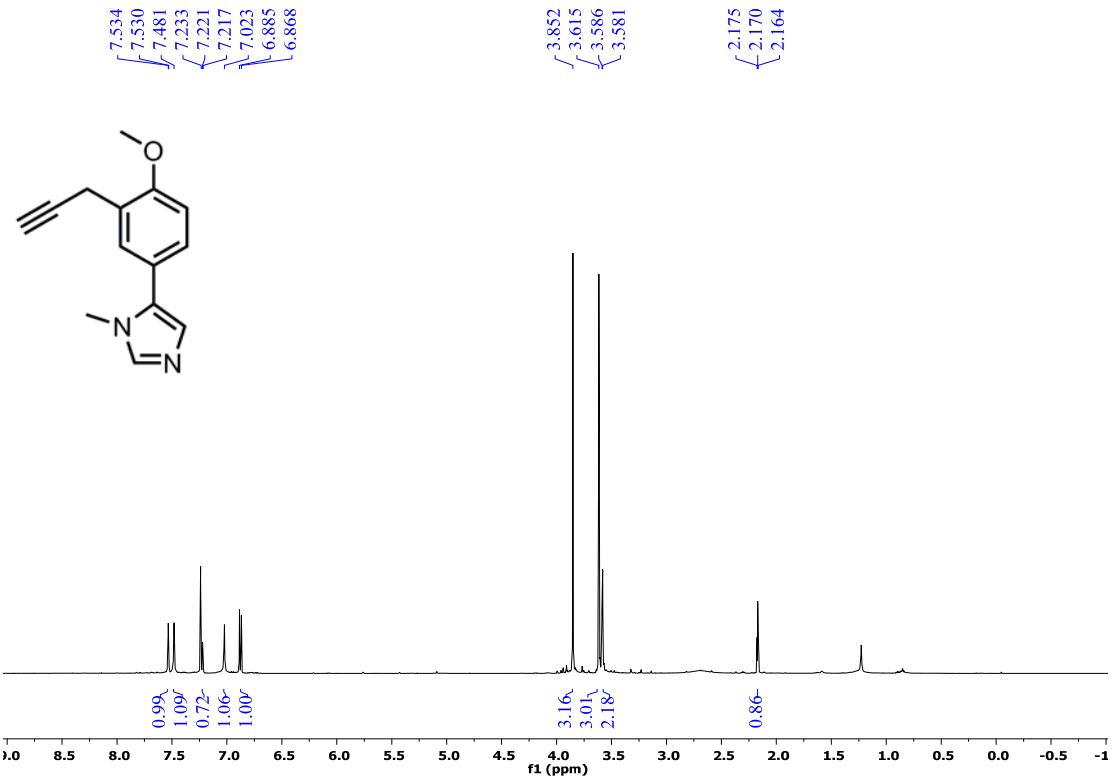
7.534
7.530
7.481
7.233
7.221
7.217
7.023
6.885
6.868
3.852
3.615
3.586
3.581
2.175
2.170
2.164
O
N
N
0.99
1.09
0.72
1.06
1.00
3.16
3.01
2.18
0.86
f1 (ppm)

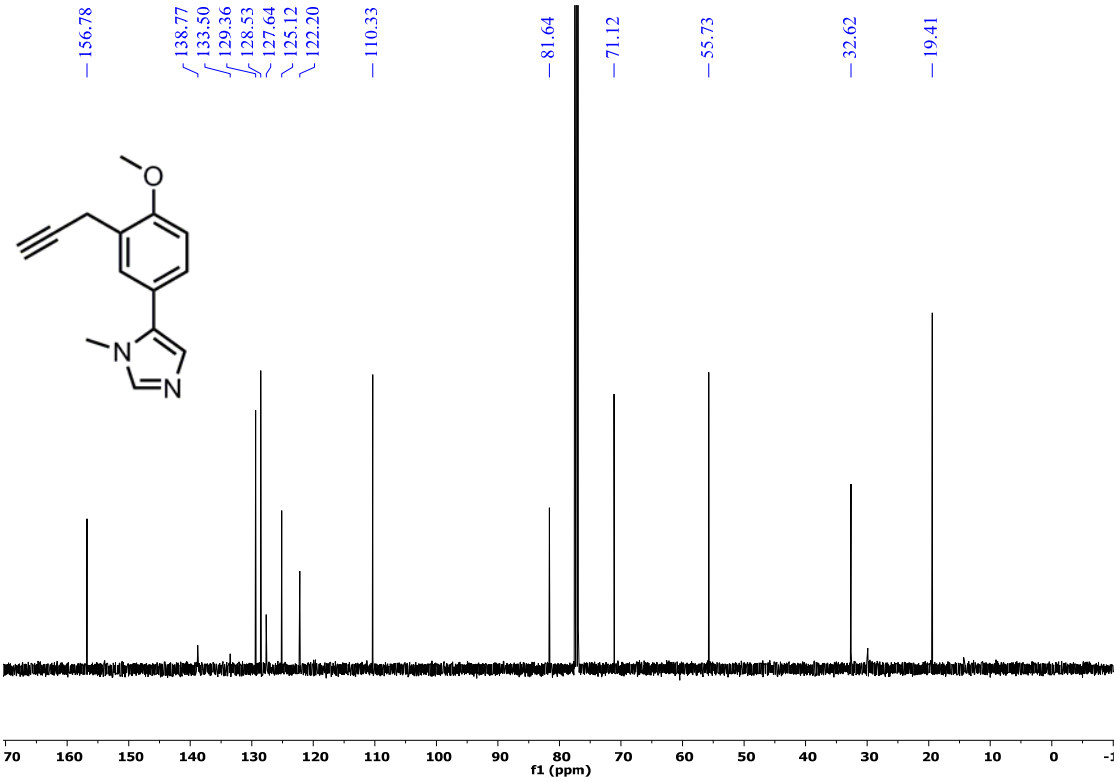
156.78
138.77
133.50
129.36
128.53
127.64
125.12
122.20
110.33
81.64
71.12
55.73
32.62
19.41
O
N
N
f1 (ppm)

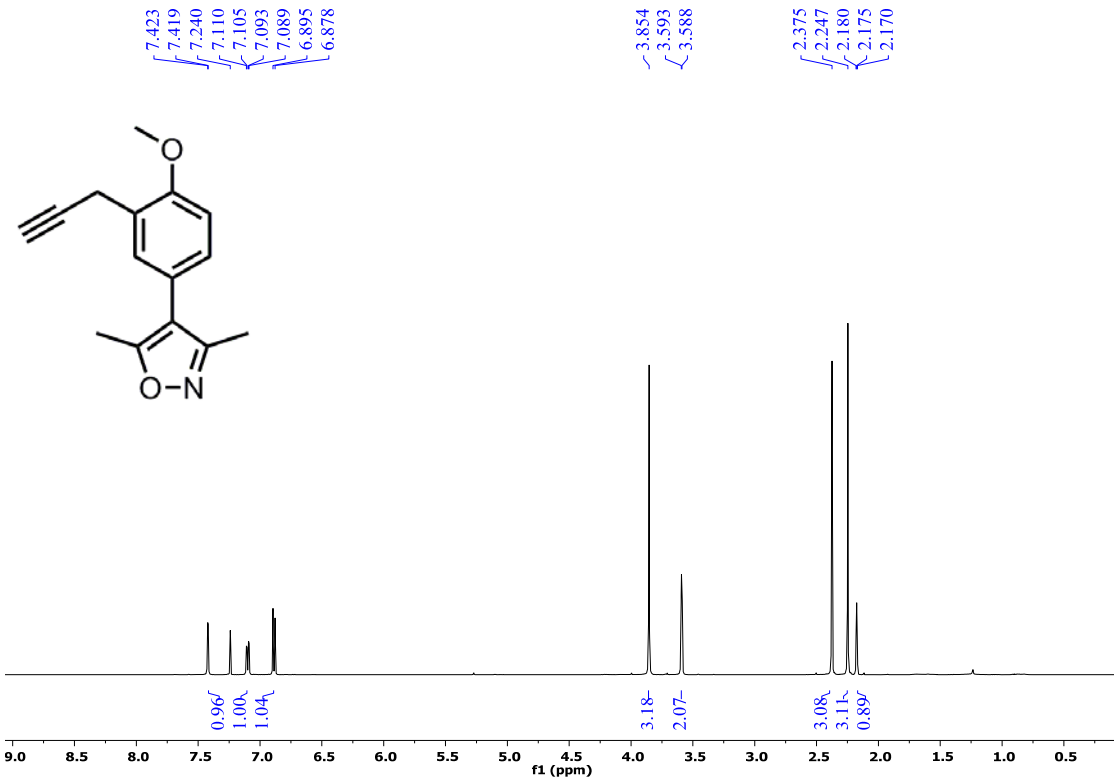
7.423
7.419
7.240
7.110
7.105
7.093
7.089
6.895
6.878
3.854
3.593
3.588
2.375
2.247
2.180
2.175
2.170
O
O–N
0.96
1.00
1.04
3.18
2.07
3.08
3.11
0.89
f1 (ppm)

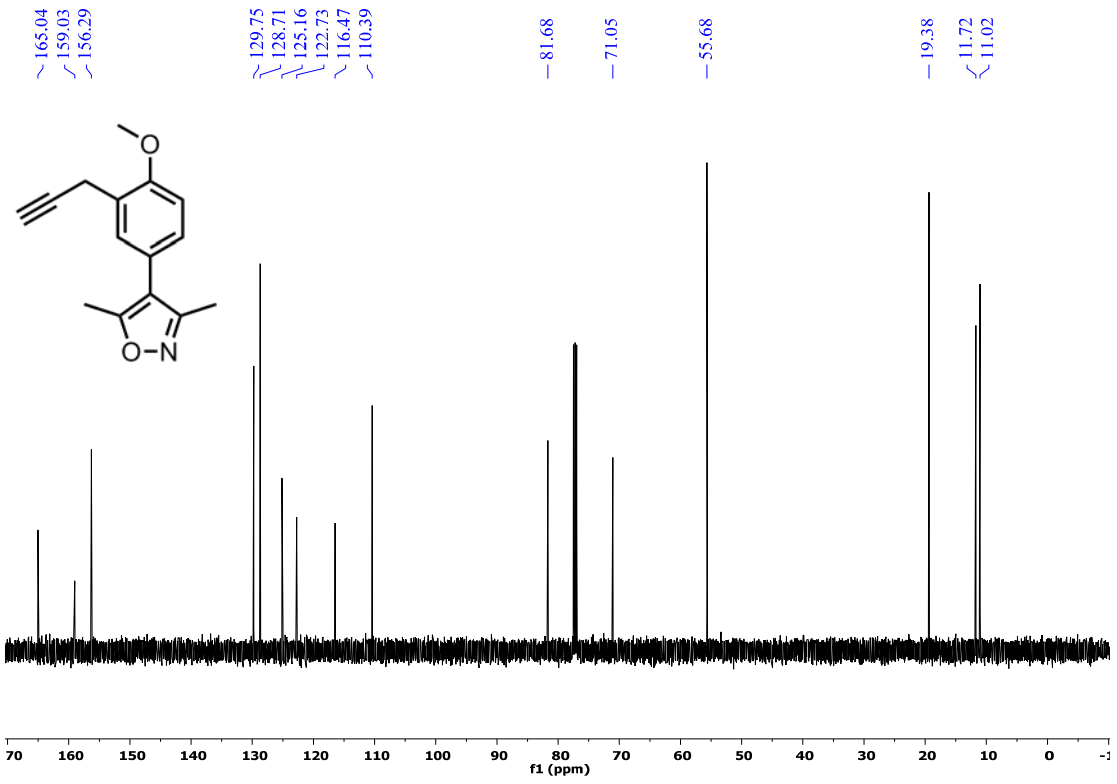
165.04
159.03
156.29
129.75
128.71
125.16
122.73
116.47
110.39
81.68
71.05
55.68
19.38
11.72
11.02
O
O–N
f1 (ppm)

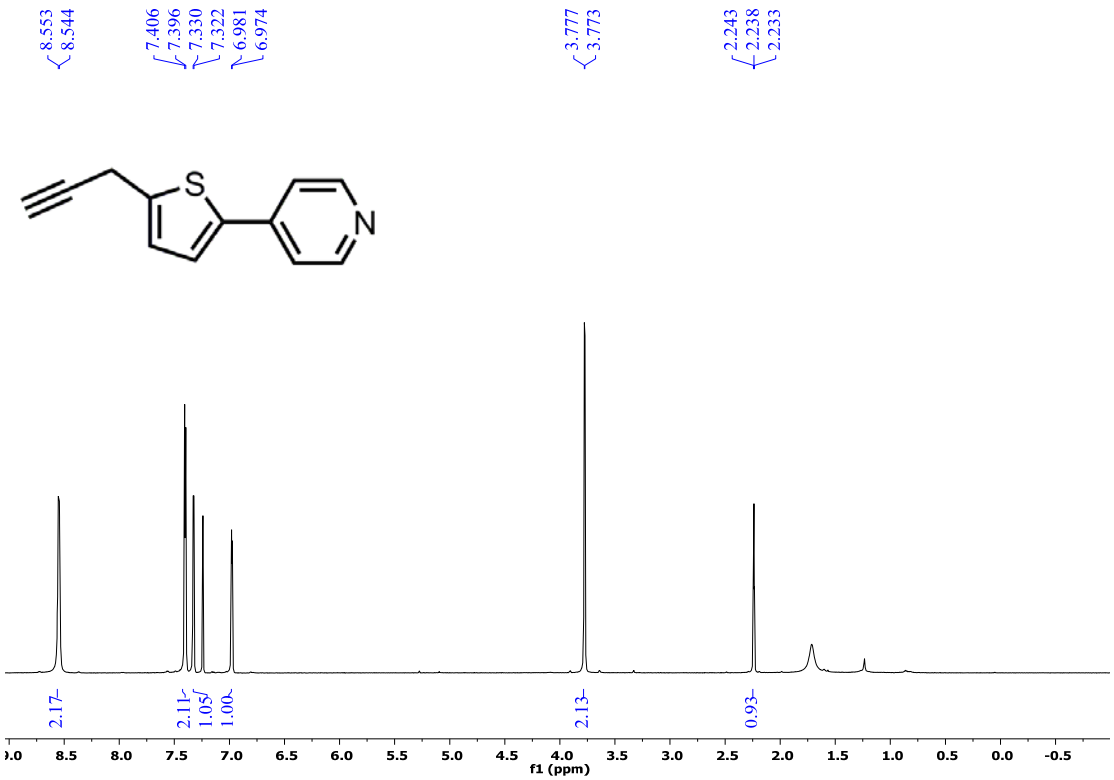
8.553
8.544
7.406
7.396
7.330
7.322
6.981
6.974
3.777
3.773
2.243
2.238
2.233
S
N
2.17
2.11
1.05
1.00
2.13
0.93
f1 (ppm)

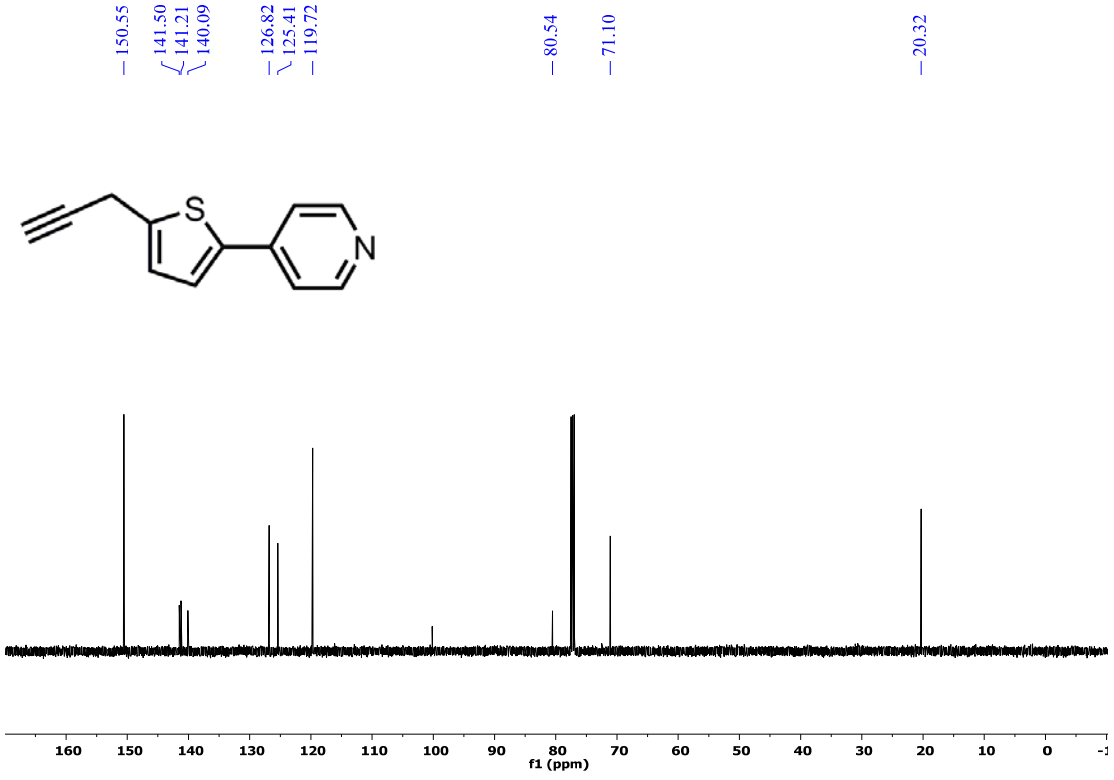
150.55
141.50
141.21
140.09
126.82
125.41
119.72
80.54
71.10
20.32
S
N
f1 (ppm)